Temporal and thermal evolution of extensional faulting in the central Gulf of Suez and detrital zircon (U-Th)/He constraints on the thermo-tectonic Paleozoic and Mesozoic history of the Sinai, Egypt

by

Edgardo J. Pujols-Vazquez
B.S., The University of Puerto Rico at Mayaguez, 2008

Submitted to the Department of Geology and the
Faculty of Graduate School of the University of Kansas
In partial fulfillment of the requirements for the
Degree of Master of Science

Advisory Committee

_____

Daniel F. Stockli (Co-chair)

_____

Douglas Walker (Co-chair)

_____

Robert Goldstein

Date Defended_____

The Thesis Committee for Edgardo Pujols certifies

that this is the approved version of the following thesis:

Temporal and thermal evolution of extensional faulting in the central Gulf of Suez and detrital zircon (U-Th)/He constraints on the thermo-tectonic Paleozoic and Mesozoic history of the Sinai, Egypt

Committee:

_____

Dr. Daniel Stockli, (Co-chair)

Date Approved:_____

ABSTRACT

Temporal and thermal evolution of extensional faulting in the central Gulf of Suez and detrital zircon (U-Th)/He constrains on the thermo-tectonic Paleozoic and Mesozoic history of the Sinai, Egypt

By

Edgardo Pujols
Department of Geology, August 26
University of Kansas

Many fundamental concepts of rifting have been influenced by observation made in the Gulf of Suez as a result of detailed structural and sedimentological studies. Although the three-dimensional structural geometry of the rift is well understood, the timing of faulting, the nature of faults linkage during progressive rifting and the influence on syn-rift sedimentation is poorly constrained. Despite ample fission track data from the Sinai rift flank, the lack of thermochronometric data from exhumed pre-rift sedimentary cover and crystalline basement blocks in a proper structural context within the rift limit the temporal and thermal reconstruction and the influence of pre-rift structures on the style of rifting. To elucidate the temporal and spatial evolution of extensional faulting and fault interaction in the central Gulf of Suez, this study presents new apatite (U-Th)/He (AHe) thermochronometric data from vertical transects and combines both surface and borehole sample arrays from normal fault blocks, integrated with structural block reconstruction of the central east margin of the Gulf of Suez. AHe data from the Sinai border fault complex at Gebel Samra (north) and Gebel Mutga (south) and surface and subsurface samples from the Hamman Faraun fault blocks explore the temporal

progression of normal faulting and the evolution of fault hard linkage in the central Gulf of Suez in the early to middle Miocene after the onset of normal faulting at ~23 Ma. As a second aspect, zircon (U-Th)/He (ZHe) dating from pre-rift strata and basement samples were analyzed to better constrain the pre-Tertiary tectonic, detrital provenance and thermal evolution of the Gulf of Suez to shed light on the Paleozoic/Mesozoic tectonic evolution and its influence on Red Sea-Gulf of Suez rifting. ZHe data from pre-rift strata in the central Gulf of Suez record a detailed Paleozoic/Mesozoic tectonic history that is highly influenced by Carboniferous, Triassic/Jurassic, and Santonian tectonism. Carboniferous Abu Thora sandstone contain detrital ZHe ages that suggest very short lag time, indicative of late Paleozoic tectonism and rapid cooling. Similarly, Triassic Qiseib sandstones, exhibits detrital ZHe ages indistinguishable from its stratigraphic age, underlining the importance of Triassic/Jurassic Neo-Tethyan rifting. Cretaceous Matulla pre-rift sandstones are dominated by Santonian detrital ZHe ages, with very short lag times, associated with the Syrian arc inverted structures and folding. The combination of AHe and ZHe ages in a detailed stratigraphic and structural context elucidates both the Neogene Gulf of Suez rift evolution and the impact of Paleozoic/Mesozoic tectonism on the structural grain of the gulf allowing for a more detailed and spatially differentiated understanding of the timing of extensional faulting and nature of fault linkage during progressive early to middle Miocene rifting in the central Gulf of Suez.

ACKNOWLEDGEMENTS

Funding for this project was provided mainly by Daniel Stockli and Apache Egypt Companies. Additional funding was provided through a DOSECC grant, a AAPG Student Scholarship, a AGI Minority Scholarship, and University of Kansas Department of Geology graduate summer research support. Special thanks go to William Bosworth and all the people in Apache Egypt, Cairo for extending their hospitality and patience. Additionally I will like to thanks my former and current laboratory partners Melissa Wolfe, Eugene Szymanski, Chris Hager, Markella Hoffman, Travis Glauser, Joe Miller, Kurt Sundell and Jordan Leigh, that even though they were extremely busy on they own research, they always find time to train me in the ways of the Isotope Geochemistry Laboratory (IGL) modus operandi or extend their help and support. In conjunction to all of this I will like to thanks greatly to Roman Kislitsyn for his everlasting patient and training.

"*A mis hermanos de laboratorio, a ustedes les debo mi progreso y crecimiento no solo exclusivo a la ciencia pero como persona. Sus puntos individuales de vista y ejemplos abrieron nuevas puertas de interés intelectual en mí y moldearon mi percepción a lo ya establecido. Agradecerles su tiempo donado es insuficiente pero imperativo, gracias por su paciencia y la ayuda provista en el Ingles que tanto necesité y principalmente por no rendirse y no perder su fe en mi. Gracias Evan Bargnesi, Kyle Goryski and Sarah Evans.*"

To my laboratory brothers, to you I owe my progress and growth not only as a scientist but as a person. Their individual points of view and example opened new doors of intellectual interest in me and shaped my perception of what is already been

established. Thank for the time donated, patience and support provided (especially in the English field) and mostly for not giving up and not losing your faith in me. Thanks Evan Bargnesi, Kyle Goryski and Sarah Evans.

Thanks go to the Faculty and Staff of the University of Kansas Department of Geology, in particular committee members Dough Walker and Bob Goldstein. Very special thanks go to coauthor, advisor, professor Daniel F. Stockli, who presented this amazing opportunity. *"Mis más sinceros agradecimientos, por tu tiempo y voluntad a ayudarme a crecer como científico, ahora estoy un paso más cerca a conseguir mis metas, acción que no será fácilmente olvidada."*

"A Yomayra Roman gracias por tu tiempo, intercambio intelectual, y apoyo continúo en todo lo que hago en esta vida, a ti y a mi familia que tanto amo y anhelo ver les dedico este trabajo. A mi Familia y a Yomy, disculpen mi ausencia física, siempre tengan en cuenta que los tengo presentes en donde este, con amor y sacrificio verdadero, Josué."

TABLE OF CONTENTS

Chapter 1

Introduction

This research provides a more comprehensive view to a failed continental rift system, the Gulf of Suez (Egypt), and its unique well preserve early architecture by integrating multiple fault blocks low temperature thermochronometric data. This project not only examines the rift flank crystalline basement as a whole unit, as previously done by Kohn and Eyal (1981) and Omar et al. (1989) in the eastern and western margin of the gulf respectively with apatite fission track data, but it also expand to nearby fault blocks and their pre- and syn-extensional sedimentary units. Furthermore it employs an unprecedented 3-D thermochronometric effort combining surface and subsurface samples in their structural and stratigraphic context. The apatite and zircon (U-Th)/He dating and thermal data derived from these blocks will grant a temporal connectivity between faulting and basin development. In summery the integration of these data will help elucidate the (1) temporal, spatial, and thermal evolution of the central eastern Gulf of Suez rift, (2) the interaction and linkage of normal faults, (3) the impact of fault linkage on early syn-rift sedimentation and provenance, (4) and the detrital pre-extensional thermal history and its influence on Early Miocene rifting.

This project was mainly funded by Dr Daniel Stockli laboratory fund and with financial and logistical assistance from Apache Egypt Corporation in an effort to understand early rifting development in a more temporal fashion. Additional funding, awarded to Edgardo Pujols was provided through AAPG and DOSECC grants, an AGI

Minority Scholarship, and University of Kansas Department of Geology graduate summer research support.

The data presented in Chapter Two entitled "*Temporal constrains on the structural and thermal development of multiple fault blocks in the central Gulf of Suez, Egypt*" yield new insights into timing of initiation and fault linkage, thermal development, and structural evolution of the central Gulf of Suez rift system through the investigation of four adjacent normal fault blocks, the Hamman Faraun and Gebel Samra, and the Gebel Araba and Gebel Mutga in the central and southern part of the east Gulf of Suez, respectively. Despite all the fission-track work done (e.g. Omar and Steckler, 1995; Omar et al., 1989, Kohn and Eyal, 1981; Kohn et al., 1996; Feinstein et al., 1996) and the already well establish structural and stratigraphic framework (Evan., 1988-1990; McClay et al., 1998; McClay & Khalil., 1998; Moustafa., 2002; Sharp et al., 2000; Bosworth., 1994, 1998, 2001; Bosworth & McClay., 2001; Younes & McClay., 2002) there is still prevailing questions on timing and mechanism for rifting evolution, initiation, progression and disproportional rift flank total uplift once balance against total extension in the Gulf of Suez. This chapter provides essential information to answer and help develop theorical models for rifting initiation, fault interaction and hydrocarbon maturation. The approach used for constraining the timing of major fault activity was to determine the low-temperature cooling histories of rocks in the footwalls of normal faults (e.g., Stockli et al., 2000, 2005). Fault slip on major normal faults leads to exhumation and cooling of the footwall such that the timing of fault slip can be determined from the age of this cooling or the modeled vertical distribution of cooling ages.

The apatite (U-Th)/He results from this study reveal that faulting in the northern study section occurred at ~19± 3 Ma and rift flank fault activation at ~23± 3 Ma. The southern Gebel Mutga block shows fault initiation at ~28± 4 Ma, although previous work in the Red Sea suggests that this age may reflect bias towards older ages due to inclusions or because the bottom of the apatite partial retention zone is not completely exposed in the southern part of the block. Two main rifting stages can be identified in this project and two models were proposed to explain the apatite thermal variation and age constrain. Zircon (U-Th)/He ages recorded an earlier thermal history in the Sinai crystalline basement and the Naqus/Araba formation that begins as early as ~525Myrs ago. This thesis chapter is as a journal manuscript to be submitted to the International Journal of Earth Sciences with Daniel Stockli, William Bosworth, and Robert Goldstein as co-authors.

The third chapter entitled *"Apatite and zircon (U-Th)/He detrital constrains on syn- and pre-rift Paleozoic and Mesozoic tectonism in central Gulf of Suez, Egypt"* discusses zircon data acquired in the ERB-B-2X borehole pre-rift sequence and several surface samples later collected with the purpose of constraining the thermal history of the Sinai and the development of early rifting architecture. This chapter provides a high-resolution pre-and syn-extensional detrital (U-Th)/He zircon data set that gives new insight on the regional tectonic evolution, sediment dispersal, detrital source, thermo-tectonic source evolution, and the consequent impact of previous tectonism on the Gulf of Suez rifting. (U-Th)/He data from pre-rift strata in the central Gulf of Suez record a detailed Paleozoic/Mesozoic tectonic history of the region that is strongly impacted by Carboniferous, Triassic/Jurassic, and Santonian (82-86 Ma) tectonism. The pre-rift units

are dominated by nearly zero depositional lag time, recording rapid exhumation related to Late Paleozoic tectonism, Jurassic/Triassic Neo-Tethyan rifting, and Syrian arc inversion on the structural grain of the Gulf of Suez. Syn-rift Abu-Zenima and Nukhul Fm. yielded ages indicative of proximal sources and recycling of pre-rift units and basement. In order to identify detrital populations we used probability density plots. This thesis chapter is written a journal manuscript to be submitted to Tectonics or Basin Research with Daniel Stockli and William Bosworth as co-authors.

All the basement and pre-rifting sequence samples were obtained mainly from the ERB-B-2X borehole provided by Apache Egypt Corporation, while surface samples were collected by Edgardo Pujols, Daniel Stockli and William Bosworth during multiple field campaigns to the Gulf of Suez. Syn-rift detrital zircon and apatite were separated from surface samples. All zircon and apatite (U-Th)/He analyses were performed at the University of Kansas Isotope Geochemistry Laboratory (KU-IGL). Fluid-inclusions Microthermometry analyses on Cambrian sandstone samples from the Gebel Samra fault block was carried out in the Fluid Inclusion Laboratory at the University of Kansas Geology Department. Inverse thermal modeling utilized code written by Chris Hager in MATLAB® (MATHWORKS, 2009b) now known as HeMP following equations from Ketcham (2005). Apatite chemically centralize ages were obtained using HelioPlot a software develop by Vermeesch in 2010 to reduced age over dispersal.

References (Chapter 1)

Bosworth, W., 1994, A model for the three-dimensional evolution of continental rift basins, north-east Africa. Geologisch Rundschau, v. 83, p. 671-688.

Bosworth, W., 1995, A high-strain rift model for the southern Gulf of Suez (Egypt): in Lambiase, J. J., ed., Hydrocarbon Habitat in Rift Basins, Geological Society, London, Special Publication, 80, p. 75-112.

Bosworth, W., and McClay, K., 2001, Structural and stratigraphic evolution of the Gulf of Suez rift, Egypt: A synthesis: in P.A. Ziegler, W. Cavazza, A.H.F. Robertson, and S. Crasquin-Soleau, eds., Peri-Tethys Memoir 6: Peri-Tethyan Rift/Wrench Basins and Passive Margins, Mémoires du Muséum National d'Histoire Naturelle de Paris, n. 186, p. 567-606.

Evans, A.L., 1990, Miocene Sandstone Provenance Relations in the Gulf of Suez: Insights into synrift Unroofing and Uplift History, American Association of Petroleum Geologists Bulletin, 74, 1386-1400.

Evan, A.L., 1988, Neogene tectonic and stratigraphic events in the Gulf of Suez rift area, Egypt, Tectonophysics **153** , p. 235–247.

Feinstein, S., Kohn, B.P., Steckler, M.S., and Eyal, M., 1996, Thermal history of the eastern margin of the Gulf of Suez, 1. Reconstruction from borehole temperature and organic maturity measurements, Tectonophysics 266 (1996), p. 203–220.

Kohn, B.P. and Eyal, M., 1981, 'History of uplift of the crystalline basement of Sinai and its relation to opening of the Red Sea as revealed by fission track dating of apatites' Earth and Planetary Science Letters, 52, p. 129–141.

Kohn, B.P., Feinstein, S., Foster, D.A., Steckler, M.S., and Eyal, M., 1996, Thermal history of the eastern Gulf of Suez, II. Reconstruction from apatite fission track and $^{40}Ar/^{39}Ar$ K-feldspar measurements.Tectonophysics. 283, p. 219-239.

McClay, K., and Khalil, S., 1998, Extensional hard linkages, eastern Gulf of Suez, Egypt, Geology 26 (1998), p. 563–566.

McClay, K.R., Nicols, G.J., Khalil, S.M., Darwish, M., and Bosworth, W., 1998, Extensional tectonics and sedimentation, eastern Gulf of Suez, Egypt: in Purser, B.H., and Bosence, D.W.J., eds., Sedimentation and Tectonics of Rift Basins: Red Sea–Gulf of Aden, Chapman and Hall, London, p. 223-238.

Omar G.I., and Steckler M.S., 1995, Fission-track evidence on the initial rifting of the Red Sea: two pulses, no propagation. Science 270, p.1341–44.

Omar, G.I., Steckler, M.S., Buck, W.R., and Kohn, B.P., 1989, Fission-track analysis of basement apatites at the western margin of the Gulf of Suez rift, Egypt: evidence for synchroneity of uplift and subsidence. Earth and Planetary Science Letters, 94, p. 316-328.

Sharp, I.R., Gawthorpe, R.L., Underhill, J.R., and Gupta, S., 2000, Fault-propagation folding in extensional settings: Examples of structural style and syn-rift sedimentary response from the Gulf of Suez Rift, Sinai, Egypt. Geological Society of America Bulletin, 112, p. 1877-1899.

Stockli, D., 2005, Application of low-temperature thermochronometry to extensional tectonic settings. Review in Mineralogy and Geochemistry. v 58, p. 411-448. in Reiners, P.W., and Ehlers, T.A., Low Temperature Thermochronology: Techniques, Interpretations and Applications, Reviews in Mineralogy and Geochemistry, v. 58, p. 123-149.

Stockli, D.F., Farley, K.A. and Dumitru, T.A., 2000, Calibration of the (U-Th)/He thermochronometer on an exhumed normal fault block in the White Mountains, eastern California and western Nevada. Geology, v. 28, n. 11, p. 983–986.

Vermeesch, P., 2010, HelioPlot, and the treatment of overdispersed (U-Th-Sm)/He data. Chemical Geology 271, p. 108-111.

Younes, A.I., and McClay, K.R., 2002, Development of accommodation zones in the Gulf of Suez-Red Sea Rift, Egypt. In: Underhill, J. R., and Trudgill, B. D., (eds.), The structure and stratigraphy of rift systems. AAPG Bulletin, 86, p. 1003-1026.

Chapter 2

Temporal constraints on the structural and thermal development of multiple fault blocks in the central Gulf of Suez, Egypt

Abstract

Many fundamental concepts of rifting have been influenced by observation made in the Gulf of Suez as a result of detailed structural and sedimentological studies. Although the three-dimensional structural geometry of the rift is well understood, the timing of faulting, the nature of fault linkage during progressive rifting and the influence on syn-rift sedimentation is poorly constrained. In order to elucidate the temporal and spatial evolution of extensional faulting and fault interaction in the central Gulf of Suez, this study presents new apatite (U-Th)/He thermochronometric data from vertical transects for both surface and borehole sample arrays from extensional fault blocks, carefully integrated with structural reconstruction of the different fault blocks. Apatite (U-Th)/He data from the Sinai border fault complex at Gebel Samra and Gebel Mutga record onset of faulting at ~23 Ma and <28 Ma, respectively. El Hamman Faraun blocks preserves the onset at ~19 Ma. These new data shed light on the temporal and thermal progression of normal faulting and the evolution of fault hard linkage in the central Gulf of Suez during early to middle Miocene faulting. These new data corroborate and refine estimates from earlier AFT studies for the timing of rift initiation at ~23 Ma in the western margin (Omar et al. 1989) and ~26 Ma along the eastern margin of the Gulf of Suez (Kohn and Eyal 1981).

Introduction

The well exposed and preserved structural and sedimentological configuration of the Gulf of Suez has captured the attention of geologists for decades due to both its hydrocarbon potential (e.g. Bosworth, 1994; McClay el al., 1998; Moustafa, 2002) and the unique opportunity to study the early stages of rifting. The exposure of early rift structures and stratigraphy is a result of the preservation of an early rift stage due to the fact that the Gulf of Suez was isolated from continued major rifting in the Red Sea and extension terminated after the onset of strike-slip faulting along the Gulf of Aqaba/Dead Sea transform at ~15-14 Ma (Evan, 1980). This failed continental rift system records and provides exclusive insights into early rift architecture, progression and early interplay between extensional faulting and sedimentation. Lesson learned from the Gulf of Suez have contributed to our fundamental understanding of early rifting dynamics and greatly influenced models and concepts of rifting evolution.

The Gulf of Suez developed as a result of the northeastward separation of the Arabian and the African plates where exhumed linked fault blocks have accommodated major crustal extension (Younes, and McClay, 2002). It was the first rift system in which large-scale, long-axis segmentation into sub-basins and tilt domains was clearly recognized. Despite ample fission-track data from the Sinai rift flank (e.g., Omar and Steckler, 1995; Omar et al., 1989, Kohn and Eyal, 1981; Kohn et al., 1996; Feinstein et al., 1996), the lack of thermochronometric data from exhumed pre-rift sedimentary cover and underlying crystalline basement, in a proper structural context within the rift, limit the temporal and thermal reconstruction and the influence of pre-rift structures on the style of rifting.

This study focuses on the central portion of the eastern Gulf of Suez (Fig. 1), which is bounded by two major transfer fault zones, the Gharandal in the north and the Sufr El Dara in the south (Moustafa, 2002). Here, we employed a detailed 3-D thermochronometric approach that utilizes an extensive apatite and zircon (U-Th)/He dataset, sampled from vertical transects from both exhumed normal fault and borehole samples that span the entire pre-rift basement and sedimentary cover sequence. Furthermore, this research targets the rift flank (Gebel Samra and Gebel Mutga) as well as individual fault blocks west of the border fault system (Hamman Faraun block and Gebel Araba block), where multiple, linked normal-fault systems take advantage of pre-existing Proterozoic to Mesozoic structural grains (Bosworth, 1995). The objective is to temporally differentiate fault-block motion and sediment provenance and shed light on the interaction and linkage of normal faults and their effect on syn-rift sedimentation. The integrated thermochronometric data in this research yields new insights into (1) the temporal, spatial, and thermal evolution of the central eastern Gulf of Suez rift, (2) the nature, interaction, and linkage of normal faults, (3) the impact of fault linkage on early syn-rift sedimentation and provenance, and (4) timing of hydrocarbon maturation and trap formation.

1. *Geology background*

1.1 *Brief pre-extension tectonic history*

The Sinai basement accreted in conjunction with a series of crystalline and metamorphic terranes that later became the west margin of the Arabian plate, now part of the Arabo-Nubian crystalline shield (Gass and Gibson 1969; Kohn and Eyal 1981; Stoeser and Camp, 1985; Genna et al., 2002). The basement rocks in the Sinai are composed of granites, gneisses, felsic metavolcanics and metasediments that were deformed and sheared during the Pan-African

Orogeny, dated regionally between 530-620 Ma (Hasson and Hashad 1990; Stern and Hedge 1985; Kohn et al., 1987; Bosworth and McClay 2001). The inherited orientation of intrusive dikes and shear zones produced during the Pan African Orogeny have been invoked to have a major impact on fault orientation and geometry during the Gulf of Suez rifting.

Pre-extensional stratigraphy is highly variable starting at the Cambrian with continental to shallow marine silisiclastics to Eocene carbonate platforms. These units generally get thinner towards the south with the exception of the Malha Fm. Deposition of thick sequences of siliciclastics (–Nubian Sandstones") overlying the Pan-African metamorphic and igneous basement resulted from repeated peneplanation of the Arabian-Nubian shield during the Paleozoic and part of the Mesozoic. Major marine incursions occurred during Cambrian, Carboniferous, Albian, and Cenomanian times (Bosworth and McClay, 2001). Zircon (U-Th)/He detrital data (Chapter, 3) constrain the top of the –Nubian" sandstones in the marine transgressive Raha Fm. at ~93 Ma (Cenomanian), younger than previous palynological studies have shown. Turonian to Santonian units range in composition from glauconitic sandstone, shale and dolomitic limestome and were overlayed by deep to shallow marine Campanian to the Eocene carbonates.

The two major Phanerozoic tectonic events affecting pre-Tertiary structures and stratigraphy of the Sinai region were (1) Triassic and Jurassic Neo-Tethyan rifting and (2) Santonian inversion related to Syrian Arc structures and the Alpine collision (s.l.). During Santonian inversion, Neo-Tethyan rift structures were reactivated in a right-lateral transtensional strain regime produced by a change in relative motion between Africa and Europe at ~84 Ma. Furthermore, these east-west trending faults were reactivated by later transfer and cross faults during the hard linkage of rift-axial trending faults in the Gulf of Suez (Bosworth and McClay,

2001). These structures may have continued to be reactivated during the Late Eocene forming right-lateral strike-slip faults in northern Egypt, as a result of ongoing shortening during the formation of the Alpine collisonal belt.

Even though the basement endured various levels of low-temperature tectonism from late Cambrian to Eocene times (i.e., Pan African Orogeny, Hercynian collision, Neo-Tethyan rifting, and Santonian inversion) the overlying Mesozoic and early Cenozoic stratigraphy appears relatively unaffected by pre-rifting tectonics (Bosworth and McClay, 2001).

1.2 *Cenozoic rifting*

The Cenozoic Red Sea continental rift system and its northern extension, the Gulf of Suez, developed as a result of the northeastward separation of the Arabian and the African plates (e.g., McKenzie et al., 1970; Coleman, 1979, 1993; Cochron, 1983; Joffe and Garfunkel, 1987; Bosworth et al., 2005). Regional extensional stress during that period was perpendicular to the rift axis. The onset of major rifting in the Red Sea was marked by the development of crustal domino-style tilt blocks and syn-rift deposition in intervening half-grabens. The earliest syn-rift strata in the Gulf of Suez basin are the latest Oligocene non-marine Abu Zenima Fm. and shallow marine Nukhul Fm. The Abu Zenima Fm. red beds, siltstones, and mudstones were deposited in continental-marginal to marine-evaporite conditions. Quickly after the deposition of this unit, sedimentation dynamics complicate after Mediterranean marine waters invade the early Gulf of Suez (Garfunkel and Borton 1977). Faulting and basin development of half grabens started to control the thickness and distribution of the syn-rift units along the Gulf during the deposition of the Nukhul Fm., which in some cases is directly deposited on top of the basement. The maximum thickness of the Nukhul Fm. is ~700 m (Richardson and Arthur, 1988).

Subsidence rates reached their maximum between ~19-16 Ma with the deposition of the Rudeis Fm., coinciding with a change to open marine conditions with water depth from ~100-1000 m (e.g., Evans, 1986, 1990; Steckler et al., 1988; Richardson and Arthur, 1988). Through this period, the Gulf of Suez and the Red Sea were linked and formed one continuous rift system that shared a kinematic and stratigraphic framework (Bosworth and McClay, 2001). During this main phase of extension, up to ~2000 m of syn-rift strata accumulated in the Gulf of Suez exhibiting major thickness and facies variations across and between adjacent fault blocks and rift segments (Gawthorpe et al., 1997; Sharp et al., 2000). The Rudeis Fm. represents the main phase of syn-tectonic deposition and rift subsidence. Deposition is interrupted at ~16.5 Ma (Mid Clysmic event of Garfunkel and Borton, 1977) resulting in the development of major unconformities. Although the Gulf of Suez was initially the northward continuation of the Red Sea, development of the Gulf of Aqaba-Dead Sea transform (~15-14 Ma) cut off the rift at an early extensional stage and preserving the early structural and stratigraphic rift records (Tamsett, 1984; Steckler and ten Brink, 1986). After onset of the Gulf of Aqaba-Dead Sea transform, basin dynamics changed significantly due to the regional extensional stress becoming oblique to the rift axis and the onset of regionally extensive evaporite deposition that included the Belayin Fm, Gharib Fm. and the Zeit Fm. During Zeit Fm. Deposition, syn-extensional salt tectonics has a major influence on basin geometry.

There is sufficient kinematic data to propose that stress fields did not vary considerably during rift progression (Angelier, 1985; Jarrige et al., 1990; Bosworth and McClay, 2001), although Quaternary units in the southern Gulf record an extensional stress field (N60E, normal to the rift axis); slightly oblique to Miocene stress field (Bosworth and McClay, 2001).

Neotectonic data from the vicinity of Gebel el Zeit show that extension is still taking place today at a rate of 0.8 to 1.2mm/yr (Bosworth and Taviani, 1996).

The total amount of extension that the Gulf of Suez is still somewhat debated, although most studies agree that the northern Gulf has experienced less extension compared to the southern portion. Estimates calculated from subsidence analysis, yielded 5-10 km and 30-40 km for the northern and southern Gulf of Suez, respectively (Richardson & Arthur, 1988). Estimates derived from structural reconstructions diverge by a factor of two from subsidence analysis given a 4-5 km of extension in the north and ~20 km in the south of the Gulf of Suez (Colletta et al., 1988). Structural estimates by Patton et al., (1994) indicate ~16 km of extension in the northern Gulf of Suez and Bosworth (1995) estimated ~ 35km in the southern part, based on extensive industry data.

1.3 *Fault Block Geometry and Orientation (Central Eastern Margin)*

Large-scale structural analyses of multiple fault blocks in the north-central region of the Gulf have been performed by Mustafa (2002). His geological and structural mapping classified the Hamman Faraun fault block and the Baba fault (bounding the Gebel Samra block) as part of a zigzag network of interconnected north-northwest-trending, rift-parallel normal faults and -south-southwest transfer faults. In this part of the Hamman Faraun fault block, pre-rift and syn-rift rocks have a principal northeast dip of about 12-14°, whereas in Paleozoic rocks on the rift-flank the strata are sub-horizontal or only gently dipping northward. The predominant northeast dip of the Hamman Faraun fault block is produced by tilting of the downthrown side toward both the rift parallel faults and the linking transfer faults. This leads to a bidirectional rollover of the

downthrown side of the rift-bounding fault due to the listric nature of the transfer faults, which develop local synclines or anticlines at the corners of the fault array. Such syn-extnesional folding likely affected the transportation direction of early rift sediments in the vicinity of these faults (Moustafa, 2002). The Gebel Mutga block belongs to the massive crystalline rift shoulder that is bounded by the border fault system and the buried Al-Qaa syncline in its hanging wall. The Gebel Araba basment-cored fault block north of the Sufr El Dara transfer zone was exposed along a southwest-dipping normal fault that delineates the eastern shore of the Gulf of Suez. This major bounding fault accommodated extensional strain through the development of small-scale, ~~"z~~ig-zag" patterned transfer-fault arrays. Additionally, this fault can be traced north where it intersects the Baba and the Markha faults which eventually converge at the rift shoulder.

2. *Thermochronology*

(U-Th)/He thermochronology is a well-established technique that uses accessory minerals (e.g., apatite and zircon) that are resistant to mechanical and chemical degradation, can incorporate radioactive parents such as Uranium, Thorium and Samarium, and can retain and/or diffuse the radioactive daughter product at constant rates. This technique takes advantage of the production, incorporation and retention of the radiogenic ^{4}He from the α-decay of ^{238}U, ^{235}U, ^{232}Th, and ^{147}Sm. The retention characteristics of He are mineral specific and the diffusive loss governed by thermally-activated volume diffusion (e.g., Shuster and Farley, 2005). The most commonly used thermochronometers with their respective closure temperature (T_c) are apatite (T_c ~80°C), titanite (T_c ~180-220°C), and zircon (T_c ~180°C) (Farley, 2000; Reiners and Farley, 1999; Stockli and Farley, 2004; Reiners et al., 2005; Wolfe and Stockli, 2010).

The closure temperature concept of Dodson (1973) is somewhat misleading in low-

temperature thermochronology as the switch from diffusively open to closed (i.e. retentive) does not occur at a discrete temperature. Rather, the system (mineral) partially opens and some of the He diffuses out and only a fraction is retained, it is said that the mineral resided in the Helium Partial Retention Zone (HePRZ). The HePRZ is best identified in vertical sample arrays of exhumed crustal sections or in boreholes. For example, Apatite encounters its HePRZ at temperatures ranging between40 to 80°C (Wolf et al., 1998; Farley, 2000) and zircon at 140 to 180°C (Reiners et al., 2002; 2004; Reiners, 2005; Stockli, 2005; Wolfe and Stockli, 2010). These temperature intervals are mainly controlled by the mineral specific diffusion kinetics of He, the cooling and exhumation rates, as well as the alpha dosage (damage) acummulated over time (Nasdala et al., 2001, 2005), and to a lesser extent grain size (Reiners and Farley, 2001). The (U-Th)/He uncorrected ages are calculated iteratively using the following equation,

$$^{4}He = 8^{238}U\,(e^{\lambda 238t} -1) + 7(^{238}U/137.88)(e^{\lambda 235t} -1) + 6^{232}Th\,(e^{\lambda 232t} -1) + {}^{147}Sm(e^{\lambda 147t} -1)$$

(equation 1)

where ^{238}U, ^{235}U, ^{232}Th, ^{147}Sm and ^{4}He are concentrations acquired by mass spectrometry usually expressed in nmol/g or ppm; $_{238}\lambda$, $_{235}\lambda$, and $_{232}\lambda$ are decay constants for their respective isotopes. Variations of this formula can be found in Vermeesch (2008). An alpha ejection correction was applied to all grains analyzed. This correction provides a statistical correction and a geometrical solution that account for the fractional loss of alpha particles from the outer ~20 m of a grain. The ~20 m approximates the travel distance of the alpha particle within an apatite or zircon (Farley, 1996).

3. *(U-Th)/He Thermochronology apply to extensional tectonic settings*

Apatite and zircon (U-Th)/He thermochronometry is a powerful tool to constrain the magnitude and timing of faulting, especially in extensional settings (e.g., Stockli, 2005). A well-established approach for dating fault motion is to determine the low-temperature cooling histories of rocks in the footwalls of normal faults (e.g., Stockli et al., 2000, 2005). Fault slip on major normal faults leads to exhumation and cooling of the footwall, such that the timing of fault slip can be determined from the age of this cooling or the modeled vertical distribution of cooling ages. Samples were strategically collected in the exposed footwall section, parallel to dip slip direction or perpendicular to strike in order to get the maximum displacement. Sampling strategy may vary according to the project goals, therefore it is crucial to assess the area prior to sample collection (e.g., the greater the fault angle, the less displacement needed to expose partial retention zones, different lithologies may or may not yield sufficient or good-quality apatite or zircon, etc.). Once the samples are analyzed, a plot of elevation vs. apatite or zircon (U-Th)/He ages will yield the timing of faulting as elevation changes but age remains constant. The combination of cooling ages from multiple fault blocks in their respective geologic context and the integration of the fault geometries and kinematics can help us understand the temporal and spatial arrangement and distribution of strain during rifting development. This information in turn will aid us in deciphering the large-scale mechanisms controlling extensional fault systems.

4. *Inverse Modeling of (U-Th)/He ages*

Inverse modeling allows us by means of algorithms and statistics to theoretically frame possible time-temperature (t-T) histories that match the obtained (U-Th)/He data. These modeled histories provide insights into how a system like the Gulf of Suez might evolve structurally and thermally through time. The time-temperature paths obtained from modeling

require the following inputs: (1) The initial and end conditions of the T-t history (can be guided by previous studies), (2) the (U-Th)/He ages for apatite and zircon and their current elevation, (3) and any other (t-T) constrain known by other geologic methods. The modeling software HeMP developed by Hager and Stockli (2011) provides the capacity to forward and inverse model sample arrays and single samples using zircon and apatite (U-Th)/He data. It will also quantify the cumulative exhumation and exhumation rates that fit the provided data and explore the thermal gradient parameter space. Interpretation of modeling results must take into account the geological structure, fault geometries, and mechanisms controlling cooling (e.g., hydrothermal fluids, topography, current geothermal gradient, etc.). The t-T path will be influenced by the geothermal gradient and the degrees of freedom between t-T constraints selected by the user. Monotonic cooling or heating is assumed between inflection points in the t-T paths.

5. *Fluid inclusion thermometry*

In addition to the thermochronometric research, fluid inclusions microthermometry was carried out to establish thermal conditions of a section in the central eastern Gulf of Suez and to estimate maximum temperatures experienced by the Cambrian strata. The need for defining maximum post-deposition temperatures arose from the observed zircon (U-Th)/He age dependency on effective uranium concentrations evident in the Naqus/Araba Fm. and crystalline basement zircons (Fig. 3). The idea to be evaluated was that the age variability due to different alpha dosage in zircons from the basement and the Naqus/Araba Fm. was controlled or affected by hydrothermal or burial temperature spikes during the Phanerozoic that should also be recorded by the fluid-inclusion data. Using sedimentary surface samples collected from the Gebel Samra fault block, we constrained the maximum and minimum thermal variations that the

Cambrian rock experienced during diagenetic quartz re-growt, by identifying the (P-T) conditions at the moment of fluid entrapment and the composition of the fluids trapped. Since most of pre-rift sediments have undergone a complex burial and thermal history after Cambrian deposition, it is expected that silica-rich fluids have provided the means for quartz re-crystallization and therefore fluid entrapment. Fluid inclusions and their petrographic context combined with (U-Th)/He ages of multiple thermochronometers deliver a relative time-temperature framework that allows a more robust reconstruction of the thermal history and the maximum temperatures experienced by the Cambrian strata and the Gulf of Suez pre-rift sequence.

6. *Methodology*

6.1 Zircon and Apatite (U-Th)/He methodology

For this research samples were collected from vertical transects from the exposed levels of different extensional fault blocks (Gebel Samra, Gebel Mutga, Gebel Araba). Additionally, borehole (wet cutting) samples from the entire pre-rift sedimentary cover sequence and basement were analyzed from the ERB-B-2X borehole (Hamman Faraun fault block) (Fig. 1-2). Borehole samples were provided by Apache Egypt Coorp.

Approximately 300 apatite and 170 zircon grains where analyzed at the University of Kansas Isotope Geochemistry Laboratory (IGL). Apatite and zircon grains were separated using standard mineral separation techniques (i.e., crushing and grinding, water table, gravimetric, magnetic and heavy-liquid density separation). Grains were subsequently handpicked according to their size (>60um), surface to volume ratio, clarity and purity (inclusion free). These characteristics were adhered to to provide an accurate alpha ejection correction (Farley et al.,

1996; Farley, 2002) and to avoid other mineral inclusion to the extent possible. The grains were individually sealed in platinum foil jackets and completely degassed with either a Nd:YAG or a CO_2 diode laser under ultra-high vacuum conditions (>10^{-9} torr). The extracted gas was spiked with ^{3}He (isotope dilution), purified cryogenically, analyzed by a quadrupole mass spectrometry.

The completely degassed grains were later dissolved according to procedures appropriate for either apatite or zircon. While apatites were dissolved using a spiked HNO_3 solution, enriched in ^{235}U, ^{230}Th and ^{149}Sm, zircons were dissolved using a two-step HF and HCl standard pressure vessel digestion procedure. Concentrations of ^{238}U (^{235}U = 1/137.88 =$^{235}U/^{238}U$), ^{232}Th and ^{147}Sm were analyzed using a high-resolution inductively coupled mass spectrometer (ICP-MS). All concentrations were calculated by means of isotope dilution.

Apatite quality for most samples from the Sinai and the Gulf of Suez was relatively poor with ubiquitous inclusions and pitted grain surfaces. Thus not surprising, many samples displayed significant scatter in apatite He ages, requiring a greater number of sample aliquots to be analyzed (>3 apatite aliquots per sample) and treated compositionally to provide a statistically correct mean age. The software Helioplot was use to calculate mean ages using a weighted mean algorithm that takes into consideration geochemical data and both analytical uncertainty and population over-dispersion simultaneously (Vermeesch, 2010). The geometric mean of the (U-Th-Sm-He) geochemical composition plotted on ternary diagrams and in logratio plots represents the calculated centralized age of one sample (Appendix 2). Centralized (mean) geochemical ages did not diverge significantly from regular average ages, meaning that the weighted sample mean age acquired from the chemical data is not significantly different from the sample mean age calculated from only the aliquots ages.

Zircon ages from the Proterozoic crystalline basement show a strong dependency on

effective Uranium concentration (as a proxy for radiation damage). A simple filter was applied to these zircon grains to exclude alpha dosage values higher that 5.E+16 events/mg after 450 m.y.. The filtered results provide a signature without partially metamict grains and therefore are more representative of a single closing temperature (Tc).

6.2 Fluid inclusion methodology

Three samples from the Cambrian Araba/Naqus Formation were analyzed for fluid inclusions. They were selected for their porosity, evident diagenetic quartz overgrowth, and proximity to basement rocks. A double-polished thin section was made for each sample using Barker and Reynolds (1984) method. The main purpose was to identify fluid inclusions in the quartz overgrowths and in the dust rims of the detrital sediments to constrain the temperature conditions of the secondary quartz growth. Fluid inclusions in quartz overgrowth tend to be present along concentric growth boundaries (Goldstein and Reynols, 1994). The measurements on the samples were made on primary and secondary inclusions using a heating and freezing stage attached to a microscope equipped with transmitted white light and incidental UV light. The heating and freezing stage, heats by passing heated air, or nitrogen over the sample and cools by passing nitrogen gas through liquid nitrogen over the sample. The maximum and minimum temperature it can reach are 600°C and -190°C, respectively. The freezing and cooling was performed multiple times for each individual fluid inclusion to find their Tm_{ice} (last crystal melt temperature), Te (eutectic temperature, first melt), Th (homogenization temperature, single phase), which constrains the fluid inclusion‘s composition and the temperatures of entrapment. Using the Te values we were able to determine the composition and subsequently the pressure conditions of the sediments assuming a geothermal gradient.

7. *Results*

7.1 *Zircon Data*

Zircon grains from the pre-rift sedimentary sequence from Thebes Fm. to the bottom of the Abu Thora Fm. display a wide range of (U-Th)/He ages that all equal or predate the depositional age of the sampled stratigraphic unit. This behavior can be seen in the ERB-B-2X borehole and in all surface samples. The Naqus/ Araba Fm. shows an even more variable (U-Th)/He age distribution with values post- and predating the depositional age. The probability density plots from this unit show three main peaks at ~450 Ma, ~350Ma , and ~250 Ma. Fully reset ages, commonly display one main peak but in this case dependency of (U-Th) ages on the eU results in multiple peaks. Therefore an alpha dosage filter was applied according to the main distribution and inflection of (U-Th)He ages with respect to alpha dosage (see Figs. 3 and 9). The remaining peak after the filter was applied on the Naqus/Araba zircons was at ~450 Ma postdating depositional age. The crystalline basement zircons display a range of (U-Th)/He ages similar to the Naqus/Araba Fm., but displays a stronger (U-Th)/He age dependency on alpha dosage variation than the Naqus/Araba Fm. The probability density plot from the basement show two main peaks at ~525 Ma and ~450 Ma, and two additional subsidiary peaks at ~325 Ma and ~240 Ma. After applying the alpha dosage filter one main peak remained at ~525Ma.

7.2 *Apatite Data*

Apatite yield in the upper pre-rift sequence in the Hamman Faraun block (ERB-B-2X) was limited to a few units. The (U-Th)/He ages acquired ranged from ~20 to 135 Ma with no apparent depth correlation. Sedimentary rocks from the upper pre-rift sequence (mostly

carbonates) lack sufficient apatite yield for detrital or thermal analysis. A more reproducible suite of apatite He ages can be seen in the lower Naqus/Araba and the granitic basement units where depth correlation can be identified (Fig. 4). The unchanging AHe ages against depth on figure 5 are at ~19 Ma (HelioPlot chemical mean age). In the Gebel Samra northern rift flank transect, ages display some age dispersal on four samples (Fig. 4), but generally apatite ages fluctuated from ~16 to 40 Ma. The most frequent ages encountered cluster around ~19-23 Ma, (Fig. 6). The Gebel Mutga transect, in the central portion rift flank, displays slightly older ages that those in the northern section of the study area, with ages varying from ~24 to 50 Ma. The AHe chemical mean age becomes less variable in depth at nearly 28 Ma (Fig. 7), while the youngest grain of the population yielded an age of ~24 Ma. The Gebel Araba transect only yielded apatite from the crystalline basement and the Naqus/Araba Fm. Aliquots ages were highly variable in almost all the samples collected in this transect due to extremely poor apatite quality. Only one sample showed reproducible aliquots ages at ~34 Ma, while the rest range in age from 34 to 150 Ma. Chemical centralized ages placed the great majority of the samples at ~70-80 Ma, but we attach little significance to them as the apatite quality is generally too poor to yield reliable ages. See appendix 5 for D.E.M. image that illustrate their spatial relationship and the chemical mean apatite (U-Th)/He ages (Appendix 5).

7.3 *(U-Th)/He apatite age scatter*

The dispersion of single aliquots apatite (U-Th)/He ages from a few samples can be explained by: (1) compositional zonation associated with high-U or low-U overgrowths on some of the grains hence influencing ejection corrections, (2) He implantation by adjacent minerals with high effective uranium concentration (parentless He), and (3) U- and Th-bearling micro-inclusions that were not completely dissolved following sample degassing such that

measurements do not reflect the total amounts of U, Th, and Sm present. Any kinetic effect or aforementioned complication is further magnified by prolonged residence in the partial retention zone of apatite. In addition, for sedimentary samples consideration of compositional and source variations are very important because, as the grains will inherit part of their previous thermal histories, if not completely thermally reset. Inherited thermal histories will complicate the distribution of ages if they are only partially reset. In the case of zircon, variation in ages from crystalline Sinai basement and Cambrian sandstones can be likely be explained by alpha dosage (damage) variations, which is controlled by the time a mineral has undergone alpha emission without annealing and the concentration and distribution of radiogenic parent (U-Th-Sm).

7.4 *Fluid Inclusion data*

Three Cambrian sandstone samples were characterized and analyzed for identifying relative temperature variations on fluid inclusions (samples GS-05, GS-07, GS-08). These sedimentary samples were directly overlain the crystalline basement on the Gebel Samra rift shoulder. They were specifically selected due to their high porosity and visible digenetic quartz growth, which increases the probability of finding good-size fluid inclusions, and their proximity to the basement rocks, in the hope of providing a temperature record that can be applied to the basement rocks as well. The reconstructed thermal conditions shed some light not only on maximum and minimum temperatures experienced by the Sinai crystalline basement since the Cambrian, but also support the idea of differential alpha-dosage control on thermal activated He diffusion in zircons from the basement and Naqus/Araba Fm., if multiple temperature events are recorded within or lower than those temperatures belonging to the zircon PRZ (T_c ~140-200).

The first sample analyzed was the *GS-05* and is a well -sorted, well-rounded, quartz-rich sub-lithic arenite. Values were obtained from the dust rim, quartz overgrowth, and digenetic quartz

growths. Temperatures of homogenization (Th) values in the dust rim were consistent along the sample giving a temperature of 152-162°C. Th values in the quartz overgrowth were widely spread ranging from 179 to 245°C. Diagenetic quartz growth Th values in a primary fluid inclusion gave values of ~186°C. Apatite inclusions in diagenetic quartz growth were visible (Appendix 3).

The second sample analyzed was the *GS-07* and is a medium to well-sorted, well-rounded, quartz-rich sub-arkose arenite. Temperature of homogenization (Th) values were obtained from the quartz dust rim and quartz overgrowth. Values from the dust rim were close to 176°C. Single two-phase fluid inclusions in the quartz overgrowth were divided into three groups based on their temperature range. The first fluid inclusion group gave values from 183-185°C. The second group gave values from 209-243°C. The third group gave lower values ranging from 132-138°C.

The third sample analyzed was the *GS-08* and is a poorly-sorted, well-rounded, sub-lithic arenite. Quartz overgrowth ranging from 90 to 350 microns in thickness was common in the majority of detrital quartz grains. Petrographic analysis revealed that quartz overgrowths formed around euhedral dolomite crystal, followed by the diagenetic quartz growth (Appendix 3). Single two-phase fluid inclusions were found in quartz overgrowths but not in the dust rim. The fluid inclusion temperature values obtained in the quartz overgrowth were divided in two groups. The first one show temperatures of homogenization (Th) ranging from 99-110°C; the second group provided Th values ranging from 133-136°C. Measurements obtained in the diagenetic quartz growth show secondary or pseudo-secondary fluid inclusions that range from Th values of 104-110°C and 176-185°C. Primary fluid inclusions showing elongation parallel to growth position gave Th values of 186-182°C. (see Appendix 3 and Table 4 for more information)

8. *Discussion*

8.1 Zircon thermo-tectonic implications

Data from multiple (U-Th)/He sample transects along the Gulf of Suez expose a complex thermal tectonic history, and show variations between AHe and ZHe ages of up to almost 500 m.y.. Low alpha-dosage (U-Th)/He zircon data from exposed basement rocks mainly record the lastest stages of the Pan-African Orogeny at ~520 Ma ages that are slightly younger than previously recorded at ~530-620 Ma by U-Pb or $^{40}Ar/^{39}Ar$ (Hasson and Hedge,1990; Stern and Hedge, 1985; Kohn et al., 1987) (Fig.9). The Naqus/Araba Fm. primarily recorded Pan-African and middle Ordovician thermal events, suggesting that the basement and the overlying Naqus Araba Fm. endure the same thermo-tectonic regime since the Cambrian. Alpha-dosage influence on (U-Th)/He zircon ages also suggests that the basement as well as the Naqus/Araba Fm. were thermally affected by ~~H~~Hercynian" (350-300 Ma) and Neo-Tethyan tectonic events (250-200 Ma) (Fig.9). Temperatures at the contact between basement and Naqus/Araba Fm. were probably oscillating near the partial retention zone of zircon during the early Carboniferous, the late Permian, and the early Jurassic as alpha dosage vs. (U-Th)/He age plot and fluid inclusion data suggest (Figs. 9 and 10). Similar age distribution pattern can be recognized almost equally along multiple fault blocks along the Gulf. These new low-temperature thermochronometric data strongly support the idea that the Sinai basment was strongly affected by multiple Phanerozoic tectonic events and that pre-existing faults likely played an important role on the style and configuration of Cenozoic rifting as suggested previously (e.g., Moustafa, 2002; Bosworth and McClay, 2001; Younes and McClay 2002). Moreover, these data explore and incorporate the kinematic role of Mesozoic tectonism (i.e., Neo-Tethyan rift-related faults and Santonian inverted structures) in the early architecture development of Cenozoic rifting as reset crystalline

basement data from multiple blocks interconnected by hard linkage suggest (i.e., Hamman Faraun block and Gebel Samra).

8.2 Apatite thermo-tectonic implications

The apatite (U-Th)/He data recorded on multiple fault blocks reveal the temporal and thermal variation along the Gulf of Suez during Neogene rifting. Gulf of Suez rift initiation in the central Gebel Samra and southern Gebel Mutga part of the rift flank began at ~23 Ma, as indicated by AHe and ZHe data from vertical transects. The northernmost block, the Hamman Faraun block recorded maximum cooling contemporaneously with maximum subsidence at ~19 Ma (Evan, 1986). Moustafa (2002), classified the east-west trending Hamman Faraun fault and the N-S trending Baba fault (that bound the Hamman Faraun block as part of a zigzag network of interconnected rift-parallel and transfer faults. Considering that these transfer faults are slightly younger than that of rift initiation (Gebel Samra ages), as suggested by AHe data from the Hamman Faraun block, we can infer that hard linkage of normal faults in the Gulf of Suez developed progressively during rift maturation and localization and do not control early rift architecture. The thermal and temporal role of these transfer faults systems along the Gulf as well as soft-linkage are still to be better constrain. The area examined in the central Gulf provided us with a good example of hard-linkage in the oblique connection between the Gebel Samra and the Hamman Faraun blocks by means of the Markha transfer fault. The borehole ERB-B-2X in the Hamman Faraun block show rapid cooling at ~19 Ma, time in which maximum strain was being accommodated along the central Gulf fault system and was coeval with subsidence. This hard-linkage, according to the previous information presented, should had

played an important role on the subsidence patter along the Gulf and thus controlling sediment dispersal during early rifting.

The pre-Miocene sedimentary thickness variation played a fundamental role on the stratigraphic location of the 80°C isotherm across the Gulf of Suez during Early Miocene. Paleodepth and cross section reconstruction, combined with the AHe data place the 80°C isotherm at ~≤2.9 km in the southern part of the Gulf (Gebel Mutga) during the Late Oligocene to Early Miocene. The same isotherm can be identified at ~1.9 km paleodepth in the Hamman Faraun block during the Early Miocene. Calculated geothermal gradients are ~25°C/km in the southern part and a ~37°C/Km in the northern part of the Gulf, which agree with the ≤40°C/km geothermal gradient previously estimated for the region (Kohn and Eyal, 1980). The overburden in the northern part was greater than in the southern part as illustrated in figure 16, where ~ 700m of Paleozoic and Mesozoic sediments are absent in the south and Early Cenozoic formations get thicker towards the northeast. The Hamman Faraun block displays a total pre-rift thickness of 1.9km compared to 1.05km at the Gebel Araba area (Fig.16). The lateral variability of this units and the detrital low-temperature thermal data showing syn-tectonic deposition during Triassic/Jurassic and Santonian (see Chapter 3), suggest that the northern part of the Gulf had experienced a different burial history that the southern part, variations probably controlled by faulting and basin development during the previously mention geologic periods. In light of the above, the burial history was primarily controlled by the Hercynian collision, Neo-Tethys opening and Santonian inversion.

One model has been proposed here to explain the differing gradients. This model invokes

a spatial solution, calling for greater volcanic activity in the northern Gulf of Suez (Bosworth, 1998; Kohn and Eyal, 1980), which comply with the geothermal heterogeneity across the Gulf illustrated by (U-Th)/He data and suggest that the APRZ recorded in the Gebel Mutga and the Gebel Samra block are temporally the same. Meaning that the early stages of rifting were preserved and exposed in Gebel Samra (northern Gulf), where we have a paleo geothermal gradient of 37°C/Km early during rifting. Thermally similar to what we found in the Hamman Faraun fault block (ERB-B-2X borehole) at ~19 Ma were the APRZ was developed during maximum onset of faulting and a greater volcanic activity rose the geothermal gradient to ~37°C/Km (Fig.15a-b). Exhumation in the central rift flank was not enough to expose the ~19Ma fully reset AHe ages and in the Southern part exhumation was not enough to exposed the ~23Ma bottom of the APRZ. Instead it preserve a well behave vertical distribution of ages that allow us to infer the approximate location of the APRZ bottom (~80°C isotherm). Extension in the Gulf started earlier in the rift flank as apatite (U-Th)/He ages recorded in Gebel Mutga and Gebel Samra suggested and the onset of maximum extension spread later to nearby inner blocks like the Hamman Faraun block that quickly cooled during maximum subsidence. According to modeled sample arrays this block was exhumed a maximum of 1.6 km since the Early Miocene. Previous work on basement apatite FT dating along the western margin of the Gulf of Suez by Omar and others (1989) yielded ages ranging from 11 to 385 Ma. The highest frequency of oldest AFT ages was located in the northern parts of the rift shoulder along the western margin. Spatial-AFT age relationships show a considerable scatter between AFT ages and the distance from the rift margin. Furthermore, young AFT ages often occur at a short distance from old AFT ages and there is no correlation with elevation.

Considering the AHe and AFT data and the different overburden along the Gulf it is possible that the rift flank did not exhumed uniformly during Miocene rifting and that heat flux was not one of the main contributors for the massive rift-flank uplift as apatite isotherm data and cross section reconstruction suggest. Mechanical unloading and isostatic compensation are more feasible mechanism for this scenario. Furthermore it is more mechanistically viable that faulting preceded volcanism in the Gulf. This is because there is no evidence of volcanism in certain areas of the gulf that have been highly extended (~50%) e.g. Gebel el Zeit. Moreover the volume of basaltic units is minimum compare to other rift systems, and the orientations of several intrusions appear to be structurally controlled. Additionally low-temperature thermochronology sample arrays show cooling by fault exhumation in the early stages of rifting and no total resetting by hot fluids (e.g., Gebel Mutga and Gebel Samra).

8.3 Hydrocarbon implications

The pre-Cenozoic results combine with the stratigraphic location of the Early Miocene ~80 $^{\circ}$C isotherm have provided a thermal history that is of importance to hydrocarbon maturation and exploration. If we start with the premise that apatite (U-Th)/He closure temperature ranges within the coldest part of the oil window and that the bottom of the zircon partial retention zone falls within the hottest part of it we can derive multiple assumptions on the hydrocarbon maturation history of Gulf of Suez. Thermal condition in the Sinai Peninsula prior to rifting and after the Pan-African orogeny mainly oscillated within the ZPRZ in the crystalline basement and probably at lower temperature above the Naqus/Araba Fm. These temperature conditions were suitable for hydrocarbon maturation in the sedimentary cover homogeneously across the Sinai during the Early Carboniferous and the Triassic/Jurassic period according to zircon (U-Th)/He

data from multiple blocks. Syn-tectonic detrital (U-Th)/He zircon ages during the Santonian explore the possibility of having a higher thermal regime in the northern part of the Sinai where Neo-Tethyan reactivated structures are the dominant feature.

During Early Miocene rifting at the southern part of the Gulf, the 80°C isotherm location was at the basement ~1800 m below the sedimentary cover according to apatite (U-Th)/He data and paleodepth reconstructions, temperature conditions in the sediments were too low for hydrocarbon maturation. Now, conditions at the northern part were more suitable having the 80°C isotherm in the Naqus/Araba Fm. or at a stratigraphically higher level. The overall thermal conditions illustrated here make the northern part of the Gulf a more favorable prospect for hydrocarbon exploration that the southern part.

8.4 Modeled thermochronology data

8.4a Pre-Cenozoic rifting modeling

When modeling (t-T) paths we applied two differently constrained models. The first model constrains thermal conditions during the Pan-African orogeny and present-day (t-T) conditions (Fig.11). For the second model we applied these constraints as well as additional t-T constraints for the Hercynian collision and Neo-Tethys rifting. (Fig.12). The sample array modeled data suggest variable scenarios where rapid cooling occurs during the Cambrian, later during the rest of the Paleozoic and Mesozoic temperatures oscillate between the coldest parts of the zircon PRZ and lower. Exhumation rates calculated with HeMP suggest possible burial during the Hercynian and Neo-Tethys opening if we consider the alpha dosage influenced grains. According to modeled sample arrays the Hamman Faraun block was exhumed a maximum of probably 3-4km

during the late Pan-African Orogeny, and 1km from the rest of the Paleozoic to and the Mesozoic, data that can be apply to the Gebel Samra as well.

8.4b Cenozoic rifting modeling

Neogene Gulf of Suez rifting exhumed the pre-rift sedimentary sequence almost completely along the rift flank, exposing crystalline basement at the central (Gebel Samra) and southern parts (Gebel Mutga) of the Gulf. The most frequent maximum modeled exhumation rate for Gebel Mutga (Southern Gulf of Suez) is ~2.2 km/m.y., a few t-T scenarios may show exhumation rates of almost ~7 km/m.y. in a short period of maximum exhumation (e.g., 23-19 Ma or 19-14 Ma) (Fig.14). The exhumation rates in the Hamman Faraun block range frequently from .3-.1Km/Myr, a few t-T scenarios may show maximum exhumation rates of almost 1.8 km/m.y. (Fig. 11-13). These rates are only true if all the exhumation is balance between various phases of extension and not as a homogeneous exhumation rate for the whole ~23 m.y. of extension. It is well documented that rapid subsidence took place in phases (Evans, 1987; Steckler et al., 1988) as well as uplift and exhumation (Garfunkel, 1988; Kohn and Eyal 1980) in the Gulf.

To provide consistency with the stratigraphic constraints by Evans (1987), the Hamman Faraun, the Gebel Mutga, and the Gebel Samra fault block AHe data, the maximum phases of exhumation should be constrain between ~23-15 Ma in the rift flank and 19-15 Ma in the basin. According to AFT data from Kohn and Eyal (1980) rift flank uplift reaches more than 5 km total. AHe modeled data for the Gebel Mutga suggest almost 2.5 km of vertical motion in the southern part of the Gulf and 1.8 km on the Hamman Faraun block since initiation of rifting at ~23 Ma. Retro-deformed cross sections from the central and southern part of the study area and the AHe

PRZ paleo-depth agree with the previously mention modeled values (Figs. 6 and 8). Almost all the single sample models agree with the t-T evolving conditions over time (Figs. 11-14, and Appendix 4). It is important to mention that the values acquired for exhumation rates are maximum values averaged over time and do not represent the real exhumation rate. More accurate exhumations rates can be derive if we temporally constrain the duration of this fast exhumation phases.

8.5 Fluid Inclusion Data

Temperatures of homogenization (Th) in the dust rim from sample GS-05 and GS-07 were similar, although values from salinity were significantly different, suggesting that these two fluid inclusion group were entrapped at different events. Sample GS-05 gave last crystal melt temperature (Tmice) of -1.7 to -2.4ºC, and GS-07 gave Tmice values of~ -4.2ºC. Petrographic evidence from both samples implies increasing temperature conditions from the dust rim to the quartz overgrowth. The large spread in entrapment temperature conditions suggests that the quartz overgrowth on the different detrital grains did not take place in a single event or simultaneously. More probably the quartz overgrowth occurred episodically. The most frequent Th values measured in the quartz overgrowth ranged from 180 to 190ºC, and higher Th values ranging from 209 to 243ºC were common in samples GS-08 and GS-07. Therefore, according to zircon closure temperature and Th values these Cambrian sediments have undergone temperatures of at least 180ºC at some time between the Late Cambrian to Late Ordovician. Primary fluid inclusions in the secondary quartz growth on samples GS-05 and GS-08 were consistent showing Th values of 182-186ºC suggesting that the secondary quartz growth took place under the same conditions. The secondary quartz growth recorded lower temperatures in

the secondary fluid inclusion assemblages (FIA). Temperature in these inclusions range from 100 to 110ºC and 130 to 140ºC recording temperature conditions probably endure by the basement sometime between the Late Ordovician to recent. Eutectic temperature data from one fluid inclusion in the quartz overgrowth indicate that the composition of the fluid is a NaCl-MgCl2-H20 system. With isochors plots we were able to identify the pressure at which the fluid was trapped. Values for this particular fluid inclusion assuming two geothermal gradients of 50ºC/km (common in extensional settings) and other of 30ºC/km (in thicker crustal settings), yield pressure estimates of 250 and 450 bars, respectively (Appendix 3). Furthermore, pressure values suggest that the fluids were entrapped at 2 – 4 km depth. This different temperature phases yield values above the apatite PRZ but within the zircon PRZ (Fig. 10), certain temporal constrain were added to the fluid inclusion data derived from (U-Th)/He thermochronometers. Since the thermal variation is evident throughout the Gulf history, alpha dosage influence on thermal activated diffusion on zircons is a viable theory according to the thermal history of the Gulf.

Conclusions

(U-Th)/He zircon ages in the Sinai basement record a ~520 Ma old low-temperature history, where the magnitude of thermo-tectonic events seems to decrease in temperature (burial) intensity through time. Four main events appear to be recorded continuously according to zircon alpha dosage variation: Late Pan–African Orogeny, Late Ordovician ?, Hercynian Orogeny, and the Neo-tethyan rifting. The lateral variability of the sedimentary cover and the detrital low-temperature thermal data showing syn-tectonic deposition during Triassic/Jurassic and

Santonian, suggest that the northern part of the Gulf had experienced a different burial history than the southern part, variations probably controlled by faulting and basin development during Triassic/Jurassic Neo-Tethyan rifiting and Santonian and younger inversion tectonics related to Syrian Arc structures. These new (U-Th)/He data explore and incorporate for the first time the kinematic role of Mezosoic tectonism (i.e., Neo-Tethyan and Santonian inverted structures) in the early architecture development of Cenozoic rifting as reset crystalline basement data from multiple blocks interconnected by hard linkage suggest (i.e., Hamman Faraun block and Gebel Samra).

The Gulf of Suez extension was not recorded by (U-Th)/He zircon data or any partially metamict grain indicating temperatures were not higher than~ 100ºC, according to fluid inclusion data and apatite fission track data (Kohn et al 1996, and Feinstein, 1995). Apatite (U-Th)/He ages were reset partially and completely from the Naqus/Araba Fm. to the crystalline basement. Transects collected in the southern part recorded early stages of rifting at 28±4 Ma probably younger according to paleo depth vs apatite He ages distribution. The Gebel Araba transects show partially reset apatite ages.

The northern borehole data (ERB-B-2X) transect display later fast exhumation at 19±3 Ma in the Hamman Faraun block, exhuming ~1.6 km at most. The Gebel Samra block transect in the east recorded fast exhumation at 23±3 Ma exhuming at least ~2.4 km with respect to the Hamman Faraun fault block. The uncertainty of the AHe ages makes the onset of faulting indistinguishable from that in the Hamman Faraun and Gebel Samra transects. The southern transect preserved a well behave APRZ and faulting initiation probably overlap with Gebel Samra. Exhumation rates according to modeled data in HeMP are 0.3-0.1 km/m.y. during rifting

early stages at the Hamman Faraun block (Figs. 11-13) and 2.2-1.2 km/m.y. at the Gebel Mutga (Fig.14) rift flank.

Cross section reconstruction and (U-Th)/He apatite data display two different geothermal gradients ~37ºC/km at the north and ~25ºC/km at the south of the study area. One model has been proposed to explain the different geothermal gradient. This model invokes a spatial solution, calling for greater volcanic activity in the northern Gulf of Suez (Bosworth 1998, Kohn and Eyal 1980), which comply with the geothermal heterogeneity across the Gulf illustrated by (U-Th)/He data and suggest that the APRZ recorded in the Gebel Mutga and the Gebel Samra block are temporally the same. This model can explain the current configuration of preserved paleo partial retention zones. It is highly likely that the rift flank did not homogeneously exhumed during Miocene rifting meaning that the southern part could have exhume faster that the northern part, rapid exhumation should had been limited to the opening of the Gulf of Aqaba. Temperature constraints acquired from apatite isotherm data and cross section reconstruction published here and in other fission track work previously mention suggest that heat flux conduction reducing the footwall density, was not one of the main contributors for the massive rift flank uplift, leaving dynamic support of rift flank topography (Zuber & Parmentier, 1986) mechanical unloading (Weissel & Karner, 1989) and isostatic compensation as the main mechanism for rift uplift in the Gulf of Suez. If we recognize the first model to be true the orientation of the Hamman Faraun transverse structure could have been mechanically facilitated by heat.

Fluid inclusion Th values and petrographic relationships in these Cambrian sediments suggest increasing temperatures condition at the moment of quartz re-growth with a minimum Th of 150 $^{\circ}$C and a maximum of 250 $^{\circ}$C. Later cooling events are recorded on the diagenetic

quartz growth in secondary fluid inclusion assemblages and in a few primary detrital quartz overgrowth inclusions, giving Th values of 100 to 140ºC temperatures which are consistent with modeled (U-Th)/He zircon and apatite data. The fluid inclusion last melt values (Tmice) range from 0-.9 to -4.8ºC and the most frequent values were -1.5 to -2.5ºC. Eutectic temperature values on a primary fluid inclusion imply that the composition of the fluid is a NaCl-$MgCl_2$-H_20. This different temperature phases yield values above the apatite PRZ but within the zircon PRZ (Fig. 10). Since the thermal variation is evident throughout the Gulf history, alpha dosage influence on thermal activated diffusion on zircons is a viable theory according to the thermal history of the Gulf.

Rapid cooling and infer faulting in the central Gulf of Suez started at 23± 3 Ma ago as constrain by Gebel Samra apatite He data. Hamman Faraun block shows cooling ages at 19±3 Ma, which suggest that transfer faulting initiation match maximum subsidence in the Gulf. Transfer faults are slightly younger that the rift initiation as AHe data suggest from the Hamman Faraun, Gebel Mutga and Gebel Samra blocks, according to this we can infer that hard linkage of normal faults developed progressively during rift maturation and localization and do not control early rift architecture. The role of Pan-African, Neo-Tethian and reactivated Santonian structures was highly important for the development of early rift architecture as zircon He data helped to confirm temporally and spatially. Calculated paleo-geothermal gradients are ~25ºC/km in the southern part and a ~37ºC/km in the northern part of the Gulf. These data suggest that geothermal gradient was mainly influenced by volcanism and not by extensional thinning of the crust. Furthermore hydrocarbon maturation may have developed greatly at the central part than in the south. Temporal faulting constrain suggest a higher probability of structural traps forming along the bounding faults of the Hamman Faraun block.

References

Angelier, J., 1985, Extension and rifting: the Zeit region, Gulf of Suez, J. Struct. Geol. 7, p. 605–612.

Barker, E. C., and Reynolds, J. T., 1984, Preparing doubly polished sections of temperature sensitive sedimentary rocks. Journal of Sedimentary Petrology, Vol. 54, n. 2, p. 635-636.

Bosworth, W., 1994, A model for the three-dimensional evolution of continental rift basins, north-east Africa. Geologisch Rundschau, v. 83, p. 671-688.

Bosworth, W., 1995, A high-strain rift model for the southern Gulf of Suez (Egypt): in Lambiase, J. J., ed., Hydrocarbon Habitat in Rift Basins, Geological Society, London, Special Publication, 80, p. 75-112.

Bosworth, W., Crevello, P., Winn, Jr., R.D., and Steinmetz, J., 1998, Structure, sedimentation, and basin dynamics during rifting of the Gulf of Suez and northwestern Red Sea: in Purser, B.H., and Bosence, D.W.J., eds., Sedimentation and Tectonics of Rift Basins: Red Sea–Gulf of Aden, Chapman and Hall, London, p. 77-96.

Bosworth, W., and McClay, K., 2001, Structural and stratigraphic evolution of the Gulf of Suez rift, Egypt: A synthesis: in P.A. Ziegler, W. Cavazza, A.H.F. Robertson, and S. Crasquin-Soleau, eds., Peri-Tethys Memoir 6: Peri-Tethyan Rift/Wrench Basins and Passive Margins, Mémoires du Muséum National d'Histoire Naturelle de Paris, n. 186, p. 567-606.

Bosworth, W., and Taviani, M., 1996, Late Quaternary reorientation of stress field and extension direction in the southern Gulf of Suez, Egypt: Evidence from uplifted coral terraces, mesoscopic fault arrays, and borehole breakouts, Tectonics 15**,** p. 791–802.

Bosworth, W., Huchon, P., and McClay, K., 2005, The Red Sea and Gulf of Aden basins, J. Afr. Earth Sci. 43, p. 334 –378.

Cochran, J. R., 1983, A model for the development of Red Sea: AAPG Bulletin, v. 67, p. 41-69.

Coleman, R.G., Hadley, D.G., Fleck, R.G., Hedge, C.E., and Donato, M.M., 1979, The Miocene Tihama Asir ophiolite and its bearing on the opening of the Red Sea, Institute of Applied Geology Bulletin, Jeddah 3, p. 173–187.

Coleman, R.G., 1993, Geologic evolution of the Red Sea, Oxford Monographs on Geology and Geophysics vol. 24**,** Oxford University Press, Oxford, p. 186 .

Colletta, B., Le Quellec, P., Letouzey, J. and Morreti, I., 1988, Longitudinal evolution of the Suez rift structure (Egypt). Tectonophysics, 153, p. 221-233

Dodson, M.H., 1973, Closure temperature in cooling geochronological and petrological systems, Contributions to Mineralogy and Petrology, v. 40, p. 259- 274.

Ehlers, T.A., and Farley, K.A., 2003, Apatite (U-Th)/He thermochronometry: methods and applications to problems in tectonics and surface processes. Earth Planet Sci Lett 206:1-14

Evans, A.L., 1990, Miocene Sandstone Provenance Relations in the Gulf of Suez: Insights into synrift Unroofing and Uplift History, American Association of Petroleum Geologists Bulletin, 74, 1386-1400.

Evan, A.L., 1988, Neogene tectonic and stratigraphic events in the Gulf of Suez rift area, Egypt, Tectonophysics 153 , p. 235–247.

Farley, K.A., 2000, Helium diffusion from apatite: General behavior as illustrated by Durango fluorapatite, Journal of Geophysical Research, v. 105, p. 2903-2914.

Farley, K.A., 2002, (U-Th)/He dating: Techniques, calibrations, and applications in: Noble Gases in Geochemistry and Cosmochemistry, Reviews in Mineralogy and Geochemistry, v. 47, p. 819-844.

Farley, K.A., Reiners, P.W., and Nenow, V., 1999, An apparatus for high-precision helium diffusion measurements from minerals. Analytical Chemistry, v. 71, p. 2059-2061.

Farley, K.A., Wolf, R., and Silver, L., 1996, The effects of long alpha-stopping distances on (U-Th)/He ages, Geochimica et Cosmochimica Acta, v. 60, p. 4223-4229.

Feinstein, S., Kohn, B.P., Steckler, M.S., and Eyal, M., 1996, Thermal history of the eastern margin of the Gulf of Suez, 1. Reconstruction from borehole temperature and organic maturity measurements, Tectonophysics 266 (1996), p. 203–220.

Joffe S., and Garfunkel, Z., 1987, Plate kinematics of the circum Red Sea — a re-evaluation, Tectonophysics 141**,** p. 5–22

Garfunkel, Z., and Bartov, Y., 1977, The tectonics of the Suez rift: Geological Survey of Israel Bulletin, v. 71, p. 44.

Gawthorpe, R.L., Sharp, I., Underhill, J.R., and Gupta, S., 1997, Linked sequence stratigraphic and structural evolution of propagating normal faults. Geology, 25, p. 795-798.

Genna, A., Nehlig, P., Le Goff, E., Guerrot C., and Shanti, M., 2002, Proterozoic tectonism of the Arabian Shield, *Precambrian Research* 117 p. 21–40.

Gass, I. G. and Gibson, I. L., 1969, The structural evolution of the rift zones in the Middle East. Nature, Lond. 221, p. 926-930.

Goldstein, R. H., and Reynols, J. T., 1994, Systematics of fluid inclusions in diagenetic minerals. SEPM short course 31, p. 15.

Hassan, M.A. and Hashad, A.H., 1990, The Geology of Egypt, Precambrian of Egypt. Balkema, Rotterdam: In: R.Said (ed.), Chapter 12, p. 201-245.

Jarrige, J., Ott d'Estevou, P., Burollet, P. F., Montenat, C., Prat, P., Richert, J.-P., and Thiriet J.-P., 1990, The multistage tectonic evolution of the Gulf of Suez and northern Red Sea continental rift from field observations, Tectonics, 9(3), p. 441–465

Kohn, B.P. and Eyal, M., 1981, ‗History of uplift of the crystalline basement of Sinai and its relation to opening of the Red Sea as revealed by fission track dating of apatites' Earth and Planetary Science Letters, 52, p. 129–141.

Kohn, B.P., Feinstein, S., Foster, D.A., Steckler, M.S., and Eyal, M., 1996, Thermal history of the eastern Gulf of Suez, II. Reconstruction from apatite fission track and 40Ar/39Ar K-feldspar measurements.Tectonophysics. 283, p. 219-239.

McClay, K., and Khalil, S., 1998, Extensional hard linkages, eastern Gulf of Suez, Egypt, Geology 26 (1998), p. 563–566.

McClay, K.R., Nicols, G.J., Khalil, S.M., Darwish, M., and Bosworth, W., 1998, Extensional tectonics and sedimentation, eastern Gulf of Suez, Egypt: in Purser, B.H., and Bosence, D.W.J., eds., Sedimentation and Tectonics of Rift Basins: Red Sea–Gulf of Aden, Chapman and Hall, London, p. 223-238.

McKenzie, D.P., Davies, D., and Molnar, P.,1970, Plate tectonics of the Red Sea and east Africa, Nature 226, p. 243–248.

Moretti, I. and Colletta, B., 1987, Spatial and temporal evolution of the Suez Rift subsidence. Journal of Geodynamics, 7, p. 151-168.

Nasdala, L., Hanchar, J.M., Kronz, A., and Whitehouse, M.J., 2005, Long-term stability of alpha particle damage in natural zircon. Chemical Geology v. 220, p. 83–103.

Nasdala, L., Wenzel, M., Vavra, G., Irmer, G., Wenzel, T., and Kober, B., 2001, Metamictisation of natural zircon: accumulation versus thermal annealing of radioactivity-induced damage. Contribution to Mineralogy Petrology v. 141, p.125–144.

Omar G.I., and Steckler M.S., 1995, Fission-track evidence on the initial rifting of the Red Sea: two pulses, no propagation. Science 270, p.1341–44

Omar, G.I., Steckler, M.S., Buck, W.R., and Kohn, B.P., 1989, Fission-track analysis of basement apatites at the western margin of the Gulf of Suez rift, Egypt: evidence for synchroneity of uplift and subsidence. Earth and Planetary Science Letters, 94, p. 316-328.

Patton, T.L., Moustafa, A.R., Nelson, R.A., and Abdine, S. A., 1994, Tectonic evolution and structural setting of the Suez Rift, in Landon, S. M., ed., Interior rift basins: American Association of Petroleum Geologists Memoir 59, p. 9–55.

Sharp, I.R., Gawthorpe, R.L., Underhill, J.R., and Gupta, S., 2000, Fault-propagation folding in extensional settings: Examples of structural style and syn-rift sedimentary response from the Gulf of Suez Rift, Sinai, Egypt. Geological Society of America Bulletin, 112, p. 1877-1899.

Shuster, D.L., and Farley, K.A., 2005, 4He/3He thermochronology: theory, practice, and potential complications. Review in Mineralogy and Geochemistry. v 58, p. 181-203.

Shuster, D.L., Farley, K.A., Sisterson, J.M., and Burnett, D.S., 2004, Quantifying the diffusion kinetics and spatial distributions of radiogenic 4He in minerals containing proton-induced 3He. Earth Planet Sci Lett 217, p. 19-32

Steckler, M.S., Berthelot F., Lyberis N. and Le Pichon X., 1988, Subsidence in the Gulf of Suez: Implications for rifting and plate kinematics. Tectonophysics, 153, p. 249-270.

Steckler, M.S. and U.S. ten Brink, 1986, Lithospheric strength variations as a control on new plate boundaries: Examples from the northern Red Sea region. Earth and Planetary Science Letters, 79, p. 120-132.

Stockli, D., 2005, Application of low-temperature thermochronometry to extensional tectonic settings. Review in Mineralogy and Geochemistry. v 58, p. 411-448. in Reiners, P.W., and Ehlers, T.A., Low Temperature Thermochronology: Techniques, Interpretations and Applications, Reviews in Mineralogy and Geochemistry, v. 58, p. 123-149.

Stockli, D.F., Farley, K.A. and Dumitru, T.A., 2000, Calibration of the (U-Th)/He thermochronometer on an exhumed normal fault block in the White Mountains, eastern California and western Nevada. Geology, v. 28, n. 11, p. 983–986.

Stosser, D. B., and V. E. Camp, 1985, Pan-African microplate accretion of the Arabian shield: Geological Society of America Bulletin, v. 96, p. 817-826.

Stern, R., and C. Hedge, 1985, Geochronological and isotopic constraint on the late Precambrian crustal evolution in the Eastern Desert of Egypt: American Journal of Science, v. 258, p. 97-127.

Reiners, P., 2005, Zircon (U-Th)/He Thermochronometry, in Reiners, P. W. and Elhers, T. A., Low Temperature Thermochronology: Techniques Interpretations and Applications, Reviews in Mineralogy and Geochemistry, v.58, p. 151-179.

Reiners, P., and Farley, K., 1999, He diffusion and (U-Th)/He thermochronometry of titanite, Geochimica et Cosmochimica Acta, v. 62, p. 3845-3859

Reiners, P.W., Farley K.A., 2001, Influence of crystal size on apatite (U-Th)/He thermochronology: an example from the Bighorn Mountains, Wyoming. Earth Planet Sci Lett 188, p. 413-420

Reiners, P., Farley, K., and Hickes, H., 2002**,** He diffusion and (U–Th)/He thermochronometry of zircon: initial results from Fish Canyon Tuff and Gold Butte. Tectonophysics, v. 349, p. 297-308.

Reiners, P., Spell, T., Nicolescu, S., Zanetti, K., 2004, Zircon (U-Th)/He thermochronometry: He diffusion and comparisons with Ar-40/Ar-39 dating. Geochimica Et Cosmochimica Acta v. 68, Ph, p. 1857-1887

Richardson, M., and Arthur, M.A., 1988. The Gulf of Suez - northern Red Sea Neogene rift: A quantitative basin analysis. Marine and Petroleum Geology, p. 247-270.

Tamsett, D., 1984, Comments on the development of rifts and transform faults during continental breakup; examples from the Gulf of Aden and northern Red Sea. Tectonophysics, 104, p. 35-46.

Vermeesch, P., 2008, Three new ways to calculate average (U-Th)/He ages. Chemical Geology 249, p. 339-347.

Vermeesch, P., 2010, HelioPlot, and the treatment of overdispersed (U-Th-Sm)/He data. Chemical Geology 271, p. 108-111.

Younes, A.I., and McClay, K.R., 2002, Development of accommodation zones in the Gulf of Suez-Red Sea Rift, Egypt. In: Underhill, J. R., and Trudgill, B. D., (eds.), The structure and stratigraphy of rift systems. AAPG Bulletin, 86, p. 1003-1026.

Zeitler, P.K., Herczeg, A.L., McDougall, I., and Honda, M., 1987, U-Th-He dating of apatite: A potential thermochronometer. Geochimica et Cosmochimica Acta, v. 51, p. 2865-2868.

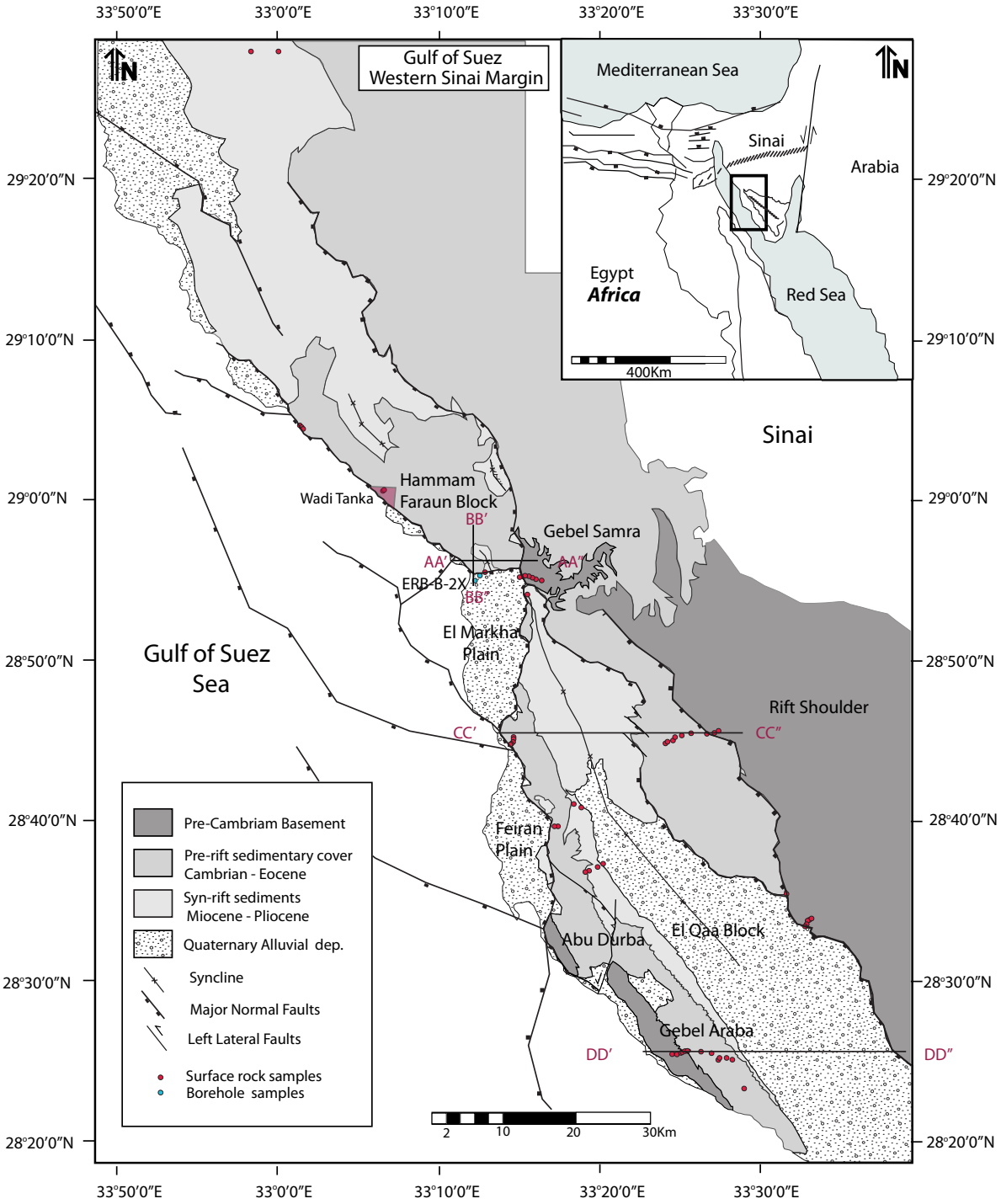
Gulf of Suez
Western Sinai Margin
Mediterranean Sea
Sinai
Arabia
Egypt
Africa
Red Sea
400Km
Sinai
Hammam
Faraun Block
Wadi Tanka
BB′
Gebel Samra
AA′
AA″
ERB-B-2X
BB″
El Markha
Plain
Gulf of Suez
Sea
Rift Shoulder
CC′
CC″
Feiran
Plain
Abu Durba
El Qaa Block
Gebel Araba
DD′
DD″
Pre-Cambriam Basement
Pre-rift sedimentary cover
Cambrian - Eocene
Syn-rift sediments
Miocene - Pliocene
Quaternary Alluvial dep.
Syncline
Major Normal Faults
Left Lateral Faults
Surface rock samples
Borehole samples
2
10
20
30Km
33°50′0″E
33°0′0″E
33°10′0″E
33°20′0″E
33°30′0″E
29°20′0″N
29°10′0″N
29°0′0″N
28°50′0″N
28°40′0″N
28°30′0″N
28°20′0″N

Figure 1. Generalized eastern Gulf of Suez geologic map showing distribution of major faults, the granitoid basement and pre- and syn-rift sedimentary sequences. Red dots are the samples collected strategically along different fault blocks. Four cross section lines (AA'-AA" to DD'-DD") were made from central to southern Gulf. (see figure 2a-d)

Cross Sections, Western Sinai

1 : 1

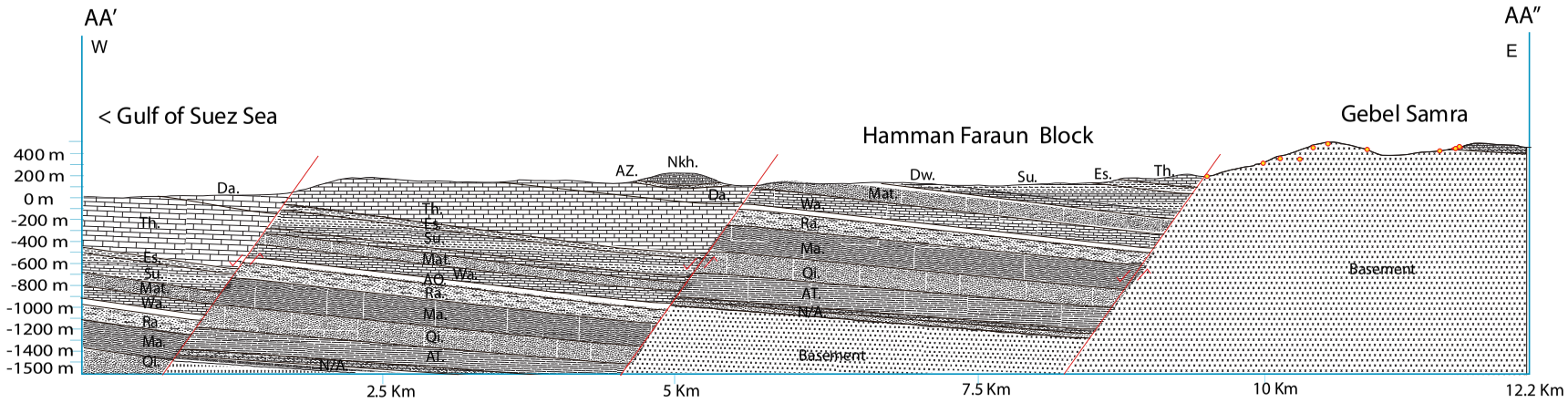

Legend

Nukhul	Nkh.		Wata	Wa.	
Abu Zenima	AZ.		Abu Qada	AQ.	
Darat	Da.		Raha	Ra.	
Thebes	Th.		Malha	Ma.	
Esna	Es.		Qiseib	Qi.	
Sudr	Su.		Abu Thora	AT.	
Duwi	Dw.		Naqus/Araba	N/A.	
Matulla	Mat.				

Cross Sections, Western Sinai

1 : 1

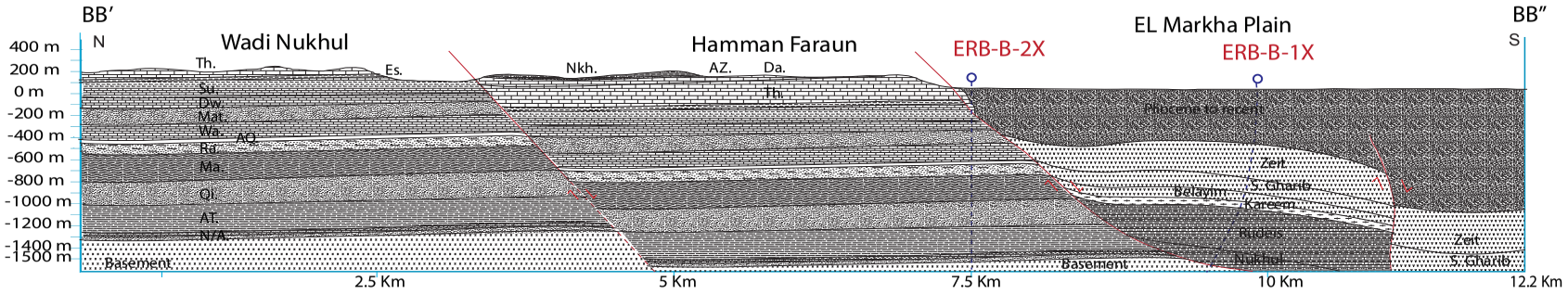

Legend

Nukhul	Nkh.		Wata	Wa.	
Abu Zenima	AZ.		Abu Qada	AQ.	
Darat	Da.		Raha	Ra.	
Thebes	Th.		Malha	Ma.	
Esna	Es.		Qiseib	Qi.	
Sudr	Su.		Abu Thora	AT.	
Duwi	Dw.		Naqus/Araba	N/A.	
Matulla	Mat.				

b

Cross Sections, Western Sinai

1 : 1

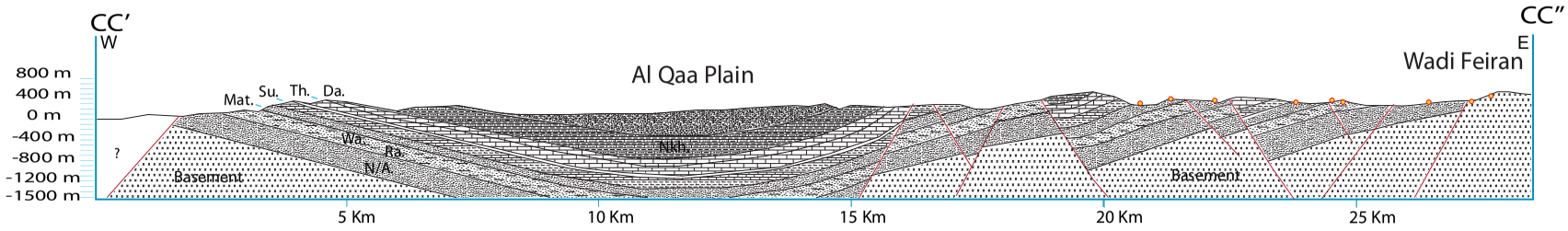

Legend

Nukhul	Nkh.		Wata	Wa.	
Abu Zenima	AZ.		Abu Qada	AQ.	
Darat	Da.		Raha	Ra.	
Thebes	Th.		Malha	Ma.	
Esna	Es.		Qiseib	Qi.	
Sudr	Su.		Abu Thora	AT.	
Duwi	Dw.		Naqus/Araba	N/A.	
Matulla	Mat.				

Cross Sections, Western Sinai

1 : 1

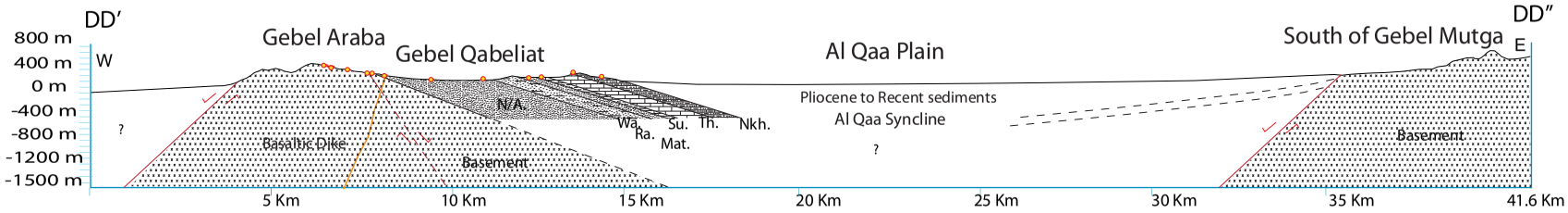

Legend

Nukhul	Nkh.		Wata	Wa.	
Abu Zenima	AZ.		Abu Qada	AQ.	
Darat	Da.		Raha	Ra.	
Thebes	Th.		Malha	Ma.	
Esna	Es.		Qiseib	Qi.	
Sudr	Su.		Abu Thora	AT.	
Duwi	Dw.		Naqus/Araba	N/A.	
Matulla	Mat.				

Figure 2a-d. Cross sections show the current eastern margin structural configuration from central to southern Gulf of Suez. The vertical transects are illustrated in three of the sections a,c-d., additionally the boreholes ERB-B-2X and 1X are illustrated in cross section b.

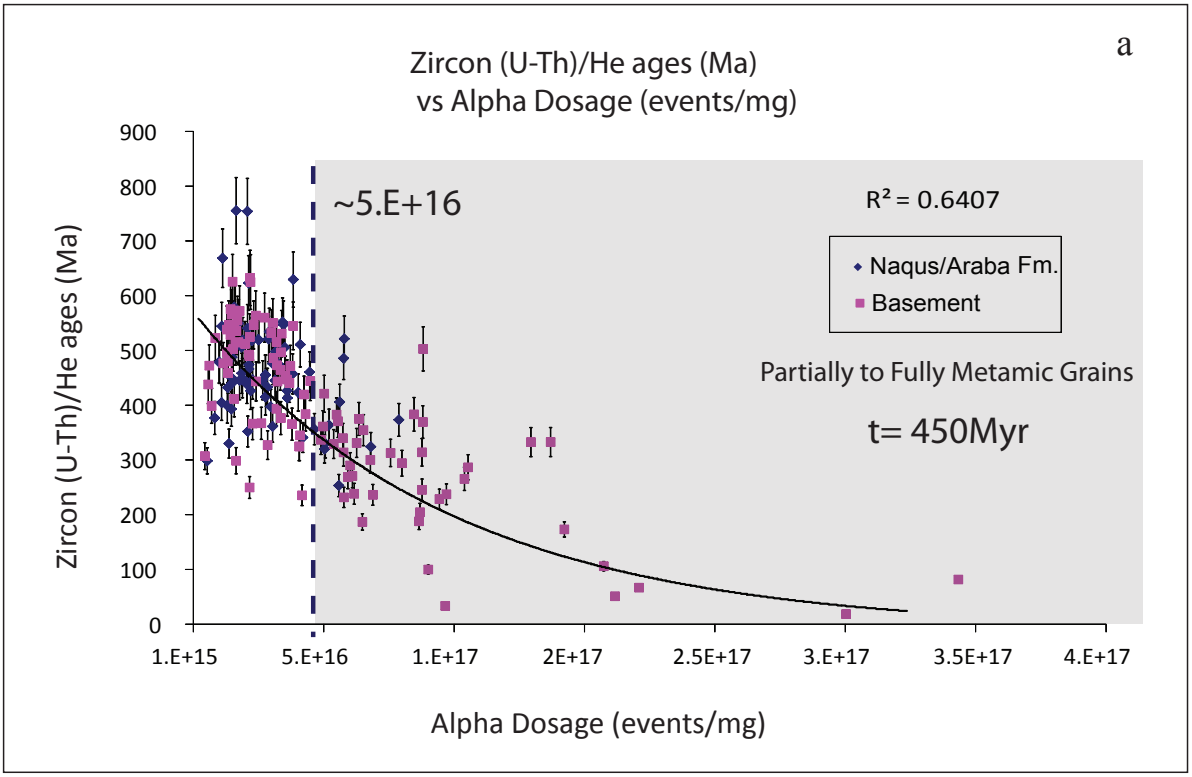
a
Zircon (U-Th)/He ages (Ma)
vs Alpha Dosage (events/mg)
Zircon (U-Th)/He ages (Ma)
900
800
700
600
500
400
300
200
100
0
~5.E+16
R² = 0.6407
Naqus/Araba Fm.
Basement
Partially to Fully Metamic Grains
t= 450Myr
1.E+15
5.E+16
1.E+17
2E+17
2.5E+17
3.E+17
3.5E+17
4.E+17
Alpha Dosage (events/mg)

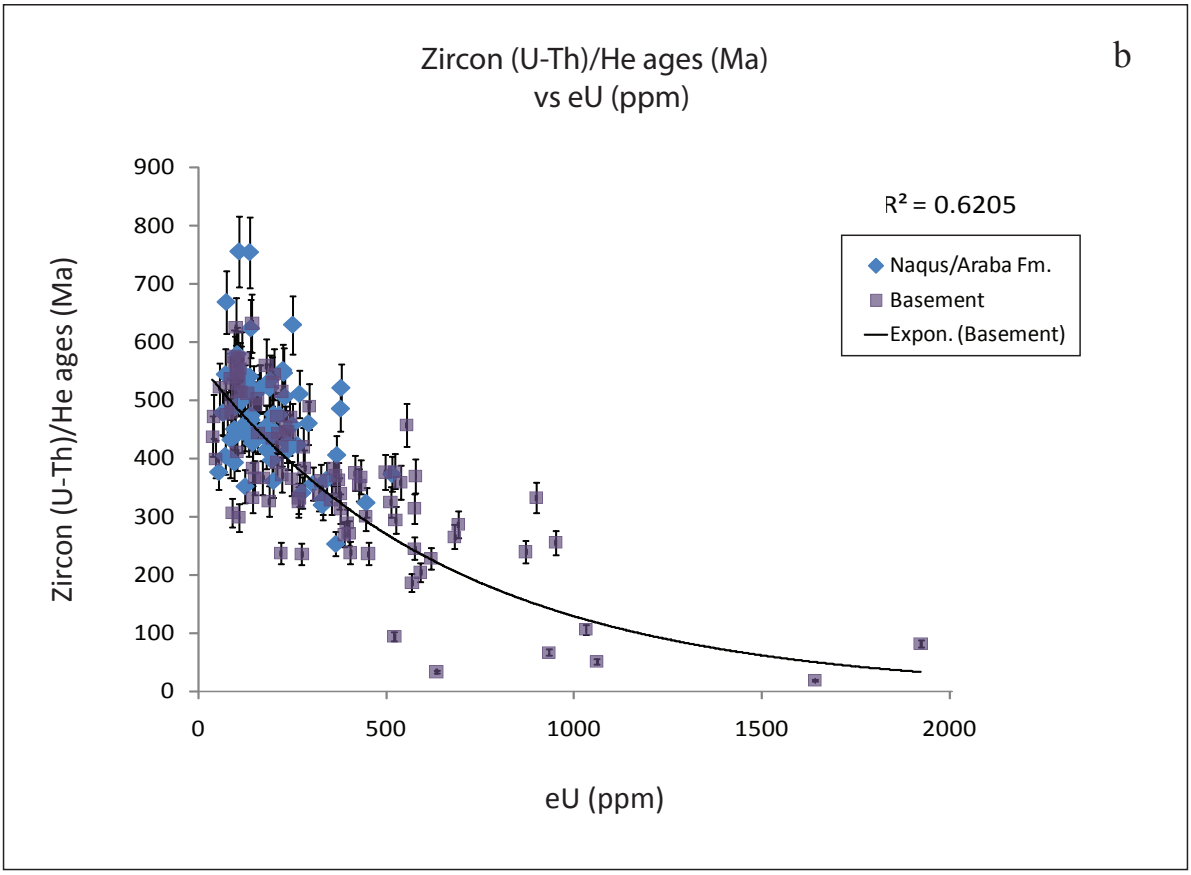
b
Zircon (U-Th)/He ages (Ma)
vs eU (ppm)
Zircon (U-Th)/He ages (Ma)
900
800
700
600
500
400
300
200
100
0
R² = 0.6205
Naqus/Araba Fm.
Basement
Expon. (Basement)
0
500
1000
1500
2000
eU (ppm)

Figure 3. Zircon (U-Th)/He ages (Ma) vs (Alpha Dosage (events/mg) (a) and eU (ppm) (b)) plots from samples in the crystalline basement (purple box) and Naqus/Araba Fm (blue box). 450 Ma represent conceivable time for full zircon annealing according to the presented thermal history of the gulf. Notice dependency of zircon (U-Th)/He ages to alpha dosage. An arbitrary line denotes at what amount of alpha dosage the grains start to disrupt the normal diffusion kinetics affecting their sensitivity. Data that was later filtered (see figure 11).

Single Grain (U-Th)/He Apatite Aliquots
Elevation (m) vs Age (Ma)

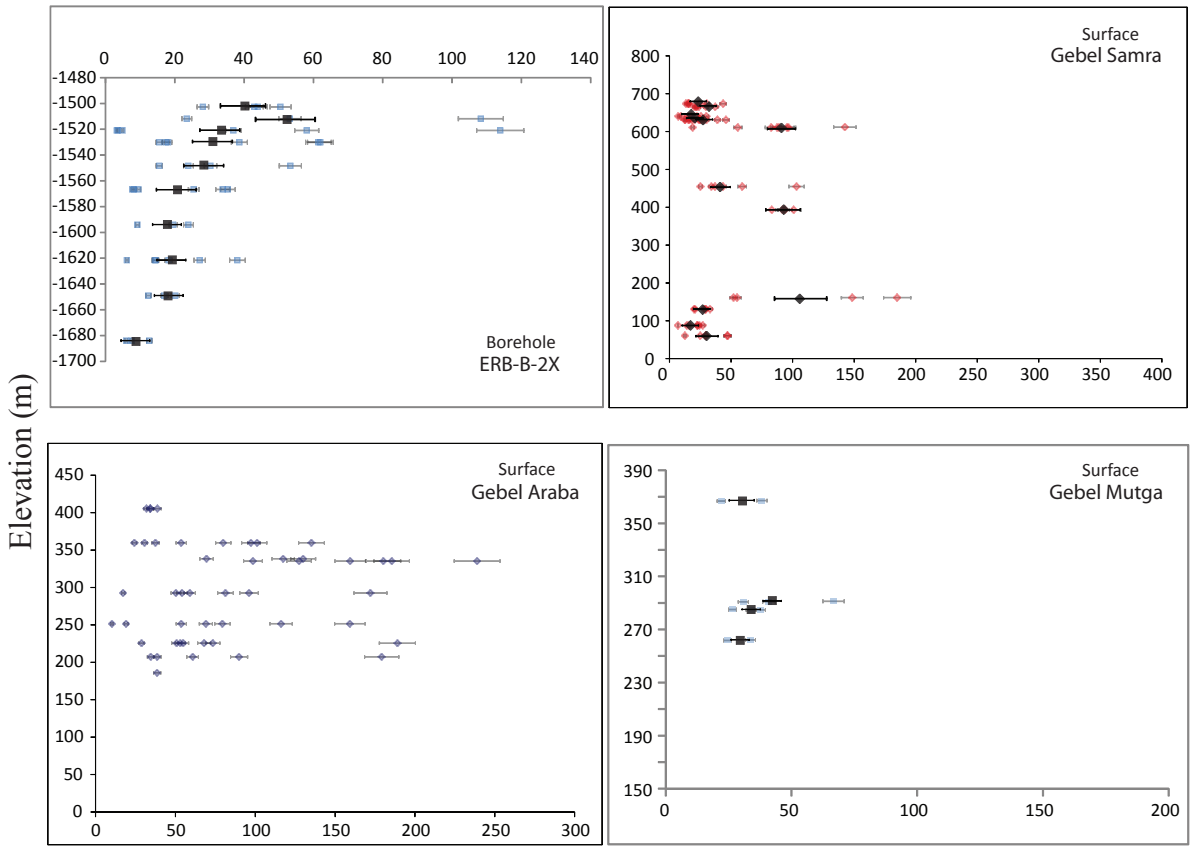

Figure 4a. Plots of elevation (m) vs Apatite (U-Th)/He ages (Ma), for all the apatite aliquots analyzed from ERB-B-2X (blue square),Gebel Samra (red diamonds), Gebel Araba (dark blue diamonds) and Gebel Mutga (light blue boxes). Data do not show aliquots that were discarded according to their high Helium extractions (inclusions), high effective Uranium concentration, small equivalent surface radius (esr) and low Uranium ICP-MS counts (analytical errors). (see (U-Th)/He apatite data tables for more details)

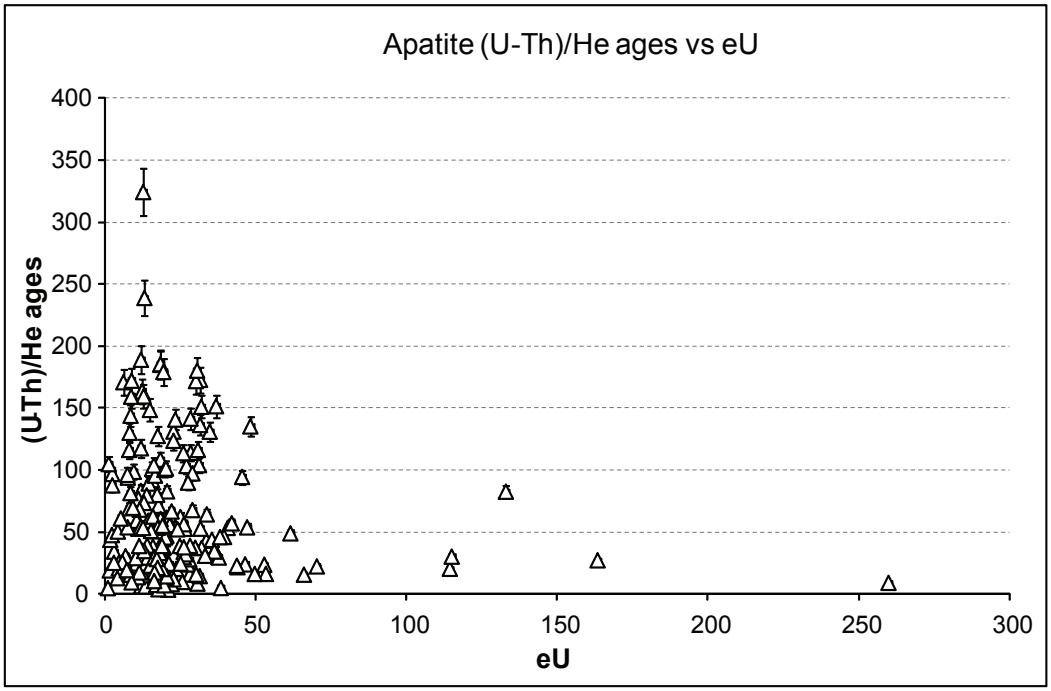
Apatite (U-Th)/He ages vs eU
(UTh)/He ages
400
350
300
250
200
150
100
50
0
0
50
100
150
200
250
300
eU

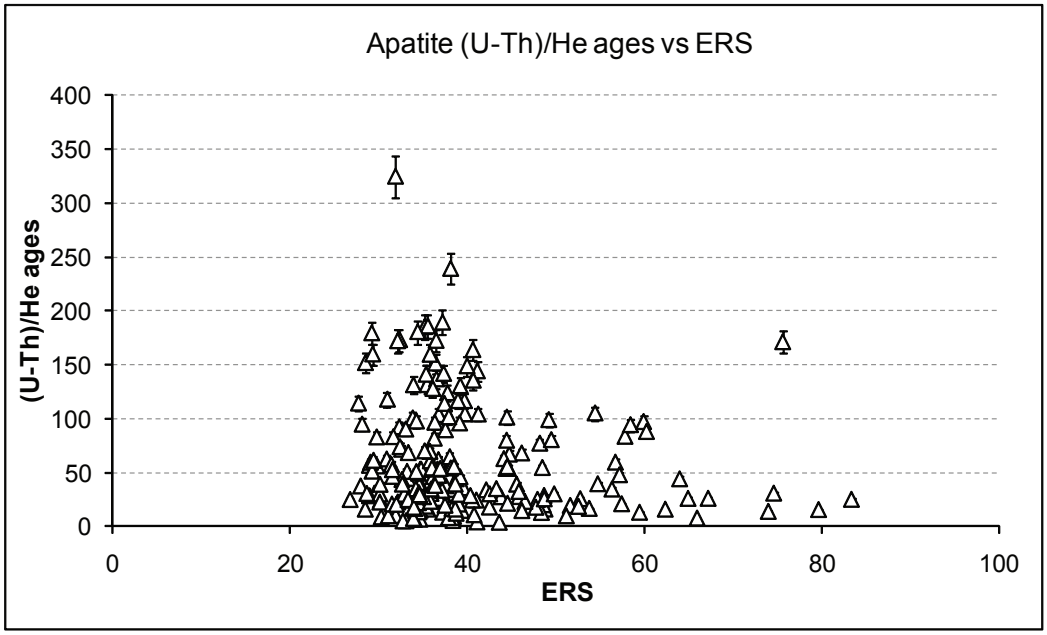
Apatite (U-Th)/He ages vs ERS
(U-Th)/He ages
400
350
300
250
200
150
100
50
0
0
20
40
60
80
100
ERS

Figure 4b. Plots of Apatite (U-Th)/He ages (Ma) vs (eU (ppm) and ERS) , these plots show all the apatite aliquots analyzed non of them display a relationship between each other and therefore they were not filtered out. These plots did not provided a solution for some of the aliquots dispersal.

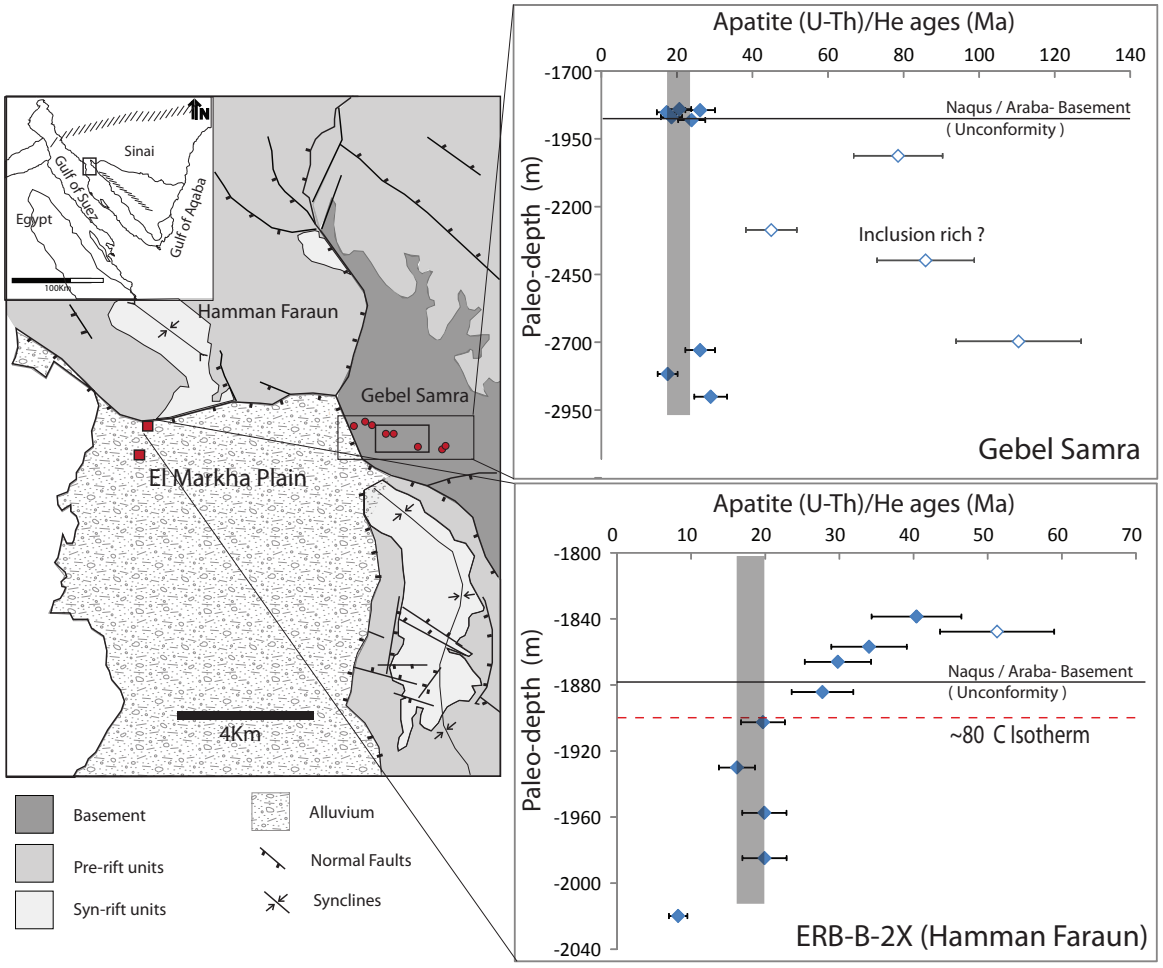
Sinai
Egypt
Gulf of Suez
Gulf of Aqaba
100Km
Hamman Faraun
Gebel Samra
El Markha Plain
4Km
Basement
Pre-rift units
Syn-rift units
Alluvium
Normal Faults
Synclines
Apatite (U-Th)/He ages (Ma)
Paleo-depth (m)
Naqus / Araba- Basement
(Unconformity)
Inclusion rich ?
Gebel Samra
~80 C Isotherm
ERB-B-2X (Hamman Faraun)

Figure 5. Simplified geologic map illustrates the current structural configuration of the El Markha Plain area and the spatial distribution of the basement and the pre- and syn-rift units. Sample location are shown in dots and squares. Right shows the paleo-depth (m) against apatite (U-Th)/He (Ma) plots for the Gebel Samra and the Hamman Faraun fault blocks.

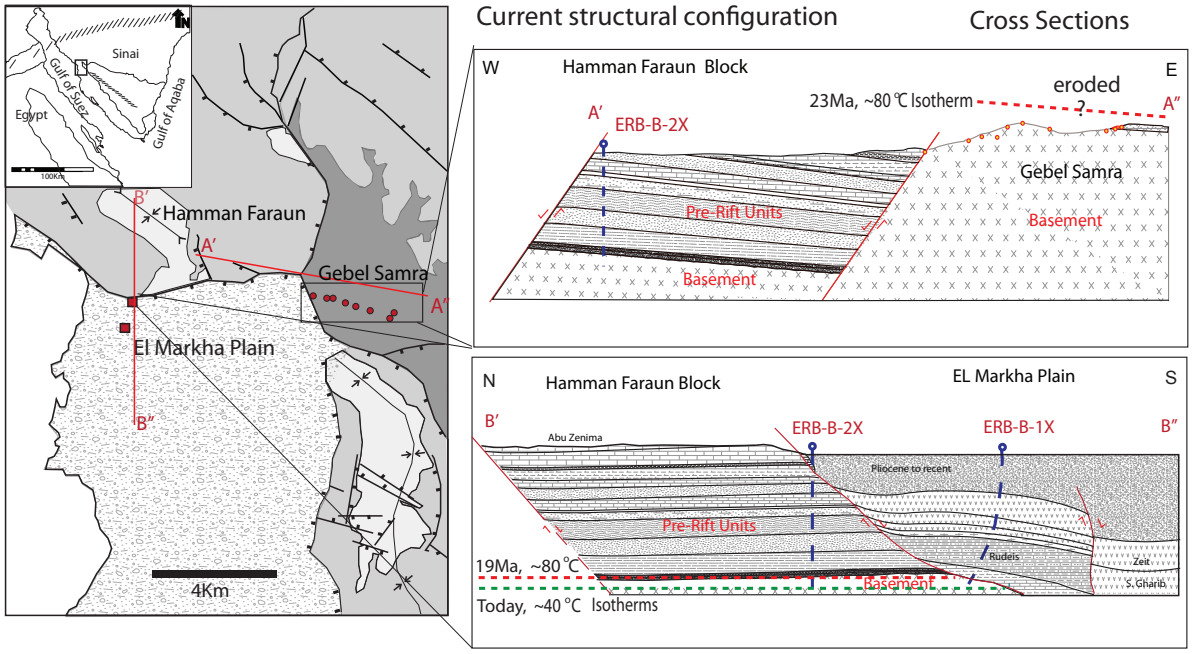

Miocene structural and thermal configuration (retro-deformed illustration)

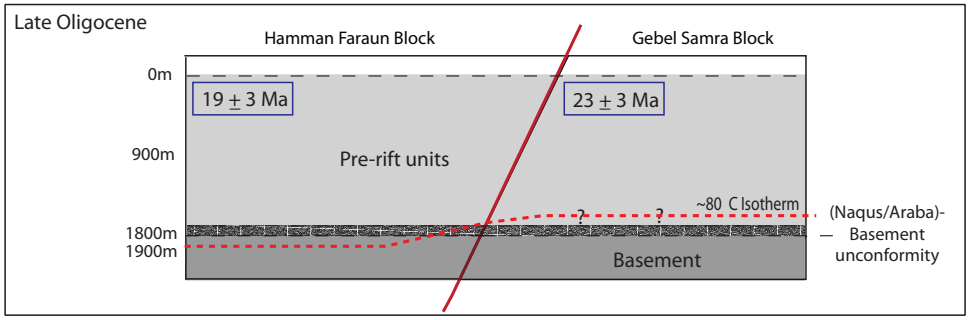

Figure 6. Map illustrates in the left corner the current structural configuration of the El Markha Plain area and the spatial distribution of the basement and the pre- and syn-rift units. Additionally it shows in two cross sections and top view the sample location and their structural relationship.Notice that the bottom of the apatite partial retention zone (APRZ dashed red line) in the ERB-B-2X borehole is at ~1900(m) during the Early-Miocene (paleo-depth) and today's top of the APRZ can be inferred from the last aliquot age values ~2020(m). The bottom of the APRZ cannot be identified in the Gebel Samra plot and therefore we infer it should be somewhere above the Naqus/Araba Fm. At the lower section of this sketch there is a retro cross-section block showing the mean apatite age of maximum exhumation and the temperature conditions pre-extension. The Naqus/Araba unit was represented as two black dashed lines with a gray fill. The red dotted line illustrates the location of the bottom APRZ or 80^{o}C isotherm. Question marks represent uncertainty.

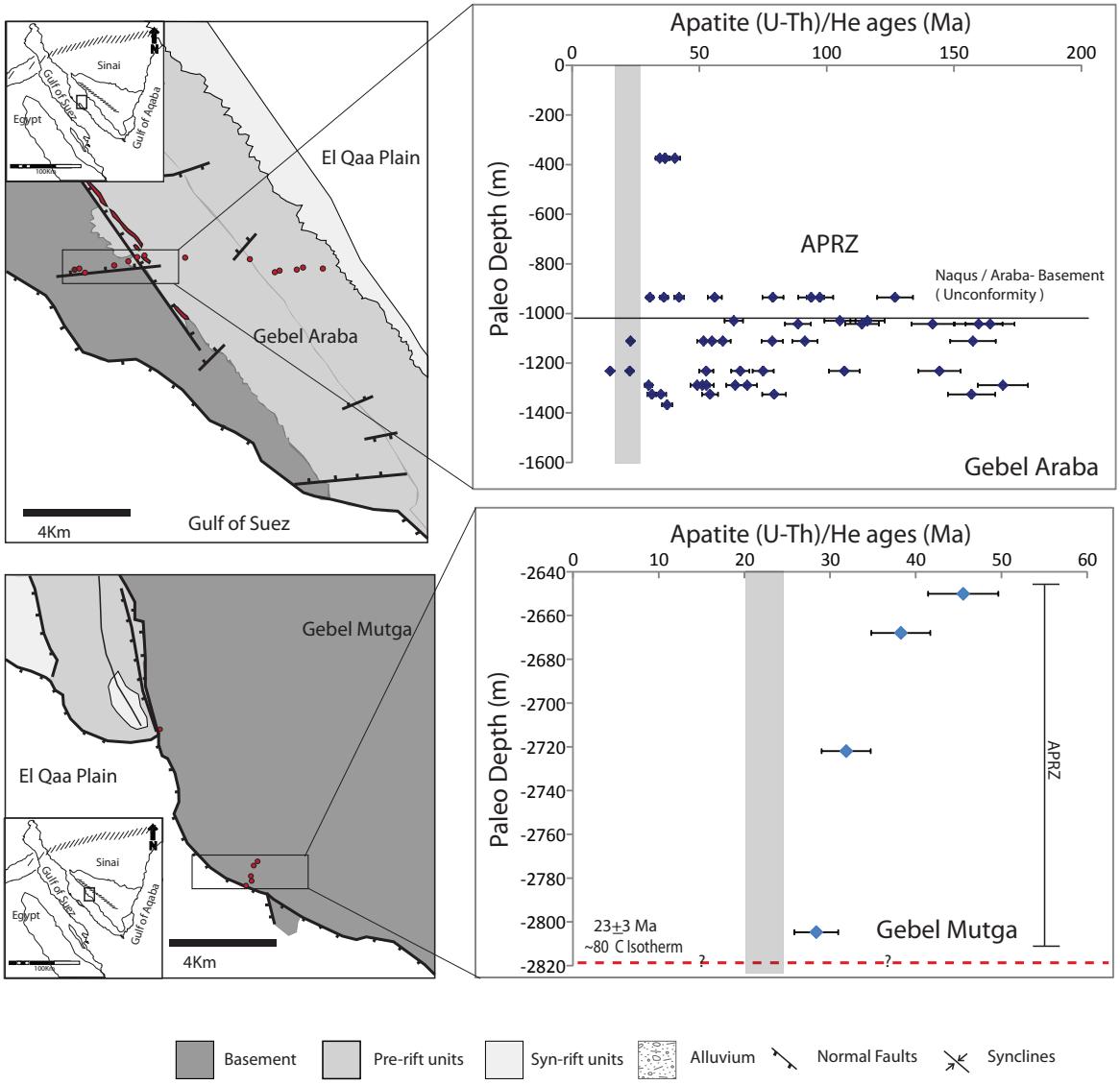
Sinai
Egypt
Gulf of Suez
Gulf of Aqaba
El Qaa Plain
Gebel Araba
4Km
Gulf of Suez
Apatite (U-Th)/He ages (Ma)
Paleo Depth (m)
APRZ
Naqus / Araba- Basement
(Unconformity)
Gebel Araba
Gebel Mutga
El Qaa Plain
23±3 Ma
~80 C Isotherm
Gebel Mutga
Basement
Pre-rift units
Syn-rift units
Alluvium
Normal Faults
Synclines

Figure 7. Map illustrates the current structural configuration of the southern part of the study area and the spatial distribution of the basement and the pre- and syn-rift units within specifically the Gebel Araba and Mutga areas. Additionally it illustrates the sample location and their top view structural relationship. In the left it is shown the paleo-depth (m) against apatite (U-Th)/He (Ma) plots for two fault blocks separated by El Qaa plain, Gebel Araba and the Gebel Mutga blocks. Notice that the bottom of the apatite partial retention zone can be approximated (APRZ) in the Gebel Mutga plot at ~2900(m) paleo-depth or deeper. The Gebel Araba transect show low reproducibility and therefore no interpretations were made out of it.

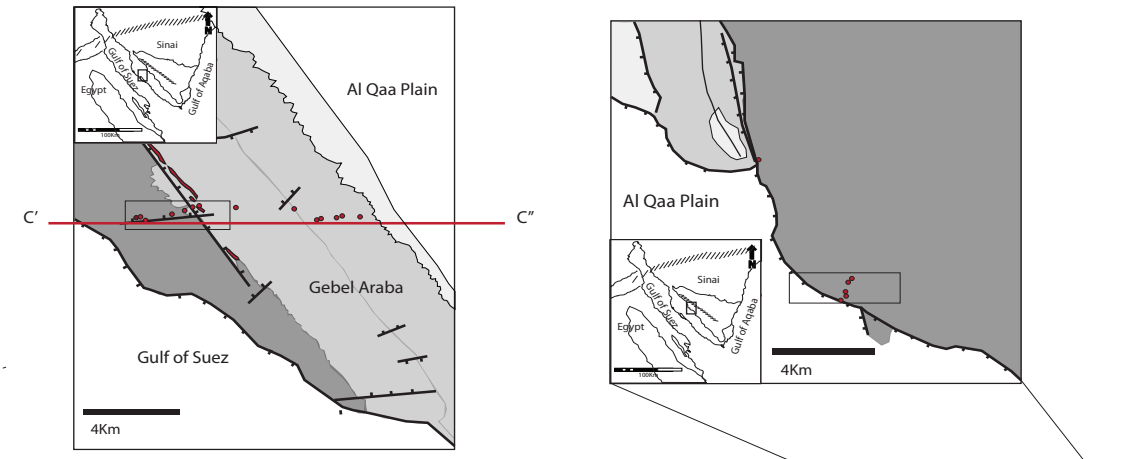

Current structural configuration

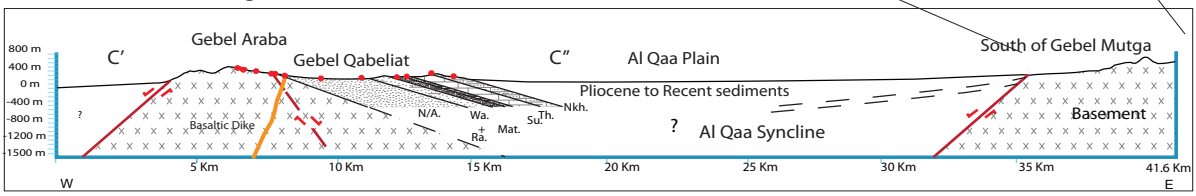

Miocene structural and thermal configuration (retro-deformed illustration)

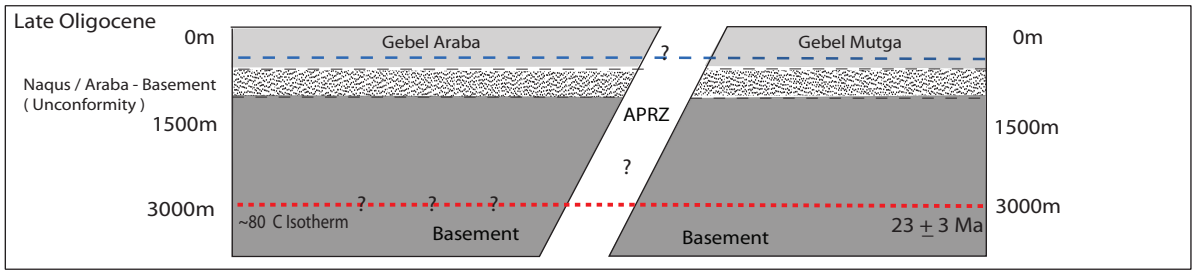

Figure 8. The map illustrates the current structural configuration of the southern part of the study area and the spatial distribution of the basement and the pre- and syn-rift units specifically the Gebel Araba and Mutga areas. Additionally it shows a cross section of the southern part of the study area. Notice that the bottom of the apatite partial retention zone can be approximated (APRZ red dashed line) in the Gebel Mutga at ~2900(m) during the Early Miocene (paleo-depth). At the lower section of this sketch there is a retrodeformed block showing the mean apatite age of maximum exhumation and the temperature conditions pre-extension. The Naqus/Araba unit was represented as two black dashed lines with a gray fill. Question marks represent uncertainty. The Gebel Araba transect show low reproducibility and therefore no interpretations were made.

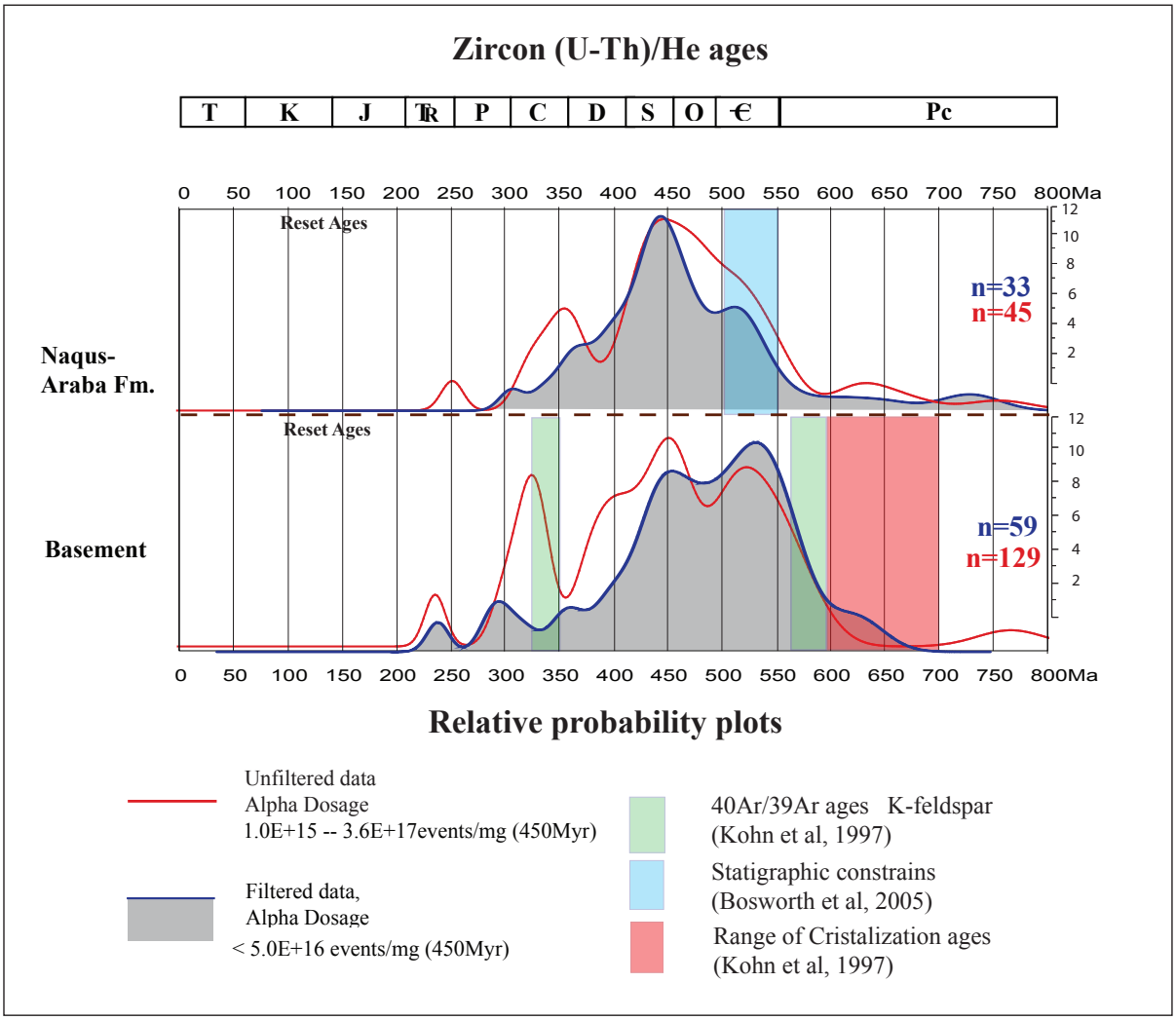
Zircon (U-Th)/He ages
T
K
J
Tr
P
C
D
S
O
Pc
0 50 100 150 200 250 300 350 400 450 500 550 600 650 700 750 800Ma
Reset Ages
n=33
n=45
Naqus-
Araba Fm.
Reset Ages
n=59
n=129
Basement
12
10
8
6
4
2
Relative probability plots
Unfiltered data
Alpha Dosage
1.0E+15 -- 3.6E+17events/mg (450Myr)
Filtered data,
Alpha Dosage
< 5.0E+16 events/mg (450Myr)
40Ar/39Ar ages K-feldspar
(Kohn et al, 1997)
Statigraphic constrains
(Bosworth et al, 2005)
Range of Cristalization ages
(Kohn et al, 1997)

Figure 9. Zircon probability density plots showing combined borehole and surface samples, This graph illustrate a variety of (U-Th)/He zircon populations found in the basement and the Naqus/Araba Fm. The columns represent stratigraphically constrained depositional age and previous analysis using (U-Pb) and Ar/Ar K-feldspar dating. Notice that the lower basement plot are zircons ages that belong to a granitoid and are recording multiple tectonic events due to their high concentration and variation on alpha dosage. Once the zircon ages with high alpha dosage were filtered out (blue curve with the gray fill) only two main peaks prevails at ~ 525Ma and ~450Ma in the basement and one main peak ~450Ma in the Naqus/Araba Fm.

(Naqus/Araba Fm.)

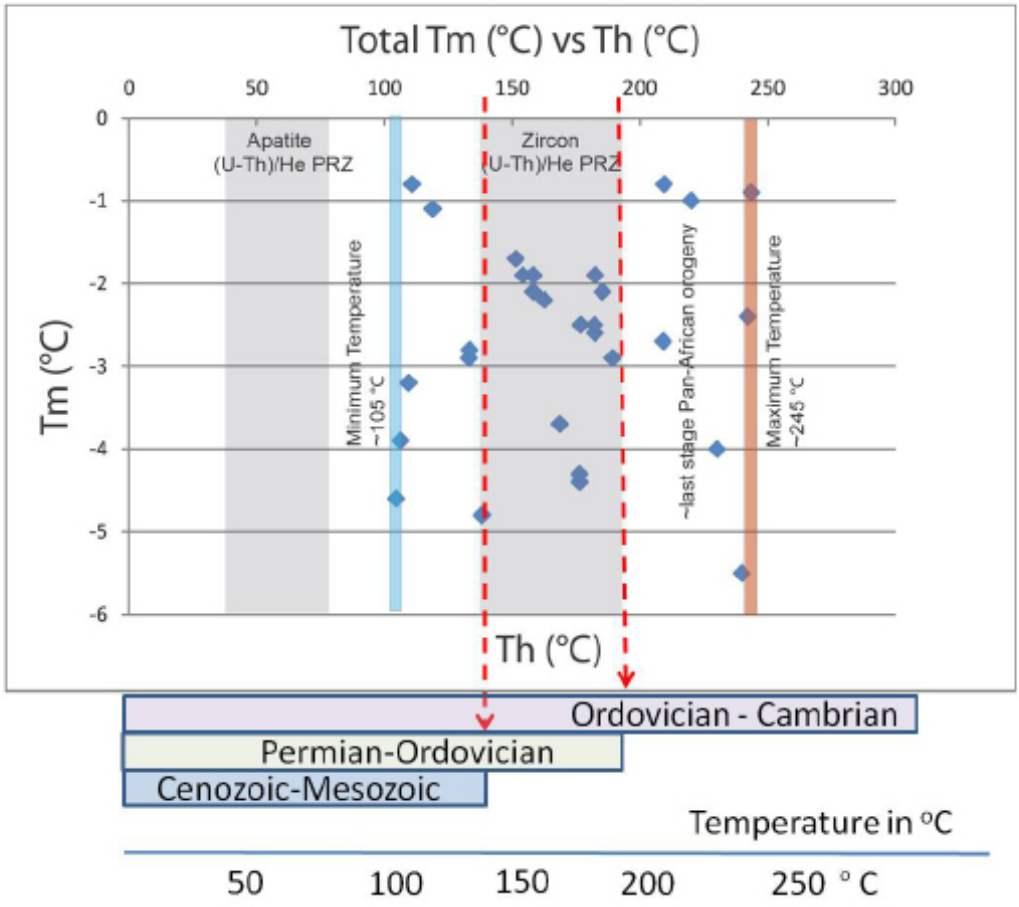

Figure 10. This Tm vs Th (temperature of homogenization) (°C) plot illustrate a range of temperature endure by the Cambrian sediments between the Late Cambrian- Late Ordovician to the Early Miocene preserved in fluid inclusions. Maximum and minimum temperatures reached by the pre-rifting sediments were ~245°C and ~105°C respectively. Notice that the great majority of homogenization temperature measured in the quartz re-growth fall within the zircon partial retention zone.

ERB-B-2X borehole

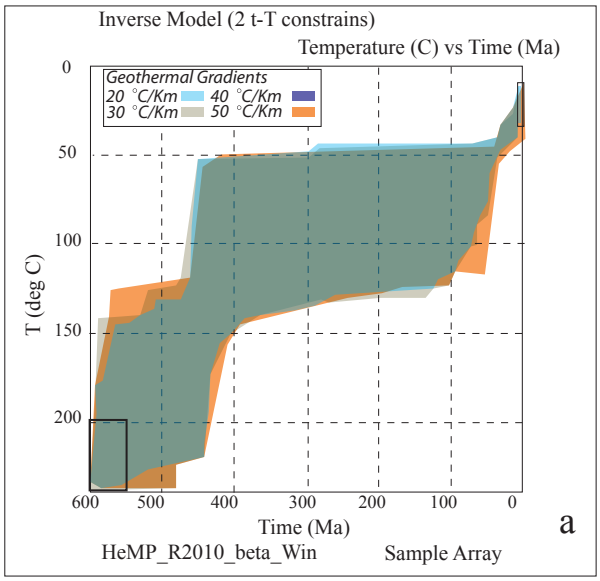

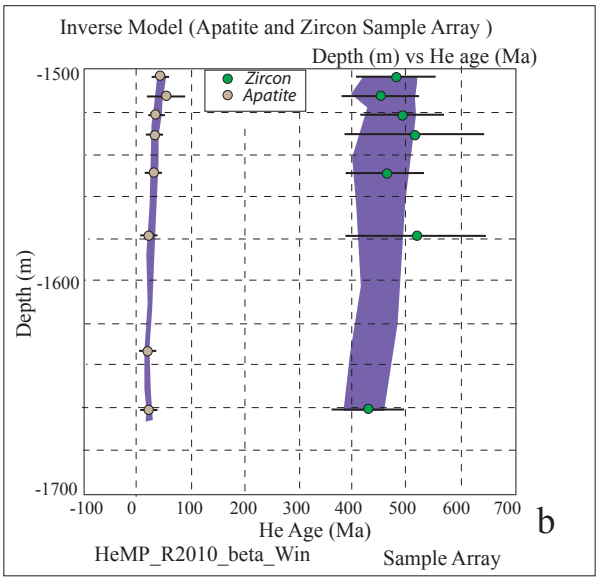

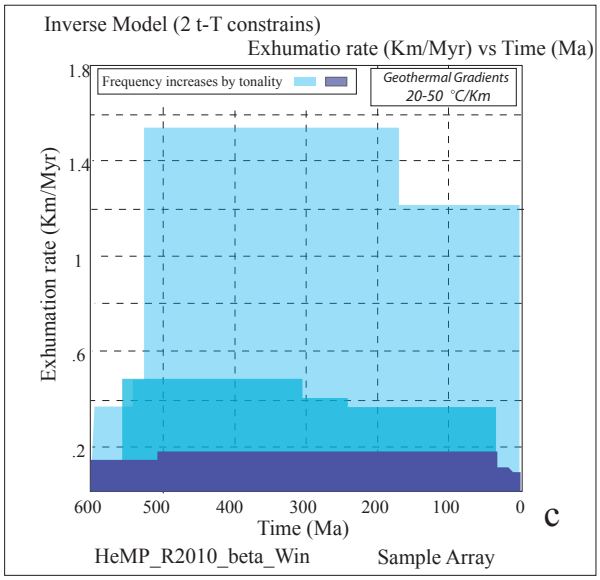

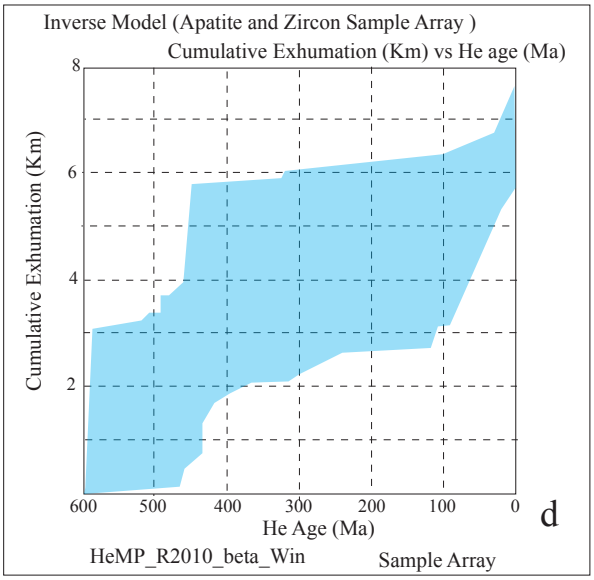

Figure 11. These graphs show the possible time temperature (t-T) paths that match the zircon and apatite (U-Th)/He ages from the ERB-B-2X borehole sample array. This data was acquired after doing inverse modeling of sample arrays in HeMP. Instead of overlapping lines we show them as patch according to specific geothermal gradients (a). Aliquots used and their depths are shown in (b). Modeled exhumation rates are highly unconstrained but a maximum of 1.4Km/Myrs during last stages of Pan-african orogeny as well as 1.2-.2Km/Myrs maximum exhumation during the Early Miocene were obtained. The more frequent estimates by HeMP were more reasonable estimates .2-.18Km/Myrs or lower (c). Cumulative exhumation gave almost 4Km during the last stages of Pan-African orogeny and 1Km during the Early Miocene in the Hamman Faraun block (d).

ERB-B-2X borehole

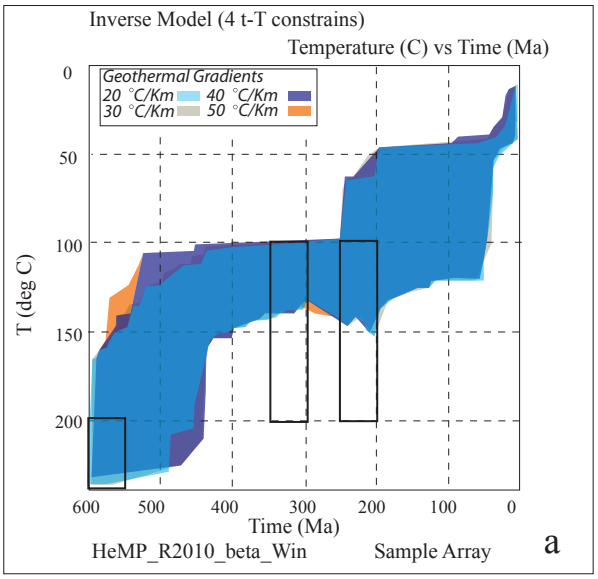

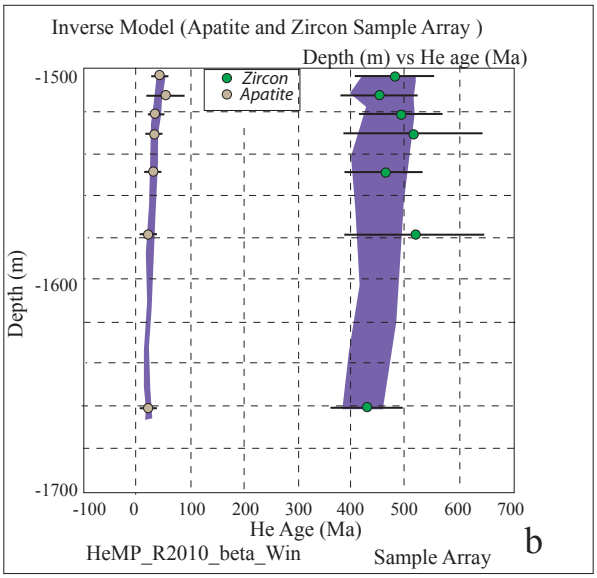

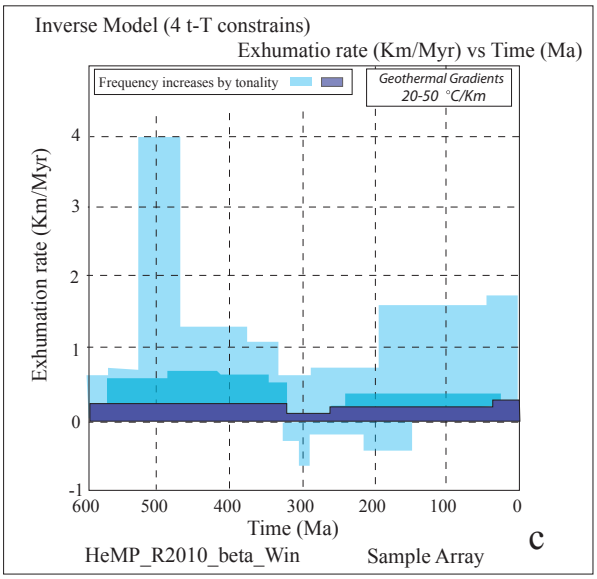

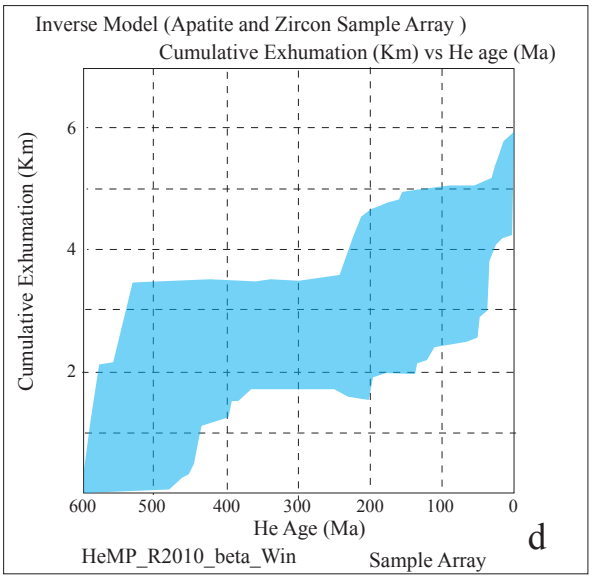

Figure 12. These graphs show the possible time temperature (t-T) paths that match the zircon and apatite (U-Th)/He ages from the ERB-B-2X borehole sample array using 4 t-T constrains. The two extra constrains came from the probability density plots with no alpha dosage filter, were at 200-250Ma and 300-350Ma zircon recorded helium loss by tectonic induced heating at lower temperature that the normal closure temperature. This data was acquired after doing inverse modeling of sample arrays in HeMP. Instead of overlapping lines we show them as patch according to specific geothermal gradients (a). Aliquots used and their depths are shown in (b). Modeled exhumation rates are more constrained than in the unconstrained model in figure 12. Maximum exhumation rates calculated by HeMP gave 4Km/Myrs during the last stages of Pan-African orogeny as well as 1.6Km/Myrs during the Early Miocene. Minimum and more frequent exhumation rates calculated by HeMP gave .6Km/Myrs during the last stages of Pan-African orogeny as well as .3-.1Km/Myrs during the Early Miocene or less (c). Cumulative exhumation gave almost 3Km during the last stages of Pan-African orogeny and 1Km during the Early Miocene in the Hamman Faraun block (d).

ERB-B-2X borehole

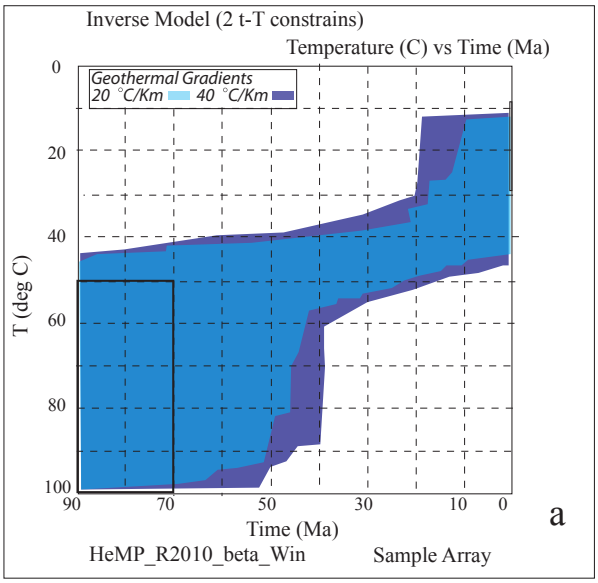

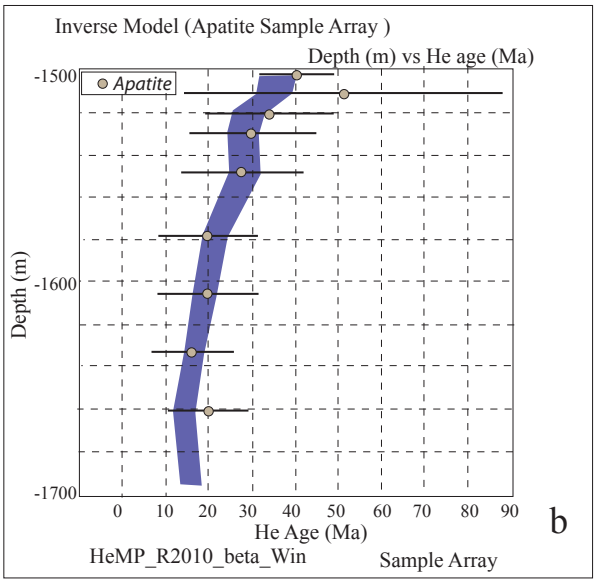

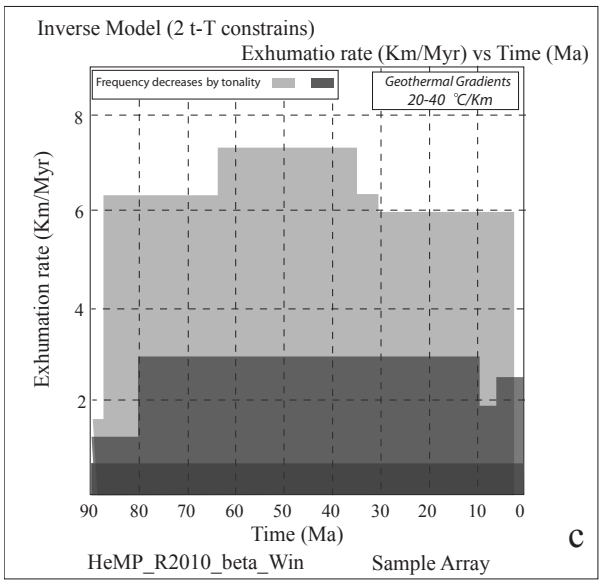

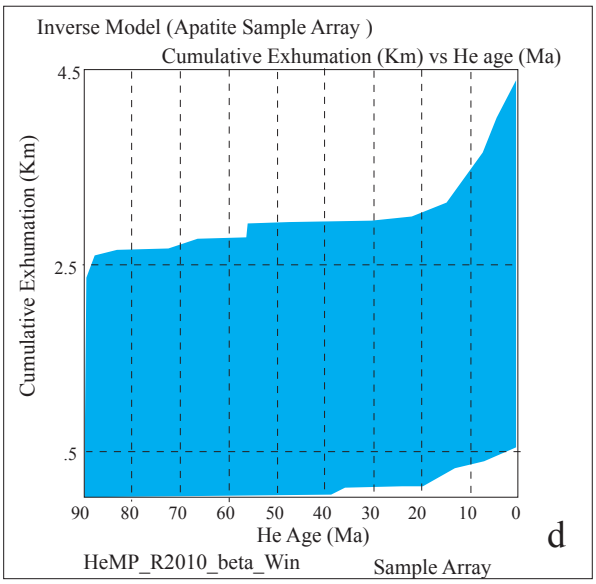

Figure 13. These graphs show the possible time temperature (t-T) paths that match the apatite (U-Th)/He ages from the ERB-B-2X borehole sample array using 2 t-T constrains. The two initial conditions are assuming temperatures from 100 to 50 ^{o}C at 90-70Ma. The data acquired after doing inverse modeling from one thermochronometer diverge slightly from the previous models. Instead of overlapping lines we show them as patch according to specific geothermal gradients (a). Aliquots used and their depths are shown in (b). Modeled exhumation rates are .4Km/Myrs during the Early Miocene (c). Cumulative exhumation gave almost 1.5Km during the Early Miocene in the Hamman Faraun block (d).

Gebel Mutga

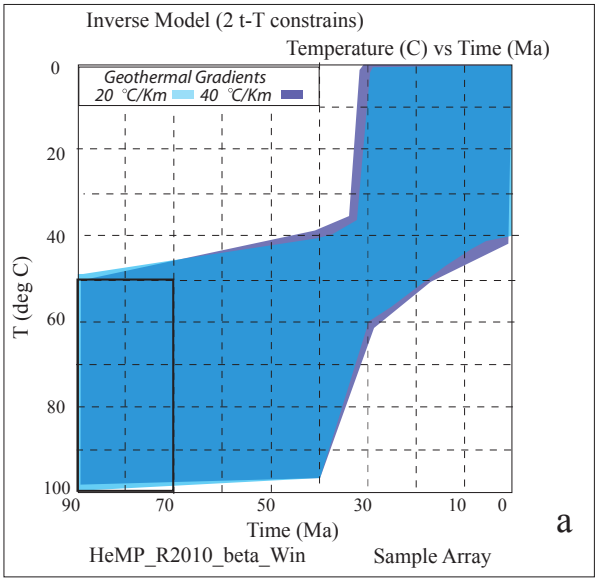
Inverse Model (2 t-T constrains)
Temperature (C) vs Time (Ma)
Geothermal Gradients
20 °C/Km 40 °C/Km
T (deg C)
Time (Ma)
HeMP_R2010_beta_Win
Sample Array
a

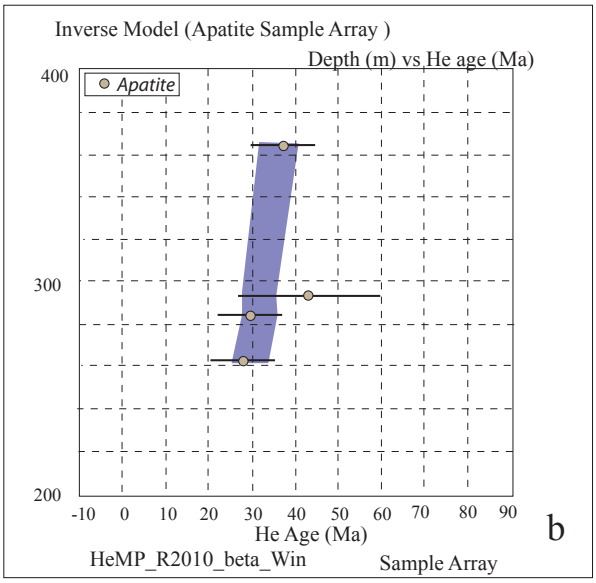
Inverse Model (Apatite Sample Array)
Depth (m) vs He age (Ma)
Apatite
He Age (Ma)
HeMP_R2010_beta_Win
Sample Array
b

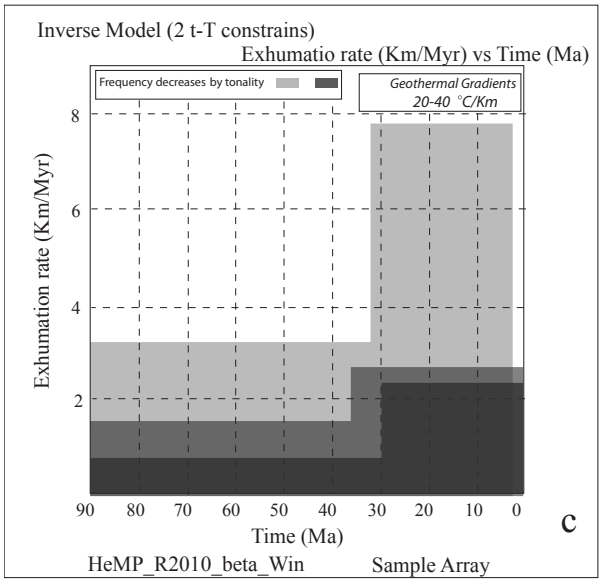
Inverse Model (2 t-T constrains)
Exhumatio rate (Km/Myr) vs Time (Ma)
Frequency decreases by tonality
Geothermal Gradients
20-40 °C/Km
Exhumation rate (Km/Myr)
Time (Ma)
HeMP_R2010_beta_Win
Sample Array
c

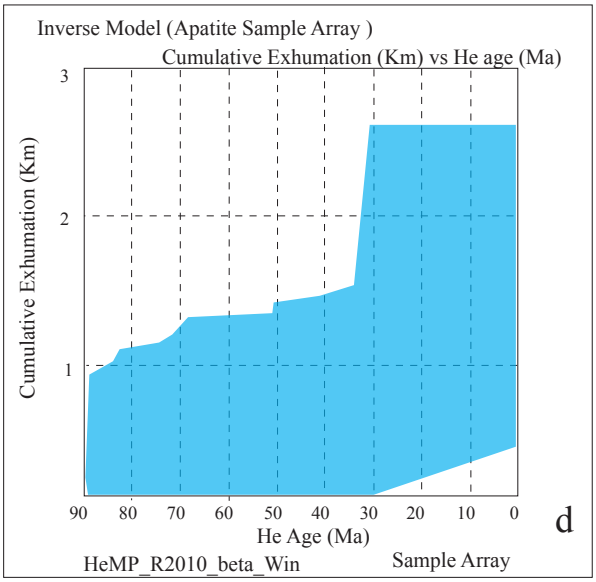
Inverse Model (Apatite Sample Array)
Cumulative Exhumation (Km) vs He age (Ma)
Cumulative Exhumation (Km)
He Age (Ma)
HeMP_R2010_beta_Win
Sample Array
d

Figure 14. These graphs show the possible time temperature (t-T) paths that match the apatite (U-Th)/He ages from the Gebel Mutga sample array using 2 t-T constrains. The two initial conditions are assuming temperatures from 100 to 50 ºC at 90-70Ma. The data acquired after doing inverse modeling from one thermochronometer correspond to the the rift flank. Instead of overlapping lines we show them as patch according to specific geothermal gradients (a). Aliquots used and their depths are shown in (b). Maximun modeled exhumation rates are 2.2Km/Myrs during the Early Miocene according to total uplift must be in an order of magnitude less (c). Cumulative exhumation gave almost 2 Km during the Early Miocene in the Gebel Mutga block (d).

Rift Basin

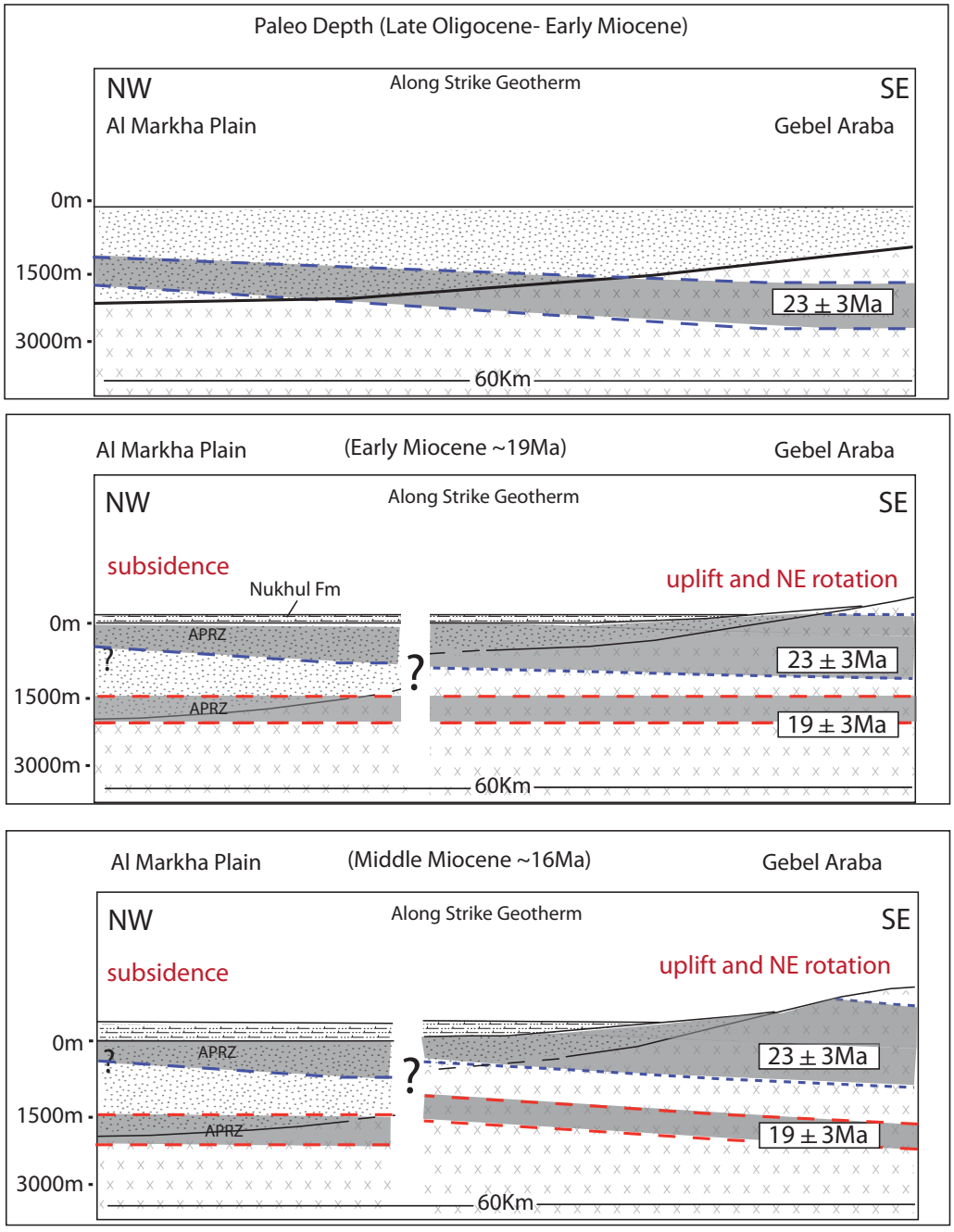
Paleo Depth (Late Oligocene- Early Miocene)
NW
Along Strike Geotherm
SE
Al Markha Plain
Gebel Araba
0m
1500m
3000m
23 ± 3Ma
60Km
Al Markha Plain
(Early Miocene ~19Ma)
Gebel Araba
NW
Along Strike Geotherm
SE
subsidence
uplift and NE rotation
Nukhul Fm
APRZ
APRZ
?
?
23 ± 3Ma
19 ± 3Ma
0m
1500m
3000m
60Km
Al Markha Plain
(Middle Miocene ~16Ma)
Gebel Araba
NW
Along Strike Geotherm
SE
subsidence
uplift and NE rotation
APRZ
APRZ
?
?
23 ± 3Ma
19 ± 3Ma
0m
1500m
3000m
60Km

Figure 15a. These cross section evolution diagrams illustrate the location of the apatite partial retention zone through time in the rift basin (constrained using ERB-B-2X data). This model illustrate a higher geothermal gradient in the northern part at the early stages of rifting (37^{o}C/Km) and a lower geothermal gradient of ~(25^{o}C/Km) in the southern part. Notice the partial retention zone are bounded by color code dashed lines and their respective time in the white rectangles.

Rift Flank

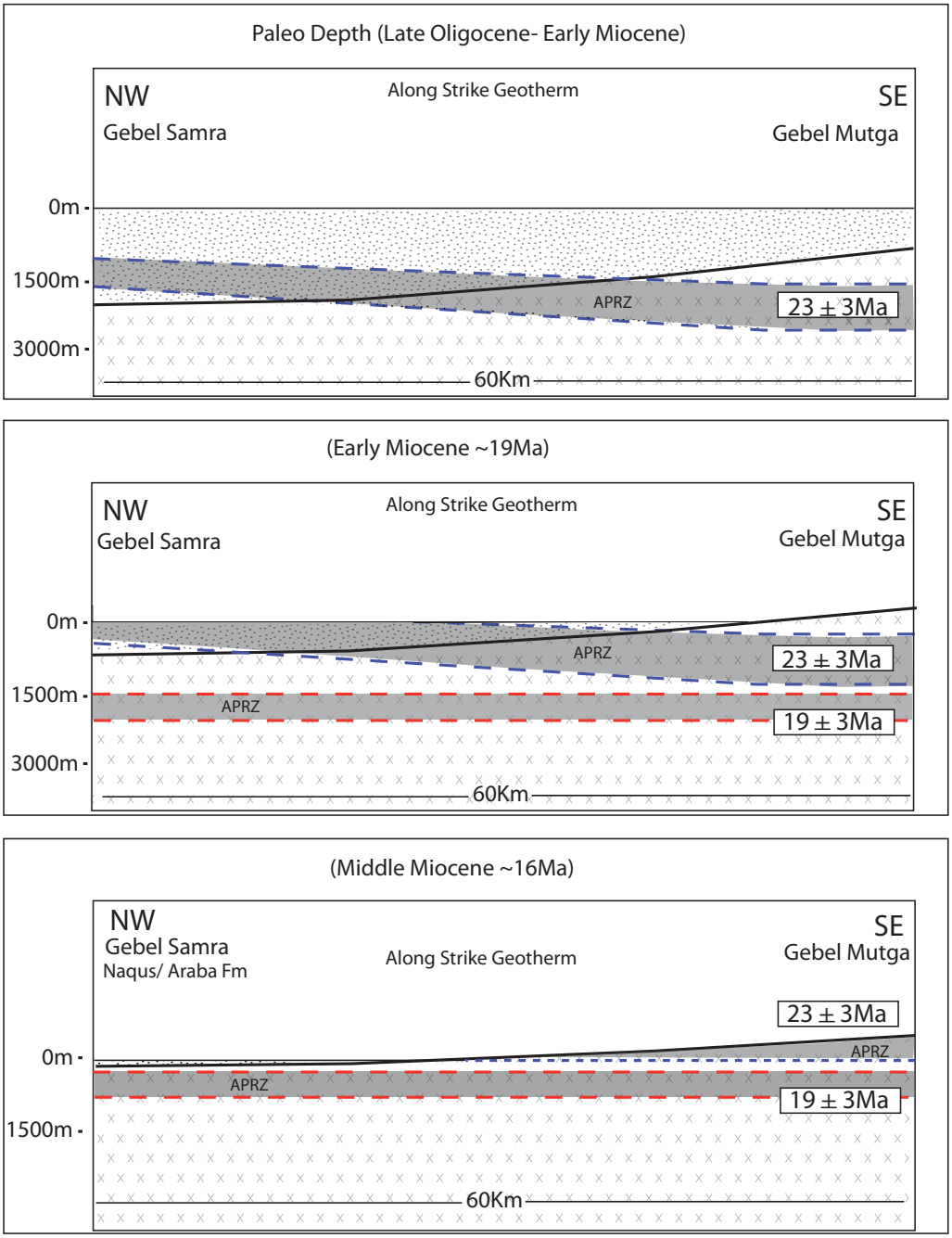
Paleo Depth (Late Oligocene- Early Miocene)
NW
Gebel Samra
Along Strike Geotherm
SE
Gebel Mutga
0m
1500m
3000m
APRZ
23 ± 3Ma
60Km
(Early Miocene ~19Ma)
NW
Gebel Samra
Along Strike Geotherm
SE
Gebel Mutga
0m
1500m
3000m
APRZ
APRZ
23 ± 3Ma
19 ± 3Ma
60Km
(Middle Miocene ~16Ma)
NW
Gebel Samra
Naqus/ Araba Fm
Along Strike Geotherm
SE
Gebel Mutga
23 ± 3Ma
0m
1500m
APRZ
APRZ
19 ± 3Ma
60Km

Figure 15b. These cross section evolution diagrams illustrate the location of the apatite partial retention zone through time in the rift flank (constrained using Gebel Mutga and Gebel Samra data). This model illustrate a higher geothermal gradient in the northern part at the early stages of rifting (37^{o}C/Km) and a lower geothermal gradient of ~(25^{o}C/Km) in the southern part. Rift flank exhumation rates were faster in the southern part ~ .4-.2Km/ Myr. Bed rotation in the southern part is greater than in the north causing the paleo Early Miocene APRZ to rotate as well as the pre rift units. This may cause a fan effect too in the new developing APRZ. Notice the partial retention zone are bounded by color code dashed lines and their respective time in the white rectangles.

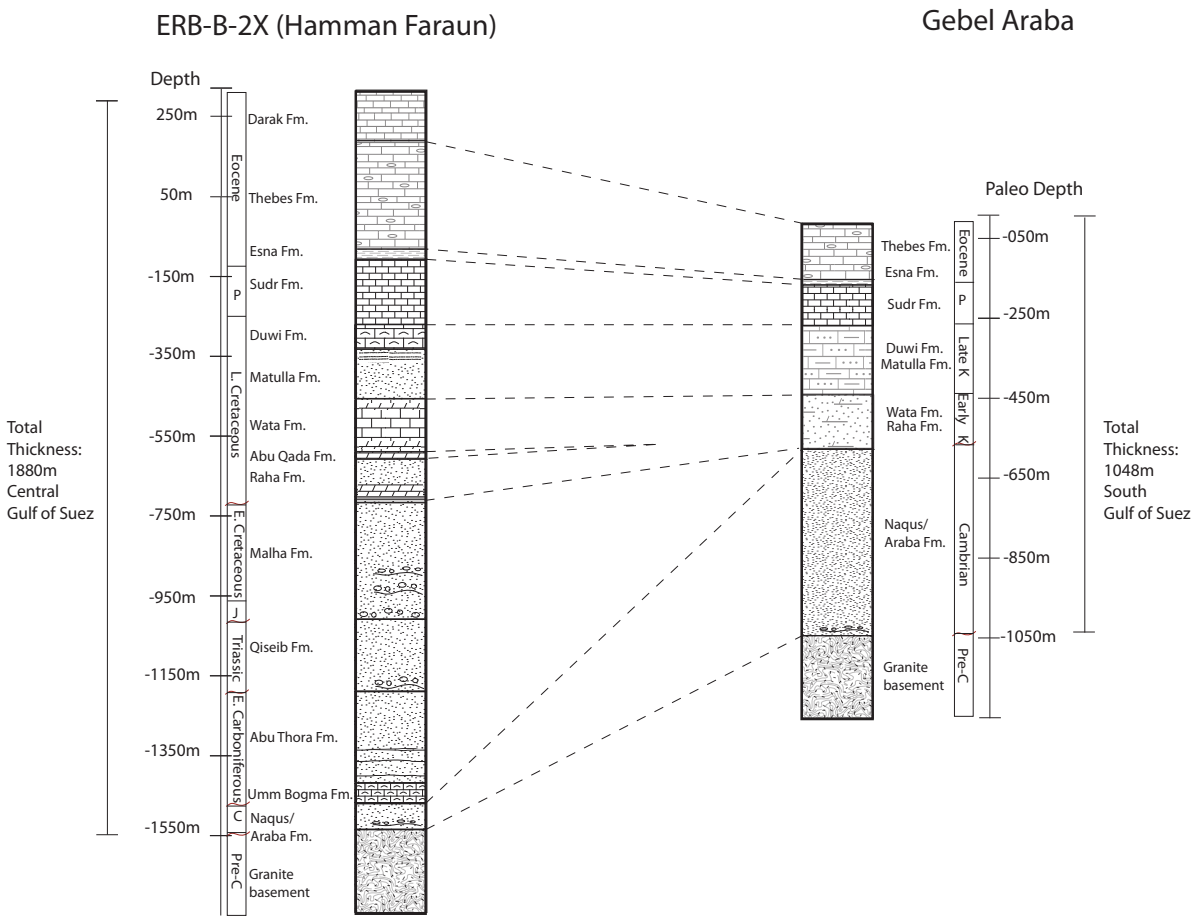
ERB-B-2X (Hamman Faraun)
Gebel Araba
Depth
250m
50m
-150m
-350m
-550m
-750m
-950m
-1150m
-1350m
-1550m
Darak Fm.
Thebes Fm.
Esna Fm.
Sudr Fm.
Duwi Fm.
Matulla Fm.
Wata Fm.
Abu Qada Fm.
Raha Fm.
Malha Fm.
Qiseib Fm.
Abu Thora Fm.
Umm Bogma Fm
Naqus/
Araba Fm.
Granite
basement
Eocene
P.
L. Cretaceous
E. Cretaceous
J.
Triassic
E. Carboniferous
C.
Pre-C
Total
Thickness:
1880m
Central
Gulf of Suez
Thebes Fm.
Esna Fm.
Sudr Fm.
Duwi Fm.
Matulla Fm.
Wata Fm.
Raha Fm.
Naqus/
Araba Fm.
Granite
basement
Eocene
P.
Late K
Early K
Cambrian
Pre-C
Paleo Depth
-050m
-250m
-450m
-650m
-850m
-1050m
Total
Thickness:
1048m
South
Gulf of Suez

Figure 16. These two stratigraphic columns are illustrating the difference in pre-rift units thickness in the Gulf of Suez. The ERB-B-2X borehole data show a more continues pre-rift sequence compare to The Gebel Araba exposures, were the entire Carboniferous to the Early Cretaceous are absent and a thinner Matulla Fm. is harder to identify. The sub basin development during those periods at the north and not in the south is highly likely if we consider zircon (U-Th)/He ages (fig.9). The thickness lateral variation illustrate a greater overburden and a diferent burial history at the northern Gulf that in the south. This different overburden played an important role on the thermal development of the Gulf during Neogene rifting and the hydrocarbon maturation history as well.

CHAPTER 3

Apatite and Zircon (U-Th)/He detrital constraints on syn and pre-rift Paleozoic and Mesozoic tectonism in the central Gulf of Suez, Egypt

Abstract

The Neogene Gulf of Suez have been subject to detailed structural and sedimentological studies for the past decades due to its high hydrocarbon potential and well exposed early rift architecture, as a result, it has a well-defined fault geometry and stratigraphy that have served as an excellent analog for continental failed rift system around the world. Despite ample fission track data from the Sinai rift flank, the lack of thermochronometric data from exhumed pre-rift sedimentary cover and crystalline basement blocks within the rift limits the understanding of the influence of pre-rift structures on the style of rifting. Zircon (U-Th)/He (ZHe) ages from pre-rift strata and basement samples were analyzed to better constrain the pre-Tertiary tectonothermal evolution of the Gulf of Suez and shed light on the influence of Paleozoic/Mesozoic tectonics on Red Sea-Gulf of Suez rifting. ZHe data from pre-rift strata in the central Gulf of Suez record a detailed Paleozoic/Mesozoic tectonic history of the region that is strongly impacted by Carboniferous, Triassic/Jurassic, and Santonian tectonism. Nearly zero depositional lag time dominates the pre-rift units recording rapid exhumation related to Late Paleozoic tectonism, Jurassic/Triassic Neo-Tethyan rifting, and Syrian arc inversion on the structural grain of the Gulf of Suez pre-rift units. Syn-rift Abu-Zenima and Nukhul Fm. yield ages indicative of proximal sources and recycling of pre-rift units and basement. Mesozoic and Paleozoic tectonic histories seem to be of a greater thermo-tectonic significance than Cenozoic history in the Sinai region.

Introduction

Many aspects of our understanding of rifting have been influenced by concepts developed in the Gulf of Suez as a result of detailed structural and sedimentological studies (e.g., Evan, 1990; Bosworth., 1994, 1998, 2007; McClay et al., 1998; McClay & Khalil., 1998; Moustafa., 2002; Sharp et al., 2000; Bosworth & McClay., 2001; Younes & McClay., 2002; Kohn & Eyal., 1980; Feinstein et al., 1996; Omar et al., 1989; Omar & Steckler., 1995; Van der Beek et al., 1993) and decades of intense hydrocarbon exploration. Although the Late Cenozoic tectonic history of the Gulf is well characterized there is not much discussion on the Paleozoic and Mesozioc tectonism experience by the Sinai and the role and influence it might have played in the current rift configuration, a key aspect when developing conceptual rift models. This research shed some light on the Paleozoic to Mesosoic detrital and thermal history of the Gulf by performing a detailed detrital zircon (U-Th)/He (DZHe) thermochronometric analysis. Furthermore it integrates borehole and surface samples strategically collected from pre- and syn-rift sedimentary units and basement along the eastern-central margin of the Gulf of Suez. The ZDHe ages explore in a regional context the link of sedimentation and tectonism by means of identifying sources, confining minimum depositional ages and lag time. Moreover it help identify and temporally constrain rapidly exhumed blocks that were contributing to basin development in western Sinai that coincide with previously constrained

temporal active tectonism along the northern Africa and west Arabia. The detrital zircon ages helped constrain a number of syn-tectonic depositional events throughout the Sinai Peninsula over the past 550 m.y. and provided for the first time thermal (U-Th)/He evidence on pre-rifting rapid cooling over areas that kinematically played a big role on early rifting architecture and orientation development along the Gulf of Suez.

1. Geology background and previous work

1.1 Paleozoic

The Sinai basement accreted in conjunction with a series of crystalline and metamorphic terranes that later become the west margin of the Arabian plate (Gass & Gibson 1969; Stoeser & Camp, 1985; and Genna et al., 2000). These terranes started to coalesce during the Late Precambrian (715-680 Ma) and consolidated completely throughout a process of continental-island arc and island arc island arc interaction approximately 70 million years later (640-610Ma). During the formation of Gondwana, the Pan-African-Brasilian orogeny produced a period of intra-cratonic shearing and rifting also known as the "Najd event" (Stern, 1985). The orientation of this fault system (NW-SE) was later adopted by accommodation zones during Cenozoic rifting (Younes and McClay, 2002). According to ZHe ages and $^{40}Ar/^{39}Ar$ from feldspar (Kohn et al., 1996) from the Sinai basement this period recorded the greatest thermal impact since the beginning of the Paleozoic. During the Cambrian

and Ordovician, the Sinai, within the craton (Beydoun, 1993), drifted along with the Arabian plate towards the south, where the dominating tectonic event was uplift inferred by major unconformities in central and west Africa. A strong glaciation period dominated the region from Late Ordovician to Early Silurian, when glacial melting produced a widely registered transgression in the northern Africa platform (McClure, 1978; Vaslet, 1990; Sutcliffe et al., 2000a). Soon after this climatic stage ended, a gentle but widely recorded tectonic event took place, producing uplift, block tilting and unconformities during the Ordovician to Silurian transition (Stump et al., 1995; Klitzsch, 2000; Guiraud and Bosworth, 1999). Deformation throughout the Early Devonian is inferred from the presence of high frequency unconformities throughout northern and western Africa (Guiraud et al, 2005; Crossley and McDougall, 1998) and likely resulted from NW-SE directed shortening and collision during early Acadian and Caledonian orogenic events (Guiraud et al., 2005).

The onset of subduction in the Early Carboniferous of the Paleo-Tethys Ocean under Gondwana produced major volcanism along the Iranian terranes, subsequent back-arc rifting and uplift heavily influenced the Arabian plate and the Sinai area respectively during the Permian (Sharland et al., 2001). The Variscan (or Hercynian) Orogeny, developed by the collision of Gondwana and Laurrusia to form Pangaea, initiated during the Early Carboniferous and peaked by latest Carboniferous to early Permian where strong folding, thrusting, and metamorphism was endured by western and northern Africa. Rifting continued, resulting in the development of the Neo-Tethys Ocean separating the Iranian terranes from the Arabian plate during the mid-

Permian to Early Jurassic. Rifting propagated westward during the Permian from NE Arabia to Morocco (Guiraud, 1998).

1.2 Mesozoic

In the eastern Mediterranean, rifting started during the Late Triassic, separating Turkey from Africa and Arabia. During the Late Jurassic the northern margin of the Arabia platform had already become a passive margin (Garfunkel, 1998). The Early Cretaceous was characterized by a decrease in tectonic activity in the northern Africa. During this period, active rifting episodes led to the break up of western Gondwana, opening the South and Equatorial Atlantic ocean (Guiraud et al., 2005). In the late Santonian the presence of multiple unconformities in the north and central African fold belts corresponds to a compressional episode during the Alpine Cycle (Guiraud & Bosworth., 1997). The change in relative motion between the African and Eurasian plates (Savostin et al., 1986) resulted in right lateral transpressional deformation along the southern margin of the Tethys Ocean. This event produced narrow fold-induced relief and the uplift of large areas in the Syrian Arc fold belt (Guiraud et al., 2005). Furthermore it reactivated older Neo-tethys structures, as was the case of the Wadi Araba Anticline in the western margin of the Gulf of Suez.

1.3 Cenozoic

During the closure of the Neo-Tethys, the Sinai did not experience any major tectonic changes, as evidenced by shallow carbonate and shale pre-rift units (Bosworth et al., 2005). Rifting started during the Early Miocene as a result of crustal weakening by the Afar plume and continued to develop as a result of the northeastward separation of the Arabian and the African plates (e.g., Bosworth et al., 2005). During this period, the Gulf of Suez and the Red Sea were linked and formed one continuous rift system that shared a kinematic and stratigraphic framework until the later opening of the Gulf of Aqaba transform system (Bosworth & McClay, 2001).

2. Pre- and Syn rift brief stratigraphic description.

The Sinai stratigraphy encompass a variety of lithologies, mainly deformed during Late Miocene rifting, that range in age from Late Pre-Cambrian (basement) to more youngest shallow marine to sillisiclastic units. The oldest Late Proterozoic basement during the accretion and cratonization process underwent a series of deformation, metamorphic, and ample intrusion (granitic-granodioritic) phases. Later uplift and extensive erosion formed the peneplain of the basement.

The units described below belong to the formations analyzed by detrital zircon (U-Th)/He thermochronology and do not include all of the pre- or syn-rift units.

The Araba and Naqus formation (collectively known as the Nubian Sandstones) are siliciclastic units that were uncomformably deposited on top of the peneplained

crystalline and metamorphic Sinai basement (Bosworth, 1999). These two units have a combined approximate thickness of 510 m (Hassan, 1967; El Barkooky, 1992).

The Carboniferous Abu Thora sandstones lies above the dolomitic Umm Bogma and black shales of the Abu Durba Formation, and is composed mainly of shallow marine sandstones with a thickness of 200m (Weissbrod, 1969; Kora, 1984). This formation was intruded and capped by basalts during the Permian.

Overlying Abu Thora is the Triassic Qiseb formation, which consists of 300m of continental and shallow marine tidal-dominated, containing minor fossiliferous stratas (Barakat et al., 1988a; Darwish, 1992).

Uncomformably overlying is the Lower Cretaceous Malha formation. This formation consists mainly of fluvial sandstones having thickness variation from 30 to 150 m and reaching a maximum of 400 m in the southern Gulf (Bosworth, 1995).

The upper Cretaceous units start unconformably with the deposition of the Raha formation, conformably overlying Raha are the Wata and Matulla formations; these units exhibit degreasing thickness towards the south (Darwish, 1994), They consist mainly of shallow marine successions and got approximate thickness of 90m, 100m and 150m respectively (Ghorab, 1961). The Cenomanian Raha consists of a sucession of shales, sandstones and limestones. The Turonian Wata formation consists mainly of limestones with a minor siliciclastic input. The Coniacian to Santonian Matulla formation consist mainly of shales and sandstones. Above these units until the Oligocene- Miocene unconformity there was insufficient number of samples, low zircon yield, or not sample.

The first syn-rift unit analyzed was the basal conglomerate and red fine-grain sandstones of the Abu-Zenima formation. This unit is above the Tayiba formation and a few basaltic flows in the central Gulf.

Unconformably overlying the Abu Zenima Fm. are the shallow marine successions of the Nukhul formation, which include calcareous sandstones, conglomerates, marls and fossiliferous limestone (Scott & Govean, 1985). The depositional environment in this unit is not homogeneously preserved along the Gulf, because individual extensional fault blocks and half-graben enlargement took place at diverse times and magnitude during early rifting stages, producing heterogeneity in early basin development.

3. Sampling method

Over 500 detrital and basement zircons where analyzed at the University of Kansas Isotope Geochemistry Laboratory (KU-IGL) for this study. A total of 47 sedimentary surface samples and 22 crystalline basement samples were collected in the central and southern part of the Gulf (Fig.1). Furthermore over 1800m of stratigraphic sequence was sampled in the form of wet cuttings belonging to the (ERB-B-2X) borehole. Apache Oil Company provided the wet cuttings to avoid resetting of apatites or zircons. The borehole was divided into 50 samples and includes almost all the pre-Miocene rift sediments from the Thebes Fm. to the Proterozoic crystalline basement (Fig.1-2). This borehole cuts through the Markha fault and the great majority of the analyzed samples, (depth < 335meters), correspond

to the footwall of the Markha Plain (Fig.2).

The detrital zircons were collected mainly from sandy sub units belonging to a variety of lithologies. An extra basement sample was extracted from the ERB-B-1X due to its proximity to the Markha Fault. In order to capture an overall representative sample from the different formations and all the possible detrital populations within a unit the samples were grouped according to their corresponding unit. There was no need to sub-divide formations for higher stratigraphic resolution because the focus was to assess major tectonic events recorded in the Sinai. Additionally we did not sub-divide formations in order to achieve an adequate number of zircons analyses for meaningful statistical purposes (see probability density plots in Figs. 3-4).

4. Thermochronology

4.1 (U-Th)/He thermochronology

(U-Th)/He thermochronology is based on the temperature-regulated diffusion of radiogenic ^{4}He out of the grain, i.e., ^{4}He that was produced and retained internally in the grain during α-decay of radioactive ^{238}U, ^{235}U, ^{232}Th and ^{147}Sm. Apatite and zircon are the most commonly used (U-Th)/He thermochronometers and they record thermal information between temperatures of ~ 40° - 200°C (Farley, 2000; Reiners and Farley, 1999; Reiners et al., 2005). The AHe thermochronometer is the most well-studied and widely applied (U-Th)/He thermochronometer. Diffusion of 4He out of the apatite crystal is controlled by temperature so that 4He is completely lost to

the surrounding at temperatures above 80°C, completely retained at temperatures below 40°C , and is partially retained between temperatures of 40 and 80°C (termed the AHe partial retention zone (PRZ)). Similarly, retention and diffusive loss of ^{4}He in zircon varies over a range of temperatures from ~ 140 – 200°C and is termed the ZHe PRZ.

The precise sensitivity or closure temperature of any chosen thermochronometer depends on a complex and variable relationship between multiple factors. The factors that need to be considered for a reliable geologic interpretation are; (1) the diffusion parameters used to calculate the closure temperature (Dodson, 1973), (2) the diffusion mechanisms applied, whether diffusion is anisotropic or not depending on the mineral (Reich et al., 2007), (3) the cooling and exhumation rates, (4) the assumed three-dimensional geometric approximations of the mineral, which have implication on the diffusion domain and the alpha ejection corrections (Farley., 1996), (5) the local thermal structure, (6) the length scale over which deformation occurs, (7) the alpha damage over time (Nasdala et al., 2001, 2005). The (U-Th)/He uncorrected ages are calculated iteratively using the following equation,

$$^{4}He = 8^{238}U\,(e^{\lambda 238t} -1) + 7(^{238}U/137.88)(e^{\lambda 235t} -1) + 6^{232}Th\,(e^{\lambda 232t} -1) + {}^{147}Sm(e^{\lambda 147t} -1) \quad \text{(equation 1)}$$

where ^{238}U, ^{235}U, ^{232}Th, ^{147}Sm and ^{4}He are acquired concentrations by mass spectrometry mainly expressed in nmol/g or ppm; $^{238}\lambda$, $^{235}\lambda$, and $^{232}\lambda$ are decay

constants for their respective isotopes. Variations of this formula can be found in Vermeesch (2008). During the radioactive decay process the alpha particles (He nuclide) is emitted with an energy of ~8 MeV from the radioactive parent. This energy allows the alpha particle to travel a certain distance within the mineral, according to the density of the mineral and the radioactive parent from which it is emitted. In the case of zircon the alpha particle tends to travel almost 20□m so it is imperative to consider the loss of alpha particles from parents located in the outer 20 □m ring of the mineral. Therefore, Farley (1996) applies a statistical correction and a geometrical solution that account for the fractional lost of alpha particles near the grain boundaries. The retention of He will vary by minerals and the He loss will be mainly by thermal diffusion (Shuster and Farley, 2005).

There is not one simple law that governs the closure temperature of a thermochronometer, but knowing these limitations and understanding the relative behavior of this system, give us a set of principles and rules that can be used to developed a precise thermo-tectonic analysis of a region. (U-Th)/He thermochronology has been applied successfully to multiple tectonic and geomorphic processes proven to have numerous applications for today's geologic questions (House et al., 1999; Farley, 2000; Reiners et al., 2000, 2007; Stockli, 2005; Mitchell and Reiners, 2003.).

4.2 (U-Th)/He Analytical Technique

Zircon were extracted from samples using a common mineral separation

process, which included crushing, grinding, water flow mineral separation (water table), heavy liquids (Bromoform and MEI) and magnetic separation. The zircons were handpicked for detrital samples, with care taken not to bias selected populations towards magmatic grains or slightly transported zircons. Characteristics like transparency, color, size and morphology variations were considered in order to reduce population bias. Grain size measurements for alpha ejection correction purposes were done using a microscope and calibrated computer measurement software. Zircon grains were individually packed in Platinum tubes and degassed using a Nd-YAG or CO_2 diode laser at temperatures over 1000 °C. The gas extracted was spiked with a known amount and ratio of $^{3}He/^{4}He$ and later analyzed by a quadrapole mass spectrometer by means of isotope dilution. Once analyzed for He content, the grains were dissolved according to a multi-step standard pressure vessel dissolution procedure using hydrofluoric, hydrochloric and nitric acid. The zircons were spiked with known quantities of ^{235}U, ^{230}Th and ^{149}Sm. Inductively coupled mass spectrometry (ICP-MS) was used to analyze the concentrations of ^{238}U (1/137.88 constant ratio with ^{235}U), ^{232}Th and ^{147}Sm. Ages were reduced by Helios software.

5. Detrital thermochronometry

5.1 Zircon (U-Th)/He detrital thermochronology

Detrital studies aim to link sedimentation and tectonism by means of identifying sources, constraining minimum depositional ages and depositional lag

time. Moreover it can help confine kinematic history models by relating dynamic changes in mass distribution and faulting controlled and recorded by rapid exhumed blocks. In the case of detrital studies, zircon is a widely used mineral due to its resistance to weathering and mechanical transportation. Furthermore, zircons are present in a wide variety of lithologies and their capacity to incorporate radioactive parents during their crystallization makes them highly useful as geo- and thermo-chronometers. Zircon is commonly use in detrital (U-Pb) dating for crystallization source ages and in (U-Th)/He thermochronology for rapid exhumed blocks and onset of faulting. Additionally this thermochronometer is less susceptible to be thermally overprinted after deposition. This (U-Th)/He cooling ages integrated into a known geologic context can be powerful tools for constraining thermal changes function of geologic processes like rapid cooling, erosional unroofing, fault exhumation, hydrothermal alteration, etc.

Zircon detrital thermochronology has been proven to give valuable information on source provenance and lag-time of rapidly exhumed blocks. The advantages of detrital thermochronology are that ages can be related to major tectonic events depending on the thermal history of the sediments encounter. Additionally it can be used to identify source rocks if the thermal history of the region is well defined. Due to their low closure temperature DZHe ages have significantly shorter erosional lag times compared to other utilized thermochronometers, or geochronometer. The final goal for the detrital analysis is to discriminate between populations of cooling ages and acquire a minimum age that can help constrain the

time of deposition. Double dating methods (e.g. U-Pb and (U-Th)/He) are highly recommended for this type of analyses (Reiners et al, 2005b; Rahl et al., 2003) but for this research we did not conduct this analyses because the current thermal history of the Gulf derive from (U-Th)/He dating provided here and in other previous works geo and thermochronometers data (e.g. Hassan and Hashad 1990; Stern and Hedge 1985; Kohn et al., 1987; Bosworth and McClay 2001) suggest that the detrital population will be entirely dominated by Pan-African signatures. (U-Th)/(He/Pb) double dating in a single detrital grain is a new method used for population identification with the advantage that is possible to differentiated between rapid tectonically (U-Th)/He cooled ages (with a different crystallization age) from volcanic zircons with the same ages (both (U-Th)/He cooling age and (U-Pb) age are the same). Additionally due to monetary and time constraints we consider them beyond the scope of this project. Results from this study, however, provide high-resolution DZHe data that gives new insight about the tectonic history, sediment dispersal, detrital source, thermo-tectonic evolution, and the impact of tectonic events on the Sinai western margin, Egypt.

5.2 Grain quantity

There has been controversy about the quantity of grains needed to achieve a satisfactory detrital study (Vermeesch, 2004). In practice the correct number of grains will depend on multiple factors. One of the first factors to consider is the number of grains needed to acquire a complete representation of all the detrital components, a value that will be influenced greatly by whether there is an unimodal distribution or

multiple components in the sample, information unattainable prior to analysis. The grain quantity will also depend on the objectives of the project and how much resolution is needed to answered the question at hand. Vermeesch (2004), presented a statistical approach that takes into account the total number of analyzed grains, the fraction of the least well-represented component, and the probability that no component was missing. The conclusion reached was that in order to be 95% confident that all the populations are represented at least 117 grains per sample should be analyzed. However, it should be noted that this approach assumes a uniform distribution of components, which is highly unlikely and representative of a worst-case scenario. Hodges et al., suggested (2005) to analyze 100 or more grains as a rule of thumb. Samples with fewer populations and populations with smaller components require a smaller quantity of grains to acquire reasonable statistical results. The number of grains used in this detrital analysis varies from n=45 to n=21. According to Vermeesch (plateau distribution), when n=45, there is 95% confidence that no fraction constituting more than 12% should be missed and when n=21 there is 95% confidence that no fraction constituting more than 20% should be missed (F_{act} >_ 0.12) (to see equations see Vermeesch. 2004).

6. He retentivity and effective uranium concentration (eU)

Changes in He retentivity have been reported multiple times in early studies, where radiation damage clearly has an effect on He diffusivity within zircon (e.g., Nasdala et al., 2004; Reiners and Farley 2001). Very old zircons with high effective

uranium concentrations (which is basically the whole contribution of alphas in relative proportion to uranium using; ^{238}U, ^{235}U, ^{232}Th, ^{147}Sm) have the tendency to destroy their crystalline internal structure by means of alpha emissions and the consequent parent recoil. The radiation damage can be healed as the mineral is subjected to high temperatures, an attribute that helps preserve an amount of radiation damage proportional to a cooling age and not the crystallization age. Since annealing kinetics of zircon are not well understood, the amount of radiation damage endured by a zircon is uncertain but can be approximated by alpha dosage calculations using an approximate annealing age according to the thermal history of the place in question. This calculation approximates how much damage a zircon has experienced based on time eU, concentration and mass, and will allow a determination of the degree of metamictization. The suites of detrital and crystalline zircons collected in the Sinai provide a consistent relationship between eU concentrations and ZHe ages that evidently show the effect of radiation damage on ^{4}He diffusion kinetics. Results lead us to believe that at higher eU concentrations (> 400ppm under Sinai zircon thermal conditions), the closure temperature of zircon will be reduced, making it more sensitive to heating events. Some DZHe ages and basement ZHe ages were excluded due to high metamictization. (See alpha dosage plots vs zircon (U-Th)/He ages in Fig. 9). Alpha dosage calculations do not quantify the amount of radiation that has effectively caused damage (Nasdala, 2004).

Palenik et al. (2003) provided a range of alpha related damage in both crystalline and amorphous Sri Lankan zircon grains by examining microstructures,

spectral signatures and the zircon birefringence using optical microscopy, micro-Raman spectroscopy, electron microprobe analysis, and transmission electron microscopy. The dosage range was 2.1 to 10.1x $10^{\wedge 15}$ alpha decay event/mg. These values are inconsistent with Nasdala et al. (2004), who found that ^{4}He loss occurred mainly on strongly metamict zircon with higher alpha dosage in the order of ~3.5 x $10^{\wedge 18}$ event/mg. They suggest that moderately metamict zircons should still retain ^{4}He. However this is not in agreement with ZHe age vs Alpha dosage plots produced by this study where a clear alpha dosage influence on the ZHe age can be identified several times. Normal distribution of Alpha dosage based on 400 m.y. of radioactive decay reveals that most zircons range between 1.5 x $10^{\wedge 15}$ to 3.0 x $10^{\wedge 16}$ events/mg (Fig. 9), with 8% out of 421 zircon grains analyzed giving higher values and a maximum of 1.3 x $10^{\wedge 17}$ events/mg. These grains belong mainly to the Proterozoic basement and Cretaceous Wata and Malha Fms. Calculated maximum Alpha dosage values, assuming an age of 550Ma, similar to basement crystallization (Kohn, 1996), gave a range of <5.0 x $10^{\wedge 16}$ to 3.6 x $10^{\wedge 17}$ events/mg. Moderate metamictization begins to occur at values higher than 5.0 x $10^{\wedge 16}$ events/mg (Fig. 9).

7. DZHe populations by units

This study combines surface and boreholes samples from a variety of units and locations along the eastern margin of the Gulf of Suez (Figs. 1-2). A great portion of the entire pre-rift sedimentary cover sequence was incorporated into this analysis; additionally the syn-rift Abu Zenima and Nukhul Fms. were analyzed. We

used probability density plots and lag time plots for all the analyzed formations. A few comparisons were made between the sediments north and south of the Markha Plain to identify spatial variations (see Figure 4).

The reset zircon (U-Th)/He ages obtained in the Naqus/Araba Formation resemble the ages recorded in the basement (Fig. 5), suggesting they both share the same thermal history. Three main signatures are characteristic of this unit: Cambrian-Ordovician, Carboniferous, and Triassic/Jurassic signatures (Fig. 4-5).

The next formation analyzed was the Carboniferous Abu Thora Formation. This unit yielded a few DZHe aliquots of Permian age, but the main age populations belong to the late Carboniferous. The age population distribution was highly dispersed suggesting multiple source terranes undergoing exhumation rather than one single, dominant source. Surface samples in the south did not show any reset Permian ages but show strong Carboniferous and Cambrian age populations. The borehole samples yield Permian reset age and Carboniferous to Silurian populations.

Overlying Abu Thora is the Triassic Qiseb formation. Qiseb probability density plots recorded a strong Triassic signature. Additionally, it has a Silurian and a Cambrian population. Unconformably on top is the Lower Cretaceous Malha Fm., as temporally constrained by the ZHe ages (Fig. 4). This formation recorded ages as young as ~110 Ma and has two main populations recorded during the Triassic/Jurassic and the Cambrian/Ordovician.

The upper Cretaceous units start unconformably with the deposition of the Raha Fm., and later Wata and Matulla Fms. The Cenomanian Raha Fm. contains ZHe

detrital ages as young as ~95 Ma. Four populations can be identified, in the Early Cretaceous, Late Jurassic, Permian, and Ordovician.

(U-Th)/He lag-time plots in the Wata Formation indicate 14m.y. depositional lag time (Fig 6). Three populations are characteristic for this unit: [1] Permo-Triassic signature with a higher frequency in the south, [2] Devonian-Silurian signatures with a greater frequency in the north, and [3] Cambrian signature recorded in the south. The Coniacian to Santonian Matulla Fm. preserved DZHe ages belonging to the Santonian (zero depositional lag-time). Other populations were found peaking at the Cambrian, the Late Carboniferous and the Triassic. These units at the south preserve stronger Cambrian and Silurian populations (Fig. 4).

The Late Cretaceous organic rich limestone of the Duwi Formation and the Eocene chert-rich limestone of the Thebes Fm., mainly recorded Triassic Jurassic and Cretaceous ages. A small number of late Paleozoic ages were also present. Mineral separates from both formations have a low zircon yield, preventing analysis of a greater number of zircons.

The Abu Zenima and the Nukhul Fms. were analyzed using detrital zircon. AHe ages were partially or completely reset but ZHe ages were not. Detrital ZHe ages populations were clearly preserved as shown in Figure 4 and 10.

The first syn-rift unit, the Abu-Zenima formation, did not provide any DZHe reset ages but preserve three main detrital populations. The first one belongs to the late Jurassic, the second population peaks at the Permian-Triassic boundary and the

third population corresponds to the Silurian–Ordivician, signature characteristic of the Naqus/Araba formation.

Unconformably overlying is the Nukhul Fm.. The upper and lower Nukhul were analyzed individually due to the high zircon yield. The upper Nukhul samples could well belong to the Lower Rudeis Fm. as there is no direct way to discriminate between them in the field and only foraminifera analysis can reveal their true nature. The Lower Nukhul Fm. shows great variety of DZHe ages starting with ages as old as Early Cretaceous, Jurassic and Triassic/Permian ages. Additionally it records Late Carboniferous, Devonian-Silurian and Cambrian populations. The upper Nukhul Fm. shows DZHe ages as old as the Jurassic and as young as the Eocene. Paleozoic population ages range from the Carboniferous to Cambrian. Notice that the major population pulse corresponds to Jurrasic/Triassic in age on the Nukhul Fm.

8. Tectonics implications and discussion

8.1 Paleozoic and Mesozoic

The zircons analyzed in the Proterozoic basement and Naqus/Araba Fm. have shown a variety of eU concentrations and therefore alpha dosages (Fig. 9), which likely has an effect on the He retentivity. Zircon with high eU concentration values have been proven to decrease He retentivity and lower T_c (Nasdala et al. 2001, 2005), thus recording events at lower temperatures.

ZHe ages from the Naqus/Araba Fm. were completely reset and appear to share the same thermal history as the basement. Above the Naqus/Araba sandstones all the ZHe ages were not reset and are considered to be detrital ages. The last stage of the Pan-African Orogeny was clearly the oldest thermal event still preserve on the Sinai basement and in the Nubian sandstones using ZHE dating. It is consider to be the finals stages of Pan-African deformation because other low temperature thermochronometers like $^{40}Ar/^{39}Ar$ on feldspar (~560-580 Ma, Kohn et al., 1997) with higher closure temperature yield ages more proximal to already establish Arabian massif deformation ages regionally constrained by U-Pb dating at 530-620Ma by Hasson and Hashad, (1990) and Stern and Hedge, (1985). Later Pan-African DZHe ages are recorded in multiple formations including Abu Thora, Qiseb, Malha, Matulla, Nukhul Fms.

The Ordovician DZHe age population was encountered to some degree throughout the stratigraphy. They could correspond to the far north Mid-Arcadian event, because no major tectonism has being recorded in the Sinai for that period. This suggestion although difficult to conceive implies that rocks near Sinai where affected by this far away stress fields or some high energy transportation mechanism carry the detrital zircons to their current location. (see possible population sources in Figure 7).

The Silurian DZHe signature might be related to deformation, uplift and local erosion by continental accretion, such as Baltica and Avalonia being accreted to Laurentia (Stampfli, 1996). Formations like Abu Thora, Qiseib, Raha and Matulla

Fms. have shown strong Silurian DZHe signatures, which are present at a lesser extent in other formations.

The late Carboniferous ("Hercynian") signature encountered in the Sinai basement and in the Nubian sandstones (Fig. 5) is more controversial and might have a more profound implication for the tectonic role of the Sinai during this period. During the Hercynian Orogeny, the Sinai province was located in northeast Africa, an area that did not undergo major deformation during collision with Gondwana, at least not enough to exposed the rocks by uplift above the partial retention zone of zircon (180°C). The peak deformation was endured by northern and western Africa during the Late Carboniferous to Early Permian and resulted in strong folding, thrusting and metamorphism along the North Algerian-Moroccan-Mauritanides Belt (Guiraud et al., 2005). A more likely mechanism for resetting those ZHe ages could be related to hydrothermal fluids produced by back-arc magmatism during the onset of subduction in the Early Carboniferous along the northwest Gondwanan margin (Fig. 5). Other sedimentary formations also recorded these populations, indicating that this source has been present almost in all the pre-rift sediments in a variety of frequencies. Carboniferous Abu Thora Fm. shows the greater frequency followed by Malha and Matulla Fm. indicating rapid cooling at the Northern and Western Africa during Abu Thora depositional time (Fig. 7). Exposure of these blocks during the Santonian inversion could explain the presence of these signatures in the Late Cretaceous units.

Abu Thora Fm. detrital grains have been partially to fully reset by Permian volcanics, volcanism generated by the initiation of Neo-Tetys rifting. Ages were reset

at the central part of the Gulf but not south of the Markha plain (Fig. 4c). This information may be useful in understanding hydrocarbon maturation, although more detrital zircon (U-Th)/He and (U-Pb) ages are needed to support this idea. This and the higher geothermal gradient recorded at the central part of the Gulf during rifting in the Gulf of Suez (acquire data not published), suggest that the central part (specifically the Hamman Faraun block) has sustained higher temperature conditions since the early Sinai tectonic history.

The dividing line between reset and detrital zircon ages is located above the Naqus/Araba Fm., which imply that the youngest ages may represent the last period at which these rocks were exposed to temperatures above or close to the partial retention zone, ~140°C. The youngest reset ZHe ages preserved in the Naqus/Araba Fm. as well as the Proterozoic basement belong to the Late Triassic to Early Jurassic. This suggests that the ZHe partial retention zone was near or above the Naqus /Araba Fm. during the deposition of the Qiseb Fm. in the Late Triassic. This would put the zircon closure temperature (~190°C isotherm) at ~500 m minimum depth below the surface in the central Gulf of Suez during that same period (Fig. 7), this without accounting for the extra overburden before the development of the upper unconformity. This suggests that the Sinai was undergoing a tectono-thermal episode of greater magnitude than that during the Early Miocene rifting. The main tectonic event of that period was the opening of the Neo-Tethys and subsequent subsidence and rifting of the Mediterranean (Guiraud et al., 2005). During the opening of the Neo-Tethys, rifting at the Northeastern part of Africa allowed Turkey to separate

from Africa, leading to the break-up and later development of the Mediterranean Sea. The main structures in the Eastern Mediterranean show faults trending NE-SW similar to the Markha fault current trend. The Triassic-Jurassic structures of the Sinai are not well documented but are likely similar to those known structures in the Eastern Mediterranean basin and north of the Eastern Desert, Egypt. All this evidence suggests that it was more than likely that the Sinai was an active cooling block at this time and that the Markha fault could be a reactivated Cambrian - Triassic structure. Further analysis on Qiseb thickness variation along the Sinai may shed some light on the matter.

The Triassic Qiseib Fm. has a distinct Triassic age signature suggesting that the major source of sediments was being rapidly exhumed and deposited (Figs. 6-7). The sediment source was likely to be the northeastern part of Africa that was undergoing a phase of uplift and erosion related to Neo-Tethys rifting during that period. Late Cretaceous Malha Fm. also shows a strong Triassic signature. Raha, Wata, Matulla and Duwi Fms. show DZHe populations corresponding to early Neo-Tethys rifting. Additionally, the thickness variation in these units is consistent with suggested transportation direction of sediments during that Late Cretaceous (Fig. 8), the northern part being the thicker and more proximal to the source.

The Early Cretaceous DZHe population corresponds to an early compressional Alpine deformational stage. Former Triassic structures were reactivated in Northeastern Africa during this period (Bosworth et al. 1999). Moreover, in Wadi Araba a few miles northwest of the Cretaceous sample collected;

there is a Santonian inversion structure, which probably supplied sediment from the Pan-African, Ordovician, Permo-Triassic and Jurassic sources during the Late Cretaceous in the Sinai (Fig. 7). The presence of Late Paleozoic to Late Mesozoic units in north central Gulf of Suez and their absence in the south contribute to the idea of basin development in the north during the Triassic-Jurassic and Santonian.

8.2 Cenozoic Rifting

The onset of rifting in the Gulf of Suez and in the Red Sea is marked by basaltic volcanism; nevertheless volcanic activity in the Gulf was considerably low compared to the Red Sea. This basaltic flow is dated at approximately 22 Ma by ^{40}K-^{39}Ar (Plaziat et al.,1998b; Stockli and Bosworth, unpublished). Whole rock K-Ar ages from other flows and dikes gave a range of ages from 27-21 Ma (Steen, 1984; Meneisy, 1990; and Plaziat et al., 1998b). Detrital ZHe ages in the Abu Zenima Fm. were mainly Ordovician-Silurian, probably belonging to the pre-rift units that were eroded and deposited in the nearby basin during rift shoulder exhumation (Fig. 8). The Nukhul Fm. shows a wide spread of ages, again due to pre-rift sediment recycling and basement input (Fig. 8). The dominant thermal signatures belong to the Pan-African and Jurrasic/Triassic Neo-Tethys events. Neogene rifting did not reset any zircons.

Detrital apatite fission track dating was employed by Kohn et al. (1996), in syn-rift sediments and Omar et al., (1989) on the western margin rift shoulder. The Syn-rift detrital analysis by Kohn et al. (1996), confirmed recorded detrital thermal signatures with AFT on younger syn-rift units. His work included the Rudeis, Kareen

and Belayin formations. The Rudeis Fm. recorded a strong Jurrasic/Triassic population and a weak Hercynian component. The Kareem Fm. shows a similar affinity as the Rudeis but a stronger Jurassic/Cretaceous and Hercynian component. The Belayim Fm. AFT detrital ages recorded mainly a Hercynian source.

9. Conclusion

In conclusion, the pre-rift detrital zircons from the western Sinai stratigraphy and basement ages, show a variety of tectonically induced thermal signatures, many of which display DZHe ages indistinguishable from their depositional age (nearly zero-lag time) (Fig. 6). One of the most important and influential cooling events recorded besides the Pan African Orogeny (which by far has the highest frequency of all the thermal signatures recorded in the Sinai sedimentary cover) is the Neo-Tethyan rift structures and associated basins that propagate further south into the Sinai area as DZHe ages and fault orientation suggest. Neo-Tethyan structures were later reactivated during the Santonian inversion. These structures contributed greatly to pre and syn-sedimentation and fault development during the early Gulf of Suez rifting.

Signatures such as Hercynian, Silurian and Devonian raise several questions regarding sedimentary dispersal, nearby active tectonism throughout specific periods and the tectonic role of the Sinai at those times. Permian volcanism resetting and sedimentary recycling was well-recorded in zircons on central Sinai on the Abu Thora Fm. Sedimentary recycling was one of the main mechanism for (U-Th)/He ages distribution along central and southern western Sinai on syn-rift sediments, idea based

upon high variability of ZHe ages on Abu Zenima and Nukhul Fms. (Figs. 4 and 8). The pre-rifting detrital thermal history illustrate recorded tectonic events at a thermal magnitude greater than the Miocene rifting in the Gulf of Suez, where no zircon resetting was produced. The new zircon (U-Th)/He data from the basement and sedimentary cover confirm and solidify the idea that pre-existing structures played a greater role in early rifting orientation and geometry development, particularly the role of Mesozoic tectonism previously absent from the literature due to the lack of concrete evidence. These pre-existing structures facilitate displacement of fault blocks and could dictate hard-linkage orientation without significant syn-rift thermal influence in the upper crust. Apatite data on these sediments are partially reset suggesting a range of temperatures from 40-70°C during Early Miocene rifting in the sedimentary cover and not earlier signature could be found using this thermochronometer (Fig. 10).

References (Chapter 3)

Barakat, M.G., Darwish, M., El Barkooky, A.N., 1988, Lithostratigraphy of the Post Carboniferous–Pre Cenomanian clastics in west central Sinai and Gulf of Suez, Egypt. In: Proc. 8th Exploration Conf. Egyptian General Petroleum Corporation, Cairo, November, 1986, v. 1, p. 380–405.

Bernet, M., 2002, Exhuming the Alps through time: Clues from detrital zircon fission-track ages. PhD Dissertation, Yale University, New Haven, Connecticut.

Bernet, M., Garver, J.I., 2005, Fission-track analysis of detrital zircon. Rev Mineral Geochem v. 58, p.205-238

Beydoun, Z.R., 1993, Evolution of the northeastern Arabian plate margin and shelf: Hydrocarbon habitad and conceptual future potential. Revue de 1'institut Francais du Petrole, v. 48, p.311-345.

Bosworth, W., 1994, A model for the three-dimensional evolution of continental rift basins, north-east Africa. Geologisch Rundschau, v. 83, p. 671-688.

Bosworth, W., 1995, A high-strain rift model for the southern Gulf of Suez (Egypt): in Lambiase, J. J., ed., Hydrocarbon Habitat in Rift Basins, Geological Society, London, Special Publication, 80, p. 75-112.

Bosworth, W., Crevello, P., Winn, Jr., R.D., and Steinmetz, J., 1998, Structure, sedimentation, and basin dynamics during rifting of the Gulf of Suez and northwestern Red Sea: in Purser, B.H., and Bosence, D.W.J., eds., Sedimentation and Tectonics of Rift Basins: Red Sea–Gulf of Aden, Chapman and Hall, London, p. 77-96.

Bosworth, W., Guiraud, R., and Kessler, L.G., 1999, Late Cretaceous (ca. 84 Ma) compressive deformation of the stable platform of northeast Africa (Egypt): far-field stress effects of the 'Santonian event' and origin of the Syrian arc deformation belt, *Geology*, **27**, p. 633–636.

Bosworth, W., and McClay, K., 2001, Structural and stratigraphic evolution of the Gulf of Suez rift, Egypt: A synthesis: in P.A. Ziegler, W. Cavazza, A.H.F. Robertson, and S. Crasquin-Soleau, eds., Peri-Tethys Memoir 6: Peri-Tethyan Rift/Wrench Basins and Passive Margins, Mémoires du Muséum National d'Histoire Naturelle de Paris, n. 186, p. 567-606.

Campbell, I.H., Reiners, P.W., Allen, C., Nicolescu, S., Upahdyay, R., 2005, He-Pb double-dating of detrital zirconsnfrom the Ganges and Indus rivers: Implication for quantifying sediment recycling, exhumation rates and provenance studies, Earth Planet Sci Lett, in press

Colletta, B., Le Quellec, P., Letouzey, J. and Morreti, I., 1988, Longitudinal evolution of the Suez rift structure (Egypt). Tectonophysics, 153, p. 221-233

Crossley, R., and McDougall, N., 1998. Lower Palaeozoic reservoirs of North Africa. In: MacGregor, D.S., Moody, R.T.J., Clark-Lowes, D.D. (Eds.), Petroleum Geology of North Africa, Special Publication Geological Society (London), v. 132, p. 157–166.

Darwish, M., 1992, Facies developments of the Upper Paleozoic–Lower Cretaceous sequences in the Northern Galala Plateau and evidences for their hydrocarbon reservoir potentiality, Northern Gulf of Suez, EgyptProceedings 1st International

Conference on Geology of the Arab World, vol. 1. Cairo University, Cairo, p. 75–214.

Darwish, M., 1994, Cenomanian–Turonian sequence stratigraphy, basin evolution and hydrocarbon potentialities of Northern EgyptProceedings of the 2nd International Conference on Geology of the Arab World, vol. 3. Cairo University, Cairo, Egypt, p. 315–362.

Dodson, M.H., 1973, Closure temperature in cooling geochronological and petrological systems, Contributions to Mineralogy and Petrology, v. 40, p. 259-274.

Ehlers, T.A., Farley, K.A., 2003, Apatite (U-Th)/He thermochronometry: methods and applications to problems in tectonics and surface processes. Earth Planet Sci Lett 206:1-14

El Barkooky, A.N., 1992, Stratigraphic framework of the Paleozoic in the Gulf of Suez Region, Egypt. In: 1st international Conference on the Geology of the Arab World. Cairo University, Cairo.

Evans, A.L., 1990, Miocene Sandstone Provenance Relations in the Gulf of Suez: Insights into synrift Unroofing and Uplift History, American Association of Petroleum Geologists Bulletin, 74, 1386-1400.

Farley, K.A., 2000, Helium diffusion from apatite: General behavior as illustrated by Durango fluorapatite, Journal of Geophysical Research, v. 105, p. 2903-2914.

Farley, K.A., 2002, (U-Th)/He dating: Techniques, calibrations, and applications in: Noble Gases in Geochemistry and Cosmochemistry, Reviews in Mineralogy and Geochemistry, v. 47, p. 819-844.

Farley, K.A., Reiners, P.W., and Nenow, V., 1999, An apparatus for high-precision helium diffusion measurements from minerals. Analytical Chemistry, v. 71, p. 2059-2061.

Farley, K.A., Wolf, R., and Silver, L., 1996, The effects of long alpha-stopping distances on (U-Th)/He ages, Geochimica et Cosmochimica Acta, v. 60, p. 4223-4229.

Feinstein, S., Kohn, B.P., Steckler, M.S., and Eyal, M., 1996, Thermal history of the eastern margin of the Gulf of Suez, 1. Reconstruction from borehole temperature and organic maturity measurements, Tectonophysics 266 (1996), p. 203–220.

Garfunkel Z., 1998, Constraints on the origin and history of the Eastern Mediterranean basin. Tectonophysics, 298, p. 5–37

Gass, I.G., and Gibson, I.L., 1969, Structural Evolution of the rift zones of the middle east. Nature, V.221, no.5184, p. 926-930.

Genna, A., Vaslet, D., Janjou, D., Le Metour, J., and Halawani M., 2000, Rifting of the Arabian platform during the proterozoic to phanerozoic interval. GeoArabia, Abstract, v. 5, n. 1, p. 94-95.

Ghorab, M.A., 1961, Abnormal stratigraphic features in Ras Gharib oil field. 3rd Arabian Petroleum Congress, Alexandria, Egypt, 10 p.

Guiraud, R., 1998, Mesozoic rifting and basin inversion along the northern African Tethyan margin: an overview. In: MacGregor, D.S., Moody, R.T.J., Clark-Lowes, D.D. (Eds.), Petroleum Geology of North Africa. Geological Society, London, Special Publication 133, p. 217–229.

Guiraud, R., and Bosworth, W., 1995, Phanerozoic geological evolution of Northern and Central Africa: an overview. Journal of African Earth Sciences.

Guiraud, R., and Bosworth, W., 1997, Senonian basin inversion and rejuvenation of rifting in Africa and Arabia: synthesis and implications to plate-scale tectonics, Tectonophysics 282, p. 39–82

Guiraud, R., and Bosworth, W., 1999, Phanerozoic geodynamic evolution of northeastern Africa and the northwestern Arabian platform. Tectonophysics 315, p. 73–108.

Guiraud, R., Bosworth, W., Thierry, J., and Delplanque, A., 2005, Phanerozoic geological evolution of Northern and Central Africa: an overview, J. Afr. Earth. Sci., 43, p. 83–143.

Guiraud, R., Issawi, B., and Bosworth, W., 2001, Phanerozic history of Egypt and surrounding areas: In: Ziegler, P.A., Cavazza, W., Robertson, A.H.F., Crasquin-Soleau, S. (Eds.), Peri-Tethys Memoir 6: Peri-Tethyan Rift/Wrench Basins and Passive Margins, Mémoires du Muséum National d'Histoire Naturelle de Paris 186, p. 469–509.

Hassan, A.A., 1967, A new Carboniferous occurrence in Abu Durba-Sinai, Egypt. In: 6th Arabian Petroleum Congress, Baghdad 2, 39 (B-3), 8 p.

Hassan, M.A. and Hashad, A.H., 1990, The Geology of Egypt, Precambrian of Egypt. Balkema, Rotterdam: In: R.Said (ed.), Chapter 12, p. 201-245.

Hodges, K.V., Ruhl, K.W., Wobus, C.W., and Pringle M.S., 2005, 40Ar/39Ar thermochronology of detrital minerals. See Reiners & Ehlers 2005, v.58, p. 239-257

House, M.A., Farley, K.A., and Kohn, B., 1999, An empirical test of helium diffusion in apatite: borehole data from the Otway basin, Australia, Earth and Planetary Science Letters, v. 170, p. 463-474.

Hurley, P.M., and Fairbairn, H.W., 1953, Radiation damage in zircons: a possible age method. Bull Geol Soc Am 64, p. 659-674.

Ketcham, R.A., Donelick, R.A., and Carlson, W.D., 1999, Variability of apatite fission-track annealing kinetics: III. Extrapolation to geological time scales. Am Mineral 84, p. 1235-1255

Klitzsch, E., 2000, The structural development of the Murzuq and Kufra basins—significance for oil and mineral exploration. In: Sola, M.A., Worsley, D. (Eds.), Geological Exploration in Murzuq Basin. Elsevier Science, Amsterdam, Chapter 7, p. 143–149.

Kora, M., 1984, The Paleozoic Outcrops of Um Bogma Area, Sinai. Ph.D.Thesis, Mansoura University, Mansoura, Egypt, 233 p.

Kohn, B.P. and Eyal, M., 1981, 'History of uplift of the crystalline basement of Sinai and its relation to opening of the Red Sea as revealed by fission track dating of apatites' Earth and Planetary Science Letters, 52, p. 129–141.

Kohn, B.P., Feinstein, S., Foster, D.A., Steckler, M.S., and Eyal, M., 1997, Thermal history of the eastern Gulf of Suez, II. Reconstruction from apatite fission track and 40Ar/39Ar K-feldspar measurements.Tectonophysics. 283, p. 219-239.

Laslett, G.M., Green, P.F., Duddy, I.R., and Gleadow, A.J.W., 1987, Thermal annealing of fission tracks in apatite. 2. A quantitative analysis. Chem Geol (Isot Geosci Sect) 65, p.1-13

McClay, K., and Khalil, S., 1998, Extensional hard linkages, eastern Gulf of Suez, Egypt, Geology 26 (1998), p. 563–566.

McClay, K.R., Nicols, G.J., Khalil, S.M., Darwish, M., and Bosworth, W., 1998, Extensional tectonics and sedimentation, eastern Gulf of Suez, Egypt: in Purser, B.H., and Bosence, D.W.J., eds., Sedimentation and Tectonics of Rift Basins: Red Sea–Gulf of Aden, Chapman and Hall, London, p. 223-238.

McClure, H.A., 1978, Early Paleozoic glaciation in Arabia. Paleogeography Palaeoclimatology palaeocology, v. 25, p. 315-326

Meneisy, M.Y., 1990, Vulcanicity. In: R. Said (ed.), The geology of Egypt Balkema, Rotterdam, Chapter 9, p. 157-172.

Mitchell, S.G., and Reiners, P.W., 2003, Influence of wildfires on apatite and zircon (UTh)/He ages. Geology, v. 31, p. 1025-1028.

Moretti, I. and Colletta, B., 1987, Spatial and temporal evolution of the Suez Rift subsidence. Journal of Geodynamics, 7, p. 151-168.

Moustafa, A.R., 1997, Controls on the development and evolution of transfer zones; the influence of basement structure and sedimentary thickness in the Suez Rift and Red Sea. Journal of Structural Geology, 19, p. 755-768.

Moustafa, A.R., 2002, Controls on the geometry of transfer zones in the Suez Rift and Northwest Red Sea; implications for the structural geometry of rift systems. In: Underhill, J. R., and Trudgill, B. D., (eds.), The structure and stratigraphy of rift systems. AAPG Bulletin, 86, p. 979-1002.

Nasdala, L., Hanchar, J.M., Kronz, A., and Whitehouse, M.J., 2005, Long-term stability of alpha particle damage in natural zircon. Chemical Geology v. 220, p. 83–103.

Nasdala, L., Wenzel, M., Vavra, G., Irmer, G., Wenzel, T., and Kober, B., 2001, Metamictisation of natural zircon: accumulation versus thermal annealing of radioactivity-induced damage. Contribution to Mineralogy Petrology v. 141, p. 125–144.

Omar G.I., and Steckler M.S., 1995, Fission-track evidence on the initial rifting of the Red Sea: two pulses, no propagation. Science 270, p.1341–44

Omar, G.I., Steckler, M.S., Buck, W.R., and Kohn, B.P., 1989, Fission-track analysis of basement apatites at the western margin of the Gulf of Suez rift, Egypt: evidence for synchroneity of uplift and subsidence. Earth and Planetary Science Letters, 94, p. 316-328.

Omar, G.I., Steckler, M.S., Buck, W.R., and Kohn, B.P., 1989, Fission-track analysis of basement apatites at the western margin of the Gulf of Suez rift, Egypt: Evidence for synchroneity of uplift and subsidence: Earth and Planetary Science Let- ters, v. 94, p. 316-328.

Patton, T.L., Moustafa, A.R., Nelson, R.A., and Abdine, S. A., 1994, Tectonic evolution and structural setting of the Suez Rift, in Landon, S. M., ed., Interior rift basins: American Association of Petroleum Geologists Memoir 59, p. 9–55.

Parrish R.R., and Noble S.R., 2003, Zircon U-Th-Pb geochronology by isotope dilution—thermal ionization mass spectrometry (ID-TIMS). Rev Mineral Geochem 53, p.183-213

Plaziat, J.C., Montenat, C., Barrier, P., Janin, M., Orszag-Sperber, F. and Philobbos, E., 1998, Stratigraphy of the Egyptian Syn-rift deposits: correlations between axial and peripheral sequences of the north-western Red Sea and Gulf of Suez and their relations with tectonics and eustacy. In: B.H. Purser & D.W.J. Bosence (eds). Sedimentation and Tectonics of rift Basins: Red Sea-Guf of Aden. Chapman and Hall, London, p. 211-222.

Savostin, L. A., Sibuet, J.C., Zonenshain, L.P., Le Pichon, X. and Roulet, M.J., 1986, Kinematic evolution of the Tethys belt from the Atlantic Ocean to the Pamirs since the Triassic. Tectonophysics, 123, p. 1-35.

Scott, R.W., and Govean, F.M., 1985, Early depositional history of a rift basin: Miocene in the western Sinai. Palaeogeography, Palaeoclimatology, Palaeoecology 52, p. 143–158.

Steen, G., 1984, Radiometric age dating of some Gulf of Suez igneous rocks. In: Proceedings of 6th Exploration seminar, Cairo, March 1982. Vol.1. Egyptian General Petroleum Corporation and Egypt Petroleum Exploration Society, Cairo, p. 199-211.

Stern, R.J., 1985, The Najd Fault system, Saudi Arabia and Egypt: a late PreCambrian rift-related transform system? Tectonics, v. 4, p. 497-511.

Stern, R., and C. Hedge, 1985, Geochronological and isotopic constraint on the late Precambrian crustal evolution in the Eastern Desert of Egypt: American Journal of Science, v. 258, p. 97-127.

Sharland, P.R., Archer, R., Casey, D.M., Davies, R.B., Hall, S.H., Heward, A.P., Horbury, A.D., and Simmons, M.D., 2001, Arabian Plate Sequence Stratigraphy. GeoArabia Special Publication 2, Gulf PetroLink, Bahrain, p. 371.

Sharp, I.R., Gawthorpe, R.L., Underhill, J.R., and Gupta, S., 2000, Fault-propagation folding in extensional settings: Examples of structural style and syn-rift sedimentary response from the Gulf of Suez Rift, Sinai, Egypt. Geological Society of America Bulletin, 112, p. 1877-1899.

Shuster, D.L., Farley, K.A., Sisterson, J.M., and Burnett, D.S., 2004, Quantifying the diffusion kinetics and spatial distributions of radiogenic 4He in minerals containing proton-induced 3He. Earth Planet Sci Lett 217, p. 19-32

Steckler, M.S., Berthelot F., Lyberis N. and Le Pichon X., 1988, Subsidence in the Gulf of Suez: Implications for rifting and plate kinematics. Tectonophysics, 153, p. 249-270.

Steckler, M.S. and U.S. ten Brink, 1986, Lithospheric strength variations as a control on new plate boundaries: Examples from the northern Red Sea region. Earth and Planetary Science Letters, 79, p. 120-132.

Stockli, D., 2005, Application of low-temperature thermochronometry to extensional tectonic settings. Review in Mineralogy and Geochemistry. v 58, p. 411-448. in Reiners, P.W., and Ehlers, T.A., Low Temperature Thermochronology: Techniques, Interpretations and Applications, Reviews in Mineralogy and Geochemistry, v. 58, p. 123-149.

Stockli, D.F., Farley, K.A. and Dumitru, T.A., 2000, Calibration of the (U-Th)/He thermochronometer on an exhumed normal fault block in the White Mountains, eastern California and western Nevada. Geology, v. 28, n. 11, p. 983–986.

Stoeser, D.B., and Camp, V.E., 1985, Pan-African Micro-plate accretion of the Arabian shield. Geological society of America Bulletin, v. 96, p.817-826.

Stump, T.E., Al-Hajri, S., and Van der Eem, J.G.L.A., 1995. Geology and biostratigraphy of the Late Precambrian through Palaeozoic sediments of Saudi Arabia. Rev. Palaeobot. Palynol. 89, p. 5–17.

Sutcliffe, O.E., Harper D.A.T., Ait Salem A., Whittington R.J., and Craig J., 2000, The development of an atypical Hirnantia-brachiopod fauna and the onset of glaciation in the late Ordovician of Gondwana. Transactions of the royal society of Edinburgh Earth Science, 90.

Reich, M., Ewing, R., Ehlers, T, Becker, U., 2007, Low-temperature anisotropic diffusion of helium in zircon: implications for zircon (U-TH)/He thermochronometry. Geochimica Et Cosmochimica Acta, v. 71, p. 2119-3130.

Reiners, P., 2005, Zircon (U-Th)/He Thermochronometry, in Reiners, P. W. and Elhers, T. A., Low Temperature Thermochronology: Techniques, Interpretations and Applications, Reviews in Mineralogy and Geochemistry, v. 58, p. 151-179.

Reiners, P., Campbell, I., Nicolescu, S., Allen, C., Hourigan. J., 2005b, (U-Th)/(He-Pb) double dating of detrital zircons. Am. J. Sci. 305, p. 259–311.

Reiners, P.W., Ehlers, T.A., Zeitler, P.K., 2005b, Past, present, and future of thermochronology. In See Reiners & Ehlers 2005, 58, p. 1–18.

Reiners, P., and Farley, K., 1999, He diffusion and (U-Th)/He thermochronometry of titanite, Geochimica et Cosmochimica Acta, v. 62, p. 3845-3859

Reiners, P.W., Farley K.A., 2001, Influence of crystal size on apatite (U-Th)/He thermochronology: an example from the Bighorn Mountains, Wyoming. Earth Planet Sci Lett 188, p. 413-420

Reiners, P., Farley, K., and Hickes, H., 2002, He diffusion and (U–Th)/He thermochronometry of zircon: initial results from Fish Canyon Tuff and Gold Butte. Tectonophysics, v. 349, p. 297-308.

Reiners, P., Spell, T., Nicolescu, S., Zanetti, K., 2004, Zircon (U-Th)/He thermochronometry: He diffusion and comparisons with Ar-40/Ar-39 dating. Geochimica Et Cosmochimica Acta v. 68, Ph, p. 1857-1887

Richardson, M., and Arthur, M.A., 1988. The Gulf of Suez - northern Red Sea Neogene rift: A quantitative basin analysis. Marine and Petroleum Geology, p. 247-270.

Tamsett, D., 1984, Comments on the development of rifts and transform faults during continental breakup; examples from the Gulf of Aden and northern Red Sea. Tectonophysics, 104, p. 35-46.

Van der Beek, P.A., Cloetingh S., and Andriessen P.A.M., 1994, Mechanisms of extensional basin formation and vertical motions at rift flanks: Constraints from tectonic modelling and fission track thermochronology. Earth Planet Sci Lett 121, p. 417–433

Vaslet, D., 1990, Upper Ordovician Glaciar Deposits in Saudi Arabia. Episodes, 13, p. 147-487.

Vermeesch, P., 2004, How many grains are needed for a provenance study?, Earth Planet. Sci. Lett. 224, p. 351–441.

Vermeesch, P., 2008, Three new ways to calculate average (U-Th)/He ages. Chemical Geology 249, p. 339-347.

Weissbrod, T., 1969, The Paleozoic of Israel and adjacent countries, part 2 The Paleozoic outcrops in southwestern Sinai and their relation with those of southern Israel, v. 48. Geological Survey of Israel, 32 p.

Younes, A.I., and McClay, K.R., 2002, Development of accommodation zones in the Gulf of Suez-Red Sea Rift, Egypt. In: Underhill, J. R., and Trudgill, B. D., (eds.), The structure and stratigraphy of rift systems. AAPG Bulletin, 86, p. 1003-1026.

Zeitler, P.K., Herczeg, A.L., McDougall, I., and Honda, M., 1987, U-Th-He dating of apatite: A potential thermochronometer. Geochimica et Cosmochimica Acta, v. 51, p. 2865-2868.

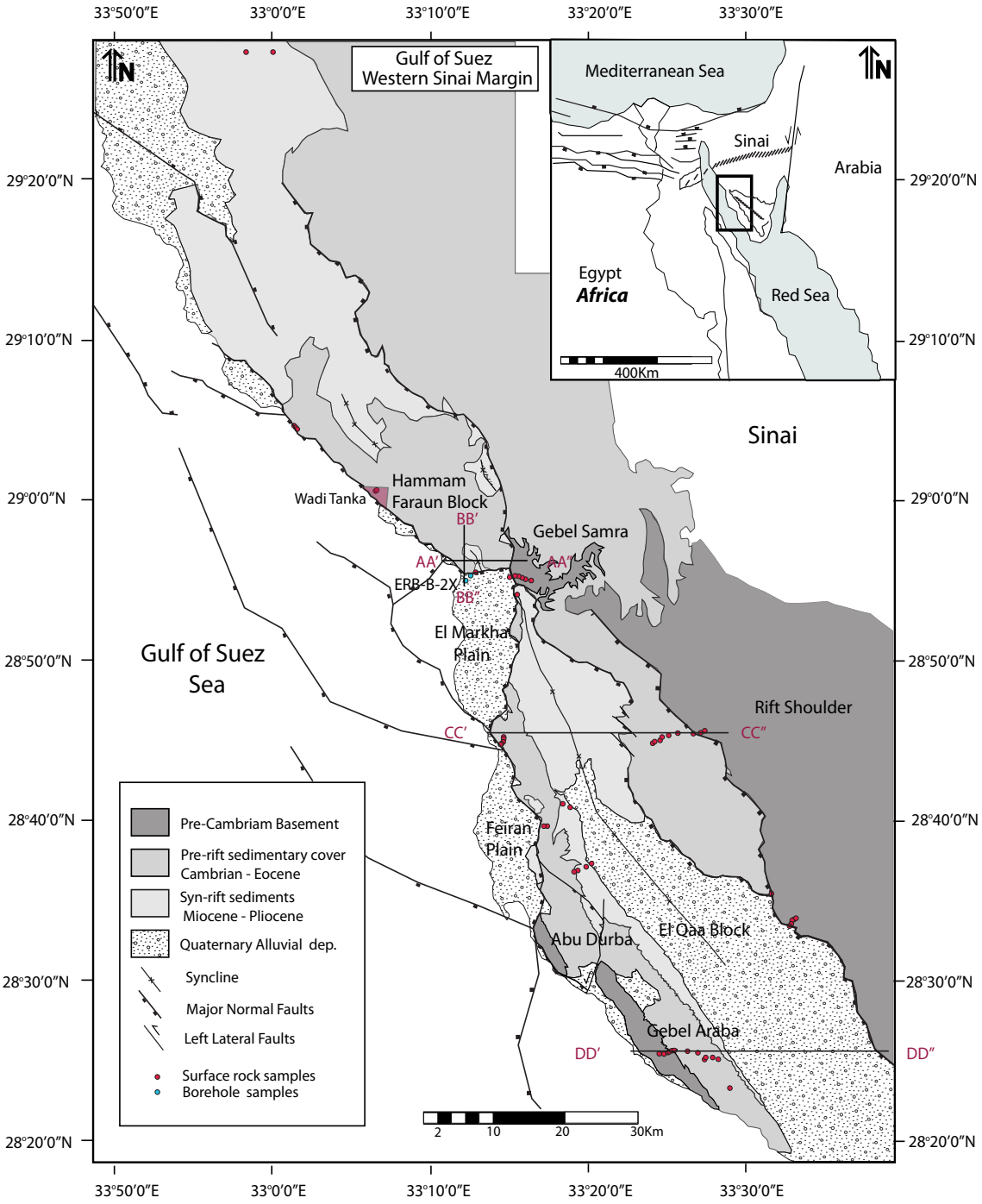
Gulf of Suez
Western Sinai Margin
Mediterranean Sea
Sinai
Arabia
Egypt
Africa
Red Sea
400Km
Sinai
Hammam
Faraun Block
Wadi Tanka
BB′
AA′
AA″
ERB-B-2X
BB″
Gebel Samra
El Markha
Plain
Gulf of Suez
Sea
Rift Shoulder
CC′
CC″
Feiran
Plain
Abu Durba
El Qaa Block
Gebel Araba
DD′
DD″
Pre-Cambriam Basement
Pre-rift sedimentary cover
Cambrian - Eocene
Syn-rift sediments
Miocene - Pliocene
Quaternary Alluvial dep.
Syncline
Major Normal Faults
Left Lateral Faults
Surface rock samples
Borehole samples
2
10
20
30Km
33°50′0″E
33°0′0″E
33°10′0″E
33°20′0″E
33°30′0″E
29°20′0″N
29°10′0″N
29°0′0″N
28°50′0″N
28°40′0″N
28°30′0″N
28°20′0″N

Figure 1. Generalized eastern Gulf of Suez geologic map showing distribution of major faults, the granitoid basement and pre- and syn-rift sedimentary sequences. Red dots are the samples collected strategically along different fault blocks, we integrate vertical transects plus surface and boreholes samples for this study. Four cross section lines were made from central to southern Gulf.

Cross Sections, Western Sinai

1 : 1

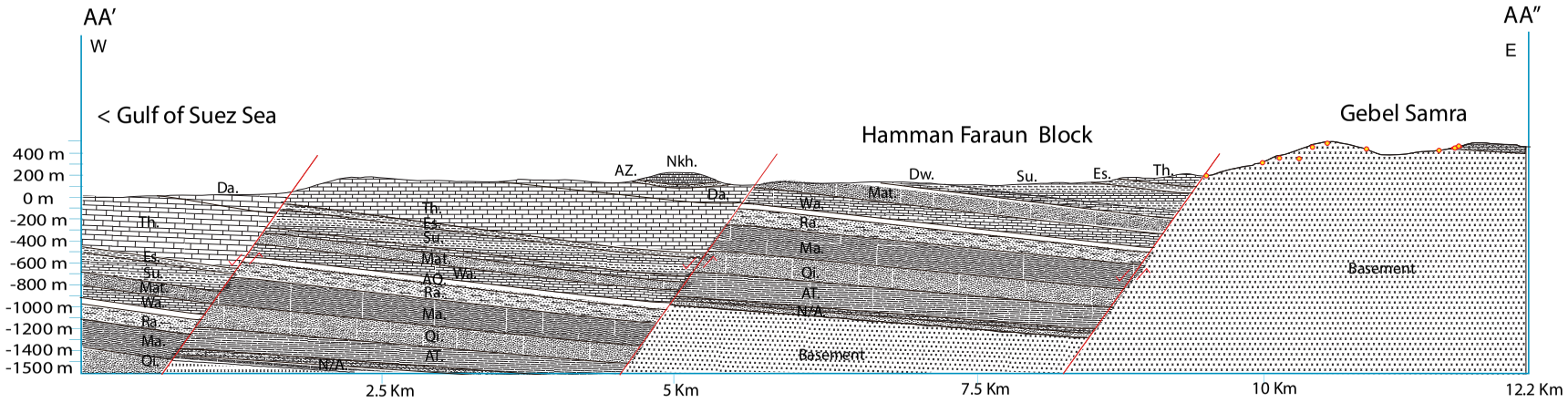

Legend

Nukhul	Nkh.		Wata	Wa.	
Abu Zenima	AZ.		Abu Qada	AQ.	
Darat	Da.		Raha	Ra.	
Thebes	Th.		Malha	Ma.	
Esna	Es.		Qiseib	Qi.	
Sudr	Su.		Abu Thora	AT.	
Duwi	Dw.		Naqus/Araba	N/A.	
Matulla	Mat.				

a

Cross Sections, Western Sinai

1 : 1

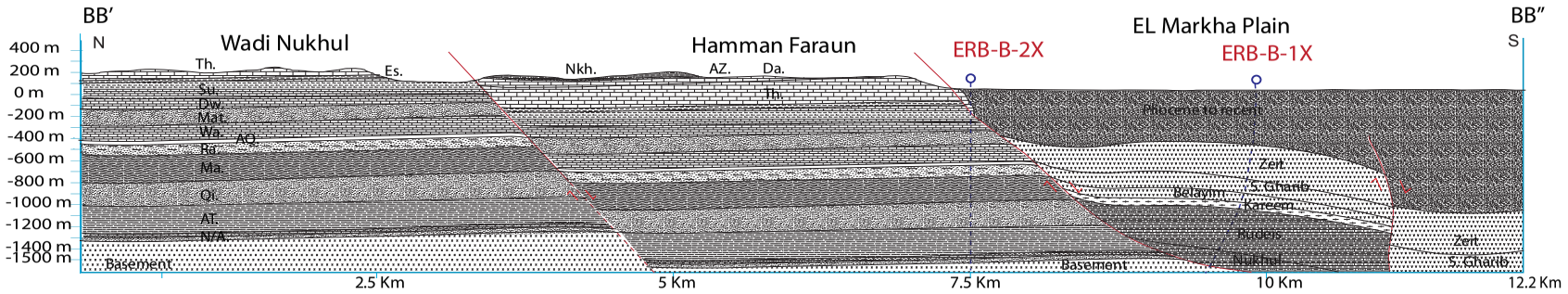

Legend

Nukhul	Nkh.		Wata	Wa.	
Abu Zenima	AZ.		Abu Qada	AQ.	
Darat	Da.		Raha	Ra.	
Thebes	Th.		Malha	Ma.	
Esna	Es.		Qiseib	Qi.	
Sudr	Su.		Abu Thora	AT.	
Duwi	Dw.		Naqus/Araba	N/A.	
Matulla	Mat.				

b

Cross Sections, Western Sinai

1 : 1

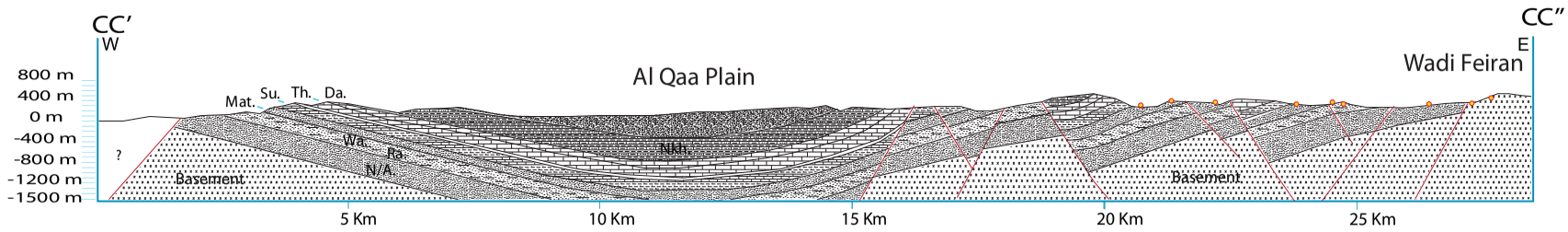

Legend

Nukhul	Nkh.		Wata	Wa.	
Abu Zenima	AZ.		Abu Qada	AQ.	
Darat	Da.		Raha	Ra.	
Thebes	Th.		Malha	Ma.	
Esna	Es.		Qiseib	Qi.	
Sudr	Su.		Abu Thora	AT.	
Duwi	Dw.		Naqus/Araba	N/A.	
Matulla	Mat.				

Cross Sections, Western Sinai

1 : 1

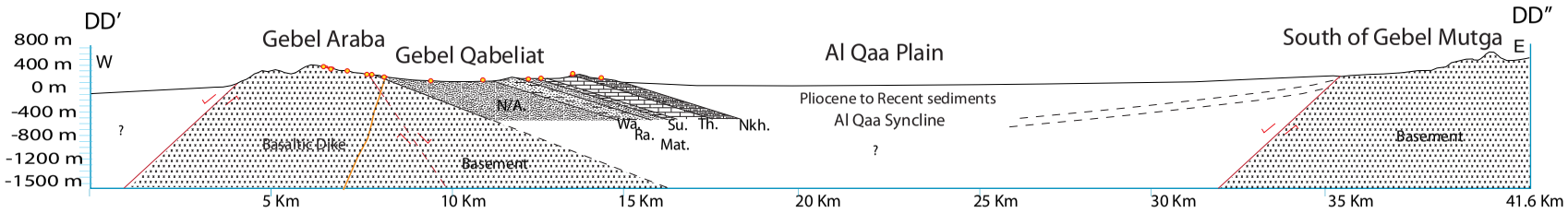

Legend

Nukhul	Nkh.		Wata	Wa.	
Abu Zenima	AZ.		Abu Qada	AQ.	
Darat	Da.		Raha	Ra.	
Thebes	Th.		Malha	Ma.	
Esna	Es.		Qiseib	Qi.	
Sudr	Su.		Abu Thora	AT.	
Duwi	Dw.		Naqus/Araba	N/A.	
Matulla	Mat.				

Figure 2a-d. Cross sections show the current eastern margin structural configuration from central to southern Gulf of Suez. The vertical transects are illustrated in three of the sections a,c-d., additionally the boreholes ERB-B-2X and 1X are illustrated in section b.

a

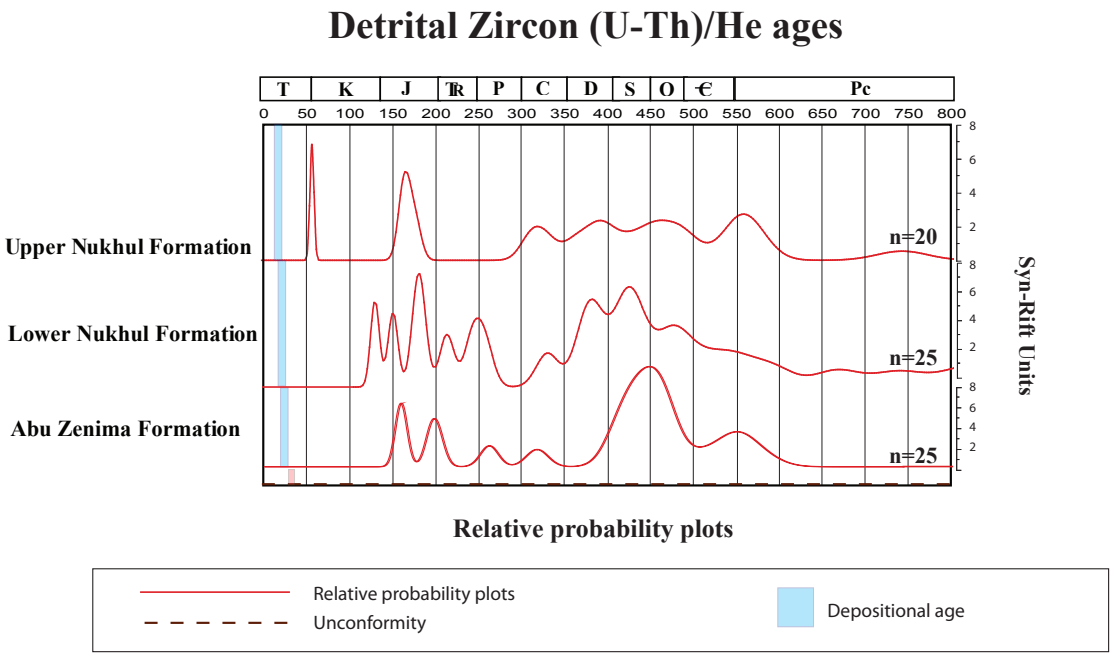
Detrital Zircon (U-Th)/He ages
T
K
J
TR
P
C
D
S
O
Pc
0 50 100 150 200 250 300 350 400 450 500 550 600 650 700 750 800
Upper Nukhul Formation
Lower Nukhul Formation
Abu Zenima Formation
n=20
n=25
n=25
Syn-Rift Units
Relative probability plots
Relative probability plots
Unconformity
Depositional age

b

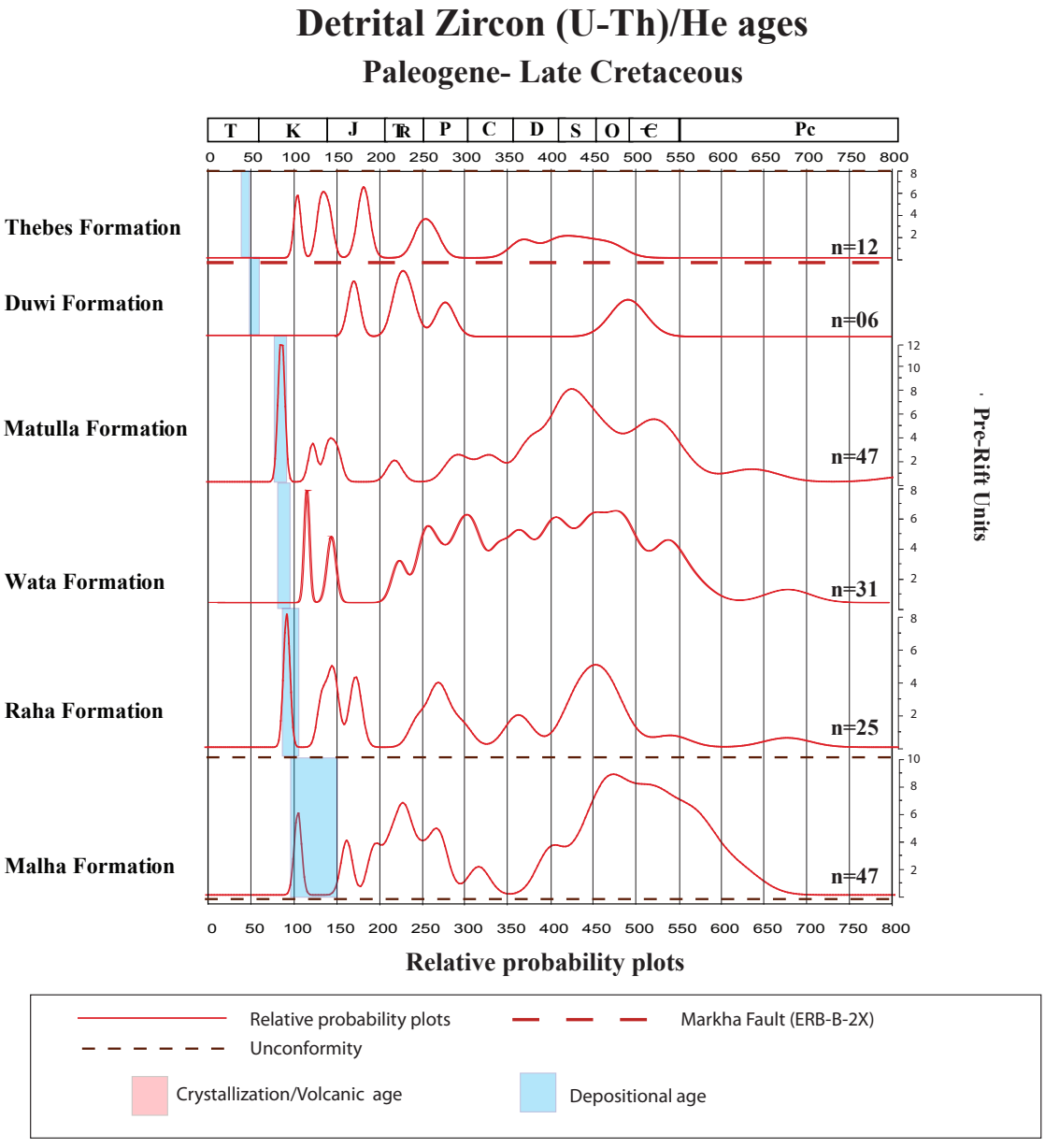
Detrital Zircon (U-Th)/He ages
Paleogene- Late Cretaceous
T
K
J
Tr
P
C
D
S
O
Pc
Thebes Formation
Duwi Formation
Matulla Formation
Wata Formation
Raha Formation
Malha Formation
n=12
n=06
n=47
n=31
n=25
n=47
Pre-Rift Units
Relative probability plots
Relative probability plots
Markha Fault (ERB-B-2X)
Unconformity
Crystallization/Volcanic age
Depositional age

C

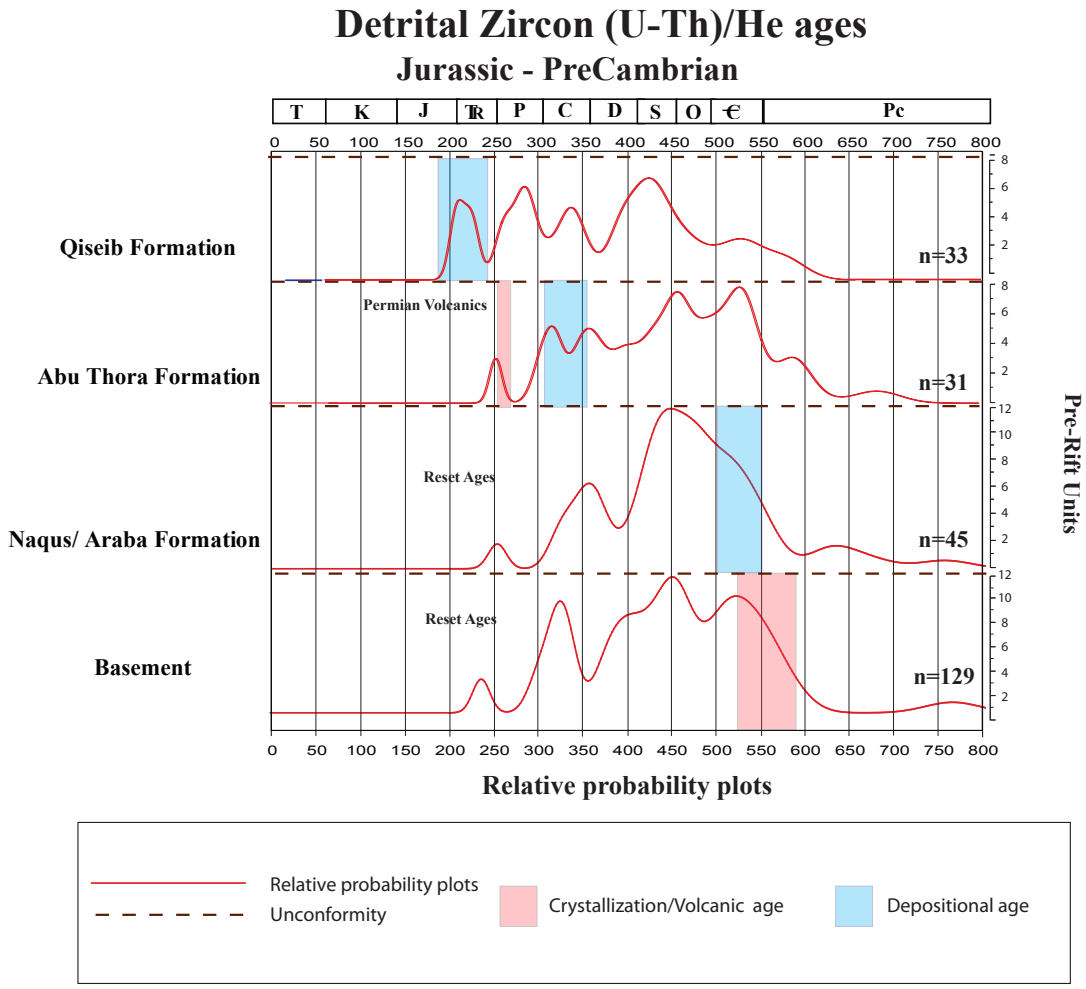
Detrital Zircon (U-Th)/He ages
Jurassic - PreCambrian
T
K
J
TR
P
C
D
S
O
Pc
0 50 100 150 200 250 300 350 400 450 500 550 600 650 700 750 800
Qiseib Formation
n=33
Permian Volcanics
Abu Thora Formation
n=31
Reset Ages
Naqus/ Araba Formation
n=45
Reset Ages
Basement
n=129
Pre-Rift Units
Relative probability plots
Relative probability plots
Unconformity
Crystallization/Volcanic age
Depositional age

Figure 3a-c. Combined borehole and surface sample zircon probability density plots showing a variety of (U-Th)/He detrital populations found in different pre- and syn rift sedimentary units. The blue smaller columns represent the stratigraphically constrained depositional age. Notice that the last plot (c) are zircons ages that belong to a granitoid basement and are recording multiple tectonic events due to their high concentration variation of eU (diffusion kinetics affected by alpha damage reducing Tc).

a

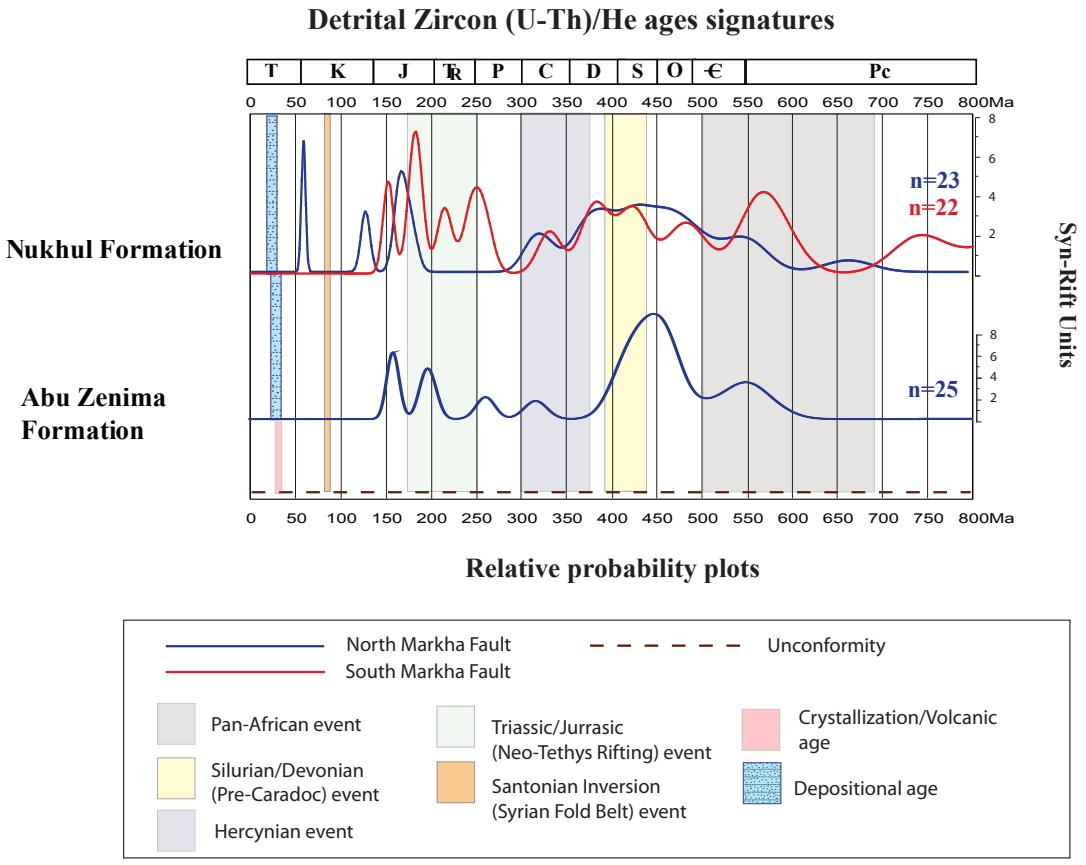
Detrital Zircon (U-Th)/He ages signatures
T
K
J
TR
P
C
D
S
O
Є
Pc
0 50 100 150 200 250 300 350 400 450 500 550 600 650 700 750 800Ma
Nukhul Formation
Abu Zenima Formation
n=23
n=22
n=25
8
6
4
2
Syn-Rift Units
Relative probability plots
North Markha Fault
South Markha Fault
Unconformity
Pan-African event
Silurian/Devonian (Pre-Caradoc) event
Hercynian event
Triassic/Jurrasic (Neo-Tethys Rifting) event
Santonian Inversion (Syrian Fold Belt) event
Crystallization/Volcanic age
Depositional age

b

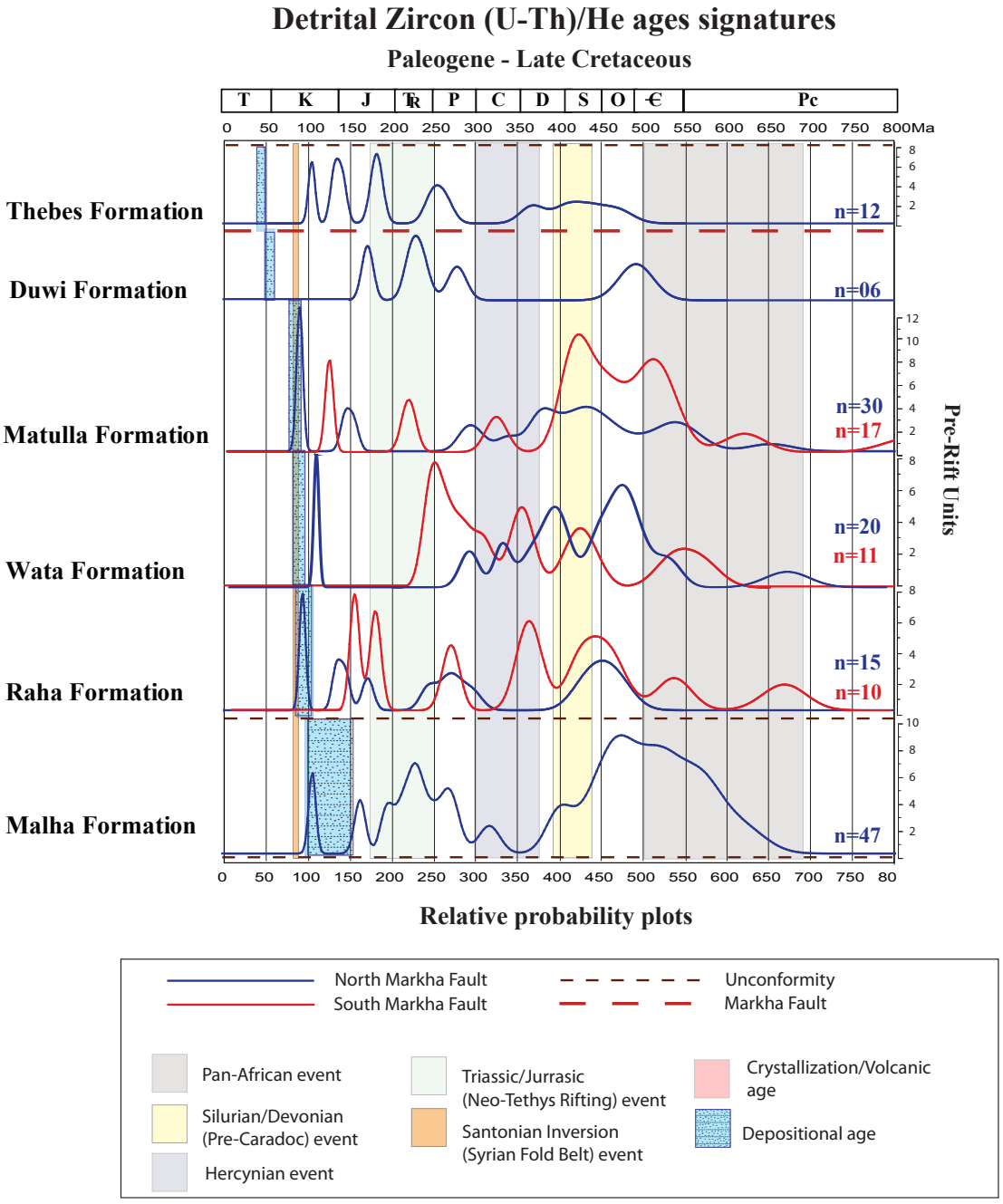
Detrital Zircon (U-Th)/He ages signatures
Paleogene - Late Cretaceous
T
K
J
Tr
P
C
D
S
O
Є
Pc
0 50 100 150 200 250 300 350 400 450 500 550 600 650 700 750 800Ma
Thebes Formation
n=12
Duwi Formation
n=06
Matulla Formation
n=30
n=17
Wata Formation
n=20
n=11
Raha Formation
n=15
n=10
Malha Formation
n=47
Pre-Rift Units
0 50 100 150 200 250 300 350 400 450 500 550 600 650 700 750 80
Relative probability plots
North Markha Fault
South Markha Fault
Unconformity
Markha Fault
Pan-African event
Silurian/Devonian
(Pre-Caradoc) event
Hercynian event
Triassic/Jurrasic
(Neo-Tethys Rifting) event
Santonian Inversion
(Syrian Fold Belt) event
Crystallization/Volcanic
age
Depositional age

C

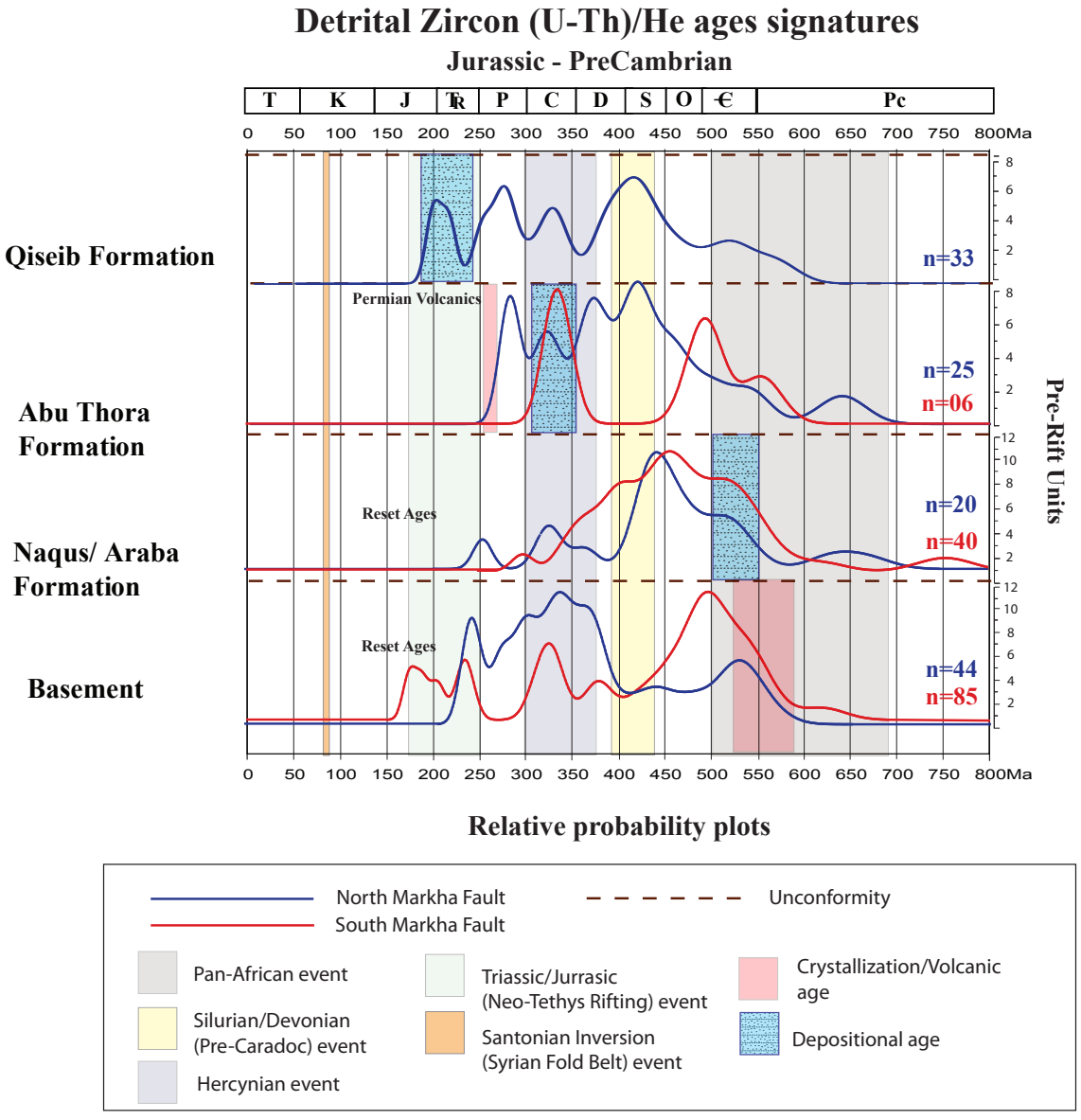
Detrital Zircon (U-Th)/He ages signatures
Jurassic - PreCambrian
T
K
J
Tr
P
C
D
S
O
Pc
0 50 100 150 200 250 300 350 400 450 500 550 600 650 700 750 800Ma
Qiseib Formation
Abu Thora Formation
Naqus/ Araba Formation
Basement
Permian Volcanics
Reset Ages
Reset Ages
n=33
n=25
n=06
n=20
n=40
n=44
n=85
Pre-Rift Units
Relative probability plots
North Markha Fault
South Markha Fault
Unconformity
Pan-African event
Silurian/Devonian (Pre-Caradoc) event
Hercynian event
Triassic/Jurrasic (Neo-Tethys Rifting) event
Santonian Inversion (Syrian Fold Belt) event
Crystallization/Volcanic age
Depositional age

Figure 4a-c. Fundamentally the same as Figure 3a-c., notice that two diferent probablility density plots were overlap with the porpuse of identifing and segregate frequency variations within the units at north and south of the Markha fault.

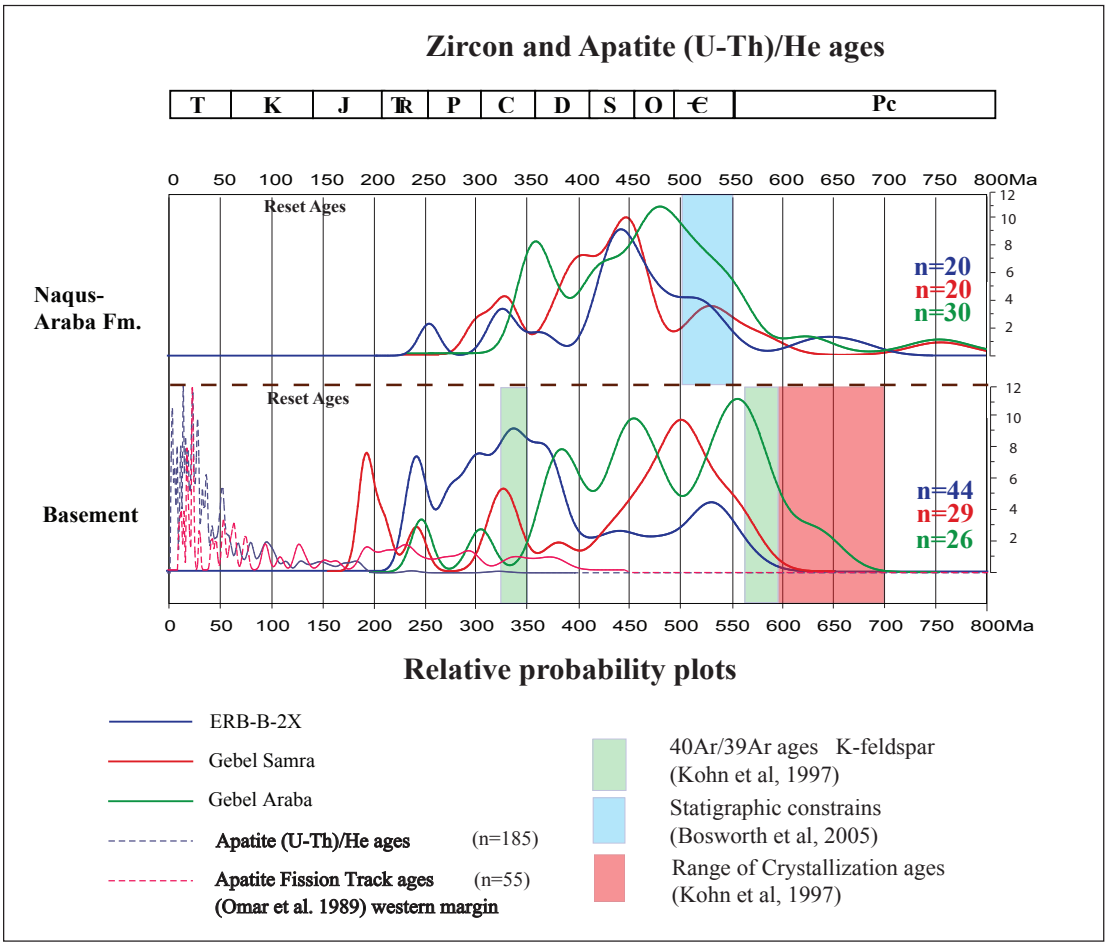
Zircon and Apatite (U-Th)/He ages
T
K
J
Tr
P
C
D
S
O
Pc
0 50 100 150 200 250 300 350 400 450 500 550 600 650 700 750 800Ma
Reset Ages
Naqus-
Araba Fm.
n=20
n=20
n=30
Reset Ages
Basement
n=44
n=29
n=26
12
10
8
6
4
2
Relative probability plots
ERB-B-2X
Gebel Samra
Gebel Araba
Apatite (U-Th)/He ages (n=185)
Apatite Fission Track ages (n=55)
(Omar et al. 1989) western margin
40Ar/39Ar ages K-feldspar
(Kohn et al, 1997)
Statigraphic constrains
(Bosworth et al, 2005)
Range of Crystallization ages
(Kohn et al, 1997)

Figure 5. The zircon (U-Th)/He ages from the Naqus-Araba Fm. were completely reset and recorded the same thermal history as the crystalline basement. There are three different probability density plots per unit, one for each transect. Additionally apatite fission track basement data from Omar et al. (1989), Ar-Ar (K-feldspar) data from Kohn et al., (1997) and apatite (U-Th)/He ages from this study were added to the plots.

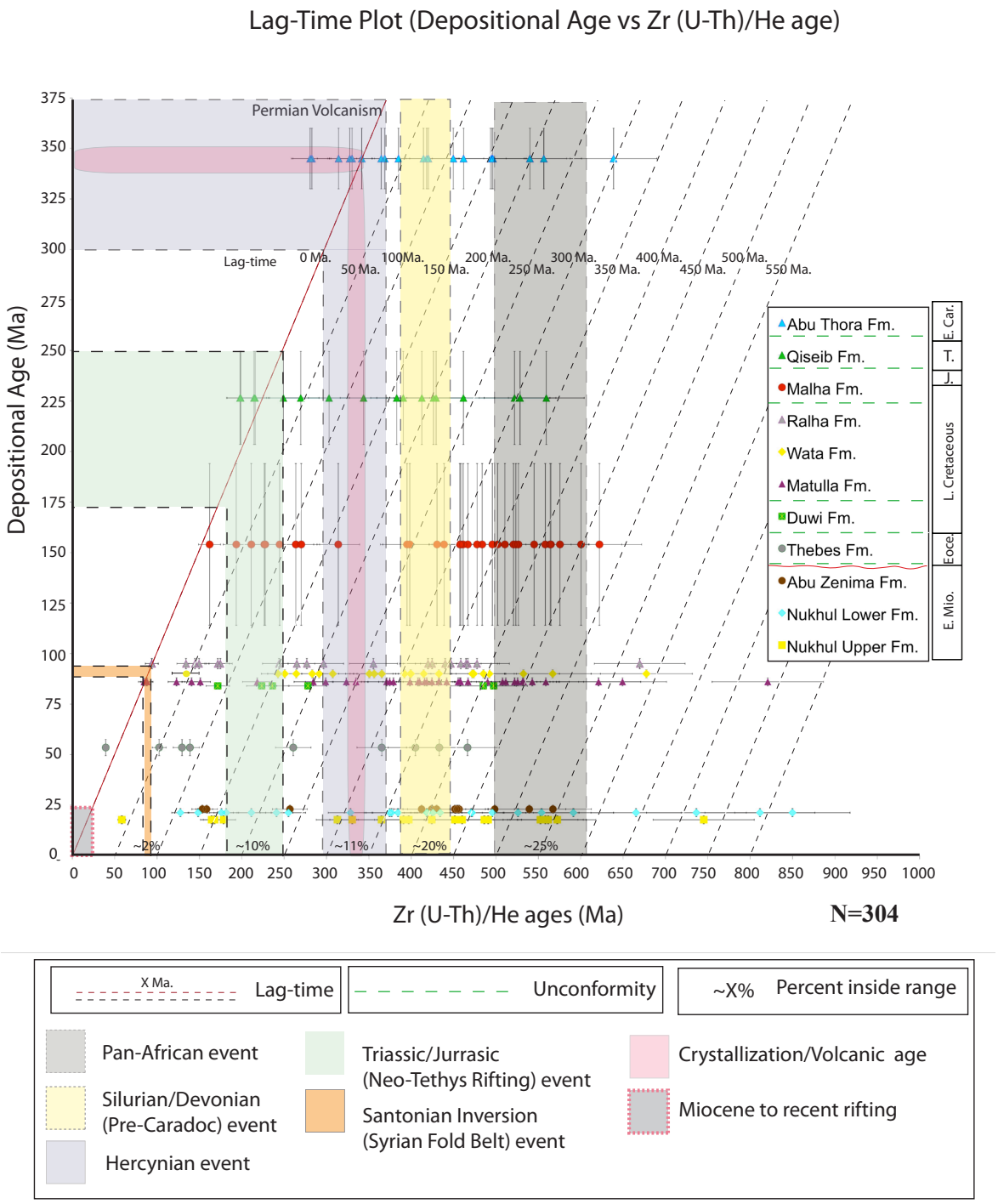
Lag-Time Plot (Depositional Age vs Zr (U-Th)/He age)
Depositional Age (Ma)
Zr (U-Th)/He ages (Ma)
N=304
Permian Volcanism
Lag-time
0 Ma.
50 Ma.
100 Ma.
150 Ma.
200 Ma.
250 Ma.
300 Ma.
350 Ma.
400 Ma.
450 Ma.
500 Ma.
550 Ma.
~2%
~10%
~11%
~20%
~25%
Abu Thora Fm.
Qiseib Fm.
Malha Fm.
Ralha Fm.
Wata Fm.
Matulla Fm.
Duwi Fm.
Thebes Fm.
Abu Zenima Fm.
Nukhul Lower Fm.
Nukhul Upper Fm.
E. Car.
T.
J.
L. Cretaceous
Eoce.
E. Mio.
X Ma.
Lag-time
Unconformity
~X%
Percent inside range
Pan-African event
Silurian/Devonian
(Pre-Caradoc) event
Hercynian event
Triassic/Jurrasic
(Neo-Tethys Rifting) event
Santonian Inversion
(Syrian Fold Belt) event
Crystallization/Volcanic age
Miocene to recent rifting

Figure 6. This lag time plot show the majority of the pre-Miocene rift units with zero depositional lag time. The age ranges of major tectonic events are represented by columns of diferent colors. The percentage given at the bottom of the column indicates how many aliquots fall within the column out of the total N analyzed.

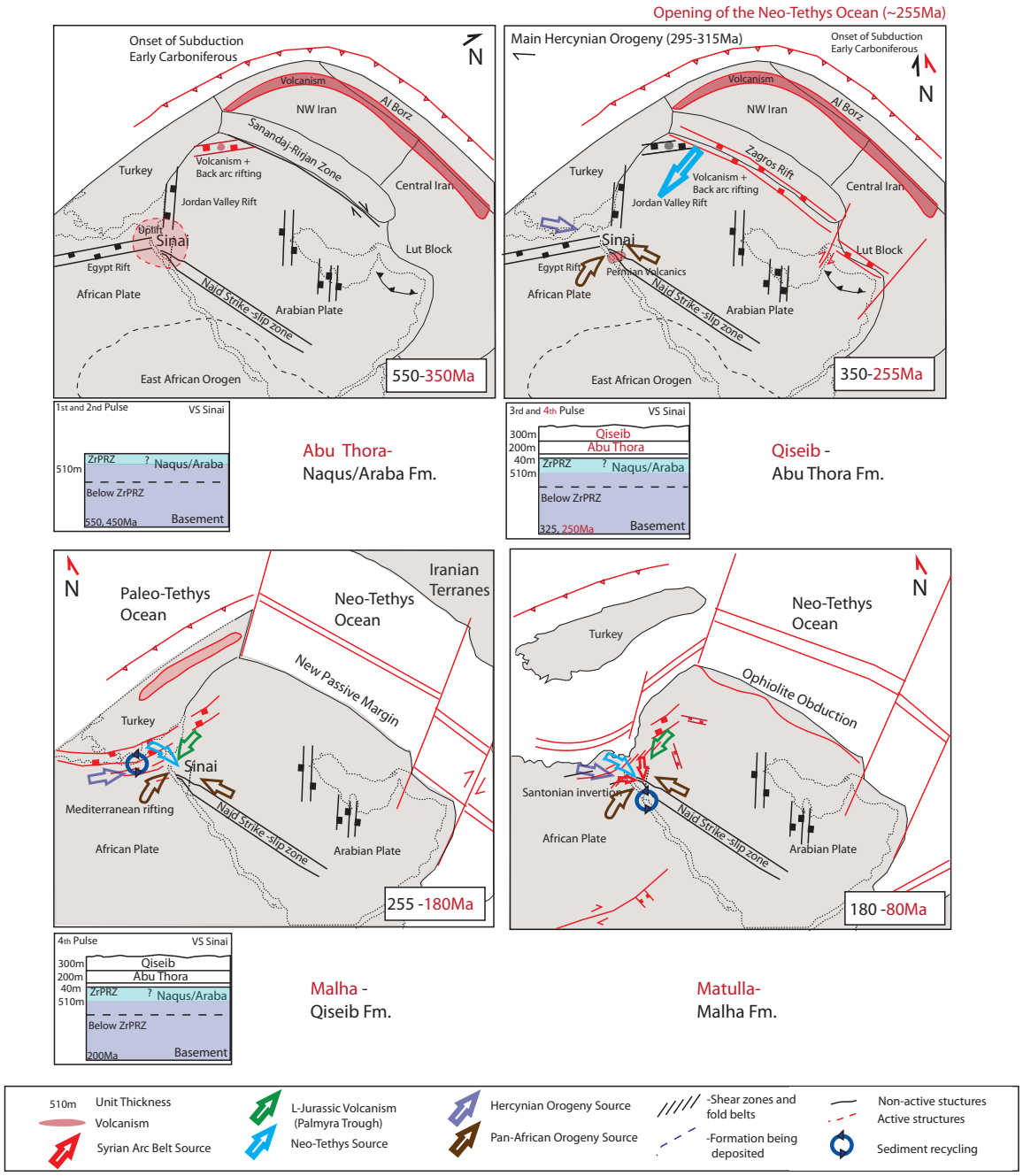
Opening of the Neo-Tethys Ocean (~255Ma)
Onset of Subduction
Early Carboniferous
N
Volcanism
NW Iran
Al Borz
Sanandaj-Rirjan Zone
Volcanism +
Back arc rifting
Turkey
Central Iran
Jordan Valley Rift
Uplift
Sinai
Egypt Rift
Lut Block
African Plate
Arabian Plate
Naid Strike -slip zone
East African Orogen
550-350Ma
Main Hercynian Orogeny (295-315Ma)
Onset of Subduction
Early Carboniferous
Zagros Rift
Permian Volcanics
350-255Ma
1st and 2nd Pulse
VS Sinai
510m
ZrPRZ
? Naqus/Araba
Below ZrPRZ
550, 450Ma
Basement
Abu Thora-
Naqus/Araba Fm.
3rd and 4th Pulse
300m
200m
40m
Qiseib
Abu Thora
325, 250Ma
Qiseib -
Abu Thora Fm.
Paleo-Tethys
Ocean
Neo-Tethys
Ocean
Iranian
Terranes
New Passive Margin
Mediterranean rifting
255 -180Ma
Ophiolite Obduction
Santonian invertion
180 -80Ma
4th Pulse
200Ma
Malha -
Qiseib Fm.
Matulla-
Malha Fm.
Unit Thickness
Volcanism
Syrian Arc Belt Source
L-Jurassic Volcanism
(Palmyra Trough)
Neo-Tethys Source
Hercynian Orogeny Source
Pan-African Orogeny Source
-Shear zones and
fold belts
-Formation being
deposited
Non-active stuctures
Active structures
Sediment recycling

Figure 7. This sketch (modified from Sharland et al., 2001) shows the transport direction of sedimentary sources according to zircon (U-Th)/He rapidly cooled ages in pre-rift units. A correlation was made between zircon (U-Th)/He ages and areas that suffered major tectonism (and likely rapid cooling) throughout the different depositional units. The small boxes at the left corner of the figures illustrate the most likely location of the zircon partial retention zone at different ages. Base map represent the previous tectonic configuration.

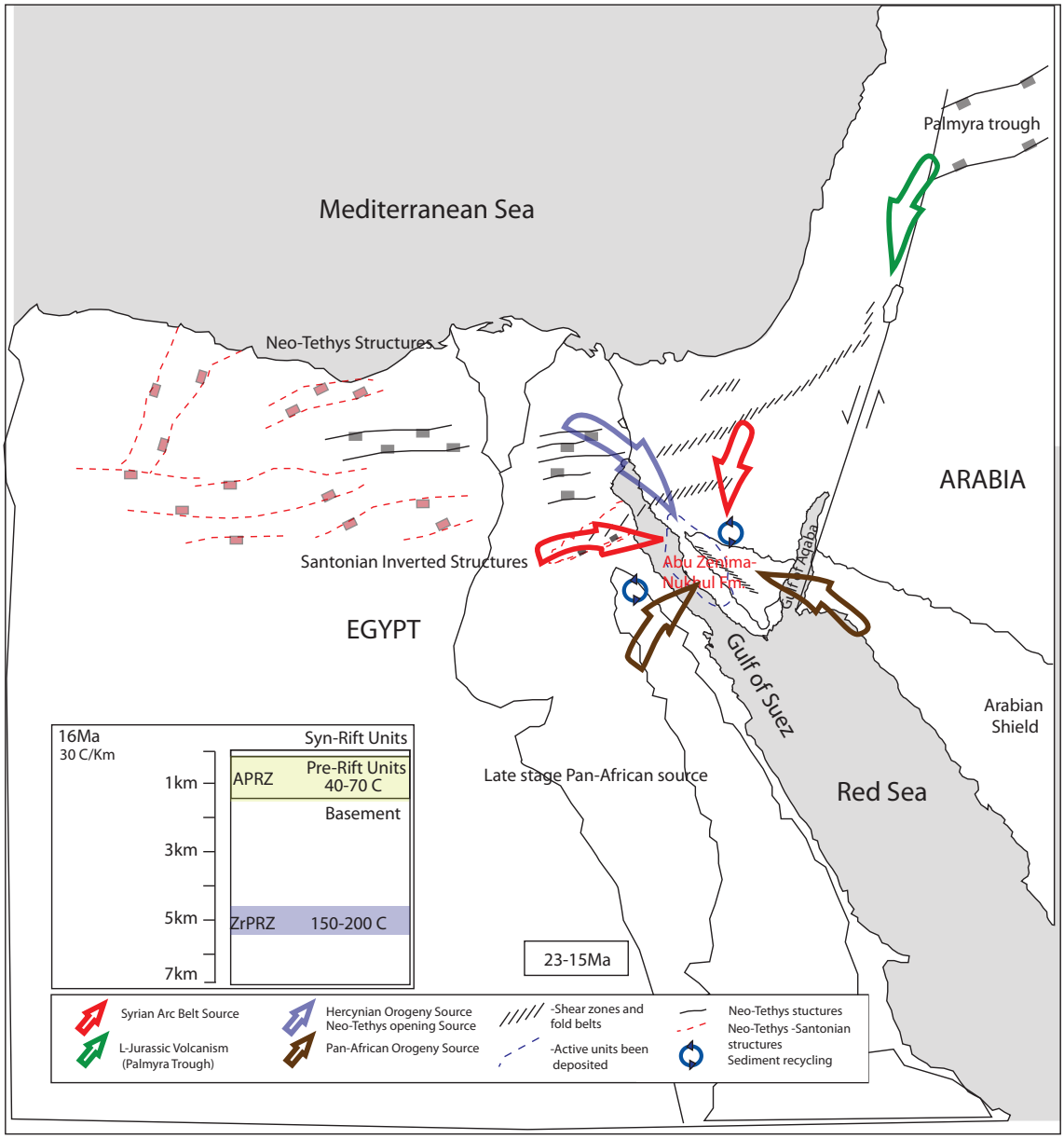
Mediterranean Sea
Palmyra trough
Neo-Tethys Structures
ARABIA
Santonian Inverted Structures
Abu Zenaima-
Nukhul Fm.
EGYPT
Gulf of Suez
Arabian
Shield
Late stage Pan-African source
Red Sea
16Ma
30 C/Km
Syn-Rift Units
1km
APRZ
Pre-Rift Units
40-70 C
Basement
3km
5km
ZrPRZ
150-200 C
7km
23-15Ma
Syrian Arc Belt Source
L-Jurassic Volcanism
(Palmyra Trough)
Hercynian Orogeny Source
Neo-Tethys opening Source
Pan-African Orogeny Source
-Shear zones and
fold belts
-Active units been
deposited
Neo-Tethys stuctures
Neo-Tethys -Santonian
structures
Sediment recycling

Figure 8. This sketch illustrates the syn-rift sedimentary sources. Recycling of pre-rift units as a result of high angle fault geometry is very common, which explains the variety of signatures in the Nukhul and Abu Zenima Fm. Detrital apatites were partially reset during Miocene rifting by thermal pulses

Alpha Dosage at 200, 350, 450, 550Ma.
Zr (U-Th)/He ages vs Alpha Dosage

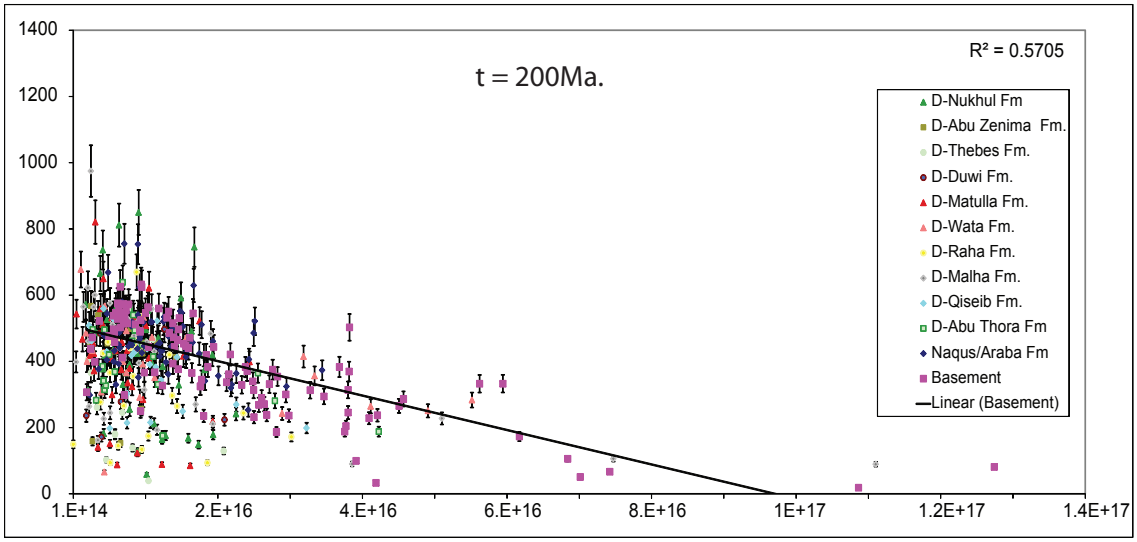

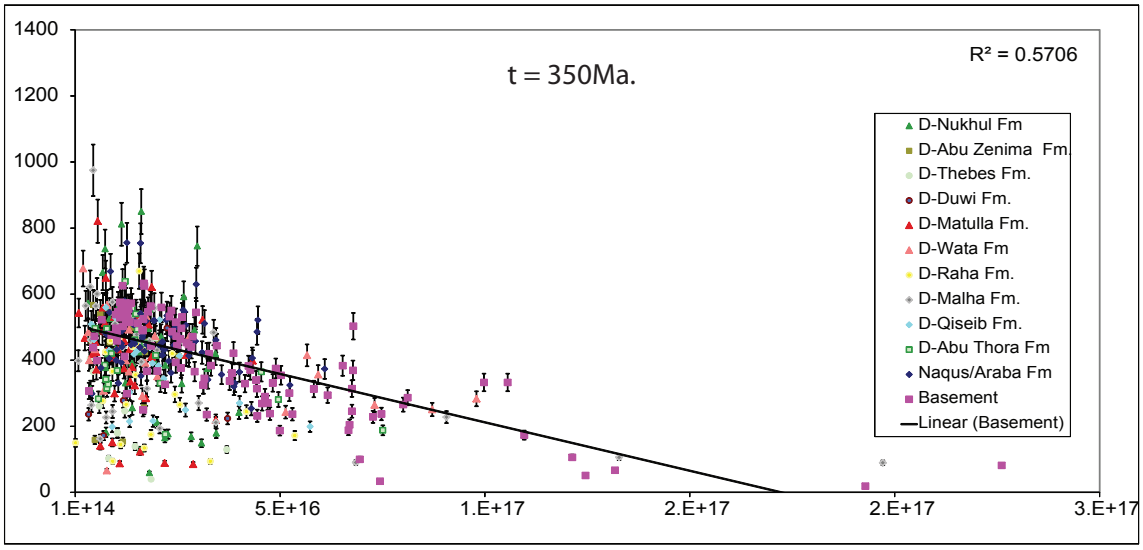

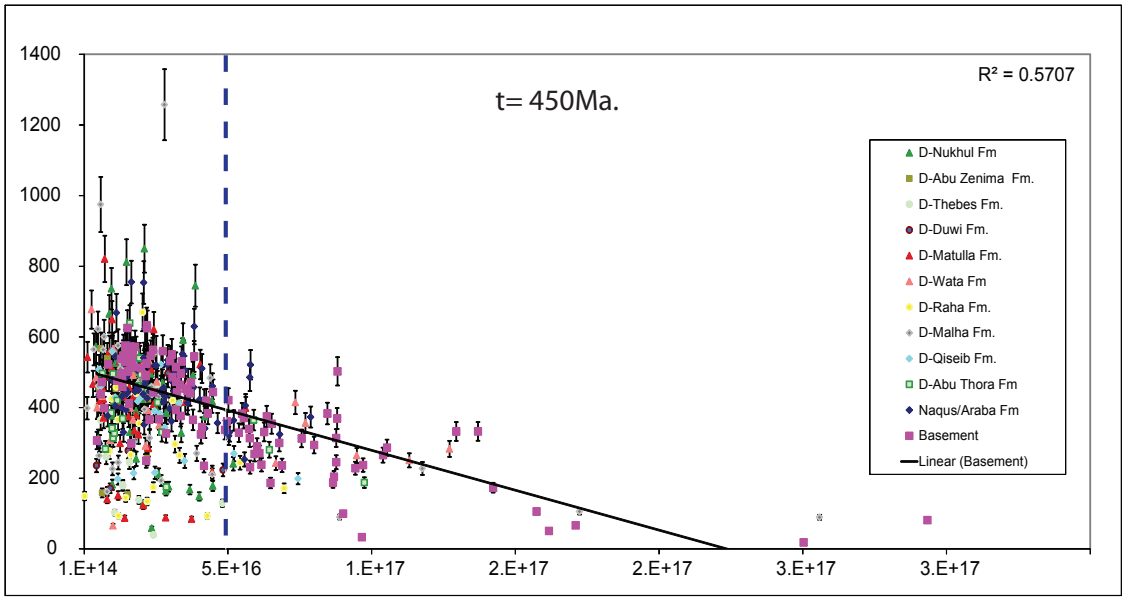
t= 450Ma.
R² = 0.5707
1400
1200
1000
800
600
400
200
0
1.E+14
5.E+16
1.E+17
2.E+17
2.E+17
3.E+17
3.E+17
D-Nukhul Fm
D-Abu Zenima Fm.
D-Thebes Fm.
D-Duwi Fm.
D-Matulla Fm.
D-Wata Fm
D-Raha Fm.
D-Malha Fm.
D-Qiseib Fm.
D-Abu Thora Fm
Naqus/Araba Fm
Basement
Linear (Basement)

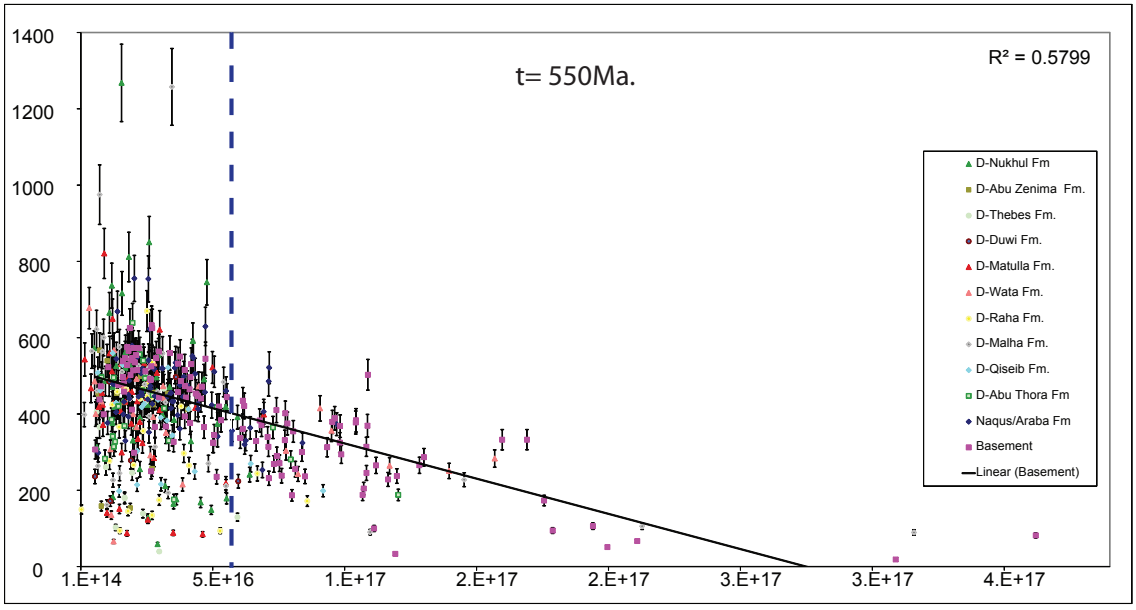
t= 550Ma.
R² = 0.5799
1400
1200
1000
800
600
400
200
0
1.E+14
5.E+16
1.E+17
2.E+17
2.E+17
3.E+17
3.E+17
4.E+17
D-Nukhul Fm
D-Abu Zenima Fm.
D-Thebes Fm.
D-Duwi Fm.
D-Matulla Fm.
D-Wata Fm.
D-Raha Fm.
D-Malha Fm.
D-Qiseib Fm.
D-Abu Thora Fm
Naqus/Araba Fm
Basement
Linear (Basement)

Figure 9. These plots show detrital zircon (U-Th)/He ages versus alpha dosage at 200, 350, 450 and 550Ma. The great majority of the detrital aliquots do not show high alpha dosage values. Basement and Naqus-Araba Fm. show an age and alpha dosage dependency. Blue dashed line (~5.0E16 and above) in the 450 and 550Ma separates zircon (U-Th)/He that show dependency to alpha dosage from those that do not.

Zircon and Apatite (U-Th)/He Chemistry Tables and Fluid Inclusion Data

Table 1. Zircon (U-Th)/He geochemistry data and ages

Sample	*Age [Ma]*	*± [Ma]*	*U (ppm)*	*Th (ppm)*	*Sm (ppm)*	*Th/U*	*He (nmol/g)*	*mass (μg)*	*Ft*	*eU*
Nukhul										
zERB01-1	255.09	20.41	111.39	34.38	0.00	0.31	110.83	1.50	0.66	119.30
zERB01-2	384.33	30.75	169.73	79.81	0.00	0.47	290.21	3.00	0.72	188.11
zERB01-3	849.85	67.99	130.30	34.03	0.00	0.26	507.37	4.50	0.75	138.13
zERB01-4	181.63	14.53	60.12	21.31	0.00	0.35	45.50	2.40	0.71	65.02
z08GS02-01	460.07	36.81	130.35	99.00	3.94	0.76	281.67	3.32	0.72	153.16
z08GS02-02	312.89	25.03	29.31	15.13	0.06	0.52	39.72	2.52	0.70	32.79
z08GS02-03	178.50	14.28	283.90	43.64	4.91	0.15	191.15	1.59	0.67	293.97
z08GS02-04	164.37	13.15	179.84	31.96	0.55	0.18	114.30	1.78	0.68	187.20
z08GS02-05	58.46	4.68	146.98	34.49	0.55	0.23	35.53	3.21	0.72	154.92
z08GS02-06	397.02	31.76	151.06	60.57	1.38	0.40	274.83	4.53	0.76	165.01
z08GS04-01	167.92	13.43	219.80	95.04	1.34	0.43	150.90	2.03	0.68	241.69
z08GS04-02	558.24	44.66	58.53	27.83	0.00	0.48	139.18	2.01	0.69	64.93
z08GS04-03	390.81	31.26	108.12	48.12	2.84	0.45	184.76	2.56	0.72	119.22
z08GS04-04	364.91	29.19	95.54	67.49	1.50	0.71	151.79	1.82	0.68	111.08
z08GS06-01	376.79	30.14	59.11	21.19	0.83	0.36	93.34	2.18	0.70	64.00

** Aliquot age was excluded from the analysis because an analitical error was made (ICP, He-line, grain broken during unpacking processs etc.)

Sample	*Age [Ma]*	*± [Ma]*	*U (ppm)*	*Th (ppm)*	*Sm (ppm)*	*Th/U*	*He (nmol/g)*	*mass (µg)*	*Ft*	*eU*
z08GS06-02	425.63	34.05	68.35	29.68	0.95	0.43	122.91	1.92	0.69	75.19
z08GS06-03	495.65	39.65	133.75	81.41	1.98	0.61	291.71	2.30	0.69	152.50
z08GS06-04	127.51	10.20	120.19	67.04	0.34	0.56	66.31	2.65	0.70	135.62
z08GS06-05**	1731.12	138.49	176.17	48.19	4.09	0.27	1385.72	1.75	0.68	187.28
z08GS06-06	434.06	34.73	75.68	40.29	0.59	0.53	134.77	1.51	0.66	84.96
z08GS07-01	418.34	33.47	66.50	7.17	0.76	0.11	120.61	4.78	0.76	68.16
z08GS07-02	470.76	37.66	169.39	42.88	0.83	0.25	345.25	3.29	0.73	179.26
z08GS07-03	665.23	53.22	51.40	28.93	0.74	0.56	166.67	4.93	0.76	58.06
z08GS07-04	525.97	42.08	64.16	33.86	0.79	0.53	154.67	3.45	0.73	71.96
z08GS14-01	552.50	44.20	100.83	29.40	0.32	0.29	242.07	2.88	0.73	107.60
z08GS14-02	486.23	38.90	45.85	17.95	0.38	0.39	95.83	2.39	0.71	49.98
z08GS14-03	330.37	26.43	97.27	34.60	0.21	0.36	142.46	4.39	0.74	105.24
z08GS14-04	451.35	36.11	141.34	61.28	1.11	0.43	289.72	4.08	0.74	155.45
z09ADGS01-1	490.76	39.26	230.71	77.74	2.31	0.34	479.87	2.33	0.70	248.62
z09ADGS01-2	572.30	45.78	22.67	21.46	0.36	0.95	67.27	4.99	0.76	27.61
z09ADGS01-3	745.13	59.61	231.14	100.33	1.92	0.43	805.17	3.73	0.74	254.25
z09ADGS01-5	561.59	44.93	81.17	40.02	0.54	0.49	205.61	3.32	0.72	90.39
z09ADGS01-6	424.23	33.94	122.68	53.00	0.76	0.43	239.62	4.69	0.75	134.89
z09ADGS02-1	148.49	11.88	243.07	87.13	1.96	0.36	154.03	3.19	0.72	263.14
z09ADGS02-2	328.30	26.26	205.99	69.77	3.34	0.34	279.98	2.14	0.70	222.07

** Aliquot age was excluded from the analysis because an analitical error was made (ICP, He-line, grain broken during unpacking processs etc.)

Sample	*Age [Ma]*	*± [Ma]*	*U (ppm)*	*Th (ppm)*	*Sm (ppm)*	*Th/U*	*He (nmol/g)*	*mass (µg)*	*Ft*	*eU*
z09ADGS02-3	811.47	64.92	89.22	34.45	1.66	0.39	312.89	2.16	0.69	97.16
z09ADGS02-4	591.32	47.31	195.94	130.56	0.79	0.67	524.90	2.27	0.70	226.00
z09ADGS02-5	471.76	37.74	107.60	134.43	1.49	1.25	264.13	3.60	0.72	138.55
z09ADGS02-6	736.44	58.92	41.79	91.38	1.70	2.19	191.31	3.68	0.73	62.83
z09WAGS04-1	470.81	37.66	53.88	47.22	1.69	0.88	125.75	3.57	0.74	64.76
z09WAGS04-2**	1267.79	101.42	68.61	59.94	2.04	0.87	480.98	6.13	0.77	82.42
z09WAGS04-3	716.09	57.29	64.74	81.02	1.64	1.25	254.66	4.55	0.75	83.40
z09WAGS04-4	521.35	41.71	68.25	95.01	1.32	1.39	205.91	6.77	0.78	90.12
z09WAGS04-5	391.33	31.31	284.03	138.30	4.85	0.49	525.93	5.38	0.77	315.90
z09WAGS04-6	527.46	42.20	92.40	32.13	1.10	0.35	226.98	5.24	0.77	99.81
z09WAGS05-1	240.97	19.28	276.44	277.86	3.99	1.01	322.98	3.02	0.72	340.42
z09WAGS05-2	176.01	14.08	120.43	314.80	1.52	2.61	136.30	4.27	0.73	192.90
z09WAGS05-3	553.73	44.30	134.48	97.52	0.38	0.73	384.67	7.32	0.79	156.93
z09WAGS05-4	418.92	33.51	280.10	52.51	0.79	0.19	517.36	4.72	0.76	292.19
z09WAGS05-5	374.28	29.94	259.67	70.60	0.84	0.27	430.65	4.40	0.75	275.93
z09WAGS05-6	211.26	16.90	158.34	52.71	0.41	0.33	136.62	2.28	0.69	170.47
Abu Zenima										
z08GS01-01	412.18	32.97	200.09	67.78	1.48	0.34	353.17	2.86	0.72	215.70
z08GS01-04	498.47	39.88	109.85	47.30	0.53	0.43	226.87	1.76	0.68	120.74
z08GS01-05	456.46	36.52	133.52	63.43	0.98	0.48	257.84	1.81	0.69	148.13
z08GS01-06	454.05	36.32	154.86	90.91	1.36	0.59	316.50	2.63	0.71	175.79

** Aliquot age was excluded from the analysis because an analitical error was made (ICP, He-line, grain broken during unpacking processs etc.)

Sample	*Age [Ma]*	*± [Ma]*	*U (ppm)*	*Th (ppm)*	*Sm (ppm)*	*Th/U*	*He (nmol/g)*	*mass (µg)*	*Ft*	*eU*
z08GS01-07	397.8	31.82	142.8	112.0	2.1	0.78	260.3	2.29	0.70	168.6
z08GS01-08	409.6	32.77	201.1	103.7	1.5	0.52	335.3	1.58	0.66	225.0
z08GS01-09	198.2	15.86	154.5	97.2	1.5	0.63	134.9	2.67	0.70	176.9
z08GS01-11	971.2	77.70	4.5	0.3	0.0	0.06	18.4	2.39	0.72	4.5
z08GS03-01	454.10	36.33	66.68	27.16	0.49	0.41	147.05	9.36	0.79	72.93
z08GS03-02	153.43	12.27	90.98	39.19	0.78	0.43	62.41	4.68	0.75	100.00
z08GS03-03	454.50	36.36	30.20	22.99	0.00	0.76	67.44	5.11	0.75	35.49
z08GS03-04	567.18	45.37	30.57	33.95	0.54	1.11	100.26	11.78	0.82	38.39
z08GS03-05	424.14	33.93	133.29	54.68	0.69	0.41	274.29	9.06	0.80	145.89
z08GS03-06	539.32	43.15	45.78	32.87	1.27	0.72	130.18	9.16	0.80	53.35
z08GS03-07	435.9	34.87	50.2	24.8	0.3	0.49	113.1	13.84	0.83	55.9
z08GS03-08	190.0	15.20	105.8	58.9	0.4	0.56	98.6	8.08	0.79	119.3
z08GS03-09	543.2	43.45	91.7	29.6	0.7	0.32	245.8	10.66	0.81	98.5
z08GS03-10	311.4	24.92	45.7	13.2	0.7	0.29	66.9	9.64	0.80	48.7
z08GS03-11	532.3	42.58	67.9	37.0	0.5	0.55	173.7	5.44	0.76	76.4
z08GS03-12	424.5	33.96	86.0	37.7	0.6	0.44	169.2	4.99	0.76	94.7
z08GS03-13	445.6	35.64	74.3	24.6	0.9	0.33	162.7	11.17	0.82	80.0
z08GS05-01	158.53	12.68	37.22	19.39	0.84	0.52	25.04	2.17	0.69	41.69
z08GS05-02	451.46	36.12	31.29	22.82	3.11	0.73	62.72	2.05	0.68	36.56
z08GS05-03	256.82	20.55	132.14	50.72	1.16	0.38	134.96	1.57	0.67	143.83
z08GS05-04	429.93	34.39	82.86	20.88	0.00	0.25	140.43	1.59	0.67	87.66

** Aliquot age was excluded from the analysis because an analitical error was made (ICP, He-line, grain broken during unpacking processs etc.)

Sample	*Age [Ma]*	*± [Ma]*	*U (ppm)*	*Th (ppm)*	*Sm (ppm)*	*Th/U*	*He (nmol/g)*	*mass (µg)*	*Ft*	*eU*
Thebes										
zERB02-1	365.19	29.22	35.44	12.20		0.34	52.50	1.80	0.68	38.25
zERB02-2	404.89	32.39	26.66	24.09		0.90	50.42	2.60	0.70	32.21
zERB02-3	433.04	34.64	118.47	56.05		0.47	232.62	4.00	0.73	131.37
zERB02-4	129.45	10.36	301.32	62.87		0.21	161.13	3.60	0.72	315.79
zERB02-5	138.76	11.10	118.94	27.99	0.14	0.24	74.75	6.77	0.79	125.38
zERB02-6	466.39	37.31	145.85	94.84	0.65	0.65	339.70	7.14	0.78	167.68
zERB02-7	260.71	20.86	45.70	22.90	0.49	0.50	54.56	3.78	0.75	50.98
zERB02-8**	39.44	3.15	137.77	89.63	0.79	0.65	23.75	2.34	0.70	158.40
zERB02-9	102.49	8.20	63.97	28.41	0.93	0.44	29.43	3.99	0.75	70.52
zERB02-10	180.67	14.45	76.89	51.20	0.00	0.67	58.19	1.55	0.66	88.68
zERB02-11	178.86	14.31	82.20	27.82	-0.51	0.34	59.27	1.81	0.69	88.60
zERB02-12	245.91	19.67	94.01	42.66	0.00	0.45	97.64	2.18	0.70	103.83
Duwi										
z08GZ14-01	497.19	39.78	169.64	95.63	10.42	0.56	422.95	8.90	0.79	191.66
z08GZ14-02	485.00	38.80	55.95	6.91	0.31	0.12	112.57	2.75	0.72	57.54
z08GZ14-03	236.04	18.88	26.83	8.73	1.41	0.33	29.85	10.45	0.80	28.84
z08GZ14-04	278.10	22.25	97.62	15.20	0.32	0.16	113.66	3.19	0.74	101.12
z08GZ14-05	171.64	13.73	49.04	46.94	2.20	0.96	39.40	2.43	0.70	59.86
z08GZ14-06	223.55	17.88	303.51	60.65	2.66	0.20	260.57	1.68	0.67	317.48

** Aliquot age was excluded from the analysis because an analitical error was made (ICP, He-line, grain broken during unpacking processs etc.)

Sample	*Age [Ma]*	*± [Ma]*	*U (ppm)*	*Th (ppm)*	*Sm (ppm)*	*Th/U*	*He (nmol/g)*	*mass (µg)*	*Ft*	*eU*
Matulla										
zERB4-1	558.82	44.71	55.69	12.43		0.22	126.16	2.10	0.69	58.55
zERB4-2	374.53	29.96	95.38	29.78		0.31	144.76	2.20	0.68	102.24
zERB4-3	88.27	7.06	169.20	75.36		0.45	67.04	4.70	0.75	186.55
zERB4-4	87.31	6.98	87.72	24.44		0.28	31.94	3.20	0.72	93.35
zERB05-1	442.8	26.57	161.6	5.2	0.0	0.03	273.7	1.66	0.68	162.8
zERB05-3	524.1	31.45	163.3	118.2	1.4	0.72	400.3	2.67	0.72	190.5
zERB05-4	487.9	29.27	74.1	61.0	2.8	0.82	192.8	8.43	0.80	88.2
zERB05-5	231.6	13.90	85.4	124.9	1.0	1.46	95.0	1.80	0.65	114.1
zERB05-6	334.6	20.08	241.0	59.3	14.3	0.25	363.9	5.50	0.77	254.8
zERB6-1	432.34	34.59	81.43	35.92		0.44	150.80	2.10	0.70	89.70
zERB6-2	490.08	39.21	122.21	68.14		0.56	259.24	2.20	0.69	137.89
zERB6-3	334.79	26.78	111.97	14.94		0.13	152.45	2.60	0.72	115.41
zERB6-4	84.64	6.77	226.70	82.78		0.37	71.69	1.30	0.64	245.75
zERB6-5	433.07	34.65	95.88	79.33		0.83	172.68	1.30	0.63	114.14
zERB6-6	649.29	51.94	53.51	47.00		0.88	162.16	2.10	0.69	64.33
z08GS08-01	621.04	49.68	124.53	150.94	0.83	1.21	428.94	5.51	0.77	159.28
z08GS08-02	457.22	36.58	94.13	40.14	0.82	0.43	211.77	10.05	0.80	103.38
z08GS08-03	525.51	42.04	126.13	54.72	1.30	0.43	311.25	4.89	0.76	138.73
z08GS08-04	122.97	9.84	120.03	66.83	0.76	0.56	68.21	4.81	0.75	135.42

** Aliquot age was excluded from the analysis because an analitical error was made (ICP, He-line, grain broken during unpacking processs etc.)

Sample	*Age [Ma]*	*± [Ma]*	*U (ppm)*	*Th (ppm)*	*Sm (ppm)*	*Th/U*	*He (nmol/g)*	*mass (µg)*	*Ft*	*eU*
z08GS08-05	418.31	33.47	33.69	13.34	0.32	0.40	61.19	2.77	0.72	36.76
z08GS10-01	284.35	22.75	143.05	19.87	6.59	0.14	159.29	1.97	0.69	147.66
z08GS10-02	378.95	30.32	107.44	51.36	0.87	0.48	182.49	3.00	0.73	119.27
z08GS10-03	398.47	31.88	318.98	216.96	20.45	0.68	558.92	2.10	0.69	369.03
z08GS10-04	424.35	33.95	39.98	19.57	3.18	0.49	74.96	3.10	0.71	44.51
z08GS10-05	542.81	43.42	6.96	5.87	1.57	0.84	200.42	1.69	0.66	8.32
z08GS10-06	521.92	41.75	249.86	67.79	1.45	0.27	561.93	3.07	0.72	265.47
z08GS11-01	370.96	29.68	39.11	25.07	1.12	0.64	66.96	3.05	0.73	44.88
z08GS11-02	458.23	36.66	86.03	48.79	9.69	0.57	181.27	3.16	0.73	97.31
z08GS11-03	455.39	36.43	36.25	28.06	1.52	0.77	79.97	4.39	0.74	42.72
z08GS11-04	407.98	32.64	72.42	35.37	1.39	0.49	133.42	3.56	0.73	80.57
z08GS13-01	298.96	23.92	75.79	29.78	0.66	0.39	99.78	3.81	0.73	82.65
z08GS13-02	151.05	12.08	72.74	23.39	1.30	0.32	50.03	6.01	0.78	78.13
z08GS13-03	140.70	11.26	48.29	21.14	0.50	0.44	30.95	4.44	0.76	53.16
z08GS13-04	532.44	42.60	114.74	56.70	1.74	0.49	280.37	3.74	0.73	127.80
z09STGS03-1	531.27	42.50	72.54	40.54	1.16	0.56	169.70	2.17	0.70	81.88
z09STGS03-2	409.82	32.79	134.30	108.80	8.48	0.81	254.00	2.47	0.70	159.39
z09STGS03-3	507.78	40.62	147.77	25.45	2.25	0.17	354.14	8.57	0.81	153.64
z09STGS03-4	415.76	33.26	183.30	206.46	10.63	1.13	375.57	2.92	0.70	230.88
z09STGS03-5	820.72	65.66	43.53	17.81	1.91	0.41	181.27	9.21	0.80	47.63

** Aliquot age was excluded from the analysis because an analitical error was made (ICP, He-line, grain broken during unpacking processs etc.)

Sample	*Age [Ma]*	*± [Ma]*	*U (ppm)*	*Th (ppm)*	*Sm (ppm)*	*Th/U*	*He (nmol/g)*	*mass (µg)*	*Ft*	*eU*
z09STGS03-6	493.81	39.50	82.51	56.88	2.74	0.69	199.58	4.89	0.76	95.62
z09STGS04-1	218.26	17.46	255.46	160.92	0.55	0.63	253.73	3.23	0.73	292.51
z09STGS04-2	441.79	35.34	127.86	25.81	0.72	0.20	256.19	6.21	0.78	133.81
z09STGS04-3	511.52	40.92	59.18	17.17	0.67	0.29	138.86	5.35	0.77	63.13
z09STGS04-4	467.00	37.36	19.09	8.14	0.28	0.43	42.79	6.28	0.78	20.97
z09STGS04-5	323.40	25.87	120.25	18.80	0.40	0.16	173.97	6.65	0.78	124.58
z09STGS04-6	427.56	34.21	60.77	23.31	2.08	0.38	115.48	3.87	0.73	66.14
Wata										
zERB07-1	677.50	54.20	16.00	6.31		0.39	54.85	10.60	0.81	17.45
zERB07-3	492.10	39.37	103.12	40.70		0.39	219.13	2.60	0.71	112.48
zERB07-4	291.37	23.31	132.28	35.46		0.27	164.17	2.90	0.73	140.44
zERB08-1	331.4	19.89	147.7	58.8	0.7	0.40	208.3	2.61	0.71	161.2
zERB08-2	105.5	6.33	139.3	74.3	0.7	0.53	57.9	1.42	0.65	156.5
zERB08-3	445.0	26.70	145.7	74.0	2.3	0.51	292.3	3.23	0.73	162.8
zERB08-5	533.3	32.00	140.3	53.1	3.4	0.38	326.8	3.02	0.72	152.5
zERB09-1	399.55	31.96	28.28	8.82		0.31	52.32	6.20	0.78	30.31
zERB09-2	473.69	37.89	81.48	23.61		0.29	179.29	6.10	0.78	86.91
zERB09-3	485.18	38.81	25.45	11.94		0.47	56.93	4.30	0.74	28.20
zERB09-4	399.16	31.93	101.02	19.81		0.20	180.02	5.40	0.77	105.58

** Aliquot age was excluded from the analysis because an analitical error was made (ICP, He-line, grain broken during unpacking processs etc.)

Sample	*Age [Ma]*	*± [Ma]*	*U (ppm)*	*Th (ppm)*	*Sm (ppm)*	*Th/U*	*He (nmol/g)*	*mass (µg)*	*Ft*	*eU*
zERB10-1	472.80	37.82	148.98	74.06		0.50	310.57	2.50	0.71	166.03
zERB10-2	391.96	31.36	134.89	49.48		0.37	217.35	1.90	0.68	146.28
zERB10-3	365.29	29.22	105.67	29.99		0.28	166.98	4.00	0.73	112.57
zERB10-4	472.06	37.76	211.02	116.01		0.55	430.15	2.00	0.69	237.72
z09STGS02-1	242.72	19.42	412.09	111.66	12.33	0.27	458.42	7.33	0.79	437.86
z09STGS02-2	350.52	28.04	160.21	50.11	0.78	0.31	250.15	4.29	0.75	171.75
z09STGS02-3	307.38	24.59	56.59	15.99	0.70	0.28	79.68	5.95	0.78	60.27
z09STGS02-4	566.94	45.36	61.66	24.72	1.07	0.40	171.07	8.64	0.79	67.36
z09STGS02-5	532.33	42.59	134.84	58.83	0.92	0.44	335.23	4.53	0.76	148.39
z09STGS02-6	432.65	34.61	38.09	16.18	0.74	0.42	73.93	3.40	0.73	41.82
z09WAGS01-1	215.15	17.21	196.34	38.95	2.39	0.20	173.33	2.62	0.72	205.32
z09WAGS01-3	303.48	24.28	343.95	302.50	9.64	0.88	481.86	2.43	0.70	413.63
z09WAGS01-4	134.73	10.78	57.29	20.00	0.43	0.35	31.54	1.93	0.70	61.89
z09WAGS01-5	541.27	43.30	99.74	38.78	3.78	0.39	217.10	1.63	0.66	108.69
z09WAGS01-6	442.41	35.39	155.35	48.96	1.86	0.32	268.32	1.74	0.66	166.63
z09WGS03-1	250.67	20.05	686.48	241.09	16.94	0.35	835.86	12.41	0.82	742.07
z09WGS03-2	283.14	22.65	764.44	300.96	21.11	0.39	957.07	3.76	0.74	833.83
z09WGS03-3	65.73	5.26	60.09	27.70	0.57	0.46	18.10	4.70	0.76	66.47
z09WGS03-4	414.64	33.17	439.94	183.43	8.81	0.42	778.39	2.54	0.70	482.21
z09WGS03-5	264.32	21.15	560.00	269.75	22.62	0.48	687.40	5.24	0.76	622.21

** Aliquot age was excluded from the analysis because an analitical error was made (ICP, He-line, grain broken during unpacking processs etc.)

Sample	*Age [Ma]*	*± [Ma]*	*U (ppm)*	*Th (ppm)*	*Sm (ppm)*	*Th/U*	*He (nmol/g)*	*mass (µg)*	*Ft*	*eU*
z09WGS03-6	356.23	28.50	460.23	195.28	10.96	0.42	739.58	4.43	0.74	505.24
Raha										
zERB13-1	93.67	7.49	238.14	186.38		0.78	98.73	2.40	0.69	281.04
zERB13-2	134.17	10.73	112.25	138.06		1.23	72.27	2.40	0.68	144.03
zERB13-3	477.59	38.21	115.10	89.32		0.78	238.24	1.60	0.66	135.66
zERB13-5	93.97	7.52	71.68	30.93	0.00	0.43	29.23	3.01	0.73	78.80
zERB13-6	424.57	33.97	49.99	59.49	0.54	1.19	99.78	1.70	0.66	63.69
zERB13-7	440.02	35.20	110.26	42.89	0.90	0.39	203.93	2.04	0.69	120.14
zERB13-8	296.44	23.72	183.07	107.23	0.00	0.59	231.01	2.14	0.68	207.76
zERB13-9	171.69	13.74	403.71	229.05	2.87	0.57	311.94	3.22	0.73	456.45
zERB13-10	466.68	37.33	113.31	53.34	0.00	0.47	252.30	5.60	0.77	125.59
zERB12-1	243.95	19.52	293.45	270.94	4.05	0.92	339.77	3.20	0.71	355.84
zERB12-2	144.79	11.58	90.12	22.68	0.00	0.25	56.56	4.22	0.75	95.34
zERB12-3	264.93	21.19	200.72	75.92	2.93	0.38	221.94	2.22	0.70	218.21
zERB12-4	458.47	36.68	64.19	41.82	0.30	0.65	137.54	3.10	0.73	73.82
zERB12-5	446.77	35.74	126.33	35.42	0.83	0.28	255.51	4.44	0.76	134.49
zERB12-6	276.77	22.14	53.71	19.54	-0.54	0.36	60.47	1.70	0.68	58.21
z09STGS01-1	355.33	28.43	114.15	52.26	10.03	0.46	182.92	3.68	0.74	126.23
z09STGS01-2	419.83	33.59	192.21	44.18	0.77	0.23	344.83	3.27	0.73	202.38
z09STGS01-3	174.66	13.97	142.88	66.82	2.89	0.47	108.48	2.90	0.72	158.28

** Aliquot age was excluded from the analysis because an analitical error was made (ICP, He-line, grain broken during unpacking processs etc.)

Sample	*Age [Ma]*	*± [Ma]*	*U (ppm)*	*Th (ppm)*	*Sm (ppm)*	*Th/U*	*He (nmol/g)*	*mass (µg)*	*Ft*	*eU*
z09STGS01-4	669.64	53.57	120.96	55.39	1.50	0.46	386.64	5.01	0.76	133.72
z09STGS01-5	464.61	37.17	84.31	33.36	0.67	0.40	178.03	3.74	0.75	91.99
z09STGS01-6	149.56	11.96	0.98	2.94	6.00	2.99	1.00	2.93	0.72	1.69
z09STGS06-1	266.16	21.29	94.52	52.64	0.53	0.56	125.37	8.47	0.80	106.64
z09STGS06-2	536.03	42.88	134.13	41.72	1.02	0.31	307.62	2.64	0.71	143.74
z09STGS06-3	443.07	35.45	115.81	115.86	2.02	1.00	256.54	3.54	0.73	142.49
z09STGS06-4	366.39	29.31	57.35	88.96	1.84	1.55	120.79	5.84	0.76	77.84
Malha										
zERB14-1	334.8	20.09	181.3	16.7	0.0	0.09	236.3	2.31	0.69	185.2
zERB14-2	553.1	33.19	59.3	50.7	1.6	0.86	171.9	6.91	0.78	70.9
zERB14-3	442.6	26.56	69.8	53.9	1.4	0.77	142.2	2.60	0.70	82.2
zERB14-4	505.1	30.31	85.1	105.0	1.6	1.23	212.6	2.37	0.69	109.3
zERB14-5	526.9	31.61	64.3	42.0	0.9	0.65	181.9	14.10	0.83	73.9
zERB14-6	261.7	15.70	61.5	52.0	1.3	0.85	71.4	2.08	0.68	73.5
zERB15-1	398.27	31.86	4.65	12.32		2.65	10.84	1.60	0.65	7.48
zERB16-2	193.52	15.48	157.65	80.69		0.51	125.83	1.70	0.68	176.23
zERB16-3	457.37	36.59	123.25	62.46		0.51	242.69	2.10	0.69	137.63
zERB16-4	974.90	77.99	36.09	9.81		0.27	158.14	3.50	0.73	38.35

** Aliquot age was excluded from the analysis because an analitical error was made (ICP, He-line, grain broken during unpacking processs etc.)

Sample	*Age [Ma]*	*± [Ma]*	*U (ppm)*	*Th (ppm)*	*Sm (ppm)*	*Th/U*	*He (nmol/g)*	*mass (µg)*	*Ft*	*eU*
zERB17-1	211.20	16.90	265.65	117.68		0.44	240.40	3.00	0.71	292.74
zERB17-2	313.85	25.11	131.52	79.56		0.60	187.21	3.30	0.72	149.84
zERB17-3	244.63	19.57	69.93	37.06		0.53	80.48	5.50	0.76	78.46
zERB17-4	477.66	38.21	120.71	34.61		0.29	294.99	23.70	0.85	128.68
zERB18-1	466.74	37.34	37.11	22.70		0.61	85.13	6.30	0.77	42.33
zERB18-2	495.62	39.65	124.92	60.53		0.48	316.85	12.50	0.82	138.86
zERB18-3	162.00	12.96	46.58	27.71		0.59	33.56	2.70	0.72	52.96
zERB18-4	438.62	35.09	86.81	54.03		0.62	174.38	3.00	0.72	99.25
zERB18-6	331.3	19.88	259.7	104.6	16.3	0.40	359.1	2.28	0.69	283.9
zERB19-1	600.43	48.03	39.06	31.21		0.80	129.25	13.20	0.82	46.24
zERB19-3	575.46	46.04	68.57	41.70		0.61	201.07	8.50	0.79	78.17
zERB19-4	483.70	38.70	237.84	217.77		0.92	597.00	5.90	0.77	287.97
zERB19-5	526.44	42.12	101.56	65.16		0.64	285.44	15.50	0.83	116.56
zERB19-6	263.73	21.10	31.29	14.56		0.47	42.91	25.30	0.85	34.64
zERB20-1	564.79	45.18	20.05	12.15		0.61	54.30	4.30	0.75	22.85
zERB20-2	1257.43	100.59	160.25	102.36		0.64	981.79	2.50	0.71	183.81
zERB20-3	461.21	36.90	28.29	21.48		0.76	70.46	13.70	0.82	33.23
zERB20-4	523.47	41.88	118.99	102.44		0.86	303.72	3.30	0.73	142.57
zERB21-1	510.49	40.84	71.47	52.67		0.74	195.87	12.80	0.82	83.60
zERB21-2	395.08	31.61	108.16	130.02		1.20	235.78	6.90	0.78	138.09

** Aliquot age was excluded from the analysis because an analitical error was made (ICP, He-line, grain broken during unpacking processs etc.)

Sample	*Age [Ma]*	*± [Ma]*	*U (ppm)*	*Th (ppm)*	*Sm (ppm)*	*Th/U*	*He (nmol/g)*	*mass (µg)*	*Ft*	*eU*
zERB21-4	520.63	41.65	113.47	101.33		0.89	321.94	11.20	0.80	136.79
zERB22-1	563.94	45.12	40.13	17.13		0.43	107.01	5.10	0.76	44.07
zERB22-2	622.06	49.76	29.00	13.46		0.46	95.37	19.70	0.84	32.10
zERB22-3	226.57	18.13	58.71	28.16		0.48	63.16	7.30	0.78	65.19
zERB22-4	502.06	40.16	112.69	77.78		0.69	278.47	5.10	0.76	130.59
zERB23-1	416.1	24.97	104.2	63.2	1.0	0.61	202.0	4.53	0.74	118.7
zERB23-2	442.5	26.55	36.4	14.5	1.0	0.40	79.4	10.37	0.81	39.7
zERB23-3	388.6	23.31	37.7	12.3	0.4	0.33	70.3	8.60	0.80	40.5
zERB23-4	471.4	28.28	141.7	70.6	3.8	0.50	320.1	6.06	0.77	157.9
zERB23-5	488.2	29.29	28.9	11.6	0.3	0.40	63.4	3.53	0.74	31.5
zERB23-6	430.8	25.85	210.1	63.1	2.2	0.30	402.9	4.30	0.75	224.7
zERB24-1	430.42	34.43	153.74	74.34		0.48	286.69	2.30	0.70	170.85
zERB24-2	544.99	43.60	87.81	33.69		0.38	224.06	5.20	0.77	95.57
zERB24-3	270.17	21.61	243.08	61.79		0.25	249.61	1.40	0.65	257.31
zERB24-4	558.07	44.65	142.32	97.97		0.69	400.11	6.80	0.77	164.87
z08GZ16-01	89.36	7.15	1588.49	387.97	20.52	0.24	623.58	5.87	0.77	1677.91
z08GZ16-02	458.39	36.67	149.14	25.99	1.37	0.17	293.39	3.63	0.74	155.13
z08GZ16-03	105.80	8.46	1099.12	136.84	3.32	0.12	501.15	5.17	0.77	1130.64
z08GZ16-04	227.65	18.21	758.51	59.62	3.42	0.08	764.31	6.97	0.79	772.25

** Aliquot age was excluded from the analysis because an analitical error was made (ICP, He-line, grain broken during unpacking processs etc.)

Sample	*Age [Ma]*	*± [Ma]*	*U (ppm)*	*Th (ppm)*	*Sm (ppm)*	*Th/U*	*He (nmol/g)*	*mass (µg)*	*Ft*	*eU*
Qiseib										
zERB25-1	508.26	40.66	31.36	14.62		0.47	70.81	2.70	0.72	34.73
zERB25-2	461.52	36.92	35.26	19.21		0.54	69.99	1.90	0.69	39.68
zERB25-3	390.54	31.24	140.14	91.90		0.66	265.03	5.20	0.76	161.29
zERB25-4	528.40	42.27	70.60	59.01		0.84	184.73	4.00	0.74	84.18
zERB26-1	343.74	27.50	157.57	118.06		0.75	254.06	3.30	0.72	184.75
zERB26-2	197.90	15.83	64.67	56.19		0.87	55.96	1.90	0.67	77.60
zERB26-3	417.75	33.42	106.67	71.06		0.67	198.91	2.20	0.70	123.03
zERB26-4	214.34	17.15	102.08	51.08		0.50	97.34	3.40	0.73	113.84
zERB26-5	275.6	22.05	200.9	139.5	4.0	0.69	262.4	4.29	0.74	233.1
zERB26-6	276.4	22.11	10.1	6.4	0.3	0.64	14.6	15.76	0.83	11.5
zERB26-7	381.3	30.50	94.4	108.2	1.3	1.15	192.1	7.08	0.76	119.4
zERB26-8	411.5	32.92	49.3	30.6	1.6	0.62	100.1	6.34	0.78	56.3
zERB26-9	327.0	26.16	203.8	65.8	1.5	0.32	291.2	3.97	0.74	219.0
zERB27-1	382.83	30.63	160.16	59.17		0.37	256.75	2.60	0.70	173.78
zERB27-2**	81.18	6.49	161.52	93.76		0.58	100.34	6.80	0.78	183.10
zERB27-3	521.85	41.75	139.21	160.64		1.15	388.56	5.10	0.75	176.19
zERB27-4	559.35	44.75	53.91	46.23		0.86	168.05	14.50	0.82	64.56
zERB27-5	254.1	20.32	143.8	72.8	2.0	0.51	156.9	2.85	0.70	160.5
zERB27-7	283.3	22.67	110.0	111.2	5.0	1.01	154.1	3.63	0.73	135.6
zERB27-8	404.8	32.39	96.5	64.0	0.9	0.66	187.1	4.52	0.75	111.3

** Aliquot age was excluded from the analysis because an analitical error was made (ICP, He-line, grain broken during unpacking processs etc.)

Sample	*Age [Ma]*	*± [Ma]*	*U (ppm)*	*Th (ppm)*	*Sm (ppm)*	*Th/U*	*He (nmol/g)*	*mass (µg)*	*Ft*	*eU*
zERB27-9	329.4	26.35	99.7	44.9	1.1	0.45	155.5	5.65	0.78	110.0
zERB27-10	453.9	36.31	106.5	38.2	2.2	0.36	210.8	3.26	0.72	115.3
zERB28-1	215.66	17.25	109.47	227.46		2.08	137.38	3.00	0.72	161.83
zERB28-2	437.36	34.99	143.62	53.48		0.37	282.26	3.60	0.74	155.93
zERB28-3	426.19	34.10	109.08	82.42		0.76	234.52	6.10	0.77	128.06
zERB28-4	249.06	19.92	199.84	130.10		0.65	245.78	6.90	0.78	229.79
zERB28-5	198.73	15.90	437.82	219.11		0.50	396.73	4.20	0.75	488.26
zERB28-6	429.29	34.34	54.42	73.23		1.35	122.73	3.40	0.72	71.28
zERB29-1	302.96	24.24	85.22	125.08	1.20	1.47	148.94	7.70	0.78	114.02
zERB29-2	269.60	21.57	334.37	34.98	0.58	0.10	427.50	15.93	0.84	342.43
zERB29-3	412.46	33.00	172.16	195.41	2.02	1.14	409.34	13.71	0.82	217.15
zERB29-4	576.4	46.11	48.6	33.7	1.6	0.69	154.8	21.89	0.84	56.3
zERB29-5	323.3	25.86	258.2	162.4	4.8	0.63	446.7	19.65	0.84	295.6
zERB29-6	484.0	38.72	120.1	26.4	0.3	0.22	276.2	8.26	0.81	126.2
Abu Thora										
zERB31-1	461.69	36.94	114.23	45.57		0.40	240.06	3.90	0.75	124.72
zERB31-2	330.11	26.41	136.53	177.87		1.30	249.61	6.10	0.77	177.47
zERB31-3	414.43	33.15	158.21	43.80		0.28	329.47	20.40	0.85	168.29
zERB31-4	364.63	29.17	369.85	75.88		0.21	553.10	2.40	0.71	387.32

** Aliquot age was excluded from the analysis because an analitical error was made (ICP, He-line, grain broken during unpacking processs etc.)

Sample	*Age [Ma]*	*± [Ma]*	*U (ppm)*	*Th (ppm)*	*Sm (ppm)*	*Th/U*	*He (nmol/g)*	*mass (µg)*	*Ft*	*eU*
zERB32-1	397.4	23.84	57.2	28.9	0.6	0.51	117.0	14.60	0.83	63.9
zERB32-2	487.1	29.23	34.6	52.4	1.4	1.51	105.6	15.11	0.83	46.7
zERB32-3	423.0	25.38	139.0	112.1	2.9	0.81	309.8	10.80	0.80	164.9
zERB32-4	229.0	13.74	88.7	36.3	1.0	0.41	97.0	8.42	0.80	97.0
zERB32-5	550.5	33.03	186.4	38.9	1.8	0.21	471.3	6.85	0.78	195.3
zERB32-6	496.4	29.78	99.6	145.9	1.1	1.47	291.7	7.40	0.79	133.2
zERB35-1	294.2	17.65	227.7	94.5	0.9	0.42	343.3	18.93	0.85	249.4
zERB35-2	467.1	28.03	135.6	71.8	0.5	0.53	340.8	22.05	0.85	152.1
zERB35-3	450.9	27.05	22.5	28.9	0.8	1.28	63.1	26.89	0.86	29.1
zERB35-4	428.8	25.73	77.9	59.0	1.9	0.76	173.9	8.24	0.79	91.5
zERB35-5	497.5	29.85	106.0	150.7	2.0	1.42	263.5	1.87	0.67	140.7
zERB37-1	384.92	30.79	50.73	50.25		0.99	102.60	5.80	0.77	62.30
zERB37-2	420.24	33.62	64.32	50.92		0.79	127.27	3.40	0.72	76.04
zERB37-3	280.73	22.46	414.57	37.13		0.09	460.03	2.60	0.71	423.12
zERB37-4	187.76	15.02	604.84	151.06		0.25	460.00	2.40	0.70	639.61
zERB37-5	418.29	33.46	266.38	34.87		0.13	449.11	2.70	0.71	274.40
zERB37-6	540.00	43.20	102.60	102.75		1.00	300.25	7.50	0.78	126.25
zERB38-1	449.58	35.97	135.92	39.92	1.00	0.29	248.42	1.82	0.69	145.12
zERB38-2	314.22	25.14	62.86	17.37	0.22	0.28	87.67	4.12	0.76	66.86
zERB39-1	368.69	29.50	76.99	49.07		0.64	131.82	3.50	0.73	88.29

** Aliquot age was excluded from the analysis because an analitical error was made (ICP, He-line, grain broken during unpacking processs etc.)

Sample	*Age [Ma]*	*± [Ma]*	*U (ppm)*	*Th (ppm)*	*Sm (ppm)*	*Th/U*	*He (nmol/g)*	*mass (µg)*	*Ft*	*eU*
zERB39-2	638.70	51.10	93.29	49.31		0.53	318.96	16.30	0.84	104.64
zERB39-3	496.38	39.71	32.64	41.03		1.26	91.71	6.70	0.78	42.08
zERB39-4	282.75	22.62	38.68	45.32		1.17	53.00	2.30	0.69	49.11
z09STGS07-1	493.56	39.48	116.33	58.27	3.09	0.50	287.76	10.15	0.80	129.75
z09STGS07-2	495.22	39.62	60.25	27.43	3.06	0.46	140.93	5.86	0.76	66.58
z09STGS07-3	556.36	44.51	101.58	75.70	3.48	0.75	288.15	5.92	0.77	119.02
z09STGS07-4	327.42	26.19	62.53	30.27	1.10	0.48	99.34	7.35	0.79	69.51
z09STGS07-5	341.59	27.33	55.85	38.12	0.61	0.68	91.57	4.42	0.75	64.63
z09STGS07-6	175.56	14.04	169.95	77.65	1.31	0.46	140.88	6.14	0.78	187.83
Naqus/Araba										
zERB41-1	363.62	29.09	296.15	197.08		0.67	514.11	4.70	0.75	341.52
zERB41-2	505.38	40.43	205.82	107.62		0.52	475.28	3.40	0.73	230.60
zERB41-3	457.14	36.57	217.96	140.34		0.64	458.51	2.90	0.72	250.27
zERB41-4	319.95	25.60	290.91	171.16		0.59	413.80	2.50	0.71	330.31
zERB42-1	438.22	35.06	106.44	125.09		1.18	254.22	6.10	0.77	135.24
zERB42-2	445.44	35.64	103.73	57.04		0.55	241.55	17.30	0.83	116.86
zERB42-3	329.85	26.39	63.26	116.90		1.85	107.56	1.80	0.65	90.17
zERB42-4	458.32	36.67	108.40	60.75		0.56	235.59	4.20	0.75	122.39
zERB42-5	519.74	41.58	147.63	70.30		0.48	343.21	3.00	0.72	163.81
zERB42-6	519.21	41.54	133.47	137.52		1.03	320.16	2.00	0.67	165.13

** Aliquot age was excluded from the analysis because an analitical error was made (ICP, He-line, grain broken during unpacking processs etc.)

Sample	*Age [Ma]*	*± [Ma]*	*U (ppm)*	*Th (ppm)*	*Sm (ppm)*	*Th/U*	*He (nmol/g)*	*mass (µg)*	*Ft*	*eU*
zERB43-1	432.08	34.57	74.15	57.01		0.77	159.83	5.00	0.76	87.28
zERB43-2	540.55	43.24	119.88	73.75		0.62	335.64	10.40	0.81	136.86
zERB43-3	432.78	34.62	145.49	179.27		1.23	353.12	8.90	0.78	186.75
zERB43-4	423.16	33.85	225.93	165.80		0.73	428.80	2.30	0.69	264.10
zERB43-5	477.92	38.23	52.20	61.58		1.18	150.11	20.40	0.84	66.38
zERB43-6	668.42	53.47	65.02	40.03		0.62	236.08	15.30	0.83	74.24
zERB44-1	629.43	50.35	168.13	361.27		2.15	677.15	6.10	0.76	251.30
zERB44-2	253.20	20.26	300.65	284.18		0.95	377.88	4.30	0.74	366.07
zERB44-3	440.37	35.23	83.96	62.17		0.74	192.08	9.40	0.79	98.27
zERB44-4	478.83	38.31	46.42	81.64		1.76	126.49	3.60	0.73	65.21
z08GZ09-01	356.18	28.49	292.95	52.17	5.74	0.18	437.67	3.30	0.73	304.99
z08GZ09-02	517.84	41.43	131.86	69.82	1.84	0.53	336.86	6.60	0.78	147.94
z08GZ09-03	466.16	37.29	116.17	104.10	1.71	0.90	285.24	7.92	0.78	140.14
z08GZ09-04	473.87	37.91	118.75	94.34	4.82	0.79	286.24	6.73	0.77	140.49
z08GZ09-05	551.86	44.15	206.57	79.84	0.34	0.39	586.65	16.50	0.84	224.95
z08GZ09-06	623.13	49.85	98.18	178.75	1.59	1.82	413.18	19.25	0.84	139.34
z08GZ10-01	475.03	38.00	195.85	81.53	1.53	0.42	464.89	11.50	0.81	214.63
z08GZ10-02	413.05	33.04	207.26	128.31	7.12	0.62	429.11	8.00	0.79	236.83
z08GZ10-03	487.53	39.00	80.43	75.33	1.71	0.94	215.33	10.27	0.81	97.78
z08GZ10-04	361.21	28.90	174.49	109.88	4.89	0.63	330.14	13.61	0.82	199.81

** Aliquot age was excluded from the analysis because an analitical error was made (ICP, He-line, grain broken during unpacking processs etc.)

Sample	*Age [Ma]*	*± [Ma]*	*U (ppm)*	*Th (ppm)*	*Sm (ppm)*	*Th/U*	*He (nmol/g)*	*mass (µg)*	*Ft*	*eU*
z08GZ10-05	404.62	32.37	61.61	43.61	0.53	0.71	134.18	15.63	0.83	71.65
z08GZ10-06	376.64	30.13	46.02	36.38	0.55	0.79	94.42	15.07	0.83	54.40
z08GZ11-01	485.53	38.84	363.03	67.68	7.07	0.19	762.41	3.83	0.74	378.65
z08GZ11-02	432.37	34.59	162.71	92.39	5.49	0.57	340.90	5.91	0.77	184.00
z08GZ11-03	460.43	36.83	262.96	130.45	12.29	0.50	524.88	2.42	0.70	293.06
z08GZ11-04	426.46	34.12	210.60	112.12	5.98	0.53	435.75	6.11	0.78	236.44
z08GZ11-05	450.35	36.03	78.83	76.54	1.64	0.97	177.02	3.40	0.73	96.46
z08GZ11-06**	7994.70	65535.00	0.00	0.10	-0.43		1.88	4.27	0.73	0.02
z08GZ12-01	351.96	28.16	120.58	73.57	5.03	0.61	188.37	2.69	0.70	124.69
z08GZ12-02	497.97	39.84	183.65	104.59	4.59	0.57	416.16	2.94	0.72	114.01
z08GZ12-03	518.69	41.50	99.77	108.24	0.89	1.08	266.77	4.15	0.74	124.69
z08GZ12-04	549.23	43.94	102.91	48.18	1.58	0.47	265.46	4.69	0.75	114.01
z08GZ12-05	506.23	40.50	88.44	144.59	1.97	1.63	242.86	2.72	0.71	121.73
z08GZ12-06	405.85	32.47	350.05	80.92	4.81	0.23	635.40	5.20	0.76	368.71
z08GZ13-01	546.77	43.74	185.92	178.64	2.92	0.96	559.99	11.07	0.80	227.06
z08GZ13-02	340.91	27.27	223.48	227.25	7.49	1.02	384.07	4.27	0.74	275.83
z08GZ13-03	753.96	60.32	119.55	73.49	2.33	0.61	412.08	2.65	0.70	136.48
z08GZ13-04	510.65	40.85	236.75	140.95	6.99	0.60	585.94	4.86	0.76	269.23
z08GZ13-05	475.63	38.05	166.78	144.58	2.75	0.87	393.06	3.89	0.74	200.08
z08GZ13-06	534.37	42.75	171.53	86.21	0.90	0.50	409.80	2.97	0.72	191.38

** Aliquot age was excluded from the analysis because an analitical error was made (ICP, He-line, grain broken during unpacking processs etc.)

Sample	*Age [Ma]*	*± [Ma]*	*U (ppm)*	*Th (ppm)*	*Sm (ppm)*	*Th/U*	*He (nmol/g)*	*mass (µg)*	*Ft*	*eU*
zGS05-1	444.99	35.60	172.99	143.06	3.98	0.83	368.06	3.30	0.72	205.94
zGS05-2	392.94	31.44	77.61	81.10	4.69	1.04	162.12	6.45	0.77	96.30
zGS05-3	446.57	35.73	122.71	116.61	4.32	0.95	299.22	9.14	0.80	149.58
zGS05-4	399.22	31.94	73.45	54.39	4.26	0.74	148.31	6.18	0.78	85.99
zGS06-1	521.17	41.69	316.89	273.11	11.54	0.86	735.63	1.94	0.67	379.82
zGS06-2	426.36	34.11	118.03	115.09	4.63	0.98	255.43	4.55	0.74	144.55
zGS06-3	579.15	46.33	76.72	116.57	2.88	1.52	227.03	1.82	0.68	103.57
zGS06-4	298.25	23.86	21.45	61.22	3.78	2.85	38.54	1.74	0.66	35.56
zGS07-01	520.85	41.67	175.55	62.04	7.51	0.35	401.50	2.98	0.73	189.87
zGS07-02	455.39	36.43	164.34	75.93	3.35	0.46	346.74	4.32	0.75	181.84
zGS07-03	373.19	29.86	258.86	1115.13	9.62	4.31	766.33	3.42	0.72	515.61
zGS07-04	397.06	31.76	179.01	70.60	6.90	0.39	300.89	2.48	0.70	195.29
zGS08-1	544.29	43.54	64.77	31.50	2.20	0.49	168.31	4.77	0.76	72.04
zGS08-2	449.42	35.95	113.52	45.93	4.24	0.40	214.75	2.17	0.69	124.12
zGS08-3	755.24	60.42	96.65	50.38	5.17	0.52	326.89	2.54	0.70	108.27
zGS08-4	454.74	36.38	168.76	56.13	2.12	0.33	322.53	2.47	0.70	181.70
zGS09-1	445.46	35.64	160.03	65.14	3.46	0.41	338.77	6.46	0.78	175.04
zGS09-2	324.12	25.93	415.35	136.33	8.11	0.33	577.37	2.92	0.72	446.78
zGS09-3	329.99	26.40	309.12	101.01	6.17	0.33	435.74	2.77	0.72	332.40
zGS09-4	415.03	33.20	168.31	59.61	7.60	0.35	285.18	1.90	0.68	182.08

** Aliquot age was excluded from the analysis because an analitical error was made (ICP, He-line, grain broken during unpacking processs etc.)

Sample	*Age [Ma]*	*± [Ma]*	*U (ppm)*	*Th (ppm)*	*Sm (ppm)*	*Th/U*	*He (nmol/g)*	*mass (µg)*	*Ft*	*eU*
Basement										
zERB45-1	479.82	38.39	70.09	73.67		1.05	182.74	6.90	0.78	87.05
zERB45-2	443.10	35.45	175.47	159.15		0.91	413.69	7.70	0.79	212.10
zERB45-3	298.51	23.88	89.78	79.32		0.88	151.76	4.90	0.75	108.04
zERB45-4	354.29	28.34	404.80	101.63		0.25	664.27	7.90	0.79	428.19
zERB46-1	514.95	41.20	101.66	53.41		0.53	256.86	7.90	0.78	113.95
zERB46-2	538.03	43.04	79.52	24.66		0.31	203.13	7.10	0.79	85.19
zERB46-3	472.24	37.78	31.15	41.60		1.34	81.42	5.90	0.76	40.73
zERB46-4	514.18	41.13	89.61	72.02		0.80	245.32	8.80	0.80	106.19
zERB46-5	531.86	42.55	160.59	156.14		0.97	442.52	5.10	0.75	196.54
zERB46-6	370.58	29.65	334.14	131.17		0.39	572.55	6.10	0.76	364.34
zERB-46-1	313.86	25.11	541.11	148.97		0.28	803.35	10.99	0.81	575.40
zERB-46-2	339.57	27.17	351.48	108.81		0.31	577.99	12.55	0.82	376.53
zERB-46-3	286.49	22.92	654.16	161.13		0.25	829.03	5.50	0.76	691.25
zERB-46-4	228.33	18.27	573.41	198.19		0.35	630.20	13.17	0.81	619.04
zERB-46-5	535.24	42.82	93.11	68.70		0.74	272.00	17.23	0.83	108.92
zERB-46-6	366.35	29.31	132.29	74.99		0.57	260.96	26.05	0.86	149.55
zERB-46-7	336.88	26.95	297.38	104.94		0.35	499.74	19.08	0.83	321.53
zERB-46-8	245.40	19.63	545.65	129.93		0.24	628.40	10.68	0.81	575.56
zERB-46-9	50.95	4.08	1016.80	190.82		0.19	249.72	24.44	0.85	1060.72

** Aliquot age was excluded from the analysis because an analitical error was made (ICP, He-line, grain broken during unpacking processs etc.)

Sample	*Age [Ma]*	*± [Ma]*	*U (ppm)*	*Th (ppm)*	*Sm (ppm)*	*Th/U*	*He (nmol/g)*	*mass (µg)*	*Ft*	*eU*
zERB47-1	369.29	29.54	544.96	141.72		0.26	871.50	4.10	0.74	577.58
zERB47-2	294.01	23.52	488.21	159.60		0.33	688.10	11.20	0.81	524.95
zERB47-3	270.79	21.66	375.20	109.61		0.29	472.13	8.00	0.79	400.44
zERB47-4	365.32	29.23	209.24	170.73		0.82	421.94	17.40	0.84	248.54
zERB-47-1	329.01	26.32	331.79	93.99		0.28	502.12	7.55	0.78	353.43
zERB-47-2	268.87	21.51	369.88	83.57		0.23	485.13	19.11	0.84	389.12
zERB-47-3	361.01	28.88	305.48	90.80		0.30	549.45	21.55	0.84	326.38
zERB-47-4	332.58	26.61	843.26	240.80		0.29	1298.36	8.56	0.79	898.69
zERB-47-5	344.87	27.59	239.33	129.24		0.54	408.14	10.33	0.79	269.08
zERB-47-6	33.33	2.67	602.69	135.14		0.22	96.67	18.73	0.85	633.80
zERB-47-7	238.23	19.06	349.87	238.37		0.68	406.35	5.60	0.77	404.75
zERB-47-8	289.93	23.19	377.95	74.40		0.20	529.19	17.53	0.84	395.08
zERB-47-10	375.00	30.00	332.89	362.85		1.09	712.03	15.42	0.82	416.42
zERB48-1	236.37	18.91	421.91	130.05	13.83	0.31	441.56	4.86	0.75	451.91
zERB48-2	300.12	24.01	422.35	101.09	6.38	0.24	599.60	10.89	0.81	445.65
zERB48-3	265.44	21.24	655.44	116.17	29.46	0.18	814.28	11.49	0.82	682.34
zERB48-4	324.58	25.97	247.54	83.02	2.19	0.34	349.00	3.43	0.73	266.66
zERB49-1	327.00	26.16	160.00	118.50	4.28	0.74	278.71	13.90	0.82	187.29
zERB49-2	398.76	31.90	40.19	27.79	0.52	0.69	86.46	15.83	0.83	46.59
zERB49-3	235.28	18.82	258.61	66.43	286.00	0.26	282.11	7.51	0.79	275.34

** Aliquot age was excluded from the analysis because an analitical error was made (ICP, He-line, grain broken during unpacking processs etc.)

Sample	*Age [Ma]*	*± [Ma]*	*U (ppm)*	*Th (ppm)*	*Sm (ppm)*	*Th/U*	*He (nmol/g)*	*mass (µg)*	*Ft*	*eU*
zERB49-4	559.85	44.79	152.67	117.55	4.29	0.77	421.37	4.46	0.74	179.75
zERB50-1	437.86	35.03	33.34	20.76	1.10	0.62	74.22	9.12	0.80	38.12
zERB50-2	419.49	33.56	249.03	129.12	20.16	0.52	497.17	5.85	0.76	278.85
zERB50-3	313.71	25.10	357.33	90.75	5.08	0.25	545.79	16.25	0.83	378.24
zERB50-4	522.40	41.79	52.23	15.61	0.87	0.30	140.53	24.19	0.85	55.82
z08GZ02-01	632.46	50.60	122.40	89.87	2.48	0.73	349.83	2.17	0.69	143.11
z08GZ02-02	471.52	37.72	211.55	141.93	10.70	0.67	479.31	4.18	0.75	244.28
z08GZ02-03	472.88	37.83	183.23	119.01	6.59	0.65	412.16	3.90	0.74	210.66
z08GZ02-04	446.86	35.75	206.33	129.51	3.26	0.63	445.50	4.56	0.76	236.16
z08GZ03-01	36.24	2.90	9.25	8.74	43.36	0.95	1.53	1.69	0.67	11.48
z08GZ03-02	382.72	30.62	317.95	184.95	14.98	0.58	589.59	5.16	0.77	360.60
z08GZ03-03	43.12	3.45	20.26	24.45	61.36	1.21	4.19	2.00	0.68	26.20
z08GZ03-04	366.93	29.35	154.20	75.20	3.41	0.49	282.28	9.12	0.81	171.53
z08GZ04-01	440.45	35.24	227.66	62.70	4.49	0.28	431.17	3.01	0.73	242.11
z08GZ04-02	393.52	31.48	199.43	44.33	3.94	0.22	331.02	3.08	0.72	209.66
z08GZ04-03	453.45	36.28	214.71	74.42	3.65	0.35	367.72	1.11	0.63	231.86
z08GZ04-04**	5.18	0.41	0.52	0.08	0.36	0.16	0.01	7.61	0.80	0.54
z08GZ05-01	528.45	42.28	79.78	60.88	2.16	0.76	223.48	8.78	0.80	93.80
z08GZ05-02	476.37	38.11	63.76	52.75	5.30	0.83	164.43	10.49	0.81	75.93

** Aliquot age was excluded from the analysis because an analitical error was made (ICP, He-line, grain broken during unpacking processs etc.)

Sample	*Age [Ma]*	*± [Ma]*	*U (ppm)*	*Th (ppm)*	*Sm (ppm)*	*Th/U*	*He (nmol/g)*	*mass (µg)*	*Ft*	*eU*
z08GZ05-03	575.29	46.02	77.47	72.40	2.53	0.93	233.59	5.88	0.77	94.15
z08GZ05-04	411.54	32.92	90.79	54.46	3.97	0.60	170.55	3.06	0.72	103.35
z08GZ06-01	625.48	50.04	85.69	58.68	2.20	0.68	269.97	5.54	0.77	99.21
z08GZ06-02	572.81	45.82	92.10	60.80	2.10	0.66	254.98	4.50	0.75	106.11
z08GZ06-03	511.97	40.96	106.31	104.98	3.51	0.99	268.60	3.08	0.72	130.50
z08GZ06-04	546.47	43.72	86.05	78.25	3.66	0.91	237.39	4.44	0.74	104.08
z08GZ07-01	540.26	43.22	84.82	75.72	7.36	0.89	218.95	2.94	0.71	102.29
z08GZ07-02	572.24	45.78	101.14	68.37	1.99	0.68	271.56	3.39	0.72	116.88
z08GZ07-03	565.43	45.23	81.37	65.67	3.94	0.81	226.42	4.11	0.74	96.51
z08GZ07-04	554.57	44.37	91.72	85.10	6.96	0.93	256.53	4.08	0.74	111.34
z08GZ08-01	443.29	35.46	138.52	85.92	5.67	0.62	287.43	3.58	0.74	158.33
z08GZ08-02	306.82	24.55	25.91	16.11	2.49	0.62	36.64	3.26	0.73	29.63
z08GZ08-03	249.66	19.97	135.22	29.78	2.05	0.22	143.23	3.29	0.74	142.08
z08GZ08-04	546.73	43.74	83.19	28.96	1.09	0.35	205.60	3.71	0.75	89.86
z08GZ17-01	383.49	30.68	271.45	49.20	1.16	0.18	482.43	8.37	0.80	282.78
z08GZ17-02	18.40	1.47	1526.56	497.55	20.75	0.33	137.64	18.97	0.84	1641.20
z08GZ17-03	81.53	6.52	1731.75	831.14	13.27	0.48	642.80	4.77	0.76	1923.15
z08GZ17-04	105.82	8.47	867.92	710.42	9.95	0.82	448.84	4.52	0.75	1031.51
zGS01-1	204.36	16.35	496.53	319.09	34.91	0.64	459.27	3.30	0.72	570.16

** Aliquot age was excluded from the analysis because an analitical error was made (ICP, He-line, grain broken during unpacking processs etc.)

Sample	*Age [Ma]*	*± [Ma]*	*U (ppm)*	*Th (ppm)*	*Sm (ppm)*	*Th/U*	*He (nmol/g)*	*mass (µg)*	*Ft*	*eU*
zGS01-2	186.69	14.94	386.41	169.73	29.91	0.44	346.26	8.13	0.80	425.63
zGS01-3	99.80	7.98	510.70	348.39	46.30	0.68	240.44	4.37	0.75	591.14
zGS01-4	187.88	15.03	505.84	269.21	116.92	0.53	477.53	13.39	0.82	568.41
zGS02-1	496.86	39.75	75.31	43.26	1.61	0.57	177.75	4.07	0.75	85.28
zGS02-2	489.50	39.16	125.54	69.08	2.41	0.55	287.25	3.82	0.74	141.45
zGS02-3	458.57	36.69	76.09	51.42	1.26	0.68	175.29	6.24	0.78	87.94
zGS02-4	443.97	35.52	265.59	125.49	3.62	0.47	547.05	4.36	0.75	294.50
zGS03-1	331.09	26.49	387.22	103.97	11.63	0.27	563.93	4.20	0.75	411.21
zGS03-2	376.39	30.11	203.13	75.40	5.27	0.37	333.63	3.24	0.73	220.51
zGS03-3	324.47	25.96	259.63	33.71	3.31	0.13	351.74	3.18	0.74	267.41
zGS03-4	312.73	25.02	473.60	99.19	4.99	0.21	572.40	1.58	0.67	496.46
zGS04-1	550.45	44.04	184.45	69.66	1.34	0.38	508.17	14.69	0.82	200.50
zGS04-2	502.76	40.22	541.79	158.90	2.83	0.29	1298.36	8.84	0.80	578.39
zGS04-3	502.37	40.19	94.15	27.84	0.69	0.30	233.78	17.22	0.82	100.57
zGS04-4	563.56	45.08	146.40	48.35	1.29	0.33	392.56	8.18	0.78	157.54
zGS11-1	544.78	43.58	229.84	94.02	1.63	0.41	568.31	4.03	0.74	251.50
zGS11-2	420.98	33.68	313.53	69.75	18.70	0.22	523.72	1.76	0.68	329.68
zGS11-3	486.23	38.90	186.33	68.19	3.48	0.37	407.64	3.78	0.74	202.04
zGS11-4	530.59	42.45	206.69	69.49	1.52	0.34	485.13	3.46	0.73	222.69

** Aliquot age was excluded from the analysis because an analitical error was made (ICP, He-line, grain broken during unpacking processs etc.)

Table 2. Apatite (U-Th)/He geochemistry data and ages

Sample	*Age [Ma]*	*± [Ma]*	*U (ppm)*	*Th (ppm)*	*147Sm (ppm)*	*Th/U*	*He (nmol/g)*	*mass (µg)*	*Ft*	*eU*	*ERS*
Syn-Rift	*Detrital*		*~23 My*								
ERB01-02	71.96	4.32	18.69	21.64	85.22	1.16	5.70	1.13	0.60	24.11	36.43
ERB01-03	109.15	6.55	11.58	12.11	61.99	1.05	5.60	1.49	0.63	14.68	40.43
ERB01-04	17.87	1.07	22.06	25.85	61.27	1.17	1.52	0.77	0.55	28.32	31.84
ERB-B-2X	*Detrital*										
ERB02-02	87.47	5.25	46.45	32.97	48.78	0.71	18.37	4.09	0.71	54.28	51.71
ERB04-01	47.86	2.87	41.90	116.24	29.05	2.77	9.10	0.60	0.51	68.80	32.77
ERB04-02	81.10	4.87	17.35	24.25	107.36	1.40	5.27	0.64	0.50	23.48	32.06
ERB04-04	7.47	0.45	12.06	44.01	58.70	3.65	0.51	0.80	0.55	22.49	36.50
ERB05-02	134.03	8.04	5.74	9.77	81.83	1.70	3.95	1.43	0.62	8.41	39.76
ERB07-01	16.22	0.97	14.69	27.27	19.41	1.86	1.10	1.28	0.59	21.07	36.51
ERB07-02	27.69	1.66	23.02	14.80	21.85	0.64	2.50	1.36	0.63	26.54	38.97
ERB08-04	16.04	0.96	13.18	36.90	48.24	2.80	1.04	0.80	0.54	21.92	31.94

Aliquot age was excluded from the analysis because; ® it shows a high Helium re- extract (inclusion) -or- * Multiple grain aliquots analized (for pressure vessel digestion with inclusions) -or- (e) high effective Uranium concentration

Sample	*Age [Ma]*	*± [Ma]*	*U (ppm)*	*Th (ppm)*	*147Sm (ppm)*	*Th/U*	*He (nmol/g)*	*mass (µg)*	*Ft*	*eU*	*ERS*
ERB09-01	70.57	4.23	15.64	11.87	113.79	0.76	4.79	2.32	0.65	18.96	41.81
ERB10-03	79.40	4.76	95.49	67.53	49.71	0.71	27.26	0.95	0.57	111.29	32.95
ERB17-02	45.47	2.73	11.47	23.15	187.26	2.02	2.29	0.56	0.50	17.76	29.01
ERB17-03	35.23	2.11	51.98	24.59	336.35	0.47	7.13	1.17	0.62	59.35	37.72
ERB17-04	42.13	2.53	7.71	5.99	139.78	0.78	1.18	0.61	0.51	9.81	28.16
ERB18-02	24.67	1.48	13.65	54.35	36.42	3.98	2.39	2.33	0.67	26.35	47.16
ERB22-01	3.89	0.23	0.76	0.89	0.65	1.16	0.02	5.69	0.76	0.97	64.03
ERB24-01	45.57	2.73	18.61	24.42	60.51	1.31	4.25	2.84	0.69	24.54	49.66
ERB41-1	44.00	2.64	7.94	47.44	92.98	5.97	2.60	1.69	0.55	19.34	33.23
ERB41-2	50.50	3.03	7.00	43.27	16.08	6.18	2.59	1.75	0.55	17.04	33.15
ERB41-4	28.10	1.69	14.00	12.34	11.99	0.88	1.78	3.06	0.69	16.90	48.63
ERB41-5 ®	4.62	0.28	29.65	38.24	11.41	1.29	0.54	0.86	0.56	38.50	33.03
ERB41-6 (e)	82.47	4.95	96.66	156.96	54.41	1.62	30.96	0.71	0.52	133.07	29.73
ERB41-3	42.94	2.58	23.38	43.97	41.99	1.88	4.36	1.80	0.55	33.71	32.58
ERB42-1	53.21	3.19	18.89	93.62	63.07	4.96	6.89	2.24	0.58	40.77	35.71
ERB42-2 ®	94.35	5.66	32.22	54.74	145.39	1.70	11.67	1.11	0.49	45.56	28.08

Aliquot age was excluded from the analysis because; ® it shows a high Helium re- extract (inclusion) -or- * Multiple grain aliquots analized (for pressure vessel digestion with inclusions) -or- (e) high effective Uranium concentration

Sample	*Age [Ma]*	*± [Ma]*	*U (ppm)*	*Th (ppm)*	*147Sm (ppm)*	*Th/U*	*He (nmol/g)*	*mass (µg)*	*Ft*	*eU*	*ERS*
ERB42-3	23.45	1.41	46.67	27.06	4.47	0.58	4.13	1.20	0.62	52.93	37.45
ERB42-4	108.32	6.50	14.06	18.77	16.42	1.33	6.62	1.25	0.61	18.47	37.42
ERB42-5 (e)	8.81	0.53	236.02	102.95	51.70	0.44	7.76	1.49	0.63	259.98	38.40
ERB43-1	4.92	0.30	5.69	58.57	72.02	10.30	0.32	3.20	0.60	19.54	38.34
ERB43-2	113.90	6.83	15.32	55.71	72.21	3.64	8.58	1.12	0.48	28.51	27.67
ERB43-3	58.06	3.48	11.24	13.87	96.68	1.23	2.94	2.84	0.61	14.92	38.11
ERB43-4	3.26	0.20	10.46	45.19	36.19	4.32	0.24	2.24	0.64	21.04	43.57
ERB43-5	3.59	0.22	5.33	54.07	11.79	10.14	0.22	1.59	0.62	17.84	41.05
ERB43-6	36.89	2.21	10.83	91.65	38.75	8.46	3.69	0.99	0.56	32.13	34.76
ERB44-1	38.64	2.32	18.95	24.35	69.71	1.29	3.53	4.25	0.67	24.91	45.53
ERB44-2	15.50	0.93	20.59	30.86	93.86	1.50	1.40	2.08	0.59	28.17	35.52
ERB44-3	61.44	3.69	14.63	23.94	73.45	1.64	4.13	2.39	0.60	20.51	36.69
ERB44-4	18.05	1.08	14.56	23.96	72.05	1.65	1.24	2.76	0.61	20.45	38.64
ERB44-6	17.39	1.04	14.22	18.52	90.77	1.30	1.17	1.92	0.65	18.94	42.46
ERB44-7	61.99	3.72	17.50	30.94	91.44	1.77	4.55	0.72	0.53	25.08	30.85
ERB45-5	33.38	2.00	14.67	13.41	58.01	0.91	2.14	1.69	0.65	18.05	42.10
ERB45-1	53.35	3.20	17.78	23.18	87.16	1.30	4.58	4.14	0.66	23.56	44.59
ERB45-2	15.53	0.93	9.78	11.24	56.59	1.15	0.74	5.79	0.69	12.65	48.73
ERB45-3	23.90	1.43	16.17	19.90	87.28	1.23	1.77	3.29	0.64	21.20	40.98
ERB45-4	30.30	1.82	11.96	15.66	73.45	1.31	1.37	1.19	0.52	15.94	29.47

Aliquot age was excluded from the analysis because; ® it shows a high Helium re- extract (inclusion) -or- * Multiple grain aliquots analized (for pressure vessel digestion with inclusions) -or- (e) high effective Uranium concentration

Sample	*Age [Ma]*	*± [Ma]*	*U (ppm)*	*Th (ppm)*	*147Sm (ppm)*	*Th/U*	*He (nmol/g)*	*mass (µg)*	*Ft*	*eU*	*ERS*
ERB46-1	67.56	4.05	21.99	28.31	111.43	1.29	7.27	4.65	0.67	29.07	46.10
ERB46-2	35.31	2.12	15.12	14.80	69.20	0.98	2.29	2.93	0.63	18.88	39.51
ERB46-3	9.55	0.57	19.39	25.47	96.51	1.31	0.74	1.54	0.55	25.74	31.87
ERB46-4 ®	64.13	3.85	26.11	31.20	110.07	1.20	7.29	2.72	0.61	33.85	37.98
ERB46-5	33.81	2.03	21.95	16.81	73.43	0.77	3.00	1.52	0.62	26.19	38.41
ERB46-6	25.43	1.53	19.84	29.97	131.28	1.51	2.30	1.25	0.60	27.40	36.80
ERB46-7	8.23	0.49	24.96	22.96	99.86	0.92	0.74	0.61	0.53	30.75	30.23
ERB46-8	7.74	0.46	18.31	15.11	79.12	0.83	0.58	1.45	0.62	22.18	38.24
ERB47-1	9.19	0.55	10.17	16.66	65.70	1.64	0.39	1.35	0.53	14.34	31.02
ERB47-2	23.93	1.44	11.55	15.75	63.28	1.36	1.29	3.03	0.63	15.50	40.53
ERB47-3	19.52	1.17	10.89	11.68	62.61	1.07	1.03	6.45	0.69	13.90	48.54
ERB48-1	14.51	0.87	15.45	16.14	58.64	1.05	0.90	1.93	0.58	19.46	34.63
ERB48-2	52.48	3.15	20.35	25.39	65.16	1.25	4.41	1.98	0.58	26.53	34.64
ERB48-3	38.05	2.28	12.40	14.24	61.36	1.15	2.00	2.16	0.60	15.99	36.51
ERB48-4	18.21	1.09	15.90	18.56	78.78	1.17	1.20	1.99	0.59	20.57	35.26
ERB48-5	14.26	0.86	27.58	15.69	62.12	0.57	1.54	1.46	0.63	31.50	39.35
ERB48-6	27.19	1.63	10.27	12.96	54.69	1.26	1.36	2.31	0.67	13.52	45.81
ERB48-7	6.19	0.37	8.47	14.19	74.90	1.67	0.24	1.07	0.57	12.11	34.61
ERB49-1	20.14	1.21	18.46	21.13	72.65	1.14	1.62	2.86	0.62	23.70	38.98
ERB49-2	37.58	2.25	14.54	20.08	81.68	1.38	2.34	2.14	0.58	19.58	34.54
ERB49-3	12.38	0.74	13.62	16.17	65.86	1.19	0.74	2.63	0.61	17.68	38.32

Aliquot age was excluded from the analysis because; ® it shows a high Helium re- extract (inclusion) -or- * Multiple grain aliquots analized (for pressure vessel digestion with inclusions) -or- (e) high effective Uranium concentration

Sample	*Age [Ma]*	*± [Ma]*	*U (ppm)*	*Th (ppm)*	*147Sm (ppm)*	*Th/U*	*He (nmol/g)*	*mass (µg)*	*Ft*	*eU*	*ERS*
ERB49-4	17.01	1.02	11.38	14.80	58.63	1.30	0.86	2.63	0.61	15.08	37.96
ERB50-1 ®	103.93	6.24	23.79	30.87	76.19	1.30	11.16	2.89	0.63	31.28	39.69
ERB50-2	5.96	0.36	9.91	14.35	60.22	1.45	0.25	2.10	0.57	13.52	33.99
ERB50-3	12.63	0.76	13.74	14.54	68.75	1.06	0.73	2.47	0.61	17.44	37.18
ERB50-4	7.57	0.45	14.15	12.88	61.69	0.91	0.44	2.65	0.61	17.43	37.83
Gebel Samra											
GS01-01	83.07	4.98	8.57	14.21	22.28	1.66	3.98	4.16	0.73	11.95	57.77
GS01-02 ®	170.85	10.25	4.93	4.96	20.42	1.01	4.63	9.33	0.79	6.18	75.59
GS01-03	93.86	5.63	6.16	6.10	19.02	0.99	2.91	4.35	0.74	7.67	58.39
GS01-04	76.69	4.60	8.77	10.08	20.14	1.15	3.22	2.57	0.69	11.20	48.15
GS201-1*	11.66	0.70	12.40	43.59	79.86	3.52	0.89	1.30	0.61	22.84	38.70
GS201-2*	91.88	5.51	12.22	14.07	45.36	1.15	4.38	1.72	0.55	15.69	32.28
GS201-3*®	131.04	7.86	17.06	23.66	58.00	1.39	9.62	2.06	0.59	22.80	35.41
GSb01-1*	123.57	7.41	19.42	12.82	84.97	0.66	9.56	8.06	0.62	22.80	37.73
GSb01-2*	100.89	6.05	12.79	11.08	76.03	0.87	5.83	13.17	0.67	15.72	44.42
GSb01-3*	163.51	9.81	10.18	8.06	69.23	0.79	7.18	10.16	0.64	12.38	40.59
GS02-01	25.15	1.51	2.76	2.13	10.44	0.77	0.32	3.21	0.71	3.31	52.71
GS02-02	59.06	3.54	11.30	13.15	30.78	1.16	3.41	3.93	0.73	14.49	56.69
GS02-03	34.07	2.04	2.41	2.69	13.07	1.11	0.42	3.85	0.73	3.10	56.29
GS02-04	43.56	2.61	1.55	1.09	8.68	0.70	0.34	5.64	0.76	1.85	63.94

Aliquot age was excluded from the analysis because; ® it shows a high Helium re- extract (inclusion) -or- * Multiple grain aliquots analized (for pressure vessel digestion with inclusions) -or- (e) high effective Uranium concentration

Sample	*Age [Ma]*	*± [Ma]*	*U (ppm)*	*Th (ppm)*	*147Sm (ppm)*	*Th/U*	*He (nmol/g)*	*mass (µg)*	*Ft*	*eU*	*ERS*
GS202-1®	140.71	8.44	18.87	18.78	42.20	0.99	10.63	2.30	0.59	23.41	35.30
GS202-2	36.95	2.22	15.52	15.44	49.64	0.99	1.95	0.96	0.50	19.33	27.91
GS202-3	103.21	6.19	21.30	23.76	67.34	1.12	9.23	2.28	0.60	27.11	36.74
GSb02-1*	130.92	7.86	26.87	33.55	45.25	1.25	14.25	5.64	0.57	34.82	33.87
GSb02-2*	136.34	8.18	25.01	27.86	42.39	1.11	14.14	7.09	0.60	31.63	36.49
GSb02-3*	116.17	6.97	24.64	26.18	46.71	1.06	12.33	9.64	0.63	30.90	39.64
GS03-01	18.85	1.13	1.35	0.77	26.56	0.57	0.13	2.95	0.71	1.67	51.59
GS03-02	96.76	5.81	2.13	1.10	23.79	0.52	1.02	4.66	0.75	2.51	59.87
GS03-03	104.75	6.29	0.97	0.99	23.42	1.01	0.57	3.65	0.72	1.32	54.39
GS03-04	87.55	5.25	1.93	1.90	29.62	0.98	0.93	4.70	0.74	2.52	60.20
GS203-1	82.72	4.96	15.22	19.74	179.02	1.30	5.20	1.71	0.54	20.67	31.61
GS203-2	143.79	8.63	6.10	8.24	111.62	1.35	4.45	3.56	0.64	8.57	41.09
GS203-3	55.51	3.33	15.54	22.07	182.21	1.42	3.47	1.39	0.52	21.55	29.77
GSb03-1*	89.10	5.35	11.10	13.08	94.41	1.18	4.38	7.99	0.61	14.59	37.48
GSb03-2*	95.44	5.73	12.53	16.17	81.05	1.29	5.46	9.10	0.62	16.66	39.09
GSb03-3*	103.72	6.22	12.10	15.90	104.95	1.31	5.99	10.79	0.64	16.28	41.20
GS04-01	20.46	1.23	3.32	5.20	26.01	1.57	0.38	4.32	0.73	4.65	57.39
GS04-02	16.17	0.97	13.41	19.12	44.07	1.43	1.14	3.35	0.71	18.03	53.73
GS04-03	25.41	1.52	3.19	6.26	28.17	1.96	0.51	6.01	0.76	4.78	64.89
GS04-04	18.05	1.08	4.47	10.99	42.03	2.46	0.51	3.15	0.70	7.21	52.52
GS204-1	23.72	1.42	16.24	45.46	146.93	2.80	1.86	1.25	0.52	27.45	30.13
GS204-2	27.89	1.67	19.79	33.14	117.26	1.67	2.18	1.19	0.51	28.02	28.90

Aliquot age was excluded from the analysis because; ® it shows a high Helium re- extract (inclusion) -or- * Multiple grain aliquots analized (for pressure vessel digestion with inclusions) -or- (e) high effective Uranium concentration

Sample	*Age [Ma]*	*± [Ma]*	*U (ppm)*	*Th (ppm)*	*147Sm (ppm)*	*Th/U*	*He (nmol/g)*	*mass (µg)*	*Ft*	*eU*	*ERS*
GS204-3	45.88	2.75	28.91	43.72	119.86	1.51	5.39	1.56	0.54	39.58	31.52
GS205-1	4.54	0.27	0.61	1.81	3.30	2.94	0.01	0.80	0.55	1.05	32.69
GS205-2	12.91	0.77	12.78	27.79	241.51	2.18	0.85	1.22	0.57	20.40	34.50
GS205-3	30.05	1.80	32.71	20.51	28.55	0.63	3.67	1.16	0.60	37.58	35.86
GS205-4	26.92	1.61	3.51	15.68	160.25	4.47	0.80	2.12	0.65	7.93	43.76
GS205-5	24.52	1.47	5.44	17.57	213.43	3.23	1.01	2.81	0.68	10.58	47.89
GS205-6	12.38	0.74	10.63	23.52	208.24	2.21	0.81	2.85	0.68	17.10	48.33
GS05-01	38.99	2.34	10.49	15.56	1.85	1.48	2.14	3.55	0.72	14.08	54.70
GS05-03	15.42	0.93	6.10	10.77	3.28	1.77	0.54	5.21	0.75	8.60	62.32
GS206-1	43.60	2.62	9.19	113.13	59.67	12.31	5.16	3.29	0.60	35.54	38.71
GS206-2	16.07	0.96	19.77	144.78	69.45	7.32	2.83	3.18	0.60	53.45	38.22
GS206-3	15.53	0.93	10.76	83.38	74.93	7.75	1.57	3.28	0.60	30.34	38.60
GS06-01	15.05	0.90	4.19	37.05	8.58	8.84	0.84	10.94	0.79	12.76	79.64
GS06-02	30.33	1.82	1.25	24.44	6.28	19.58	0.90	9.03	0.78	6.91	74.57
GS06-03	13.39	0.80	2.42	37.04	10.09	15.31	0.63	8.91	0.78	11.00	73.96
GS06-04	24.57	1.47	3.72	42.88	10.13	11.51	1.48	12.82	0.80	13.65	83.35
GS207-1	29.55	1.77	21.13	19.54	111.61	0.92	2.35	1.64	0.55	26.19	30.07
GS207-2	23.73	1.42	39.03	29.88	129.15	0.77	3.23	1.36	0.53	46.57	32.54
GS207-3	48.78	2.93	45.60	66.36	139.42	1.46	9.25	1.89	0.56	61.59	34.44
GS07-01	22.00	1.32	7.68	34.32	7.25	4.47	0.96	0.60	0.51	15.62	30.07
GS07-02®	71.13	4.27	12.66	22.25	6.50	1.76	3.81	0.94	0.55	17.81	32.54

Aliquot age was excluded from the analysis because; ® it shows a high Helium re- extract (inclusion) -or- * Multiple grain aliquots analized (for pressure vessel digestion with inclusions) -or- (e) high effective Uranium concentration

Sample	*Age [Ma]*	*± [Ma]*	*U (ppm)*	*Th (ppm)*	*147Sm (ppm)*	*Th/U*	*He (nmol/g)*	*mass (µg)*	*Ft*	*eU*	*ERS*
GS07-03	21.45	1.29	35.45	37.05	8.14	1.05	2.97	1.07	0.58	44.02	34.44
GS07-04	20.19	1.21	95.54	80.53	77.77	0.84	6.88	0.77	0.55	114.47	31.44
GSb07-1*	45.77	2.75	26.99	47.06	85.38	1.74	5.66	7.10	0.59	38.25	36.10
GSb07-2*	37.14	2.23	21.06	37.32	73.99	1.77	3.69	7.69	0.60	30.02	37.55
GSb07-3*	66.49	3.99	14.47	31.92	73.78	2.21	5.35	13.35	0.66	22.18	44.70
GS208-1	22.11	1.33	59.67	41.52	220.68	0.70	4.75	1.70	0.56	70.36	32.10
GS208-2	30.00	1.80	95.13	84.13	116.86	0.88	9.58	1.09	0.51	115.09	28.61
GS208-3	15.45	0.93	57.26	37.63	29.92	0.66	2.83	1.06	0.51	66.08	28.43
GS08-01®	7.16	0.43	13.65	14.75	8.95	1.08	0.51	6.19	0.76	17.09	65.92
GS08-02	25.53	1.53	3.05	11.67	20.30	3.82	0.63	6.86	0.76	5.84	67.16
GS08-03	17.24	1.03	7.68	16.22	8.61	2.11	0.73	2.45	0.68	11.46	47.71
GS08-04	9.22	0.55	5.51	14.65	5.36	2.66	0.31	3.19	0.70	8.91	51.14
GS09-01	25.01	1.50	1.76	5.12	18.59	2.91	0.29	2.48	0.68	3.03	48.65
GS09-02	12.55	0.75	2.85	4.86	44.03	1.71	0.22	4.72	0.74	4.19	59.42
GS09-03®	100.12	6.01	15.25	17.91	81.33	1.17	6.23	0.94	0.57	19.78	33.80
GS09-04	29.63	1.78	9.52	13.41	70.16	1.41	1.47	2.67	0.69	12.97	49.77
GS09-05	47.37	2.84	1.28	4.32	20.02	3.38	0.46	4.03	0.72	2.37	57.15
GS209-1	29.31	1.76	29.33	33.36	156.58	1.14	3.41	1.68	0.56	37.80	32.84
GS209-2®	151.07	9.06	24.66	28.31	163.91	1.15	16.01	2.39	0.60	32.01	36.37
GS209-3	46.91	2.81	15.66	17.98	131.63	1.15	3.20	2.56	0.60	20.47	36.75
GSb09-1*	56.86	3.41	32.37	39.14	150.03	1.21	7.14	4.42	0.54	42.14	31.38
GSb09-2*	52.57	3.15	23.53	32.68	141.07	1.39	5.50	7.06	0.60	31.76	36.59

Aliquot age was excluded from the analysis because; ® it shows a high Helium re- extract (inclusion) -or- * Multiple grain aliquots analized (for pressure vessel digestion with inclusions) -or- (e) high effective Uranium concentration

Sample	*Age [Ma]*	*± [Ma]*	*U (ppm)*	*Th (ppm)*	*147Sm (ppm)*	*Th/U*	*He (nmol/g)*	*mass (µg)*	*Ft*	*eU*	*ERS*
GSb09-3*	52.55	3.15	8.61	9.56	63.80	1.11	1.88	6.16	0.58	11.13	34.74
GS10-01®	324.47	19.47	9.91	9.70	123.82	0.98	12.91	0.94	0.55	12.76	31.85
GS10-02	24.38	1.46	14.17	30.80	4.06	2.17	1.33	0.43	0.47	21.28	26.72
GS10-03	6.85	0.41	15.65	16.74	49.19	1.07	0.42	1.00	0.57	19.75	33.87
GS10-04	27.03	1.62	106.89	244.81	47.91	2.29	13.88	1.14	0.58	163.48	35.01
GS10-05	22.62	1.36	19.48	105.11	28.11	5.40	3.61	2.59	0.66	43.81	46.47
GS10-06	14.09	0.85	8.52	51.93	23.47	6.09	1.05	2.37	0.66	20.59	46.12
GS10-07	16.00	0.96	13.87	155.42	21.42	11.21	2.43	0.99	0.55	49.75	34.01
GS210-1®	56.16	3.37	17.94	34.68	64.19	1.93	4.07	1.20	0.50	26.25	28.90
GS210-2	22.72	1.36	10.42	18.72	86.91	1.80	1.12	2.31	0.59	15.17	35.80
GS11-01	29.63	1.78	12.28	16.65	76.28	1.36	1.74	3.87	0.65	16.49	42.49
GS11-02	32.96	1.98	13.11	20.22	90.86	1.54	1.99	2.53	0.60	18.22	37.11
GS11-03	28.04	1.68	12.28	19.48	101.89	1.59	1.69	3.47	0.63	17.27	40.30
GS11-04	20.93	1.26	12.43	20.35	87.72	1.64	1.34	5.08	0.66	17.55	44.51
GS211-1	29.22	1.75	10.57	13.39	123.30	1.27	1.44	2.88	0.62	14.29	38.99
GS211-2	19.95	1.20	13.65	20.57	146.35	1.51	1.16	1.78	0.55	19.14	31.95
GS211-3®	60.31	3.62	13.07	20.53	146.69	1.57	3.66	2.19	0.59	18.54	35.78
GSb11-1*	45.53	2.73	15.00	19.87	95.36	1.33	3.12	9.00	0.62	20.05	39.13
GSb11-2*	62.37	3.74	12.00	15.64	80.01	1.30	3.63	12.99	0.66	16.00	44.09
GSb11-3*	53.35	3.20	13.39	16.45	86.51	1.23	3.43	12.62	0.66	17.61	44.33
GS12-01	54.92	3.30	4.16	3.05	159.00	0.73	1.23	2.03	0.67	5.67	44.47

Aliquot age was excluded from the analysis because; ® it shows a high Helium re- extract (inclusion) -or- * Multiple grain aliquots analized (for pressure vessel digestion with inclusions) -or- (e) high effective Uranium concentration

Sample	*Age [Ma]*	*± [Ma]*	*U (ppm)*	*Th (ppm)*	*147Sm (ppm)*	*Th/U*	*He (nmol/g)*	*mass (µg)*	*Ft*	*eU*	*ERS*
GS12-02	52.08	3.12	20.81	10.94	160.98	0.53	3.85	2.12	0.55	24.15	31.50
GS12-03	148.48	8.91	10.47	15.91	164.73	1.52	7.86	1.42	0.63	14.97	39.94
GS12-04	184.90	11.09	14.99	12.13	133.60	0.81	11.23	1.02	0.59	18.46	35.14
GSb12-1*	171.77	10.31	24.30	22.03	176.13	0.91	16.02	4.86	0.55	30.26	32.09
GSb12-2*	141.50	8.49	23.03	19.44	190.05	0.84	13.65	8.40	0.61	28.45	37.28
GSb12-3*	113.57	6.81	21.88	14.31	182.01	0.65	10.10	8.29	0.61	26.08	37.38
Gebel Araba											
08GZ02-01	34.35	2.06	30.47	25.17	11.81	0.83	3.92	0.92	0.58	36.33	34.16
08GZ02-02	38.74	2.32	21.56	28.89	16.21	1.34	3.67	1.51	0.62	28.30	38.59
08GZ02-03	34.17	2.05	28.07	35.56	22.04	1.27	4.00	1.19	0.59	36.36	35.87
08GZ02-04	31.90	1.91	17.53	39.06	52.43	2.23	3.11	2.44	0.66	26.79	45.78
08GZ03-01	30.70	1.84	26.31	28.96	58.42	1.10	3.23	0.92	0.58	33.27	34.49
08GZ03-02	135.19	8.11	36.92	47.28	98.53	1.28	22.71	1.90	0.63	48.31	40.63
08GZ03-03	101.16	6.07	15.85	18.25	50.52	1.15	6.89	1.24	0.61	20.31	37.87
08GZ03-04	79.93	4.80	15.25	8.12	54.99	0.53	5.34	2.84	0.70	17.40	49.45
08GZ03-05	37.53	2.25	20.82	22.10	64.29	1.06	3.22	1.05	0.60	26.23	36.32
08GZ03-06	24.33	1.46	20.71	18.10	54.58	0.87	1.90	0.85	0.57	25.15	33.26
08GZ03-07	53.63	3.22	36.81	43.50	80.04	1.18	8.48	1.35	0.61	47.23	38.08
08GZ03-08	97.25	5.83	24.22	19.90	55.89	0.82	8.97	1.09	0.58	29.08	34.21

Aliquot age was excluded from the analysis because; ® it shows a high Helium re- extract (inclusion) -or- * Multiple grain aliquots analized (for pressure vessel digestion with inclusions) -or- (e) high effective Uranium concentration

Sample	*Age [Ma]*	*± [Ma]*	*U (ppm)*	*Th (ppm)*	*147Sm (ppm)*	*Th/U*	*He (nmol/g)*	*mass (µg)*	*Ft*	*eU*	*ERS*
08GZ04-1	185.47	11.13	17.55	2.99	47.62	0.17	11.44	3.51	0.61	18.48	35.51
08GZ04-2	127.46	7.65	16.77	2.50	43.83	0.15	7.52	3.22	0.61	17.57	36.07
08GZ04-3	159.47	9.57	12.24	2.00	36.73	0.16	6.06	1.76	0.54	12.89	29.27
08GZ04-4	238.91	14.33	12.38	2.58	39.09	0.21	10.94	1.24	0.63	13.17	38.08
08GZ04-5	180.25	10.81	25.80	20.01	45.91	0.78	17.62	0.96	0.58	30.64	34.35
08GZ04-6	98.55	5.91	9.07	1.33	51.58	0.15	3.71	2.65	0.71	9.64	49.16
08GZ05-1	96.09	5.77	3.99	14.76	31.04	3.70	2.35	3.86	0.58	7.54	36.29
08GZ05-2	50.27	3.02	2.48	7.82	14.04	3.15	0.68	2.84	0.56	4.35	34.20
08GZ05-3	81.33	4.88	4.17	18.00	44.42	4.31	2.25	3.45	0.58	8.54	36.23
08GZ05-4	17.24	1.03	10.74	24.25	41.95	2.26	0.88	0.90	0.56	16.53	33.93
08GZ05-5	172.14	10.33	4.58	17.92	39.23	3.91	5.00	1.07	0.59	8.90	36.44
08GZ05-6	58.99	3.54	5.13	22.17	66.04	4.32	1.73	0.54	0.50	10.56	29.02
08GZ05-7	54.10	3.25	5.66	26.01	63.16	4.59	2.44	2.83	0.68	11.96	48.43
08GZ06-1	69.11	4.15	4.43	15.69	17.60	3.54	1.79	3.77	0.58	8.13	35.73
08GZ06-2	53.69	3.22	4.39	13.52	13.25	3.08	1.30	3.36	0.58	7.57	35.96
08GZ06-3	159.19	9.55	5.20	15.15	15.59	2.92	4.47	3.21	0.58	8.76	35.76
08GZ06-4	19.10	1.15	4.24	12.70	27.57	3.00	0.46	1.43	0.60	7.30	37.44
08GZ06-5	79.43	4.77	8.11	24.54	34.64	3.03	3.98	2.10	0.65	13.93	44.40
08GZ06-6	116.16	6.97	5.90	9.31	13.67	1.58	3.19	1.44	0.62	8.11	38.91
08GZ06-7	10.25	0.62	11.03	22.71	28.42	2.06	0.58	1.54	0.63	16.40	40.72
08GZ07-1	50.74	3.04	8.92	27.21	33.87	3.05	2.15	1.18	0.50	15.36	29.20

Aliquot age was excluded from the analysis because; ® it shows a high Helium re- extract (inclusion) -or- * Multiple grain aliquots analized (for pressure vessel digestion with inclusions) -or- (e) high effective Uranium concentration

Sample	*Age [Ma]*	*± [Ma]*	*U (ppm)*	*Th (ppm)*	*147Sm (ppm)*	*Th/U*	*He (nmol/g)*	*mass (µg)*	*Ft*	*eU*	*ERS*
08GZ07-2	73.42	4.40	7.84	22.00	22.16	2.80	2.86	2.50	0.54	13.02	32.35
08GZ07-3	67.98	4.08	7.18	18.62	17.34	2.59	2.40	2.72	0.56	11.56	33.29
08GZ07-4	28.79	1.73	7.63	11.03	24.15	1.45	0.93	0.92	0.58	10.29	34.56
08GZ07-5	53.15	3.19	8.67	17.04	26.14	1.97	2.21	1.27	0.60	12.72	36.90
08GZ07-6	189.03	11.34	6.74	22.40	21.68	3.32	7.45	1.28	0.59	12.01	37.16
08GZ07-7	54.96	3.30	11.37	32.77	52.69	2.88	3.52	1.60	0.61	19.18	38.45
08GZ09-1	89.81	5.39	24.09	15.08	10.16	0.63	7.68	1.78	0.57	27.62	33.01
08GZ09-2	34.51	2.07	9.23	16.32	20.25	1.77	1.60	4.14	0.65	13.09	43.24
08GZ09-3	38.65	2.32	12.28	28.56	25.81	2.32	2.21	1.97	0.55	18.99	32.62
08GZ09-4 ®	179.15	10.75	10.68	36.73	64.70	3.44	9.68	0.65	0.50	19.46	29.17
08GZ09-5	60.81	3.65	3.45	7.84	12.31	2.27	0.90	0.58	0.51	5.32	29.36
08GZ16-1	38.53	2.31	6.77	19.31	42.68	2.85	1.25	0.59	0.52	11.43	30.10
08GZ17-1	130.01	7.80	4.88	13.53	50.16	2.77	3.67	4.18	0.61	8.25	39.16
08GZ17-2	117.51	7.05	6.74	21.43	65.54	3.18	4.13	1.43	0.53	12.01	30.94
08GZ17-3	69.50	4.17	2.51	28.48	53.01	11.35	2.06	1.91	0.57	9.34	35.14
Saint Chaterine	*Road*										
09STGS08-1	131.98	7.92	29.88	67.94	85.17	2.27	22.87	2.94	0.68	45.94	49.04
09STGS08-2	78.34	4.70	17.97	24.24	75.07	1.35	7.01	2.56	0.68	23.92	47.53

Aliquot age was excluded from the analysis because; ® it shows a high Helium re- extract (inclusion) -or- * Multiple grain aliquots analized (for pressure vessel digestion with inclusions) -or- (e) high effective Uranium concentration

Table 3.Zircon (U-Th)/He alpha dosage and spatial data

Sample	*alpha dosage (200myr)*	*alpha dosage (350myr)*	*alpha dosage (450myr)*	*alpha dosage (550myr)*	*Elev./ Depth (m)*	*Latitude*	*Longitude*
Nukhul							
zERB01-1	7.904E+15	1.402E+16	1.820E+16	2.246E+16	-156	28.995243°	33.193448°
zERB01-2	1.247E+16	2.212E+16	2.871E+16	3.541E+16	-156	28.995243°	33.193448°
zERB01-3	9.149E+15	1.624E+16	2.107E+16	2.601E+16	-156	28.995243°	33.193448°
zERB01-4	4.309E+15	7.645E+15	9.922E+15	1.224E+16	-156	28.995243°	33.193448°
z08GS02-01	1.017E+16	1.802E+16	2.338E+16	2.883E+16	90	29.10040568°	33.07043167°
z08GS02-02	2.175E+15	3.857E+15	5.004E+15	6.173E+15	90	29.10040568°	33.07043167°
z08GS02-03	1.946E+16	3.454E+16	4.484E+16	5.534E+16	90	29.10040568°	33.07043167°
z08GS02-04	1.239E+16	2.200E+16	2.855E+16	3.524E+16	90	29.10040568°	33.07043167°
z08GS02-05	1.026E+16	1.821E+16	2.363E+16	2.917E+16	90	29.10040568°	33.07043167°
z08GS02-06	1.094E+16	1.940E+16	2.518E+16	3.106E+16	90	29.10040568°	33.07043167°
z08GS04-01	1.602E+16	2.842E+16	3.688E+16	4.550E+16	125	29.100476°	33.07322645°
z08GS04-02	4.305E+15	7.637E+15	9.909E+15	1.222E+16	125	29.100476°	33.07322645°
z08GS04-03	7.903E+15	1.402E+16	1.819E+16	2.244E+16	125	29.100476°	33.07322645°
z08GS04-04	7.373E+15	1.307E+16	1.696E+16	2.091E+16	125	29.100476°	33.07322645°
z08GS06-01	4.241E+15	7.524E+15	9.764E+15	1.205E+16	112	28.99681893°	33.20001489°

** Aliquot age was excluded from the analysis because an analitical error was made (ICP, He-line, grain broken during unpacking processs etc.)

Sample	*alpha dosage (200myr)*	*alpha dosage (350myr)*	*alpha dosage (450myr)*	*alpha dosage (550myr)*	*Elev./ Depth (m)*	*Latitude*	*Longitude*
z08GS06-02	4.984E+15	8.842E+15	1.147E+16	1.415E+16	112	28.99681893°	33.20001489°
z08GS06-03	1.012E+16	1.794E+16	2.328E+16	2.871E+16	112	28.99681893°	33.20001489°
z08GS06-04	8.996E+15	1.595E+16	2.070E+16	2.553E+16	112	28.99681893°	33.20001489°
z08GS06-05**	1.240E+16	2.201E+16	2.857E+16	3.525E+16	112	28.99681893°	33.20001489°
z08GS06-06	5.635E+15	9.994E+15	1.297E+16	1.599E+16	112	28.99681893°	33.20001489°
z08GS07-01	4.510E+15	8.007E+15	1.039E+16	1.283E+16	254	28.99743316°	33.20038897°
z08GS07-02	1.187E+16	2.107E+16	2.735E+16	3.375E+16	254	28.99743316°	33.20038897°
z08GS07-03	3.851E+15	6.830E+15	8.861E+15	1.093E+16	254	28.99743316°	33.20038897°
z08GS07-04	4.772E+15	8.464E+15	1.098E+16	1.355E+16	254	28.99743316°	33.20038897°
z08GS14-01	7.128E+15	1.265E+16	1.642E+16	2.026E+16	531	29.69878111°	32.89274001°
z08GS14-02	3.313E+15	5.877E+15	7.626E+15	9.409E+15	531	29.69878111°	32.89274001°
z08GS14-03	6.974E+15	1.237E+16	1.606E+16	1.981E+16	531	29.69878111°	32.89274001°
z08GS14-04	1.030E+16	1.828E+16	2.372E+16	2.926E+16	531	29.69878111°	32.89274001°
z09ADGS01-1	1.647E+16	2.923E+16	3.793E+16	4.680E+16	213	28.62903°	33.34855°
z09ADGS01-2	1.835E+15	3.251E+15	4.216E+15	5.198E+15	213	28.62903°	33.34855°
z09ADGS01-3	1.685E+16	2.990E+16	3.880E+16	4.786E+16	213	28.62903°	33.34855°
z09ADGS01-5	5.993E+15	1.063E+16	1.379E+16	1.702E+16	213	28.62903°	33.34855°
z09ADGS01-6	8.942E+15	1.586E+16	2.058E+16	2.539E+16	213	28.62903°	33.34855°
z09ADGS02-1	1.744E+16	3.094E+16	4.015E+16	4.954E+16	301	28.62584°	33.34223°
z09ADGS02-2	1.471E+16	2.611E+16	3.388E+16	4.180E+16	301	28.62584°	33.34223°

** Aliquot age was excluded from the analysis because an analitical error was made (ICP, He-line, grain broken during unpacking processs etc.)

Sample	*alpha dosage (200myr)*	*alpha dosage (350myr)*	*alpha dosage (450myr)*	*alpha dosage (550myr)*	*Elev./ Depth (m)*	*Latitude*	*Longitude*
z09ADGS02-3	6.439E+15	1.142E+16	1.482E+16	1.829E+16	301	28.62584°	33.34223°
z09ADGS02-4	1.500E+16	2.659E+16	3.450E+16	4.255E+16	301	28.62584°	33.34223°
z09ADGS02-5	9.216E+15	1.632E+16	2.116E+16	2.608E+16	301	28.62584°	33.34223°
z09ADGS02-6	4.191E+15	7.415E+15	9.604E+15	1.183E+16	301	28.62584°	33.34223°
z09WAGS04-1	4.301E+15	7.623E+15	9.887E+15	1.219E+16	134	28.70114°	33.32197°
z09WAGS04-2**	5.474E+15	9.702E+15	1.258E+16	1.551E+16	134	28.70114°	33.32197°
z09WAGS04-3	5.547E+15	9.826E+15	1.274E+16	1.570E+16	134	28.70114°	33.32197°
z09WAGS04-4	5.998E+15	1.062E+16	1.377E+16	1.697E+16	134	28.70114°	33.32197°
z09WAGS04-5	2.095E+16	3.715E+16	4.820E+16	5.947E+16	134	28.70114°	33.32197°
z09WAGS04-6	6.613E+15	1.173E+16	1.523E+16	1.879E+16	134	28.70114°	33.32197°
z09WAGS05-1	2.262E+16	4.009E+16	5.198E+16	6.408E+16	114	28.70529°	33.31232°
z09WAGS05-2	1.288E+16	2.278E+16	2.950E+16	3.631E+16	114	28.70529°	33.31232°
z09WAGS05-3	1.042E+16	1.847E+16	2.396E+16	2.954E+16	114	28.70529°	33.31232°
z09WAGS05-4	1.934E+16	3.434E+16	4.457E+16	5.501E+16	114	28.70529°	33.31232°
z09WAGS05-5	1.828E+16	3.243E+16	4.210E+16	5.195E+16	114	28.70529°	33.31232°
z09WAGS05-6	1.130E+16	2.004E+16	2.601E+16	3.209E+16	114	28.70529°	33.31232°
Abu Zenima							
z08GS01-01	1.429E+16	2.536E+16	3.291E+16	4.061E+16	113	29.10028154°	33.07031105°
z08GS01-04	8.004E+15	1.420E+16	1.842E+16	2.273E+16	113	29.10028154°	33.07031105°
z08GS01-05	9.821E+15	1.742E+16	2.260E+16	2.789E+16	113	29.10028154°	33.07031105°

** Aliquot age was excluded from the analysis because an analitical error was made (ICP, He-line, grain broken during unpacking processs etc.)

Sample	*alpha dosage (200myr)*	*alpha dosage (350myr)*	*alpha dosage (450myr)*	*alpha dosage (550myr)*	*Elev./ Depth (m)*	*Latitude*	*Longitude*
z08GS01-06	1.166E+16	2.068E+16	2.683E+16	3.309E+16	113	29.10028154°	33.07031105°
z08GS01-07	1.119E+16	1.984E+16	2.574E+16	3.174E+16	113	29.10028154°	33.07031105°
z08GS01-08	1.492E+16	2.646E+16	3.433E+16	4.235E+16	113	29.10028154°	33.07031105°
z08GS01-09	1.174E+16	2.081E+16	2.700E+16	3.330E+16	113	29.10028154°	33.07031105°
z08GS01-11	2.997E+14	5.322E+14	6.909E+14	8.529E+14	113	29.10028154°	33.07031105°
z08GS03-01	4.834E+15	8.576E+15	1.113E+16	1.373E+16	86	29.09981836°	33.07093483°
z08GS03-02	6.629E+15	1.176E+16	1.526E+16	1.883E+16	86	29.09981836°	33.07093483°
z08GS03-03	2.356E+15	4.177E+15	5.418E+15	6.682E+15	86	29.09981836°	33.07093483°
z08GS03-04	2.552E+15	4.522E+15	5.863E+15	7.227E+15	86	29.09981836°	33.07093483°
z08GS03-05	9.670E+15	1.715E+16	2.226E+16	2.746E+16	86	29.09981836°	33.07093483°
z08GS03-06	3.541E+15	6.278E+15	8.143E+15	1.004E+16	86	29.09981836°	33.07093483°
z08GS03-07	3.706E+15	6.574E+15	8.530E+15	1.052E+16	86	29.09981836°	33.07093483°
z08GS03-08	7.916E+15	1.404E+16	1.821E+16	2.247E+16	86	29.09981836°	33.07093483°
z08GS03-09	6.527E+15	1.158E+16	1.503E+16	1.855E+16	86	29.09981836°	33.07093483°
z08GS03-10	3.225E+15	5.724E+15	7.429E+15	9.167E+15	86	29.09981836°	33.07093483°
z08GS03-11	5.070E+15	8.993E+15	1.167E+16	1.439E+16	86	29.09981836°	33.07093483°
z08GS03-12	6.277E+15	1.113E+16	1.445E+16	1.783E+16	86	29.09981836°	33.07093483°
z08GS03-13	5.297E+15	9.399E+15	1.220E+16	1.505E+16	86	29.09981836°	33.07093483°
z08GS05-01	2.764E+15	4.903E+15	6.361E+15	7.847E+15	116	28.99703183°	33.19974013°
z08GS05-02	2.426E+15	4.301E+15	5.578E+15	6.879E+15	116	28.99703183°	33.19974013°
z08GS05-03	9.532E+15	1.691E+16	2.195E+16	2.708E+16	116	28.99703183°	33.19974013°
z08GS05-04	5.806E+15	1.030E+16	1.337E+16	1.650E+16	116	28.99703183°	33.19974013°

** Aliquot age was excluded from the analysis because an analitical error was made (ICP, He-line, grain broken during unpacking processs etc.)

Sample	*alpha dosage (200myr)*	*alpha dosage (350myr)*	*alpha dosage (450myr)*	*alpha dosage (550myr)*	*Elev./ Depth (m)*	*Latitude*	*Longitude*
Thebes							
zERB02-1	2.534E+15	4.497E+15	5.836E+15	7.201E+15	-193	28.995243°	33.193448°
zERB02-2	2.139E+15	3.792E+15	4.918E+15	6.063E+15	-193	28.995243°	33.193448°
zERB02-3	8.710E+15	1.545E+16	2.005E+16	2.473E+16	-193	28.995243°	33.193448°
zERB02-4	2.091E+16	3.711E+16	4.817E+16	5.945E+16	-194	28.995243°	33.193448°
zERB02-5	8.303E+15	1.474E+16	1.913E+16	2.361E+16	-194	28.995243°	33.193448°
zERB02-6	1.113E+16	1.973E+16	2.560E+16	3.157E+16	-194	28.995243°	33.193448°
zERB02-7	3.380E+15	5.996E+15	7.779E+15	9.596E+15	-193	28.995243°	33.193448°
zERB02-8**	1.051E+16	1.864E+16	2.418E+16	2.982E+16	-193	28.995243°	33.193448°
zERB02-9	4.675E+15	8.292E+15	1.076E+16	1.328E+16	-193	28.995243°	33.193448°
zERB02-10	5.885E+15	1.044E+16	1.354E+16	1.670E+16	-193	28.995243°	33.193448°
zERB02-11	5.871E+15	1.042E+16	1.352E+16	1.668E+16	-193	28.995243°	33.193448°
zERB02-12	6.884E+15	1.221E+16	1.585E+16	1.955E+16	-193	28.995243°	33.193448°
Duwi							
z08GZ14-01	1.271E+16	2.255E+16	2.925E+16	3.608E+16	184	28.383167°	33.512778°
z08GZ14-02	3.808E+15	6.760E+15	8.776E+15	1.083E+16	184	28.383167°	33.512778°
z08GZ14-03	1.911E+15	3.390E+15	4.400E+15	5.429E+15	184	28.383167°	33.512778°
z08GZ14-04	6.694E+15	1.188E+16	1.542E+16	1.904E+16	184	28.383167°	33.512778°
z08GZ14-05	3.977E+15	7.048E+15	9.139E+15	1.127E+16	184	28.383167°	33.512778°
z08GZ14-06	2.102E+16	3.731E+16	4.843E+16	5.977E+16	184	28.383167°	33.512778°

** Aliquot age was excluded from the analysis because an analitical error was made (ICP, He-line, grain broken during unpacking processs etc.)

Sample	*alpha dosage (200myr)*	*alpha dosage (350myr)*	*alpha dosage (450myr)*	*alpha dosage (550myr)*	*Elev./ Depth (m)*	*Latitude*	*Longitude*
Matulla							
zERB4-1	3.877E+15	6.881E+15	8.932E+15	1.102E+16	-400	28.995243°	33.193448°
zERB4-2	6.774E+15	1.202E+16	1.560E+16	1.925E+16	-400	28.995243°	33.193448°
zERB4-3	1.237E+16	2.194E+16	2.847E+16	3.512E+16	-400	28.995243°	33.193448°
zERB4-4	6.183E+15	1.097E+16	1.424E+16	1.757E+16	-400	28.995243°	33.193448°
zERB05-1	1.077E+16	1.912E+16	2.483E+16	3.065E+16	-432	28.995243°	33.193448°
zERB05-3	1.265E+16	2.242E+16	2.909E+16	3.587E+16	-432	28.995243°	33.193448°
zERB05-4	5.856E+15	1.038E+16	1.346E+16	1.660E+16	-432	28.995243°	33.193448°
zERB05-5	7.597E+15	1.345E+16	1.744E+16	2.148E+16	-432	28.995243°	33.193448°
zERB05-6	1.687E+16	2.994E+16	3.886E+16	4.795E+16	-432	28.995243°	33.193448°
zERB6-1	5.946E+15	1.055E+16	1.369E+16	1.689E+16	-454	28.995243°	33.193448°
zERB6-2	9.147E+15	1.622E+16	2.105E+16	2.596E+16	-454	28.995243°	33.193448°
zERB6-3	7.638E+15	1.356E+16	1.760E+16	2.173E+16	-454	28.995243°	33.193448°
zERB6-4	1.629E+16	2.889E+16	3.750E+16	4.627E+16	-454	28.995243°	33.193448°
zERB6-5	7.580E+15	1.344E+16	1.743E+16	2.149E+16	-454	28.995243°	33.193448°
zERB6-6	4.273E+15	7.574E+15	9.822E+15	1.211E+16	-454	28.995243°	33.193448°
z08GS08-01	1.059E+16	1.877E+16	2.433E+16	2.999E+16	280	28.96956543°	33.25395201°
z08GS08-02	6.853E+15	1.216E+16	1.577E+16	1.946E+16	280	28.96956543°	33.25395201°
z08GS08-03	9.196E+15	1.631E+16	2.117E+16	2.612E+16	280	28.96956543°	33.25395201°

** Aliquot age was excluded from the analysis because an analitical error was made (ICP, He-line, grain broken during unpacking processs etc.)

Sample	*alpha dosage (200myr)*	*alpha dosage (350myr)*	*alpha dosage (450myr)*	*alpha dosage (550myr)*	*Elev./ Depth (m)*	*Latitude*	*Longitude*
z08GS08-04	8.982E+15	1.593E+16	2.067E+16	2.549E+16	280	28.96956543°	33.25395201°
z08GS08-05	2.436E+15	4.322E+15	5.609E+15	6.920E+15	280	28.96956543°	33.25395201°
z08GS10-01	9.771E+15	1.735E+16	2.252E+16	2.779E+16	43	29.17831203°	32.96910368°
z08GS10-02	7.908E+15	1.403E+16	1.820E+16	2.245E+16	43	29.17831203°	32.96910368°
z08GS10-03	2.449E+16	4.341E+16	5.632E+16	6.945E+16	43	29.17831203°	32.96910368°
z08GS10-04	2.950E+15	5.233E+15	6.790E+15	8.376E+15	43	29.17831203°	32.96910368°
z08GS10-05	5.522E+14	9.788E+14	1.269E+15	1.565E+15	43	29.17831203°	32.96910368°
z08GS10-06	1.758E+16	3.120E+16	4.050E+16	4.998E+16	43	29.17831203°	32.96910368°
z08GS11-01	2.978E+15	5.280E+15	6.850E+15	8.449E+15	86	29.18029921°	32.96890226°
z08GS11-02	6.452E+15	1.144E+16	1.484E+16	1.831E+16	86	29.18029921°	32.96890226°
z08GS11-03	2.836E+15	5.027E+15	6.521E+15	8.041E+15	86	29.18029921°	32.96890226°
z08GS11-04	5.342E+15	9.475E+15	1.229E+16	1.517E+16	86	29.18029921°	32.96890226°
z08GS13-01	5.478E+15	9.718E+15	1.261E+16	1.556E+16	557	29.70215935°	32.9447685°
z08GS13-02	5.176E+15	9.184E+15	1.192E+16	1.471E+16	557	29.70215935°	32.9447685°
z08GS13-03	3.524E+15	6.251E+15	8.112E+15	1.001E+16	557	29.70215935°	32.9447685°
z08GS13-04	8.474E+15	1.503E+16	1.950E+16	2.406E+16	557	29.70215935°	32.9447685°
z09STGS03-1	5.431E+15	9.631E+15	1.250E+16	1.541E+16	311	28.78594°	33.43802°
z09STGS03-2	1.058E+16	1.876E+16	2.433E+16	3.000E+16	311	28.78594°	33.43802°
z09STGS03-3	1.017E+16	1.805E+16	2.343E+16	2.892E+16	311	28.78594°	33.43802°
z09STGS03-4	1.535E+16	2.719E+16	3.525E+16	4.346E+16	311	28.78594°	33.43802°

** Aliquot age was excluded from the analysis because an analitical error was made (ICP, He-line, grain broken during unpacking processs etc.)

Sample	*alpha dosage (200myr)*	*alpha dosage (350myr)*	*alpha dosage (450myr)*	*alpha dosage (550myr)*	*Elev./ Depth (m)*	*Latitude*	*Longitude*
z09STGS03-5	3.157E+15	5.600E+15	7.267E+15	8.966E+15	311	28.78594°	33.43802°
z09STGS03-6	6.346E+15	1.125E+16	1.459E+16	1.800E+16	311	28.78594°	33.438
z09STGS04-1	1.941E+16	3.442E+16	4.465E+16	5.507E+16	344	28.78852°	33.43971°
z09STGS04-2	8.859E+15	1.572E+16	2.041E+16	2.519E+16	344	28.78852°	33.43971°
z09STGS04-3	4.182E+15	7.421E+15	9.631E+15	1.189E+16	344	28.78852°	33.43971°
z09STGS04-4	1.390E+15	2.465E+15	3.199E+15	3.947E+15	344	28.78852°	33.43971°
z09STGS04-5	8.247E+15	1.464E+16	1.900E+16	2.345E+16	344	28.78852°	33.43971°
z09STGS04-6	4.383E+15	7.776E+15	1.009E+16	1.245E+16	344	28.78852°	33.43971°
Wata							
zERB07-1	1.157E+15	2.052E+15	2.663E+15	3.286E+15	-527	28.995243°	33.193448°
zERB07-3	7.455E+15	1.323E+16	1.716E+16	2.118E+16	-527	28.995243°	33.193448°
zERB07-4	9.302E+15	1.651E+16	2.143E+16	2.644E+16	-527	28.995243°	33.193448°
zERB08-1	1.068E+16	1.895E+16	2.460E+16	3.035E+16	-552	28.995243°	33.193448°
zERB08-2	1.038E+16	1.840E+16	2.388E+16	2.945E+16	-552	28.995243°	33.193448°
zERB08-3	1.079E+16	1.914E+16	2.484E+16	3.064E+16	-552	28.995243°	33.193448°
zERB08-5	1.011E+16	1.793E+16	2.327E+16	2.871E+16	-552	28.995243°	33.193448°
zERB09-1	2.008E+15	3.563E+15	4.624E+15	5.706E+15	-560	28.995243°	33.193448°
zERB09-2	5.757E+15	1.022E+16	1.326E+16	1.636E+16	-560	28.995243°	33.193448°
zERB09-3	1.870E+15	3.317E+15	4.304E+15	5.309E+15	-560	28.995243°	33.193448°

** Aliquot age was excluded from the analysis because an analitical error was made (ICP, He-line, grain broken during unpacking processs etc.)

Sample	*alpha dosage (200myr)*	*alpha dosage (350myr)*	*alpha dosage (450myr)*	*alpha dosage (550myr)*	*Elev./ Depth (m)*	*Latitude*	*Longitude*
zERB09-4	6.991E+15	1.241E+16	1.611E+16	1.988E+16	-560	28.995243°	33.193448°
zERB10-1	1.101E+16	1.953E+16	2.534E+16	3.126E+16	-569	28.995243°	33.193448°
zERB10-2	9.694E+15	1.720E+16	2.232E+16	2.754E+16	-569	28.995243°	33.193448°
zERB10-3	7.457E+15	1.323E+16	1.717E+16	2.119E+16	-569	28.995243°	33.193448°
zERB10-4	1.577E+16	2.796E+16	3.628E+16	4.475E+16	-569	28.995243°	33.193448°
z09STGS02-1	2.900E+16	5.146E+16	6.679E+16	8.242E+16	334	28.7845°	33.43047°
z09STGS02-2	1.138E+16	2.019E+16	2.620E+16	3.233E+16	334	28.7845°	33.43047°
z09STGS02-3	3.992E+15	7.084E+15	9.195E+15	1.135E+16	334	28.7845°	33.43047°
z09STGS02-4	4.464E+15	7.920E+15	1.028E+16	1.268E+16	334	28.7845°	33.43047°
z09STGS02-5	9.837E+15	1.745E+16	2.264E+16	2.793E+16	334	28.7845°	33.43047°
z09STGS02-6	2.772E+15	4.918E+15	6.381E+15	7.873E+15	334	28.7845°	33.43047°
z09WAGS01-1	1.359E+16	2.413E+16	3.132E+16	3.865E+16	163	28.67687°	33.28896°
z09WAGS01-3	2.747E+16	4.869E+16	6.315E+16	7.786E+16	163	28.67687°	33.28896°
z09WAGS01-4	4.101E+15	7.277E+15	9.443E+15	1.165E+16	163	28.67687°	33.28896°
z09WAGS01-5	7.202E+15	1.278E+16	1.658E+16	2.046E+16	163	28.67687°	33.28896°
z09WAGS01-6	1.104E+16	1.959E+16	2.542E+16	3.137E+16	163	28.67687°	33.28896°
z09WGS03-1	4.917E+16	8.723E+16	1.132E+17	1.397E+17	109	28.78333°	33.23573°
z09WGS03-2	5.526E+16	9.803E+16	1.272E+17	1.570E+17	109	28.78333°	33.23573°
z09WGS03-3	4.407E+15	7.817E+15	1.014E+16	1.251E+16	109	28.78333°	33.23573°
z09WGS03-4	3.196E+16	5.670E+16	7.358E+16	9.077E+16	109	28.78333°	33.23573°

** Aliquot age was excluded from the analysis because an analitical error was made (ICP, He-line, grain broken during unpacking processs etc.)

Sample	*alpha dosage (200myr)*	*alpha dosage (350myr)*	*alpha dosage (450myr)*	*alpha dosage (550myr)*	*Elev./ Depth (m)*	*Latitude*	*Longitude*
z09WGS03-5	4.125E+16	7.317E+16	9.494E+16	1.171E+17	109	28.78333°	33.23573°
z09WGS03-6	3.349E+16	5.941E+16	7.709E+16	9.511E+16	109	28.78333°	33.23573°
Raha							
zERB13-1	1.866E+16	3.308E+16	4.291E+16	5.291E+16	-650	28.995243°	33.193448°
zERB13-2	9.580E+15	1.697E+16	2.200E+16	2.711E+16	-650	28.995243°	33.193448°
zERB13-3	9.008E+15	1.597E+16	2.071E+16	2.554E+16	-650	28.995243°	33.193448°
zERB13-5	5.224E+15	9.267E+15	1.202E+16	1.484E+16	-650	28.995243°	33.193448°
zERB13-6	4.236E+15	7.504E+15	9.728E+15	1.199E+16	-650	28.995243°	33.193448°
zERB13-7	7.962E+15	1.413E+16	1.833E+16	2.262E+16	-650	28.995243°	33.193448°
zERB13-8	1.378E+16	2.444E+16	3.171E+16	3.911E+16	-650	28.995243°	33.193448°
zERB13-9	3.028E+16	5.370E+16	6.966E+16	8.593E+16	-650	28.995243°	33.193448°
zERB13-10	8.327E+15	1.477E+16	1.917E+16	2.364E+16	-650	28.995243°	33.193448°
zERB12-1	2.364E+16	4.190E+16	5.433E+16	6.699E+16	-627	28.995243°	33.193448°
zERB12-2	6.315E+15	1.121E+16	1.455E+16	1.795E+16	-627	28.995243°	33.193448°
zERB12-3	1.446E+16	2.565E+16	3.329E+16	4.108E+16	-627	28.995243°	33.193448°
zERB12-4	4.898E+15	8.686E+15	1.127E+16	1.390E+16	-627	28.995243°	33.193448°
zERB12-5	8.908E+15	1.581E+16	2.052E+16	2.532E+16	-627	28.995243°	33.193448°
zERB12-6	3.858E+15	6.844E+15	8.882E+15	1.096E+16	-627	28.995243°	33.193448°
z09STGS01-1	8.366E+15	1.484E+16	1.926E+16	2.375E+16	292	28.7832°	33.42948°
z09STGS01-2	1.340E+16	2.378E+16	3.087E+16	3.810E+16	292	28.7832°	33.42948°

** Aliquot age was excluded from the analysis because an analitical error was made (ICP, He-line, grain broken during unpacking processs etc.)

Sample	*alpha dosage (200myr)*	*alpha dosage (350myr)*	*alpha dosage (450myr)*	*alpha dosage (550myr)*	*Elev./ Depth (m)*	*Latitude*	*Longitude*
z09STGS01-3	1.049E+16	1.861E+16	2.415E+16	2.980E+16	292	28.7832°	33.42948°
z09STGS01-4	8.865E+15	1.572E+16	2.040E+16	2.517E+16	292	28.7832°	33.42948°
z09STGS01-5	6.097E+15	1.082E+16	1.404E+16	1.732E+16	292	28.7832°	33.42948°
z09STGS01-6	1.111E+14	1.963E+14	2.542E+14	3.128E+14	292	28.7832°	33.42948°
z09STGS06-1	7.074E+15	1.254E+16	1.628E+16	2.008E+16	317	28.79531°	33.46012°
z09STGS06-2	9.523E+15	1.690E+16	2.193E+16	2.706E+16	317	28.79531°	33.46012°
z09STGS06-3	9.469E+15	1.678E+16	2.176E+16	2.682E+16	317	28.79531°	33.46012°
z09STGS06-4	5.183E+15	9.176E+15	1.189E+16	1.465E+16	317	28.79531°	33.46012°
Malha							
zERB14-1	1.225E+16	2.175E+16	2.824E+16	3.486E+16	-759	28.79531°	33.46012°
zERB14-2	4.711E+15	8.350E+15	1.083E+16	1.335E+16	-759	28.79531°	33.46012°
zERB14-3	5.459E+15	9.677E+15	1.255E+16	1.548E+16	-759	28.79531°	33.46012°
zERB14-4	7.271E+15	1.288E+16	1.670E+16	2.058E+16	-759	28.79531°	33.46012°
zERB14-5	4.907E+15	8.700E+15	1.129E+16	1.392E+16	-759	28.79531°	33.46012°
zERB14-6	4.883E+15	8.655E+15	1.123E+16	1.384E+16	-759	28.79531°	33.46012°
zERB15-1	4.998E+14	8.839E+14	1.144E+15	1.409E+15	-781	28.995243°	33.193448°
zERB16-2	1.169E+16	2.073E+16	2.689E+16	3.318E+16	-804	28.995243°	33.193448°
zERB16-3	9.127E+15	1.619E+16	2.100E+16	2.591E+16	-804	28.995243°	33.193448°
zERB16-4	2.540E+15	4.507E+15	5.850E+15	7.219E+15	-804	28.995243°	33.193448°

** Aliquot age was excluded from the analysis because an analitical error was made (ICP, He-line, grain broken during unpacking processs etc.)

Sample	*alpha dosage (200myr)*	*alpha dosage (350myr)*	*alpha dosage (450myr)*	*alpha dosage (550myr)*	*Elev./ Depth (m)*	*Latitude*	*Longitude*
zERB17-1	1.941E+16	3.443E+16	4.467E+16	5.511E+16	-832	28.995243°	33.193448°
zERB17-2	9.941E+15	1.763E+16	2.287E+16	2.821E+16	-832	28.995243°	33.193448°
zERB17-3	5.204E+15	9.229E+15	1.197E+16	1.477E+16	-832	28.995243°	33.193448°
zERB17-4	8.524E+15	1.513E+16	1.963E+16	2.423E+16	-832	28.995243°	33.193448°
zERB18-1	2.809E+15	4.981E+15	6.461E+15	7.969E+15	-854	28.995243°	33.193448°
zERB18-2	9.208E+15	1.633E+16	2.119E+16	2.614E+16	-854	28.995243°	33.193448°
zERB18-3	3.513E+15	6.230E+15	8.083E+15	9.970E+15	-854	28.995243°	33.193448°
zERB18-4	6.585E+15	1.168E+16	1.515E+16	1.869E+16	-854	28.995243°	33.193448°
zERB18-6	1.881E+16	3.337E+16	4.331E+16	5.343E+16			
zERB19-1	3.070E+15	5.443E+15	7.059E+15	8.705E+15	-873	28.995243°	33.193448°
zERB19-3	5.186E+15	9.197E+15	1.193E+16	1.472E+16	-873	28.995243°	33.193448°
zERB19-4	1.913E+16	3.391E+16	4.397E+16	5.421E+16	-873	28.995243°	33.193448°
zERB19-5	7.735E+15	1.372E+16	1.779E+16	2.194E+16	-873	28.995243°	33.193448°
zERB19-6	2.297E+15	4.075E+15	5.287E+15	6.522E+15	-873	28.995243°	33.193448°
zERB20-1	1.516E+15	2.688E+15	3.488E+15	4.302E+15	-899	28.995243°	33.193448°
zERB20-2	1.220E+16	2.163E+16	2.806E+16	3.461E+16	-899	28.995243°	33.193448°
zERB20-3	2.206E+15	3.912E+15	5.074E+15	6.257E+15	-899	28.995243°	33.193448°
zERB20-4	9.470E+15	1.679E+16	2.177E+16	2.684E+16	-899	28.995243°	33.193448°
zERB21-1	5.550E+15	9.839E+15	1.276E+16	1.574E+16	-926	28.995243°	33.193448°

** Aliquot age was excluded from the analysis because an analitical error was made (ICP, He-line, grain broken during unpacking processs etc.)

Sample	*alpha dosage (200myr)*	*alpha dosage (350myr)*	*alpha dosage (450myr)*	*alpha dosage (550myr)*	*Elev./ Depth (m)*	*Latitude*	*Longitude*
zERB21-2	9.184E+15	1.627E+16	2.109E+16	2.600E+16	-926	28.995243°	33.193448°
zERB21-4	9.087E+15	1.611E+16	2.089E+16	2.575E+16	-926	28.995243°	33.193448°
zERB22-1	2.922E+15	5.183E+15	6.726E+15	8.298E+15	-949	28.995243°	33.193448°
zERB22-2	2.128E+15	3.775E+15	4.899E+15	6.044E+15	-949	28.995243°	33.193448°
zERB22-3	4.323E+15	7.668E+15	9.949E+15	1.227E+16	-949	28.995243°	33.193448°
zERB22-4	8.668E+15	1.537E+16	1.993E+16	2.459E+16	-949	28.995243°	33.193448°
zERB23-1	7.878E+15	1.397E+16	1.812E+16	2.236E+16	967	28.995243°	33.193448°
zERB23-2	2.632E+15	4.670E+15	6.060E+15	7.477E+15	967	28.995243°	33.193448°
zERB23-3	2.684E+15	4.763E+15	6.182E+15	7.628E+15	967	28.995243°	33.193448°
zERB23-4	1.047E+16	1.857E+16	2.410E+16	2.973E+16	967	28.995243°	33.193448°
zERB23-5	2.091E+15	3.709E+15	4.813E+15	5.938E+15	967	28.995243°	33.193448°
zERB23-6	1.488E+16	2.641E+16	3.427E+16	4.229E+16	967	28.995243°	33.193448°
zERB24-1	1.133E+16	2.009E+16	2.607E+16	3.216E+16	-990	28.995243°	33.193448°
zERB24-2	6.334E+15	1.124E+16	1.458E+16	1.799E+16	-990	28.995243°	33.193448°
zERB24-3	1.704E+16	3.024E+16	3.925E+16	4.844E+16	-990	28.995243°	33.193448°
zERB24-4	1.094E+16	1.940E+16	2.517E+16	3.104E+16	-990	28.995243°	33.193448°
z08GZ16-01	1.111E+17	1.972E+17	2.560E+17	3.159E+17	185	28.384944°	33.505722°
z08GZ16-02	1.027E+16	1.823E+16	2.366E+16	2.920E+16	185	28.384944°	33.505722°
z08GZ16-03	7.483E+16	1.328E+17	1.724E+17	2.129E+17	185	28.384944°	33.505722°
z08GZ16-04	5.110E+16	9.071E+16	1.178E+17	1.454E+17	185	28.384944°	33.505722°

** Aliquot age was excluded from the analysis because an analitical error was made (ICP, He-line, grain broken during unpacking processs etc.)

Sample	*alpha dosage (200myr)*	*alpha dosage (350myr)*	*alpha dosage (450myr)*	*alpha dosage (550myr)*	*Elev./ Depth (m)*	*Latitude*	*Longitude*
Qiseib							
zERB25-1	2.302E+15	4.084E+15	5.299E+15	6.538E+15	-1018	28.995243°	33.193448°
zERB25-2	2.632E+15	4.668E+15	6.057E+15	7.471E+15	-1018	28.995243°	33.193448°
zERB25-3	1.070E+16	1.898E+16	2.462E+16	3.036E+16	-1018	28.995243°	33.193448°
zERB25-4	5.591E+15	9.910E+15	1.285E+16	1.585E+16	-1018	28.995243°	33.193448°
zERB26-1	1.227E+16	2.174E+16	2.820E+16	3.478E+16	-1042	28.995243°	33.193448°
zERB26-2	5.154E+15	9.136E+15	1.185E+16	1.461E+16	-1042	28.995243°	33.193448°
zERB26-3	8.165E+15	1.448E+16	1.878E+16	2.316E+16	-1042	28.995243°	33.193448°
zERB26-4	7.549E+15	1.339E+16	1.737E+16	2.143E+16	-1042	28.995243°	33.193448°
zERB26-5	1.547E+16	2.743E+16	3.558E+16	4.388E+16	-1042	28.995243°	33.193448°
zERB26-6	7.655E+14	1.357E+15	1.761E+15	2.172E+15	-1042	28.995243°	33.193448°
zERB26-7	7.936E+15	1.406E+16	1.823E+16	2.247E+16	-1042	28.995243°	33.193448°
zERB26-8	3.735E+15	6.623E+15	8.592E+15	1.060E+16	-1042	28.995243°	33.193448°
zERB26-9	1.451E+16	2.575E+16	3.341E+16	4.123E+16	-1042	28.995243°	33.193448°
zERB27-1	1.152E+16	2.043E+16	2.652E+16	3.272E+16	-1062	28.995243°	33.193448°
zERB27-2**	1.215E+16	2.154E+16	2.795E+16	3.447E+16	-1062	28.995243°	33.193448°
zERB27-3	1.172E+16	2.076E+16	2.691E+16	3.317E+16	-1062	28.995243°	33.193448°
zERB27-4	4.288E+15	7.600E+15	9.857E+15	1.215E+16	-1062	28.995243°	33.193448°
zERB27-5	1.065E+16	1.888E+16	2.450E+16	3.022E+16	-1062	28.995243°	33.193448°
zERB27-7	8.131E+15	1.442E+16	1.870E+16	2.306E+16	-1062	28.995243°	33.193448°

** Aliquot age was excluded from the analysis because an analitical error was made (ICP, He-line, grain broken during unpacking processs etc.)

Sample	*alpha dosage (200myr)*	*alpha dosage (350myr)*	*alpha dosage (450myr)*	*alpha dosage (550myr)*	*Elev./ Depth (m)*	*Latitude*	*Longitude*
zERB27-8	9.011E+15	1.597E+16	2.070E+16	2.552E+16	-1062	28.995243°	33.193448°
zERB27-9	7.384E+15	1.309E+16	1.698E+16	2.095E+16	-1062	28.995243°	33.193448°
zERB27-10	7.293E+15	1.294E+16	1.679E+16	2.071E+16	-1062	28.995243°	33.193448°
	7.640E+15	1.355E+16	1.759E+16	2.170E+16			
zERB28-1	1.079E+16	1.910E+16	2.474E+16	3.047E+16	-1103	28.995243°	33.193448°
zERB28-2	1.033E+16	1.833E+16	2.379E+16	2.936E+16	-1103	28.995243°	33.193448°
zERB28-3	8.502E+15	1.507E+16	1.955E+16	2.411E+16	-1103	28.995243°	33.193448°
zERB28-4	1.525E+16	2.704E+16	3.508E+16	4.326E+16	-1103	28.995243°	33.193448°
zERB28-5	3.238E+16	5.743E+16	7.451E+16	9.192E+16	-1103	28.995243°	33.193448°
zERB28-6	4.743E+15	8.400E+15	1.089E+16	1.342E+16	-1103	28.995243°	33.193448°
zERB29-1	7.590E+15	1.344E+16	1.742E+16	2.146E+16	-1130	28.995243°	33.193448°
zERB29-2	2.266E+16	4.023E+16	5.223E+16	6.447E+16	-1130	28.995243°	33.193448°
zERB29-3	1.444E+16	2.558E+16	3.316E+16	4.088E+16	-1130	28.995243°	33.193448°
zERB29-4	3.739E+15	6.630E+15	8.600E+15	1.061E+16	-1130	28.995243°	33.193448°
zERB29-5	1.961E+16	3.478E+16	4.512E+16	5.565E+16	-1130	28.995243°	33.193448°
zERB29-6	8.358E+15	1.483E+16	1.925E+16	2.376E+16	-1130	28.995243°	33.193448°
Abu Thora							
zERB31-1	8.266E+15	1.466E+16	1.903E+16	2.348E+16	-1194	28.995243°	33.193448°
zERB31-2	1.181E+16	2.091E+16	2.711E+16	3.341E+16	-1194	28.995243°	33.193448°
zERB31-3	1.115E+16	1.978E+16	2.567E+16	3.168E+16	-1194	28.995243°	33.193448°
zERB31-4	2.565E+16	4.552E+16	5.908E+16	7.292E+16	-1194	28.995243°	33.193448°

** Aliquot age was excluded from the analysis because an analitical error was made (ICP, He-line, grain broken during unpacking processs etc.)

Sample	*alpha dosage (200myr)*	*alpha dosage (350myr)*	*alpha dosage (450myr)*	*alpha dosage (550myr)*	*Elev./ Depth (m)*	*Latitude*	*Longitude*
zERB32-1	4.236E+15	7.513E+15	9.748E+15	1.202E+16	-1222	28.995243°	33.193448°
zERB32-2	3.109E+15	5.505E+15	7.135E+15	8.791E+15	-1222	28.995243°	33.193448°
zERB32-3	1.095E+16	1.940E+16	2.517E+16	3.103E+16	-1222	28.995243°	33.193448°
zERB32-4	6.432E+15	1.141E+16	1.481E+16	1.827E+16	-1222	28.995243°	33.193448°
zERB32-5	1.293E+16	2.296E+16	2.980E+16	3.677E+16	-1222	28.995243°	33.193448°
zERB32-6	8.866E+15	1.570E+16	2.035E+16	2.507E+16	-1222	28.995243°	33.193448°
zERB35-1	1.653E+16	2.933E+16	3.806E+16	4.696E+16	-1313	28.995243°	33.193448°
zERB35-2	1.009E+16	1.789E+16	2.322E+16	2.864E+16	-1313	28.995243°	33.193448°
zERB35-3	1.937E+15	3.432E+15	4.448E+15	5.482E+15	-1313	28.995243°	33.193448°
zERB35-4	6.073E+15	1.077E+16	1.397E+16	1.722E+16	-1313	28.995243°	33.193448°
zERB35-5	9.365E+15	1.658E+16	2.150E+16	2.649E+16	-1313	28.995243°	33.193448°
zERB37-1	4.140E+15	7.337E+15	9.513E+15	1.173E+16	-1374	28.995243°	33.193448°
zERB37-2	5.049E+15	8.950E+15	1.161E+16	1.432E+16	-1374	28.995243°	33.193448°
zERB37-3	2.800E+16	4.971E+16	6.453E+16	7.966E+16	-1374	28.995243°	33.193448°
zERB37-4	4.236E+16	7.518E+16	9.758E+16	1.204E+17	-1374	28.995243°	33.193448°
zERB37-5	1.816E+16	3.224E+16	4.185E+16	5.166E+16	-1374	28.995243°	33.193448°
zERB37-6	8.390E+15	1.487E+16	1.928E+16	2.377E+16	-1374	28.995243°	33.193448°
zERB38-1	9.613E+15	1.706E+16	2.214E+16	2.732E+16	-1402	28.995243°	33.193448°
zERB38-2	4.428E+15	7.859E+15	1.020E+16	1.259E+16	-1402	28.995243°	33.193448°

** Aliquot age was excluded from the analysis because an analitical error was made (ICP, He-line, grain broken during unpacking processs etc.)

Sample	*alpha dosage (200myr)*	*alpha dosage (350myr)*	*alpha dosage (450myr)*	*alpha dosage (550myr)*	*Elev./ Depth (m)*	*Latitude*	*Longitude*
zERB39-1	5.858E+15	1.039E+16	1.348E+16	1.662E+16	-1420	28.995243°	33.193448°
zERB39-2	6.940E+15	1.231E+16	1.597E+16	1.970E+16	-1420	28.995243°	33.193448°
zERB39-3	2.800E+15	4.959E+15	6.428E+15	7.923E+15	-1420	28.995243°	33.193448°
zERB39-4	3.266E+15	5.786E+15	7.501E+15	9.245E+15	-1420	28.995243°	33.193448°
z09STGS07-1	8.603E+15	1.526E+16	1.980E+16	2.442E+16	343	28.79452°	33.47968°
z09STGS07-2	4.413E+15	7.828E+15	1.016E+16	1.253E+16	343	28.79452°	33.47968°
z09STGS07-3	7.900E+15	1.401E+16	1.817E+16	2.240E+16	343	28.79452°	33.47968°
z09STGS07-4	4.609E+15	8.175E+15	1.061E+16	1.308E+16	343	28.79452°	33.47968°
z09STGS07-5	4.289E+15	7.606E+15	9.866E+15	1.217E+16	343	28.79452°	33.47968°
z09STGS07-6	1.245E+16	2.209E+16	2.866E+16	3.536E+16	343	28.79452°	33.47968°
Naqus/Araba							
zERB41-1	2.266E+16	4.019E+16	5.213E+16	6.429E+16	-1502	28.995243°	33.193448°
zERB41-2	1.529E+16	2.712E+16	3.519E+16	4.341E+16	-1502	28.995243°	33.193448°
zERB41-3	1.661E+16	2.945E+16	3.820E+16	4.712E+16	-1502	28.995243°	33.193448°
zERB41-4	2.191E+16	3.886E+16	5.042E+16	6.219E+16	-1502	28.995243°	33.193448°
zERB42-1	8.994E+15	1.593E+16	2.066E+16	2.546E+16	-1511	28.995243°	33.193448°
zERB42-2	7.751E+15	1.375E+16	1.784E+16	2.200E+16	-1511	28.995243°	33.193448°
zERB42-3	6.010E+15	1.064E+16	1.378E+16	1.698E+16	-1511	28.995243°	33.193448°
zERB42-4	8.118E+15	1.440E+16	1.868E+16	2.304E+16	-1511	28.995243°	33.193448°
zERB42-5	1.086E+16	1.927E+16	2.500E+16	3.084E+16	-1511	28.995243°	33.193448°

** Aliquot age was excluded from the analysis because an analitical error was made (ICP, He-line, grain broken during unpacking processs etc.)

Sample	*alpha dosage (200myr)*	*alpha dosage (350myr)*	*alpha dosage (450myr)*	*alpha dosage (550myr)*	*Elev./ Depth (m)*	*Latitude*	*Longitude*
zERB42-6	1.098E+16	1.945E+16	2.522E+16	3.109E+16	-1511	28.995243°	33.193448°
zERB43-1	5.795E+15	1.027E+16	1.332E+16	1.643E+16	-1520	28.995243°	33.193448°
zERB43-2	9.080E+15	1.610E+16	2.089E+16	2.577E+16	-1520	28.995243°	33.193448°
zERB43-3	1.242E+16	2.200E+16	2.853E+16	3.516E+16	-1520	28.995243°	33.193448°
zERB43-4	1.753E+16	3.108E+16	4.032E+16	4.972E+16	-1520	28.995243°	33.193448°
zERB43-5	4.414E+15	7.820E+15	1.014E+16	1.250E+16	-1520	28.995243°	33.193448°
zERB43-6	4.926E+15	8.735E+15	1.133E+16	1.398E+16	-1520	28.995243°	33.193448°
zERB44-1	1.676E+16	2.966E+16	3.842E+16	4.731E+16	-1530	28.995243°	33.193448°
zERB44-2	2.432E+16	4.311E+16	5.590E+16	6.892E+16	-1530	28.995243°	33.193448°
zERB44-3	6.524E+15	1.157E+16	1.500E+16	1.850E+16	-1530	28.995243°	33.193448°
zERB44-4	4.345E+15	7.691E+15	9.966E+15	1.228E+16	-1530	28.995243°	33.193448°
z08GZ09-01	2.019E+16	3.584E+16	4.652E+16	5.741E+16	207	28.394750°	33.458056°
z08GZ09-02	9.811E+15	1.740E+16	2.258E+16	2.785E+16	207	28.394750°	33.458056°
z08GZ09-03	9.309E+15	1.650E+16	2.140E+16	2.638E+16	207	28.394750°	33.458056°
z08GZ09-04	9.327E+15	1.653E+16	2.144E+16	2.644E+16	207	28.394750°	33.458056°
z08GZ09-05	1.491E+16	2.645E+16	3.432E+16	4.235E+16	207	28.394750°	33.458056°
z08GZ09-06	9.286E+15	1.644E+16	2.129E+16	2.623E+16	207	28.394750°	33.458056°
z08GZ10-01	1.423E+16	2.524E+16	3.275E+16	4.041E+16	121	28.391750°	33.486083°
z08GZ10-02	1.571E+16	2.786E+16	3.614E+16	4.458E+16	121	28.391750°	33.486083°
z08GZ10-03	6.496E+15	1.151E+16	1.493E+16	1.841E+16	121	28.391750°	33.486083°

** Aliquot age was excluded from the analysis because an analitical error was made (ICP, He-line, grain broken during unpacking processs etc.)

Sample	*alpha dosage (200myr)*	*alpha dosage (350myr)*	*alpha dosage (450myr)*	*alpha dosage (550myr)*	*Elev./ Depth (m)*	*Latitude*	*Longitude*
z08GZ10-04	1.326E+16	2.351E+16	3.050E+16	3.761E+16	121	28.391750°	33.486083°
z08GZ10-05	4.756E+15	8.432E+15	1.094E+16	1.349E+16	121	28.391750°	33.486083°
z08GZ10-06	3.612E+15	6.403E+15	8.305E+15	1.024E+16	121	28.391750°	33.486083°
z08GZ11-01	2.507E+16	4.449E+16	5.775E+16	7.128E+16	134	28.393333°	33.473194°
z08GZ11-02	1.220E+16	2.164E+16	2.808E+16	3.464E+16	134	28.393333°	33.473194°
z08GZ11-03	1.943E+16	3.446E+16	4.471E+16	5.516E+16	134	28.393333°	33.473194°
z08GZ11-04	1.568E+16	2.781E+16	3.608E+16	4.451E+16	134	28.393333°	33.473194°
z08GZ11-05	6.409E+15	1.136E+16	1.473E+16	1.816E+16	134	28.393333°	33.473194°
z08GZ11-06**	1.586E+12	2.785E+12	3.590E+12	4.399E+12	134	28.393333°	33.473194°
z08GZ12-01	9.124E+15	1.618E+16	2.099E+16	2.589E+16	121	28.384278°	33.495139°
z08GZ12-02	1.378E+16	2.444E+16	3.170E+16	3.911E+16	121	28.384278°	33.495139°
z08GZ12-03	8.289E+15	1.469E+16	1.904E+16	2.347E+16	121	28.384278°	33.495139°
z08GZ12-04	7.558E+15	1.341E+16	1.740E+16	2.146E+16	121	28.384278°	33.495139°
z08GZ12-05	8.108E+15	1.435E+16	1.860E+16	2.292E+16	121	28.384278°	33.495139°
z08GZ12-06	2.442E+16	4.333E+16	5.624E+16	6.941E+16	121	28.384278°	33.495139°
z08GZ13-01	1.509E+16	2.674E+16	3.467E+16	4.274E+16	143	28.385472°	33.496750°
z08GZ13-02	1.833E+16	3.248E+16	4.212E+16	5.192E+16	143	28.385472°	33.496750°
z08GZ13-03	9.054E+15	1.606E+16	2.083E+16	2.569E+16	143	28.385472°	33.496750°
z08GZ13-04	1.786E+16	3.167E+16	4.109E+16	5.068E+16	143	28.385472°	33.496750°
z08GZ13-05	1.329E+16	2.355E+16	3.055E+16	3.766E+16	144	28.385472°	33.496750°
z08GZ13-06	1.269E+16	2.251E+16	2.921E+16	3.603E+16	144	28.385472°	33.496750°

** Aliquot age was excluded from the analysis because an analitical error was made (ICP, He-line, grain broken during unpacking processs etc.)

Sample	*alpha dosage (200myr)*	*alpha dosage (350myr)*	*alpha dosage (450myr)*	*alpha dosage (550myr)*	*Elev./ Depth (m)*	*Latitude*	*Longitude*
zGS05-1	1.368E+16	2.424E+16	3.144E+16	3.877E+16	630	28.987056°	33.270917°
zGS05-2	6.400E+15	1.134E+16	1.470E+16	1.813E+16	630	28.987056°	33.270917°
zGS05-3	9.937E+15	1.761E+16	2.284E+16	2.816E+16	630	28.987056°	33.270917°
zGS05-4	5.707E+15	1.012E+16	1.312E+16	1.619E+16	630	28.987056°	33.270917°
zGS06-1	2.522E+16	4.471E+16	5.798E+16	7.149E+16	640	28.988250°	33.271778°
zGS06-2	9.604E+15	1.702E+16	2.207E+16	2.721E+16	640	28.988250°	33.271778°
zGS06-3	6.895E+15	1.221E+16	1.582E+16	1.950E+16	640	28.988250°	33.271778°
zGS06-4	2.375E+15	4.198E+15	5.436E+15	6.691E+15	640	28.988250°	33.271778°
zGS07-01	1.258E+16	2.232E+16	2.896E+16	3.574E+16	665	28.987917°	33.271667°
zGS07-02	1.206E+16	2.138E+16	2.775E+16	3.423E+16	665	28.987917°	33.271667°
zGS07-03	3.454E+16	6.100E+16	7.891E+16	9.706E+16	665	28.987917°	33.271667°
zGS07-04	1.294E+16	2.296E+16	2.979E+16	3.676E+16	665	28.987917°	33.271667°
zGS08-1	4.776E+15	8.471E+15	1.099E+16	1.356E+16	673	28.987056°	33.270917°
zGS08-2	8.225E+15	1.459E+16	1.894E+16	2.336E+16	673	28.987056°	33.270917°
zGS08-3	7.179E+15	1.273E+16	1.652E+16	2.038E+16	673	28.987056°	33.270917°
zGS08-4	1.204E+16	2.136E+16	2.772E+16	3.420E+16	673	28.987056°	33.270917°
zGS09-1	1.160E+16	2.058E+16	2.671E+16	3.295E+16	60	28.992917°	33.247361°
zGS09-2	2.960E+16	5.252E+16	6.816E+16	8.410E+16	60	28.992917°	33.247361°
zGS09-3	2.202E+16	3.907E+16	5.071E+16	6.257E+16	60	28.992917°	33.247361°

** Aliquot age was excluded from the analysis because an analitical error was made (ICP, He-line, grain broken during unpacking processs etc.)

Sample	*alpha dosage (200myr)*	*alpha dosage (350myr)*	*alpha dosage (450myr)*	*alpha dosage (550myr)*	*Elev./ Depth (m)*	*Latitude*	*Longitude*
zGS09-4	1.206E+16	2.140E+16	2.778E+16	3.427E+16	60	28.992917°	33.247361°
Basement							
zERB45-1	5.786E+15	1.025E+16	1.329E+16	1.639E+16	-1548	28.995243°	33.193448°
zERB45-2	1.409E+16	2.497E+16	3.239E+16	3.993E+16	-1548	28.995243°	33.193448°
zERB45-3	7.177E+15	1.272E+16	1.650E+16	2.034E+16	-1548	28.995243°	33.193448°
zERB45-4	2.836E+16	5.033E+16	6.532E+16	8.061E+16	-1548	28.995243°	33.193448°
zERB46-1	7.558E+15	1.340E+16	1.739E+16	2.145E+16	-1566	28.995243°	33.193448°
zERB46-2	5.644E+15	1.001E+16	1.300E+16	1.604E+16	-1566	28.995243°	33.193448°
zERB46-3	2.710E+15	4.800E+15	6.222E+15	7.667E+15	-1566	28.995243°	33.193448°
zERB46-4	7.052E+15	1.250E+16	1.621E+16	1.999E+16	-1566	28.995243°	33.193448°
zERB46-5	1.306E+16	2.314E+16	3.001E+16	3.700E+16	-1566	28.995243°	33.193448°
zERB46-6	2.415E+16	4.284E+16	5.559E+16	6.859E+16	-1566.	28.995243°	33.193448°
zERB-46-1	3.811E+16	6.763E+16	8.778E+16	1.083E+17	-1566	28.995243°	33.193448°
zERB-46-2	2.495E+16	4.426E+16	5.745E+16	7.089E+16	-1566	28.995243°	33.193448°
zERB-46-3	4.578E+16	8.124E+16	1.055E+17	1.301E+17	-1566	28.995243°	33.193448°
zERB-46-4	4.102E+16	7.278E+16	9.445E+16	1.165E+17	-1566	28.995243°	33.193448°
zERB-46-5	7.231E+15	1.282E+16	1.663E+16	2.051E+16	-1566	28.995243°	33.193448°
zERB-46-6	9.920E+15	1.759E+16	2.283E+16	2.815E+16	-1566	28.995243°	33.193448°
zERB-46-7	2.131E+16	3.780E+16	4.906E+16	6.053E+16	-1566	28.995243°	33.193448°
zERB-46-8	3.812E+16	6.764E+16	8.780E+16	1.084E+17	-1566	28.995243°	33.193448°

** Aliquot age was excluded from the analysis because an analitical error was made (ICP, He-line, grain broken during unpacking processs etc.)

Sample	*alpha dosage (200myr)*	*alpha dosage (350myr)*	*alpha dosage (450myr)*	*alpha dosage (550myr)*	*Elev./ Depth (m)*	*Latitude*	*Longitude*
zERB-46-9	7.023E+16	1.246E+17	1.618E+17	1.997E+17	-1566	28.995243°	33.193448°
zERB47-1	3.825E+16	6.789E+16	8.812E+16	1.087E+17	-1594	28.995243°	33.193448°
zERB47-2	3.478E+16	6.171E+16	8.009E+16	9.883E+16	-1594	28.995243°	33.193448°
zERB47-3	2.653E+16	4.707E+16	6.109E+16	7.539E+16	-1594	28.995243°	33.193448°
zERB47-4	1.650E+16	2.926E+16	3.795E+16	4.679E+16	-1594	28.995243°	33.193448°
zERB-47-1	2.341E+16	4.154E+16	5.392E+16	6.654E+16	-1594	28.995243°	33.193448°
zERB-47-2	2.577E+16	4.573E+16	5.936E+16	7.326E+16	-1594	28.995243°	33.193448°
zERB-47-3	2.162E+16	3.837E+16	4.980E+16	6.145E+16	-1594	28.995243°	33.193448°
zERB-47-4	5.953E+16	1.056E+17	1.371E+17	1.692E+17	-1594	28.995243°	33.193448°
zERB-47-5	1.785E+16	3.165E+16	4.107E+16	5.066E+16	-1594	28.995243°	33.193448°
zERB-47-6	4.197E+16	7.449E+16	9.669E+16	1.193E+17	-1594	28.995243°	33.193448°
zERB-47-7	2.686E+16	4.763E+16	6.178E+16	7.620E+16	-1594	28.995243°	33.193448°
zERB-47-8	2.616E+16	4.643E+16	6.027E+16	7.438E+16	-1594	28.995243°	33.193448°
zERB-47-10	2.768E+16	4.905E+16	6.360E+16	7.840E+16	-1594	28.995243°	33.193448°
zERB48-1	2.993E+16	5.312E+16	6.894E+16	8.507E+16	-1621	28.995243°	33.193448°
zERB48-2	2.951E+16	5.237E+16	6.798E+16	8.389E+16	-1621	28.995243°	33.193448°
zERB48-3	4.516E+16	8.016E+16	1.041E+17	1.284E+17	-1621	28.995243°	33.193448°
zERB48-4	1.767E+16	3.135E+16	4.068E+16	5.020E+16	-1621	28.995243°	33.193448°
zERB49-1	1.243E+16	2.204E+16	2.859E+16	3.526E+16	-1648	28.995243°	33.193448°
zERB49-2	3.092E+15	5.482E+15	7.111E+15	8.770E+15	-1648	28.995243°	33.193448°

** Aliquot age was excluded from the analysis because an analitical error was made (ICP, He-line, grain broken during unpacking processs etc.)

Sample	*alpha dosage (200myr)*	*alpha dosage (350myr)*	*alpha dosage (450myr)*	*alpha dosage (550myr)*	*Elev./ Depth (m)*	*Latitude*	*Longitude*
zERB49-3	1.814E+16	3.219E+16	4.179E+16	5.157E+16	-1648	28.995243°	33.193448°
zERB49-4	1.193E+16	2.115E+16	2.744E+16	3.384E+16	-1648	28.995243°	33.193448°
zERB50-1	2.529E+15	4.485E+15	5.818E+15	7.176E+15	-1684	28.995243°	33.193448°
zERB50-2	1.849E+16	3.279E+16	4.254E+16	5.248E+16	-1684	28.995243°	33.193448°
zERB50-3	2.505E+16	4.445E+16	5.770E+16	7.120E+16	-1684	28.995243°	33.193448°
zERB50-4	3.698E+15	6.562E+15	8.516E+15	1.051E+16	-1684	28.995243°	33.193448°
z08GZ02-01	9.499E+15	1.684E+16	2.184E+16	2.694E+16	405	28.389694°	33.437528°
z08GZ02-02	1.621E+16	2.874E+16	3.728E+16	4.598E+16	405	28.389694°	33.437528°
z08GZ02-03	1.398E+16	2.478E+16	3.215E+16	3.965E+16	405	28.389694°	33.437528°
z08GZ02-04	1.567E+16	2.778E+16	3.604E+16	4.446E+16	405	28.389694°	33.437528°
z08GZ03-01	7.480E+14	1.326E+15	1.719E+15	2.119E+15	359	28.390056°	33.439500°
z08GZ03-02	2.392E+16	4.241E+16	5.503E+16	6.787E+16	359	28.390056°	33.439500°
z08GZ03-03	1.722E+15	3.050E+15	3.954E+15	4.873E+15	359	28.390056°	33.439500°
z08GZ03-04	1.137E+16	2.017E+16	2.617E+16	3.229E+16	359	28.390056°	33.439500°
z08GZ04-01	1.604E+16	2.846E+16	3.693E+16	4.558E+16	335	28.389222°	33.441972°
z08GZ04-02	1.388E+16	2.464E+16	3.198E+16	3.947E+16	335	28.389222°	33.441972°
z08GZ04-03	1.536E+16	2.726E+16	3.537E+16	4.365E+16	335	28.389222°	33.441972°
z08GZ04-04**	3.571E+13	6.339E+13	8.229E+13	1.016E+14	335	28.389222°	33.441972°
z08GZ05-01	6.227E+15	1.104E+16	1.432E+16	1.766E+16	292	28.391417°	33.446639°

** Aliquot age was excluded from the analysis because an analitical error was made (ICP, He-line, grain broken during unpacking processs etc.)

Sample	*alpha dosage (200myr)*	*alpha dosage (350myr)*	*alpha dosage (450myr)*	*alpha dosage (550myr)*	*Elev./ Depth (m)*	*Latitude*	*Longitude*
z08GZ05-02	5.041E+15	8.936E+15	1.159E+16	1.429E+16	292	28.391417°	33.446639°
z08GZ05-03	6.254E+15	1.108E+16	1.437E+16	1.772E+16	292	28.391417°	33.446639°
z08GZ05-04	6.855E+15	1.216E+16	1.577E+16	1.945E+16	292	28.391417°	33.446639°
z08GZ06-01	6.584E+15	1.167E+16	1.514E+16	1.868E+16	251	28.393722°	33.451639°
z08GZ06-02	7.041E+15	1.248E+16	1.620E+16	1.997E+16	251	28.393722°	33.451639°
z08GZ06-03	8.671E+15	1.537E+16	1.993E+16	2.456E+16	251	28.393722°	33.451639°
z08GZ06-04	6.913E+15	1.225E+16	1.589E+16	1.959E+16	251	28.393722°	33.451639°
z08GZ07-01	6.793E+15	1.204E+16	1.561E+16	1.925E+16	225	28.394667°	33.453944°
z08GZ07-02	7.757E+15	1.375E+16	1.784E+16	2.200E+16	225	28.394667°	33.453944°
z08GZ07-03	6.407E+15	1.136E+16	1.473E+16	1.816E+16	225	28.394667°	33.453944°
z08GZ07-04	7.395E+15	1.311E+16	1.700E+16	2.095E+16	225	28.394667°	33.453944°
z08GZ08-01	1.050E+16	1.863E+16	2.416E+16	2.980E+16	224	28.395444°	33.456194°
z08GZ08-02	1.965E+15	3.485E+15	4.521E+15	5.576E+15	224	28.395444°	33.456194°
z08GZ08-03	9.408E+15	1.670E+16	2.167E+16	2.675E+16	224	28.395444°	33.456194°
z08GZ08-04	5.954E+15	1.056E+16	1.371E+16	1.692E+16	224	28.395444°	33.456194°
z08GZ17-01	1.872E+16	3.323E+16	4.313E+16	5.324E+16	335	28.595222°	33.579947°
z08GZ17-02	1.087E+17	1.929E+17	2.504E+17	3.090E+17	338	28.595222°	33.579947°
z08GZ17-03	1.275E+17	2.262E+17	2.935E+17	3.620E+17	338	28.595222°	33.579947°
z08GZ17-04	6.850E+16	1.214E+17	1.575E+17	1.942E+17	338	28.595222°	33.579947°

** Aliquot age was excluded from the analysis because an analitical error was made (ICP, He-line, grain broken during unpacking processs etc.)

Sample	*alpha dosage (200myr)*	*alpha dosage (350myr)*	*alpha dosage (450myr)*	*alpha dosage (550myr)*	*Elev./ Depth (m)*	*Latitude*	*Longitude*
zGS01-1	3.782E+16	6.707E+16	8.700E+16	1.073E+17	393	28.991417°	33.255889°
zGS01-2	2.821E+16	5.004E+16	6.493E+16	8.010E+16	393	28.991417°	33.255889°
zGS01-3	3.922E+16	6.954E+16	9.020E+16	1.112E+17	393	28.991417°	33.255889°
zGS01-4	3.766E+16	6.679E+16	8.666E+16	1.069E+17	393	28.991417°	33.255889°
zGS02-1	5.657E+15	1.003E+16	1.301E+16	1.605E+16	454	28.991361°	33.258194°
zGS02-2	9.382E+15	1.664E+16	2.159E+16	2.663E+16	454	28.991361°	33.258194°
zGS02-3	5.836E+15	1.035E+16	1.342E+16	1.655E+16	454	28.991361°	33.258194°
zGS02-4	1.953E+16	3.463E+16	4.494E+16	5.544E+16	454	28.991361°	33.258194°
zGS03-1	2.723E+16	4.833E+16	6.273E+16	7.741E+16	610	28.987972°	33.264444°
zGS03-2	1.461E+16	2.592E+16	3.364E+16	4.151E+16	610	28.987972°	33.264444°
zGS03-3	1.770E+16	3.142E+16	4.078E+16	5.034E+16	610	28.987972°	33.264444°
zGS03-4	3.287E+16	5.834E+16	7.573E+16	9.346E+16	610	28.987972°	33.264444°
zGS04-1	1.329E+16	2.357E+16	3.059E+16	3.774E+16	630	28.987056°	33.270917°
zGS04-2	3.831E+16	6.799E+16	8.824E+16	1.089E+17	630	28.987056°	33.270917°
zGS04-3	6.662E+15	1.182E+16	1.534E+16	1.893E+16	630	28.987056°	33.270917°
zGS04-4	1.044E+16	1.852E+16	2.404E+16	2.966E+16	630	28.987056°	33.270917°
zGS11-1	1.667E+16	2.957E+16	3.838E+16	4.735E+16	130	28.993917°	33.252333°
zGS11-2	2.182E+16	3.873E+16	5.028E+16	6.205E+16	130	28.993917°	33.252333°
zGS11-3	1.339E+16	2.375E+16	3.083E+16	3.803E+16	130	28.993917°	33.252333°
zGS11-4	1.475E+16	2.618E+16	3.398E+16	4.192E+16	130	28.993917°	33.252333°

** Aliquot age was excluded from the analysis because an analitical error was made (ICP, He-line, grain broken during unpacking processs etc.)

Sample	*alpha dosage (200myr)*	*alpha dosage (350myr)*	*alpha dosage (450myr)*	*alpha dosage (550myr)*	*Elev./ Depth (m)*	*Latitude*	*Longitude*
zGS12-01	1.389E+16	2.465E+16	3.199E+16	3.947E+16	161	28.993361°	33.252583°
zGS12-02	4.218E+16	7.485E+16	9.715E+16	1.199E+17	161	28.993361°	33.252583°
zGS12-03	1.467E+16	2.602E+16	3.377E+16	4.166E+16	161	28.993361°	33.252583°
zGS12-04	1.454E+16	2.579E+16	3.347E+16	4.130E+16	161	28.993361°	33.252583°
z09STGS08-1	5.631E+16	9.986E+16	1.296E+17	1.598E+17	348	28.79454°	33.48954°
z09STGS08-2	3.692E+16	6.537E+16	8.472E+16	1.044E+17	348	28.79454°	33.48954°
z09STGS08-3	9.584E+15	1.699E+16	2.204E+16	2.717E+16	348	28.79454°	33.48954°
z09STGS09-1	9.298E+15	1.649E+16	2.140E+16	2.640E+16	430	28.79693°	33.49402°
z09STGS09-2	9.446E+15	1.676E+16	2.175E+16	2.683E+16	430	28.79693°	33.49402°
z09STGS09-3	1.010E+16	1.791E+16	2.324E+16	2.867E+16	430	28.79693°	33.49402°
z09SGS01-1	2.166E+16	3.841E+16	4.984E+16	6.148E+16	262	28.55046°	33.60435°
z09SGS01-2	2.614E+16	4.637E+16	6.018E+16	7.424E+16	262	28.55046°	33.60435°
z09SGS01-3	1.298E+16	2.303E+16	2.988E+16	3.686E+16	262	28.55046°	33.60435°
z09SGS02-1	2.867E+16	5.085E+16	6.598E+16	8.140E+16	367	28.55159°	33.60621°
z09SGS02-2	2.732E+16	4.847E+16	6.290E+16	7.760E+16	367	28.55159°	33.60621°
z09SGS02-3	6.304E+16	1.118E+17	1.451E+17	1.789E+17	367	28.55159°	33.60621°
z09SGS04-1	3.459E+16	6.136E+16	7.963E+16	9.825E+16	285	28.55287°	33.60587°
z09SGS04-2	3.361E+16	5.961E+16	7.735E+16	9.543E+16	285	28.55287°	33.60587°

** Aliquot age was excluded from the analysis because an analitical error was made (ICP, He-line, grain broken during unpacking processs etc.)

Sample	*alpha dosage (200myr)*	*alpha dosage (350myr)*	*alpha dosage (450myr)*	*alpha dosage (550myr)*	*Elev./ Depth (m)*	*Latitude*	*Longitude*
z09SGS04-3	3.392E+16	6.017E+16	7.807E+16	9.631E+16	285	28.55287°	33.60587°
z09SGS05-1	7.432E+16	1.318E+17	1.710E+17	2.110E+17	291	28.55682°	33.60695°
z09SGS05-2	2.510E+16	4.454E+16	5.782E+16	7.136E+16	291	28.55682°	33.60695°
z09SGS05-3	6.181E+16	1.097E+17	1.424E+17	1.757E+17	291	28.55682°	33.60695°
z09SGS06-1	3.673E+16	6.515E+16	8.454E+16	1.043E+17	465	28.55775°	33.60775°
z09SGS06-2	3.944E+16	6.996E+16	9.078E+16	1.120E+17	465	28.55775°	33.60775°
z09SGS06-3	3.464E+16	6.145E+16	7.973E+16	9.837E+16	465	28.55775°	33.60775°

** Aliquot age was excluded from the analysis because an analitical error was made (ICP, He-line, grain broken during unpacking processs etc.)

Table 4. Fluid Inclusion Data (Naqus/Araba Fm.)

Sample # GS-08

Tn (°C)	*Te (°C)*	*Tm (°C)*	*Th (°C)*	*error (°C)*	*sub L*	*classification*	*petrography*
			136.8	1	A	P	q-overgrowth
-44.9		-1.1	118.9	1	B	P	q-overgrowth
-45.4		-0.8	110.8	1	B	P	q-overgrowth
-45.3	-30.9	-2.9	133.1	1	B	P	q-overgrowth
-44.7	-32.1	-2.8	133.4	1	B	P	q-overgrowth
-45.7		-2.5	176.9	1	B	S or PS	P q-growth
-46.9		-2.6	182.4	1	B	S or PS	P q-growth
-53.4		-0.8	209.5	1	B	S or PS	S q-growth
-47.9		-4.6	104.6	1	B	S or PS	S q-growth
-48.6		-3.2	109.5	1	B	S or PS	S q-growth
-47.3		-3.9	106.3	1	B	S or PS	S q-growth
-46.5		-2.9	189.3	1	C	primary in amorphous silica	P q-growth

Sample # GS-07

Tn (°C)	*Te (°C)*	*Tm (°C)*	*Th (°C)*	*error (°C)*	*sub L*	*classification*	*petrography*
			183.8	1	C	P	q-overgrowth
			132.2	1	C	P	q-overgrowth
			173.2	1	C	S or PS	q-overgrowth
			103.8	1	C	P	q-overgrowth
-42.3		-2.7	209.1	1	C	P	q-overgrowth
-46.8		-4	230.2	1	C	P	q-overgrowth
-41		-1	220.1	1	C	P	q-overgrowth
-43.4		-0.9	243.6	1	C	P	q-overgrowth
-37.8		-2.5	182.2	1	C	U	q-overgrowth
-43.1		-2.1	185.3	1	C	U	q-overgrowth
-47.5		-4.8	138.2	1	A	P	q-overgrowth
-46.6		-3.7	168.7	1	A	dust rim	
-42.3		-1.9	182.5	1	G	U	q-overgrowth
-51.4		-4.4	176.4	1	G	dust rim	
-51.7		-4.3	176.3	1	G	dust rim	

Sample # GS-05

Tn (°C)	*Te (°C)*	*Tm (°C)*	*Th (°C)*	*error (°C)*	*sub L*	*classification*	*petrography*
			186.1	1	E	P	S q-growth
			221.5	1	A	P	q-overgrowth
			203.1	1	A	P	q-overgrowth
			160.3	1	E	dust rim	
			172.1	1	E		q-overgrowth
			179.4	1	E	P	S q-growth
-58.9		-5.5	239.9	1	A	P	q-overgrowth
-56.7		-2.4	242.2	1	E	P	q-overgrowth
-55.6		-1.9	158.3	1	E	dust rim	
-57.1		-1.7	151.4	1	E	dust rim	
-58.1		-1.9	154.2	1	E	dust rim	
-57.4		-2.1	158.3	1	D	dust rim	
-41.7		-2.2	162.6	1	D	dust rim	

Tn = first crystal melt
Te = eutactic temperature
Tm_{ice} = last crystal melt temperature
Th = Temperature of homogenization = minimun temp.of entrapment
* sub L = spatial location in the thin section,
* Classifications; (P) primary, (S) secundary, (PS) pseudo-secundary, or (U) unknown, additionaly inclusion in the dust rim sometimes were classified as unknown.
* To see the petrographic context of the fluid inclusions go to appendix 3

Appendix

Appendix **1**

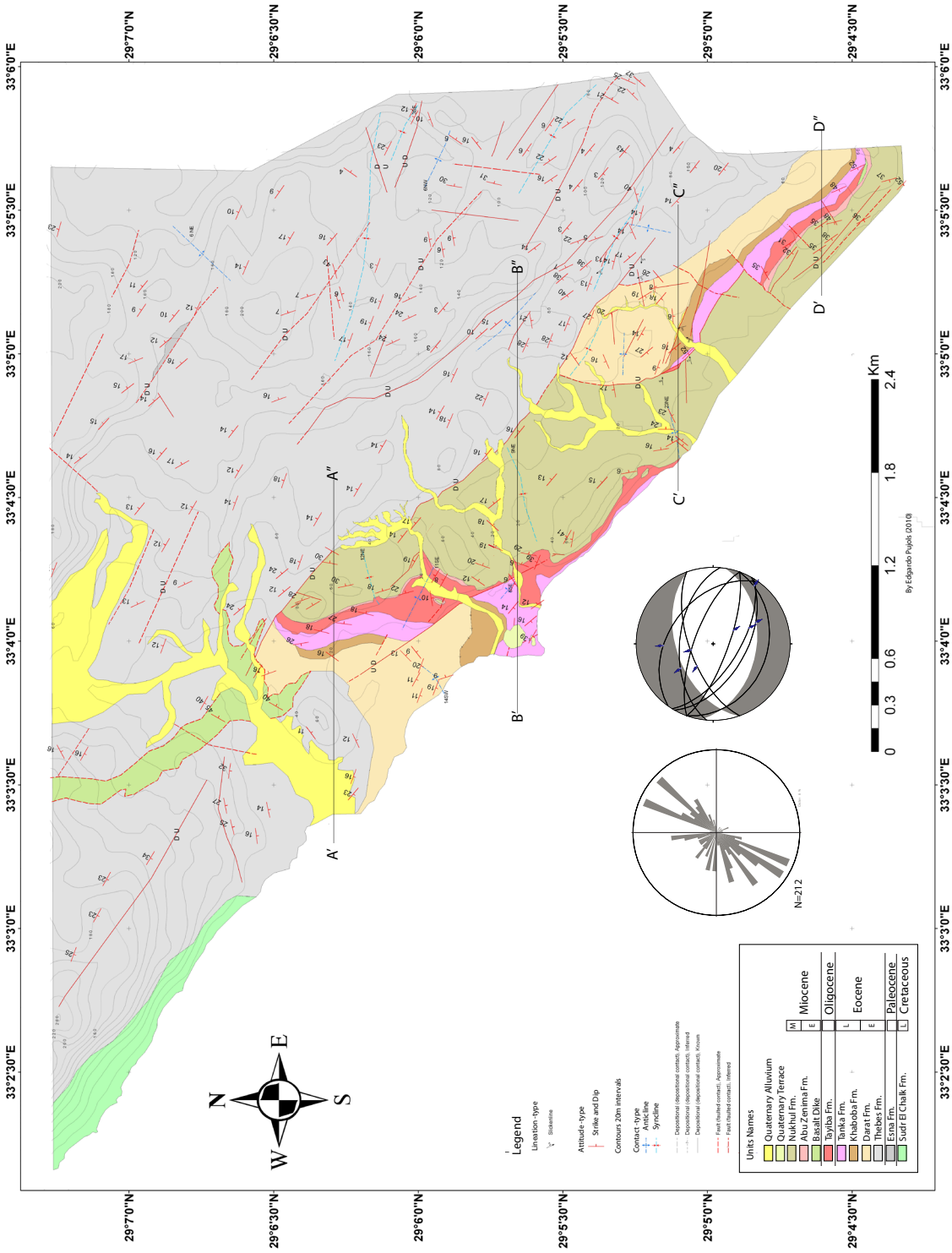
29°7'0"N
29°6'30"N
29°6'0"N
29°5'30"N
29°5'0"N
29°4'30"N
33°2'30"E
33°3'0"E
33°3'30"E
33°4'0"E
33°4'30"E
33°5'0"E
33°5'30"E
33°6'0"E
A'
A''
B'
B''
C'
C''
D'
D''
N
S
E
W
N=212
0 0.3 0.6 1.2 1.8 2.4 Km
By Edgardo Pujols (2018)
Legend
Lineation -type
Bidirectional
Attitude -type
Strike and Dip
Contours 20m intervals
Contact -type
Anticline
Syncline
Depositional (depositional contact), Approximate
Depositional (depositional contact), Inferred
Depositional (depositional contact), Known
Fault (faulted contact), Approximate
Fault (faulted contact), Inferred
Units Names
Quaternary Alluvium
Quaternary Terrace
Nukhul Fm.
Abu Zenima Fm.
Basalt Dike
Tayiba Fm.
Tanka Fm.
Khaboba Fm.
Darat Fm.
Thebes Fm.
Esna Fm.
Sudr El Chalk Fm.
M
E
Miocene
Oligocene
L
E
Eocene
Paleocene
L
Cretaceous

Cross Sections for Wadi Tanka

1 : 1

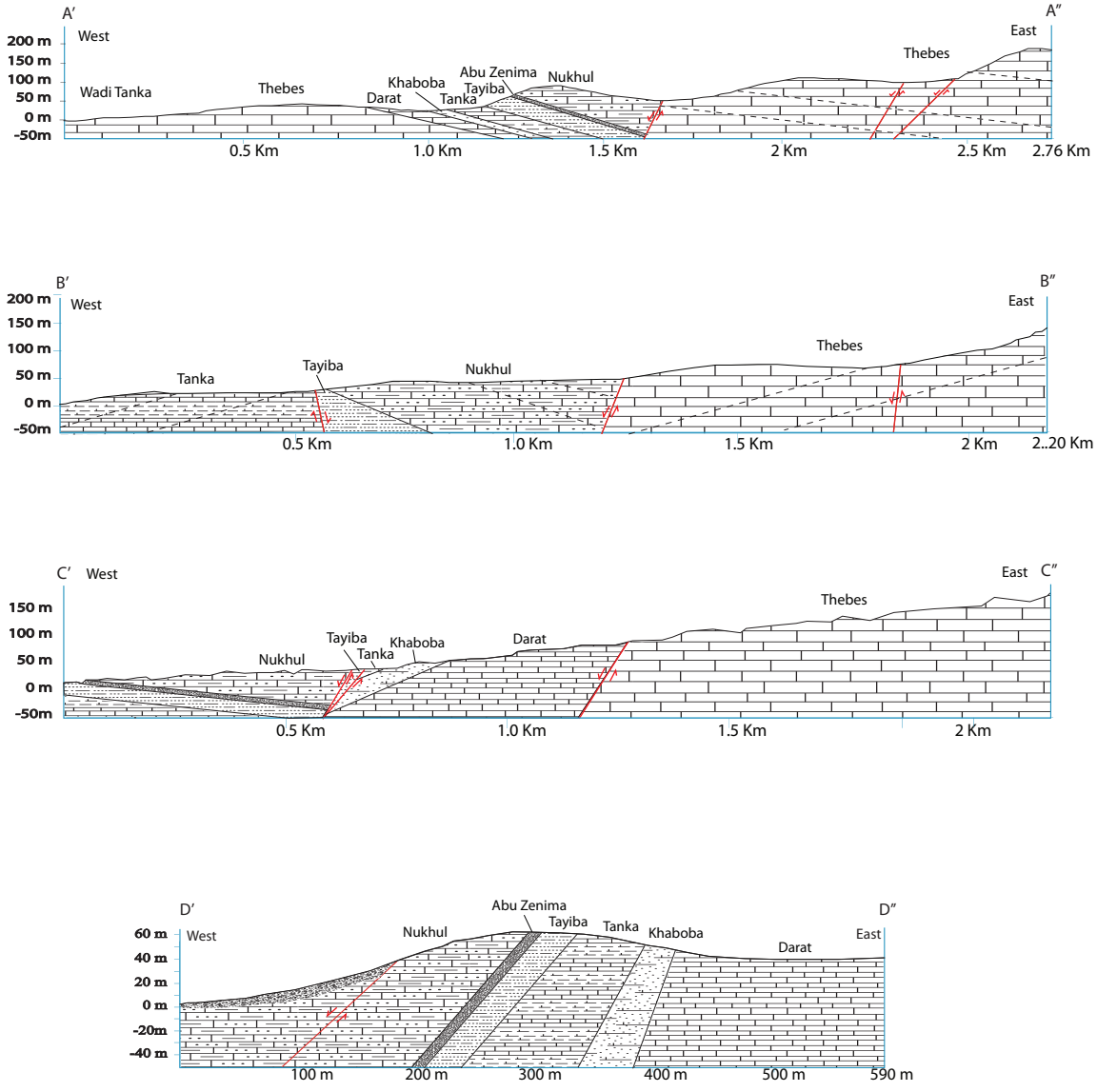

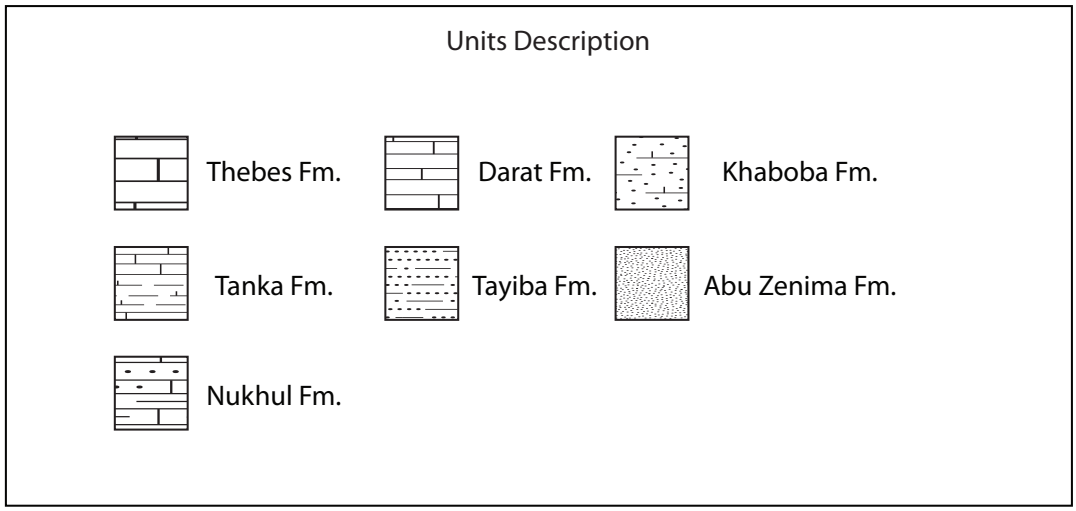

Thebes Fm. = Pale-brown to tan interbedded wackestone , lime-mudstone and cherty limestone, The wackestone exhibit bedding and is mainly compose of limestone clast and skeletal shell fragments, the lime-mudstone don't preserve any sedimentary structure and it is always thinner that the wackestone. * Several thicker wackestone sub units display sub-rounded chert within the beds, really characteristic from this cliff forming unit.
"Shallow to deeper marine limestone"

Darak Fm. = Pale brown mudstone interbedded with fine sandstones. ~1meter unconsolidated mudstone beds and 1.5meter unconsolidated calcareous sandstones beds.

Khaboba Fm. = Orange –reddish-brownish unconsolidated mudstone beds, it is a calcareous mudstone to fine sandstone, extremely fractured with authigenic calcite and gypsum veins.

Tanka Fm. = Light brown, highly homogenious planar bedded limestone, beds have approximately 50cm spacing.
"Shallow marine limestone"

Tayiba Fm. = five sub units were identified:
Lower sub unit 1, Light to brown mudstones 3-4meters
Sub unit 2, pale brown homogeneous sandstone ~2meters
**Sub unit 3,* Red and purple mudstone and fine sandstones, show fissility and oxidation marks perpendicular to the fissility in a few areas, 10cm calcite veins are common. Mudstone and silts were found occasionally in a lenticular shape within the same fine sandstones or mudstones. This sub unit is the thickest and therefore the one mainly associated to Tayiba Fm. It is also commonly found alone in Wadi Tanka. ~9meters
Sub unit 4, pale brown homogeneous sandstone ~2meters
Upper unit 5, pale brown lime-mudstone to shale <1meters

"This unit varies in thickness regionally and display characteristic of a restricted, low energy depositional environment in the thicker sub units. Possible sub aerial exposures and later high energy events ere preserve in the smaller sub units"

Basatic volcanism, = highly weathered basalts, no mains structures were preserved due to weathering. According to the orientation of the basalt and the slightly bake zone at the upper part of the Tayiba Fm but not at the lower part of the Abu Zenima make us believe it was a basaltic flow.

Abu Zenima Fm. = Reddish poorly sorted fine sandstones; this unit starts with a scoured contact above the basaltic flow or the Tayiba Fm. The lower sub unit is an ortho-conglomerate mainly compose of angular clast of basalt, chert and limestone, in a calcareous matrix.
Lower sub unit, Brown ortho-conglomerate in a calcareous mud matrix, well rounded clast of chert limestone and basalt can be identified, lens of coarse sandstones are at the bottom of this unit and the contact with the basalts.
Middle sub unit, pink- purple fine sandstones, Grain supported with a calcareous matrix and few coarse quartz grains. Approximate clast composition: ~25% skeletal fragments, ~ 20% quartz,~20% calcareous fragments, ~7% lithics and <5% calcareous matrix. (It can be confuse with Abu Zenima).
Upper sub unit, is mainly reddish fine sandstone or siltstone with occasional small pebbles of basalt. No sedimentary structures were preserved.
"This unit gets thinner towards the northwest in Wadi Tanka and it displays characteristics of a fluvial continental depositional environment"

Nukhul Fm. = Pale brown to brown mudstone, wackstones, sandstones and conglomerates, This units lies conformably above the Abu Zenima Fm. and sometimes above Tayiba Fm., this unit display multiple sedimentary structures; mud lens, planar lamination and through cross bedding. Pebble size clast in the conglomerate units are mainly angular mudstone and chert.
"This unit display a characteristic deeping upward sequence, it developed in several pulses, from small conglomerates to deeper marine mudstone, with small regressions in between"

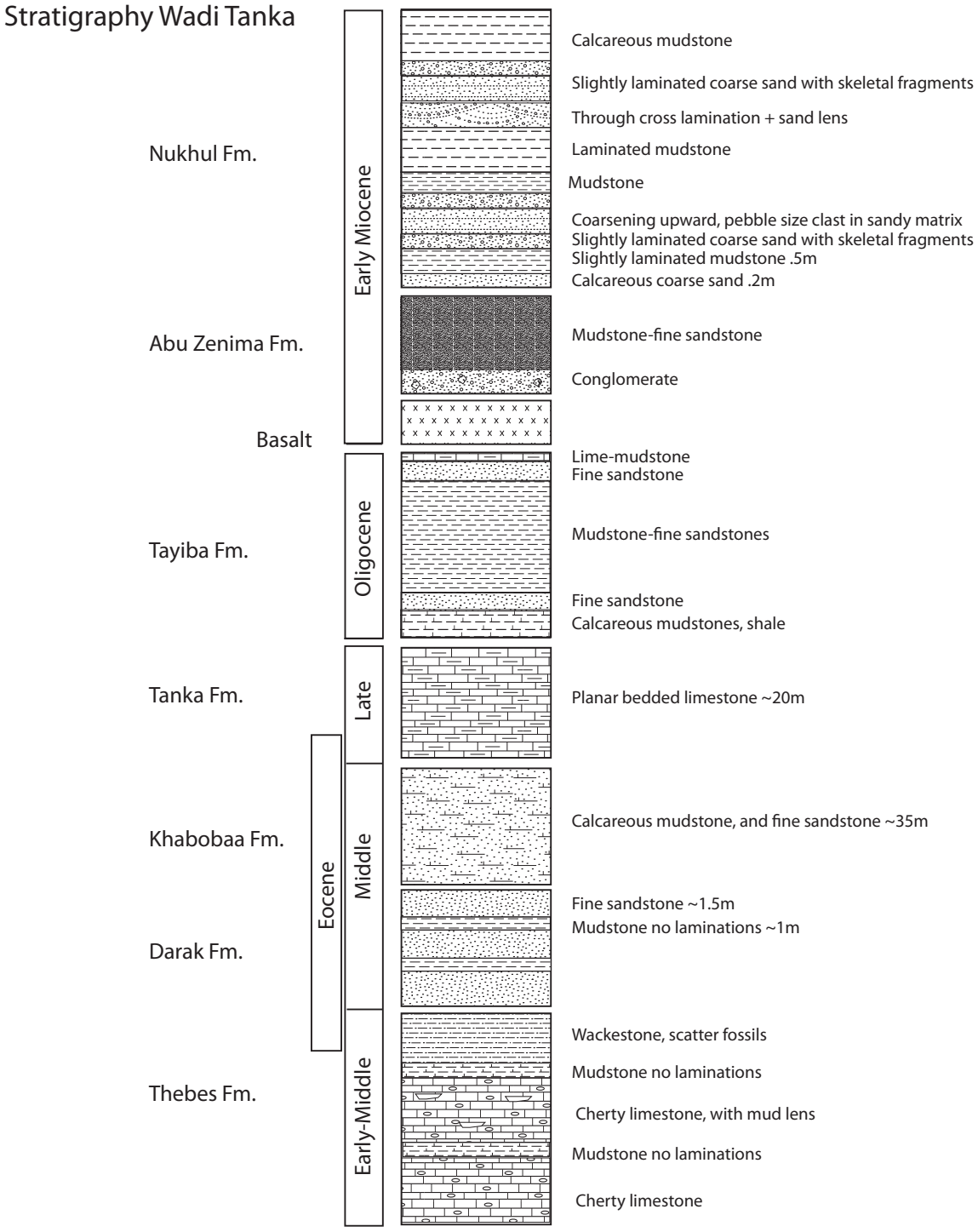
Stratigraphy Wadi Tanka
Nukhul Fm.
Abu Zenima Fm.
Basalt
Tayiba Fm.
Tanka Fm.
Khabobaa Fm.
Darak Fm.
Thebes Fm.
Early Miocene
Oligocene
Late
Middle
Early-Middle
Eocene
Calcareous mudstone
Slightly laminated coarse sand with skeletal fragments
Through cross lamination + sand lens
Laminated mudstone
Mudstone
Coarsening upward, pebble size clast in sandy matrix
Slightly laminated coarse sand with skeletal fragments
Slightly laminated mudstone .5m
Calcareous coarse sand .2m
Mudstone-fine sandstone
Conglomerate
Lime-mudstone
Fine sandstone
Mudstone-fine sandstones
Fine sandstone
Calcareous mudstones, shale
Planar bedded limestone ~20m
Calcareous mudstone, and fine sandstone ~35m
Fine sandstone ~1.5m
Mudstone no laminations ~1m
Wackestone, scatter fossils
Mudstone no laminations
Cherty limestone, with mud lens
Mudstone no laminations
Cherty limestone

Appendix **1**

Arithmetic mean = 40.88 Ma, s.e. = 4.20 Ma, MSWD = 13.71
Geometric mean = 40.40 Ma, s.e. = 4.39 Ma, MSWD = 10.67

ERB-41

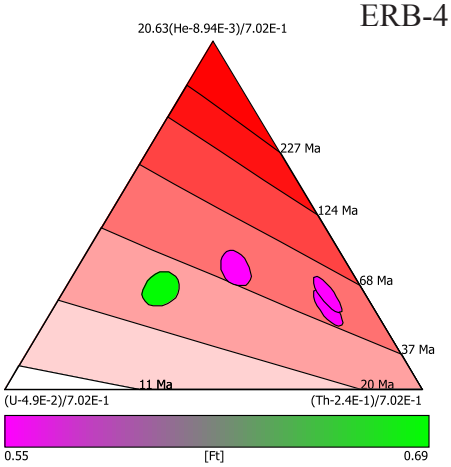

Arithmetic mean = 60.77 Ma, s.e. = 20.05 Ma, MSWD = 214.32
Geometric mean = 51.28 Ma, s.e. = 18.49 Ma, MSWD = 94.36
Central age = 55.33 Ma, s.e. = 23.56 Ma, MSWD = 119.4
95% C.I = [22.42 Ma, 116.80 Ma]

ERB-42

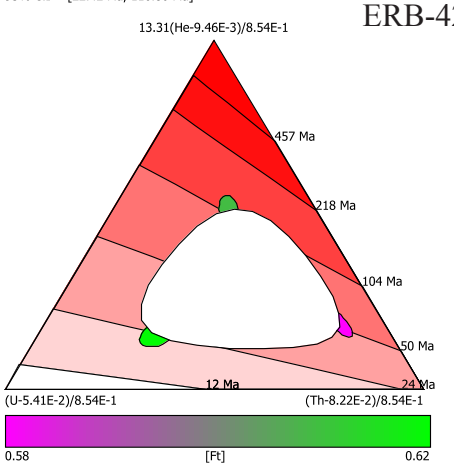

Arithmetic mean = 34.00 Ma, s.e. = 7.47 Ma, MSWD = 7140.6
Geometric mean = 15.48 Ma, s.e. = 9.06 Ma, MSWD = 445.86
Central age = 16.59 Ma, s.e. = 9.93 Ma, MSWD = 281.82
95% C.I = [5.13 Ma, 49.11 Ma]

ERB-43

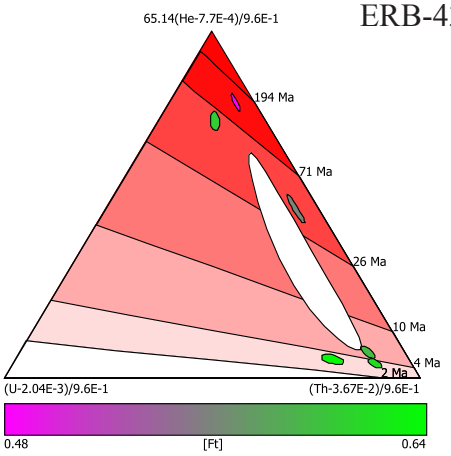

Arithmetic mean = 34.90 Ma, s.e. = 8.07 Ma, MSWD = 132.83
Geometric mean = 29.79 Ma, s.e. = 7.19 Ma, MSWD = 71.83
Central age = 29.84 Ma, s.e. = 7.24 Ma, MSWD = 38.72
95% C.I = [19.29 Ma, 46.13 Ma]

ERB-44

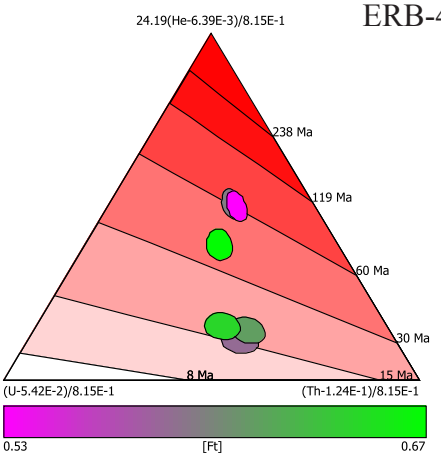

Arithmetic mean = 30.20 Ma, s.e. = 6.83 Ma, MSWD = 64.43
Geometric mean = 27.71 Ma, s.e. = 6.17 Ma, MSWD = 44.12
Central age = 27.72 Ma, s.e. = 7.16 Ma, MSWD = 23.42
95% C.I = [12.80 Ma, 12.80 Ma]

ERB-45

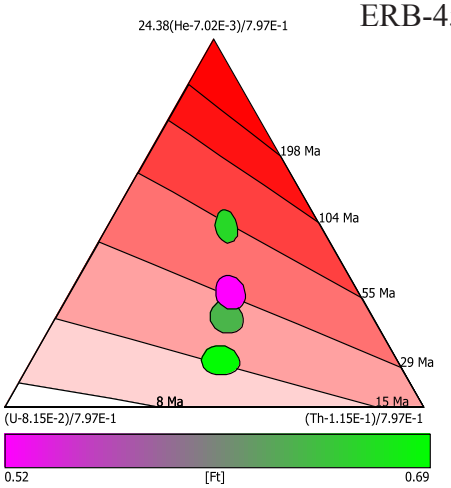

Arithmetic mean = 25.79 Ma, s.e. = 6.98 Ma, MSWD = 368.06
Geometric mean = 19.69 Ma, s.e. = 5.80 Ma, MSWD = 116.03
Central age = 19.78 Ma, s.e. = 5.85 Ma, MSWD = 68.6
95% C.I = [11.33 Ma, 33.74 Ma]

ERB-46

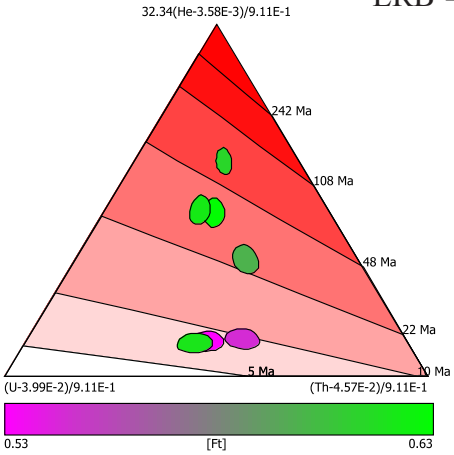

Arithmetic mean = 17.29 Ma, s.e. = 3.60 Ma, MSWD = 76.42
Geometric mean = 16.18 Ma, s.e. = 3.86 Ma, MSWD = 43.8
Central age = 16.22 Ma, s.e. = 4.74 Ma, MSWD = 30.58
95% C.I = [6.40 Ma, 6.40 Ma]

ERB-47

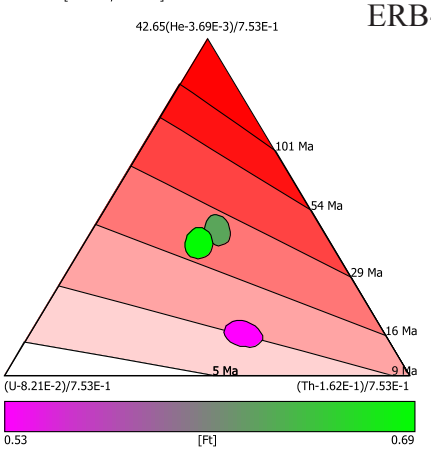

Arithmetic mean = 23.96 Ma, s.e. = 5.49 Ma, MSWD = 282.27
Geometric mean = 19.88 Ma, s.e. = 4.96 Ma, MSWD = 85.9
Central age = 20.02 Ma, s.e. = 4.97 Ma, MSWD = 54.88
95% C.I = [12.44 Ma, 31.48 Ma]

ERB-48

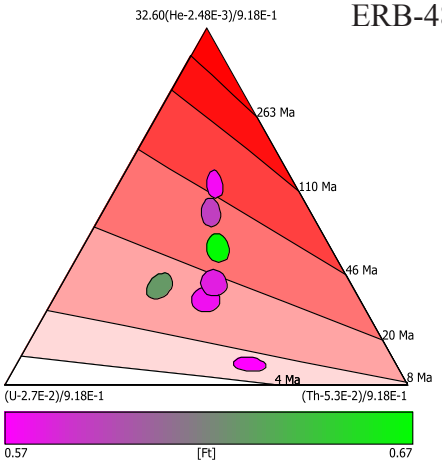

Arithmetic mean = 21.36 Ma, s.e. = 4.59 Ma, MSWD = 44.25
Geometric mean = 19.90 Ma, s.e. = 4.02 Ma, MSWD = 36.57
Central age = 19.91 Ma, s.e. = 4.66 Ma, MSWD = 19.42
95% C.I = [13.75 Ma, 15.61 Ma]

ERB-49

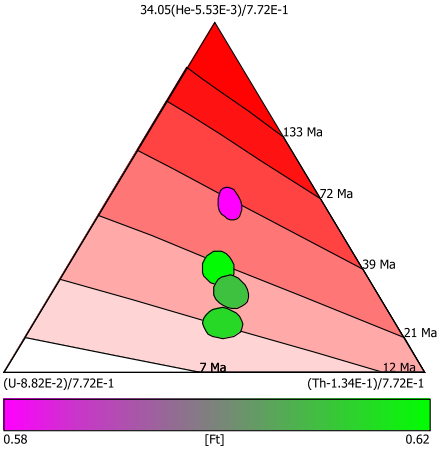

Arithmetic mean = 8.56 Ma, s.e. = 1.59 Ma, MSWD = 26.81
Geometric mean = 8.25 Ma, s.e. = 1.50 Ma, MSWD = 24.64
Central age = 8.27 Ma, s.e. = 1.83 Ma, MSWD = 20.06
95% C.I = [5.72 Ma, 8.93 Ma]

ERB-50

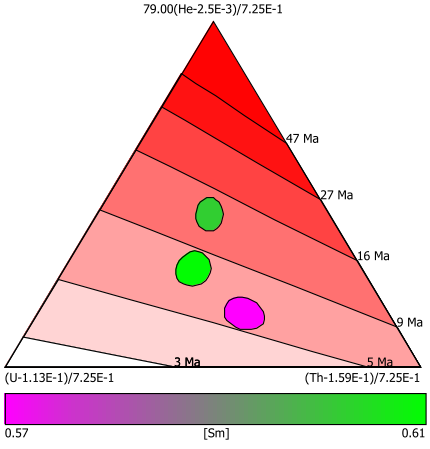

Arithmetic mean = 85.13 Ma, s.e. = 3.48 Ma, MSWD = 1.44
Geometric mean = 85.86 Ma, s.e. = 3.43 Ma, MSWD = 1.42
Central age = 86.21 Ma, s.e. = 3.53 Ma, MSWD = 5
95% C.I = [79.53 Ma, 93.09 Ma]

GS-01

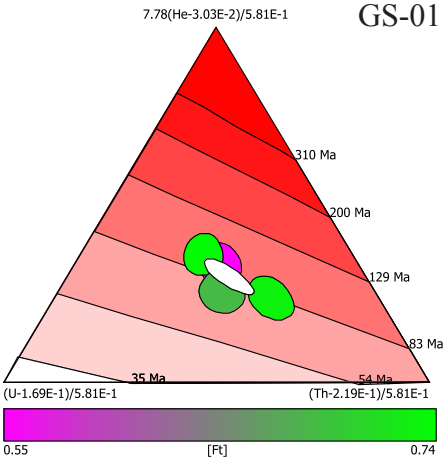

Arithmetic mean = 49.38 Ma, s.e. = 10.04 Ma, MSWD = 50.51
Geometric mean = 45.00 Ma, s.e. = 8.28 Ma, MSWD = 39.53
Central age = 45.14 Ma, s.e. = 8.37 Ma, MSWD = 23.24
95% C.I = [31.90 Ma, 63.09 Ma]

GS-02

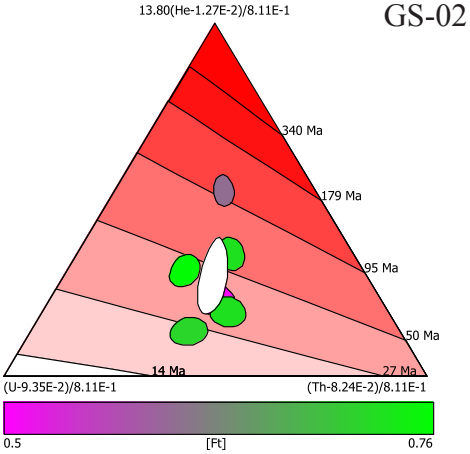

Arithmetic mean = 86.13 Ma, s.e. = 9.79 Ma, MSWD = 232.01
Geometric mean = 78.55 Ma, s.e. = 13.13 Ma, MSWD = 48.44
Central age = 79.28 Ma, s.e. = 13.27 Ma, MSWD = 33.76
95% C.I = [57.69 Ma, 107.68 Ma]

GS-03

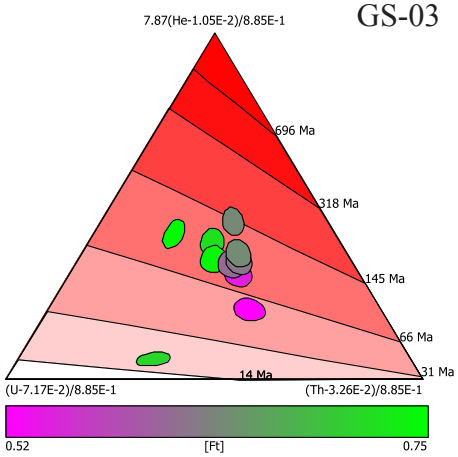

Arithmetic mean = 24.86 Ma, s.e. = 3.23 Ma, MSWD = 20.32
Geometric mean = 23.91 Ma, s.e. = 2.86 Ma, MSWD = 20.16
Central age = 24.04 Ma, s.e. = 2.88 Ma, MSWD = 15.79
95% C.I = [19.09 Ma, 30.11 Ma]

GS-04

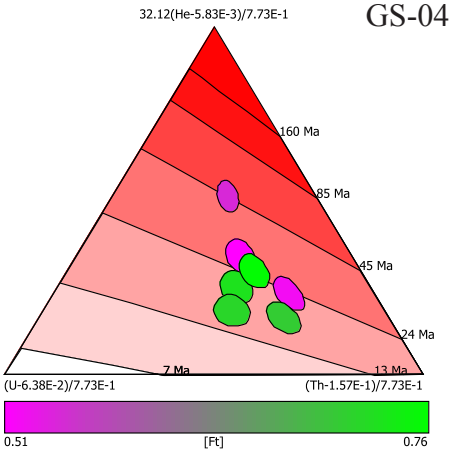

Arithmetic mean = 20.29 Ma, s.e. = 3.69 Ma, MSWD = 350.34
Geometric mean = 17.31 Ma, s.e. = 3.92 Ma, MSWD = 83.18
Central age = 17.72 Ma, s.e. = 4.10 Ma, MSWD = 70.39
95% C.I = [11.24 Ma, 27.23 Ma]

GS-05

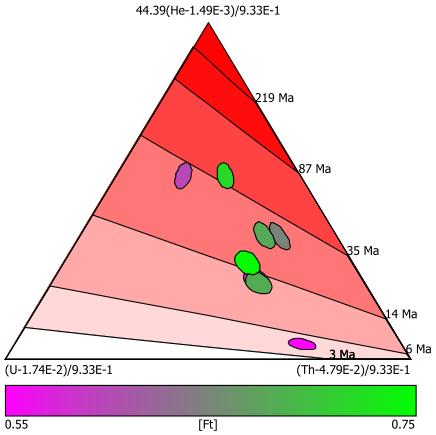

Arithmetic mean = 22.28 Ma, s.e. = 3.73 Ma, MSWD = 38.49
Geometric mean = 20.68 Ma, s.e. = 3.19 Ma, MSWD = 33.39
Central age = 20.92 Ma, s.e. = 3.23 Ma, MSWD = 30.6
95% C.I = [15.39 Ma, 27.91 Ma]

GS-06

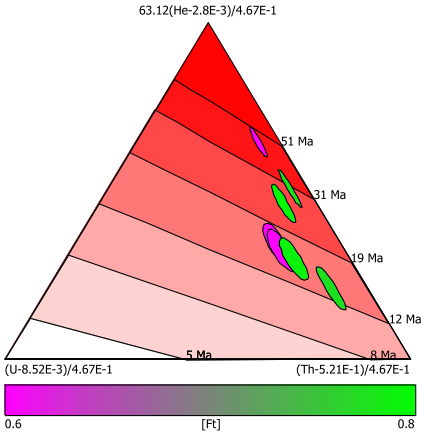

Arithmetic mean = 27.10 Ma, s.e. = 3.76 Ma, MSWD = 15.62
Geometric mean = 26.17 Ma, s.e. = 3.22 Ma, MSWD = 18.41
Central age = 27.13 Ma, s.e. = 3.21 Ma, MSWD = 40.63
95% C.I = [21.35 Ma, 33.85 Ma]

GS-07

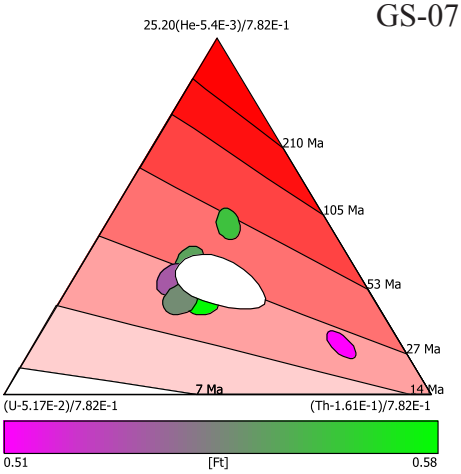

Arithmetic mean = 19.65 Ma, s.e. = 2.77 Ma, MSWD = 55.79
Geometric mean = 18.58 Ma, s.e. = 2.92 Ma, MSWD = 31.11
Central age = 19.42 Ma, s.e. = 3.10 Ma, MSWD = 62.14
95% C.I = [14.13 Ma, 25.95 Ma]

GS-08

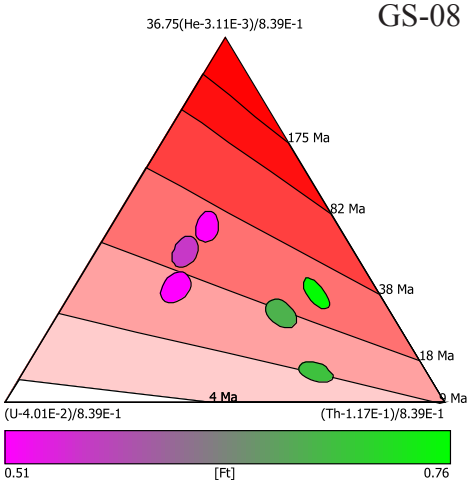

Arithmetic mean = 31.27 Ma, s.e. = 4.94 Ma, MSWD = 88.17
Geometric mean = 28.95 Ma, s.e. = 5.27 Ma, MSWD = 41.31
Central age = 29.46 Ma, s.e. = 5.49 Ma, MSWD = 37.23
95% C.I = [20.54 Ma, 42.23 Ma]

GS-09

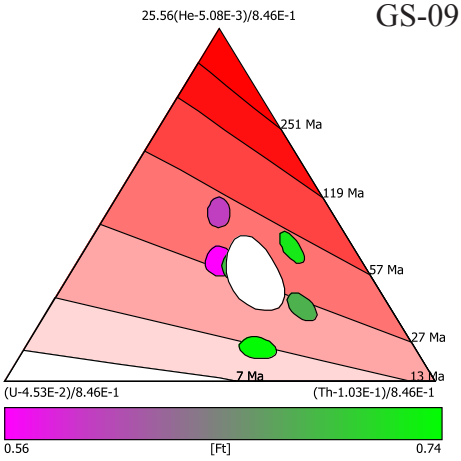

Arithmetic mean = 18.88 Ma, s.e. = 2.51 Ma, MSWD = 96.16
Geometric mean = 17.57 Ma, s.e. = 2.94 Ma, MSWD = 38.84
Central age = 18.83 Ma, s.e. = 2.89 Ma, MSWD = 64.29
95% C.I = [13.73 Ma, 24.73 Ma]

GS-10

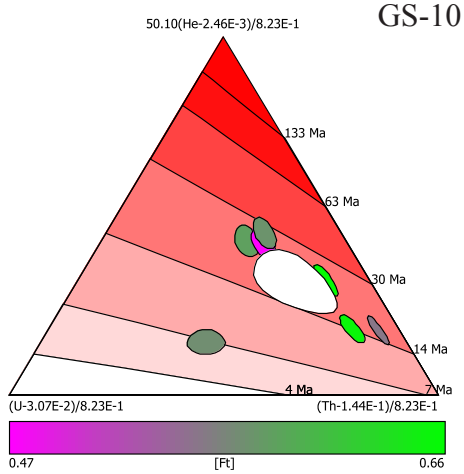

Arithmetic mean = 26.32 Ma, s.e. = 1.97 Ma, MSWD = 8.29
Geometric mean = 26.16 Ma, s.e. = 2.00 Ma, MSWD = 7.2
Central age = 26.19 Ma, s.e. = 2.01 Ma, MSWD = 5.12
95% C.I = [22.54 Ma, 30.14 Ma]

GS-11

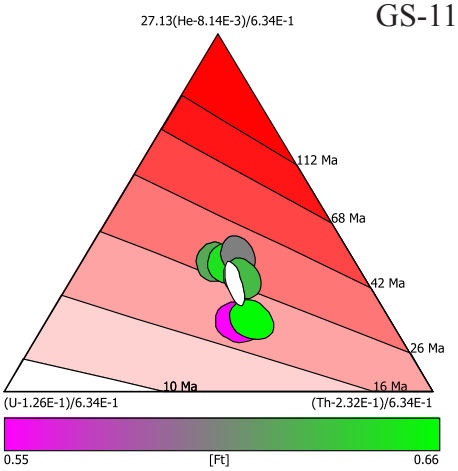

Arithmetic mean = 121.23 Ma, s.e. = 18.64 Ma, MSWD = 93.71
Geometric mean = 110.45 Ma, s.e. = 20.48 Ma, MSWD = 43.39
Central age = 111.22 Ma, s.e. = 20.97 Ma, MSWD = 26.95
95% C.I = [78.58 Ma, 155.83 Ma]

GS-12

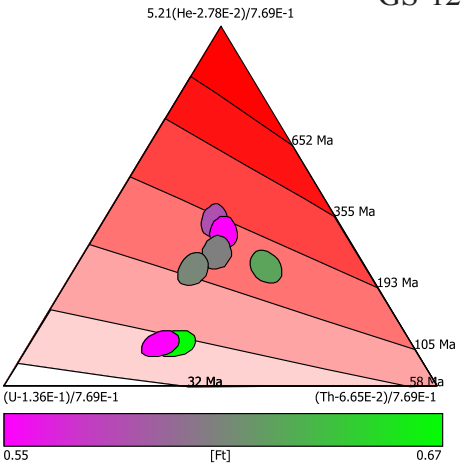

Arithmetic mean = 34.39 Ma, s.e. = 1.33 Ma, MSWD = 1.09
Geometric mean = 34.64 Ma, s.e. = 1.33 Ma, MSWD = 1.13
Central age = 35.05 Ma, s.e. = 1.27 Ma, MSWD = 13.07
95% C.I = [31.88 Ma, 37.79 Ma]

08GZ-02

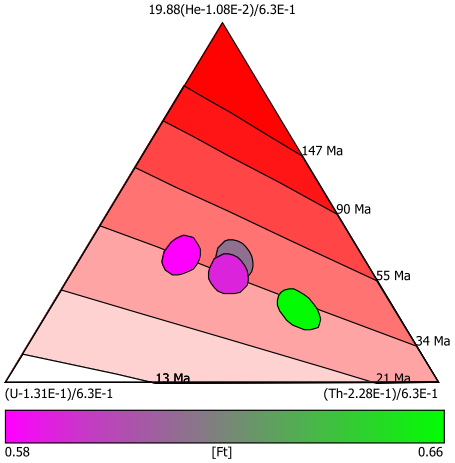

Arithmetic mean = 68.87 Ma, s.e. = 12.93 Ma, MSWD = 143.37
Geometric mean = 59.48 Ma, s.e. = 12.32 Ma, MSWD = 63.84
Central age = 59.83 Ma, s.e. = 12.57 Ma, MSWD = 43.54
95% C.I = [40.19 Ma, 87.47 Ma]

08GZ-03

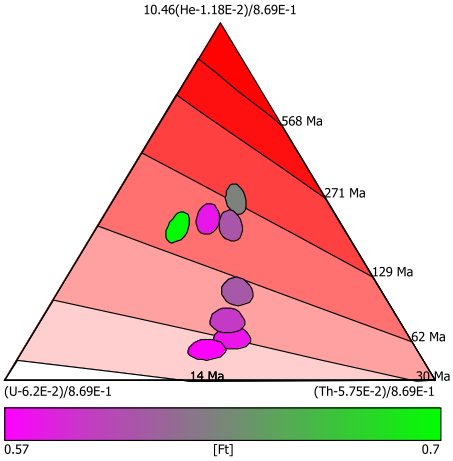

Arithmetic mean = 162.16 Ma, s.e. = 17.92 Ma, MSWD = 17.62
Geometric mean = 158.30 Ma, s.e. = 18.32 Ma, MSWD = 13.59
Central age = 160.06 Ma, s.e. = 19.33 Ma, MSWD = 38.66
95% C.I = [128.40 Ma, 198.59 Ma]

08GZ-04

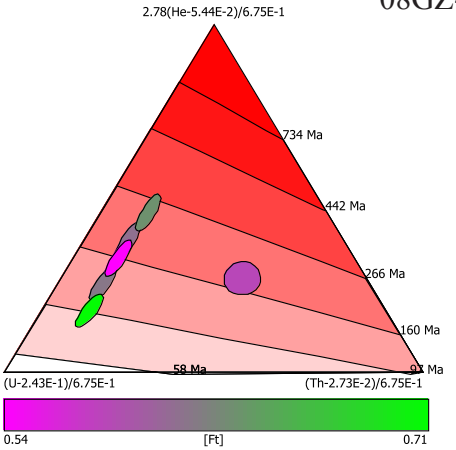

Arithmetic mean = 74.17 Ma, s.e. = 16.59 Ma, MSWD = 353.25
Geometric mean = 62.13 Ma, s.e. = 15.38 Ma, MSWD = 90.18
Central age = 62.51 Ma, s.e. = 15.44 Ma, MSWD = 48.35
95% C.I = [40.03 Ma, 97.31 Ma]

08GZ-05

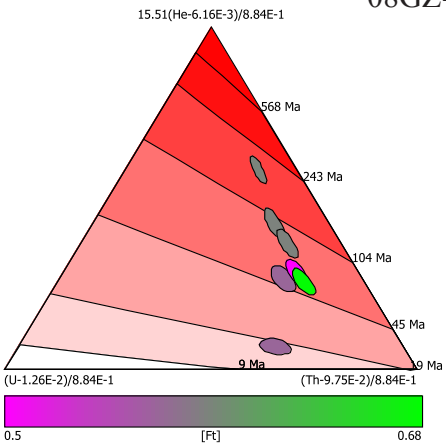

Arithmetic mean = 71.17 Ma, s.e. = 16.79 Ma, MSWD = 1295.28
Geometric mean = 52.15 Ma, s.e. = 17.94 Ma, MSWD = 172.28
Central age = 52.61 Ma, s.e. = 18.28 Ma, MSWD = 95.63
95% C.I = [26.60 Ma, 98.38 Ma]

08GZ-06

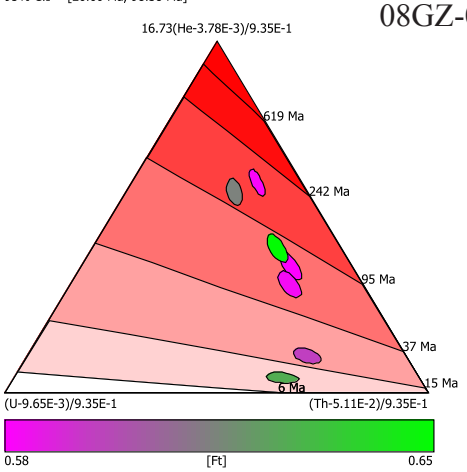

Arithmetic mean = 72.47 Ma, s.e. = 17.45 Ma, MSWD = 90.34
Geometric mean = 63.03 Ma, s.e. = 12.56 Ma, MSWD = 57.37
Central age = 63.57 Ma, s.e. = 151.62 Ma, MSWD = 32.88
95% C.I = [.00 ka, 5.18 ka]

08GZ-07

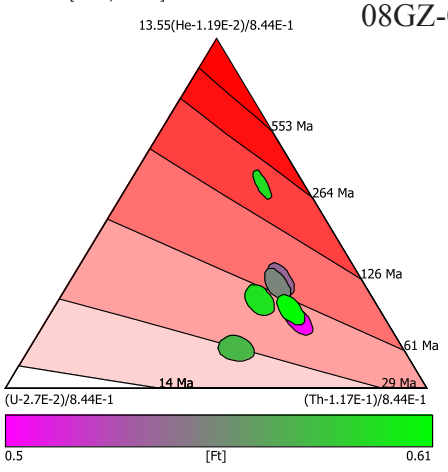

Arithmetic mean = 79.06 Ma, s.e. = 22.94 Ma, MSWD = 140.93
Geometric mean = 66.36 Ma, s.e. = 17.80 Ma, MSWD = 79.67
Central age = 68.45 Ma, s.e. = 19.26 Ma, MSWD = 73.81
95% C.I = [39.78 Ma, 113.10 Ma]

08GZ-09

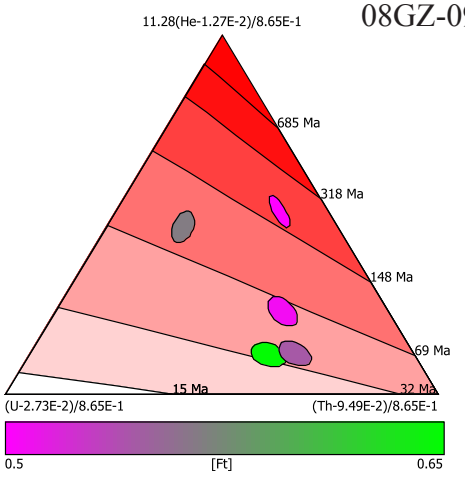

Arithmetic mean = 103.79 Ma, s.e. = 15.28 Ma, MSWD = 26.82
Geometric mean = 101.23 Ma, s.e. = 16.05 Ma, MSWD = 19.95
Central age = 105.80 Ma, s.e. = 18.70 Ma, MSWD = 46.2
95% C.I = [48.99 Ma, 48.99 Ma]

08GZ-17

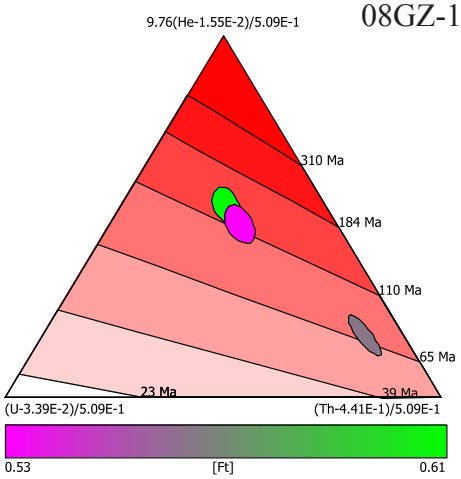

Arithmetic mean = 89.70 Ma, s.e. = 16.74 Ma, MSWD = 26.35
Geometric mean = 86.39 Ma, s.e. = 15.61 Ma, MSWD = 25.16
Central age = 87.20 Ma, s.e. = 19.84 Ma, MSWD = 18.54
95% C.I = [72.35 Ma, 72.35 Ma]

09STGS-08

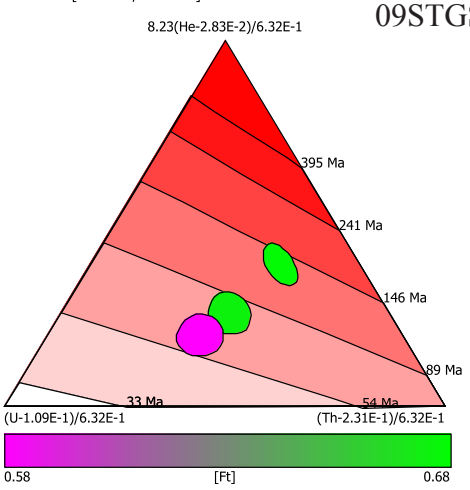

Arithmetic mean = 26.55 Ma, s.e. = 2.09 Ma, MSWD = 4.89
Geometric mean = 26.62 Ma, s.e. = 2.12 Ma, MSWD = 4.97
Central age = 26.62 Ma, s.e. = 1.16 Ma, MSWD = 2.75
95% C.I = [24.44 Ma, 28.90 Ma]

09STGS-09

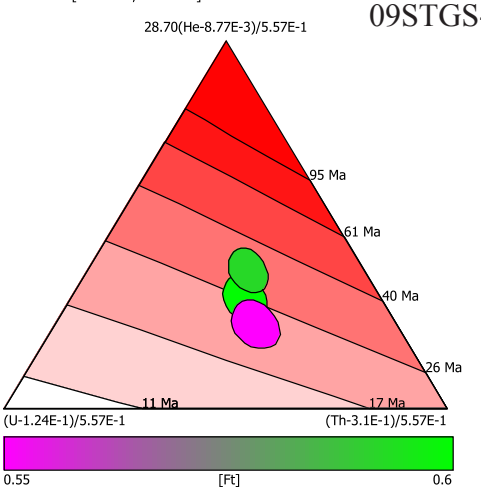

Arithmetic mean = 28.39 Ma, s.e. = 3.23 Ma, MSWD = 9.67
Geometric mean = 28.34 Ma, s.e. = 3.23 Ma, MSWD = 9.47
Central age = 30.10 Ma, s.e. = 4.88 Ma, MSWD = 4.89
95% C.I = [18.05 Ma, 18.05 Ma]

09SGS-01

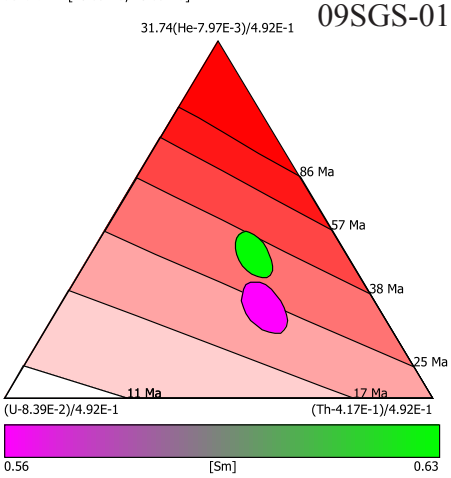

Arithmetic mean = 31.88 Ma, s.e. = 2.70 Ma, MSWD = 6.27
Geometric mean = 31.88 Ma, s.e. = 2.71 Ma, MSWD = 5.81
Central age = 31.93 Ma, s.e. = 3.33 Ma, MSWD = 3.95
95% C.I = [22.30 Ma, 22.30 Ma]

09SGS-04

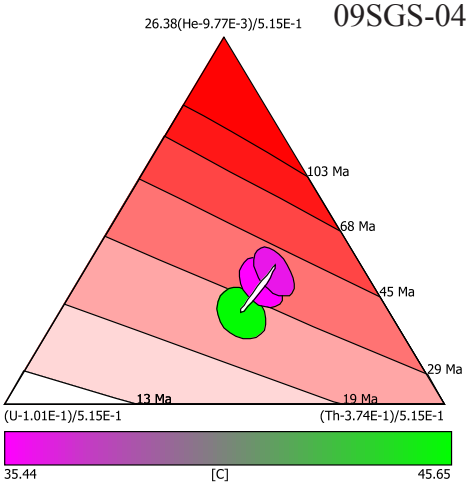

Arithmetic mean = 45.54 Ma, s.e. = 8.65 Ma, MSWD = 28.43
Geometric mean = 43.78 Ma, s.e. = 8.19 Ma, MSWD = 25.03
Central age = 43.89 Ma, s.e. = 10.08 Ma, MSWD = 20.76
95% C.I = [21.88 Ma, 21.88 Ma]

09SGS-05

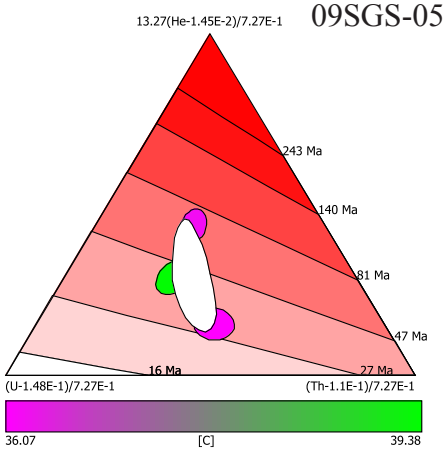

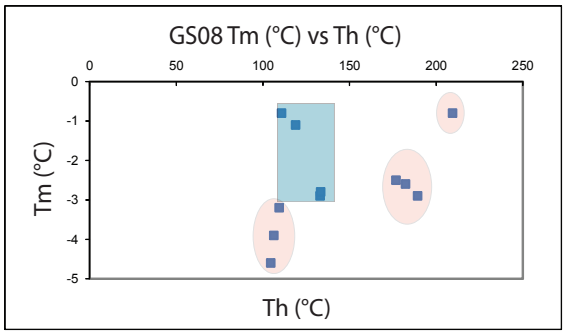
GS08 Tm (°C) vs Th (°C)
Tm (°C)
Th (°C)

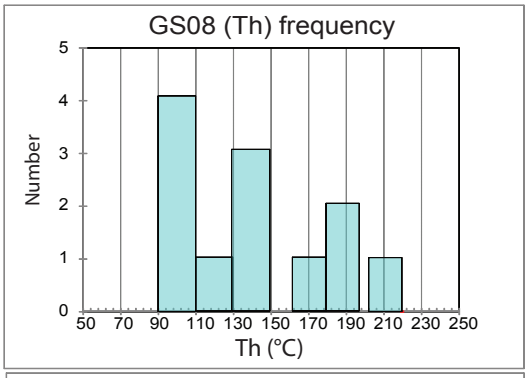
GS08 (Th) frequency
Number
Th (°C)

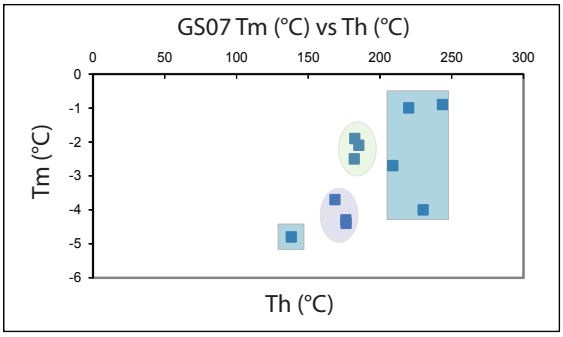
GS07 Tm (°C) vs Th (°C)
Tm (°C)
Th (°C)

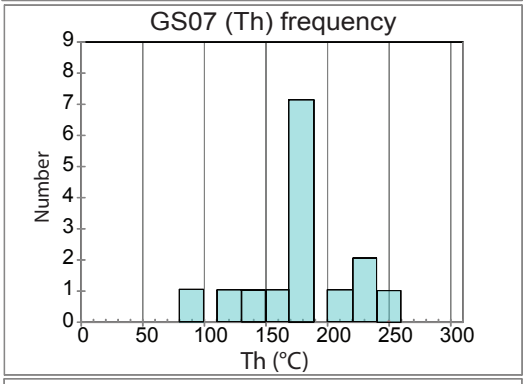
GS07 (Th) frequency
Number
Th (°C)

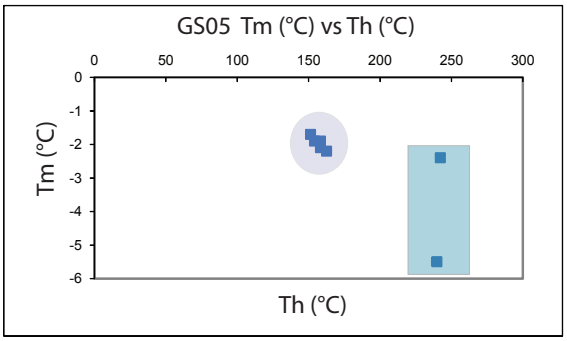
GS05 Tm (°C) vs Th (°C)
Tm (°C)
Th (°C)

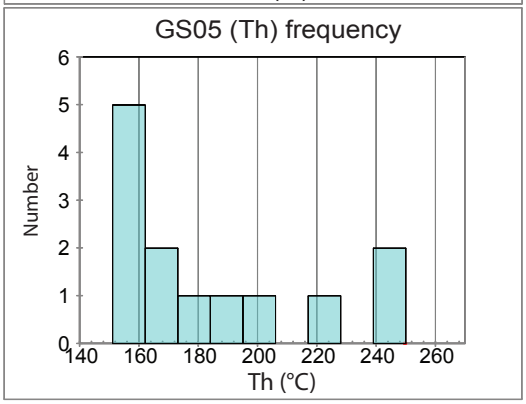
GS05 (Th) frequency
Number
Th (°C)

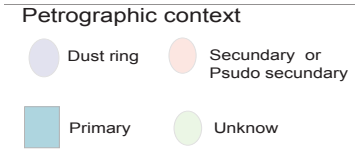
Petrographic context
Dust ring
Secundary or
Psudo secundary
Primary
Unknow

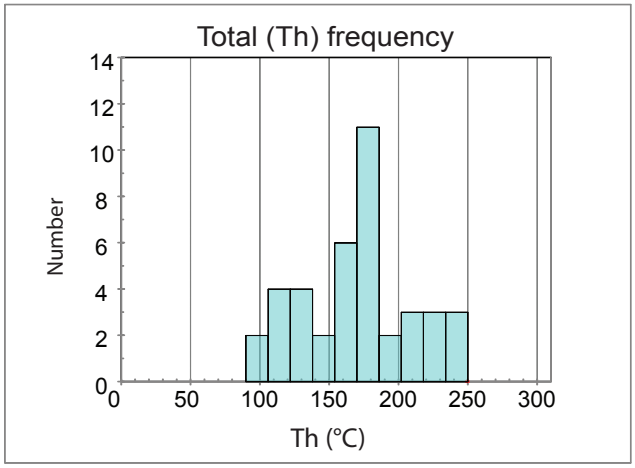

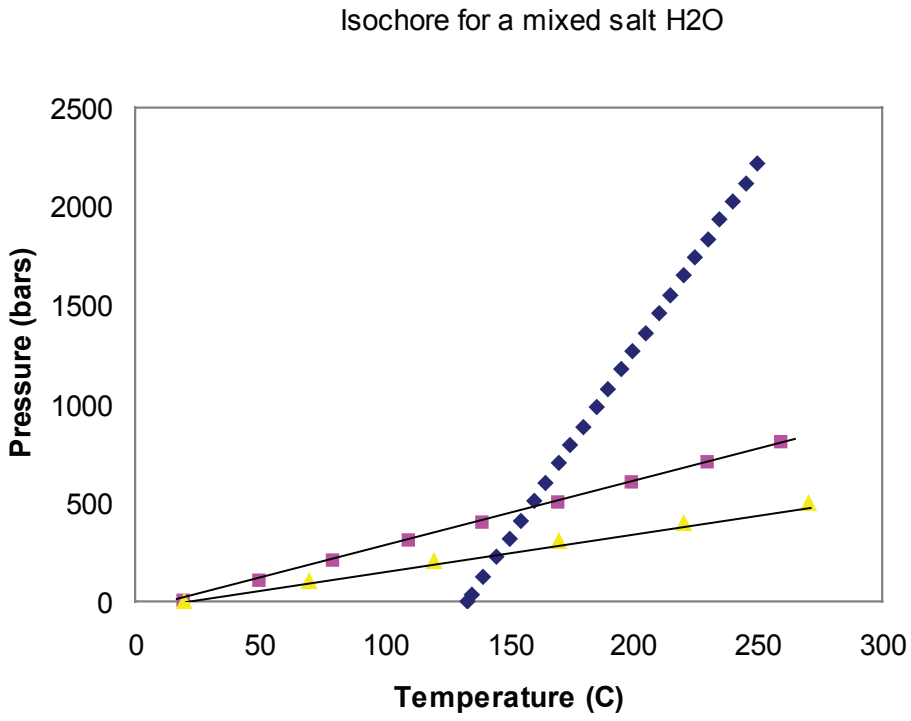

This graph shows pressuere values for a single fluid inclusion assuming two geothermal gradient one of 50 °C/km (common in highly extended settings - yellow triangles) and other of 25 °C/km (in non faulted setting-purple boxes) gave pressure of 250- 450 bars respectively. Mixed salt model provided the isochore line (dark blue boxes).
Te (eutectic temp.) gave = NaCl-MgCl2-H20
Tm= -2.8, Te=-32.1, Th=133.4 (°C)in quartz overgrowth (GS-08)

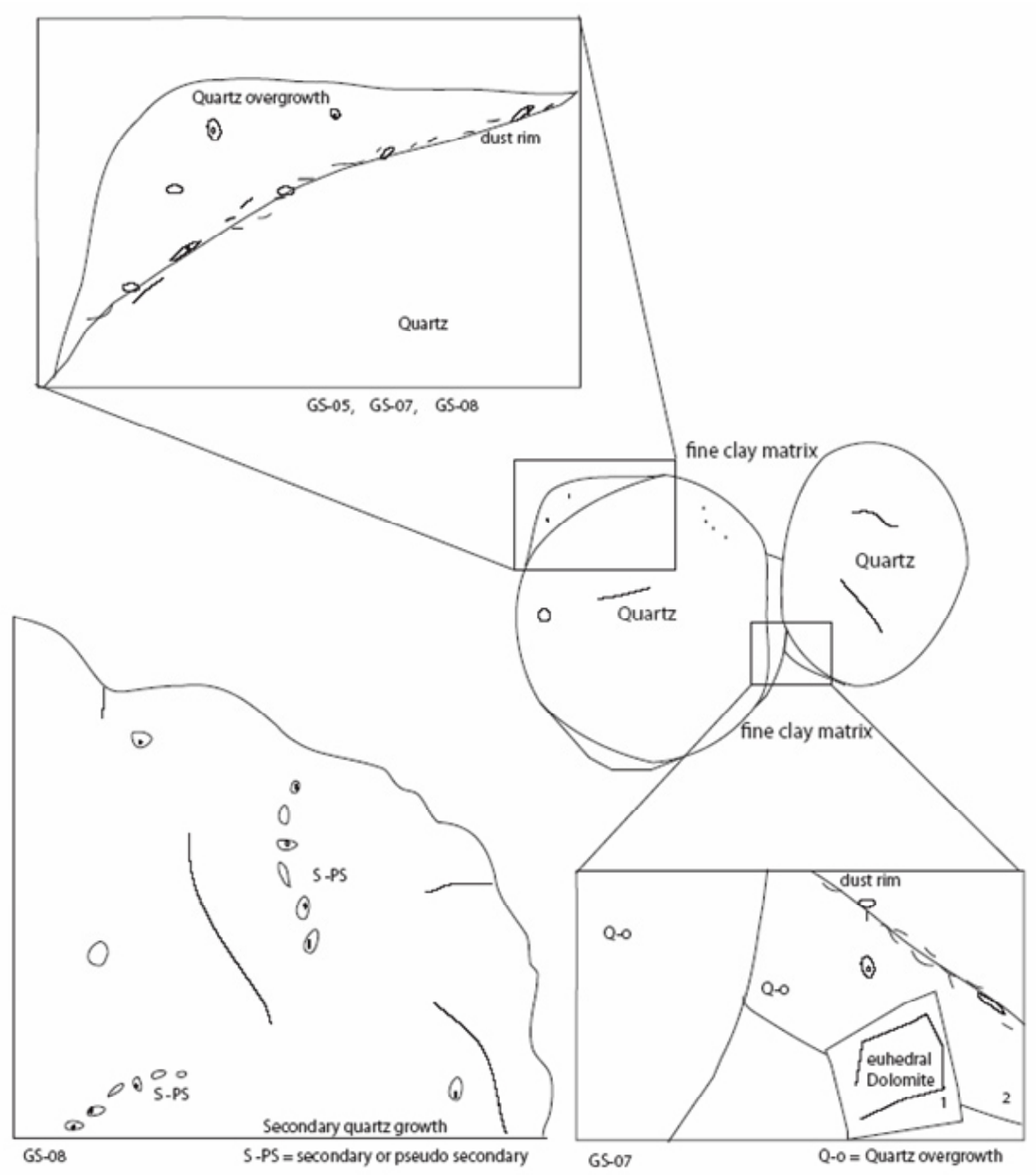

Figure 3A.1 Sketch illustrate the petrography of all three samples. Fluids inclusions mainly range from 15 to 25 microns. Many solid inclusions where found in the dust rim only a few percent were single two phase fluid inclusions. The great majority were classified as primary and undeterminable fluid inclusions.

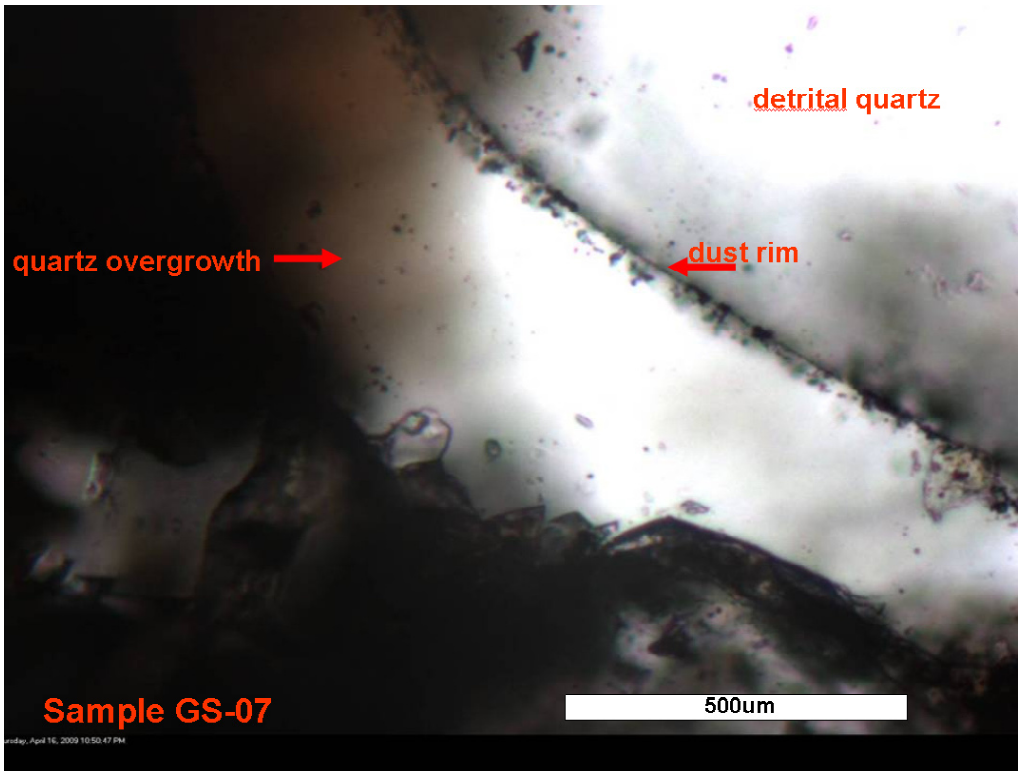

Figure 3A.2. Image illustrate the main characteristics shown in all thin sections. In where the dust rim and the quartz overgrowth are easy to recognize. Fluid inclusions in quartz concentric growth were one of the main characteristic observed.

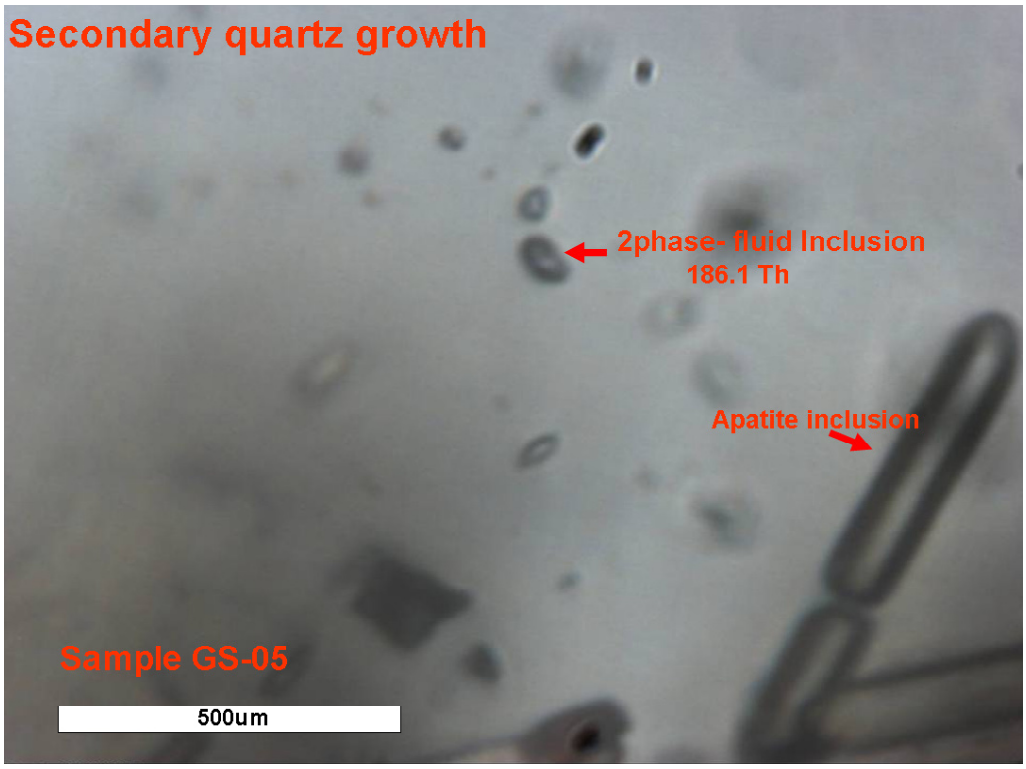

Figure 3A.3. Petrographic evidence showing an apatite almost 500 microns of a fluid inclusion that gave an homogenization temperature of 186.1 oC. This imply that using (U-Th)/He method on the apatite in this sample might provide ages must younger that expected due to partial or complete loss of He in the detrital apatite and zircon. Ages obtain can be related to this events if the thermal history is well defined.

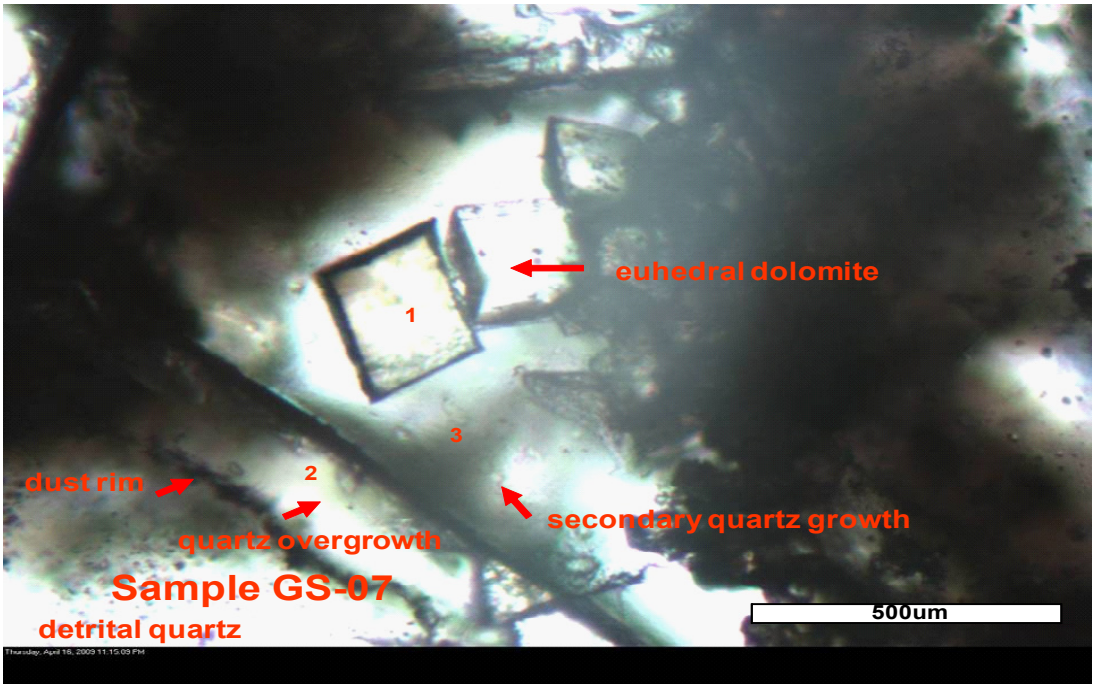

Figure 3A.4 Image shows the petrography and sequence of events in sample GS-07. Euhedral dolomite precipitated first, second the quartz overgrowth and third the secondary quartz growth. The quartz overgrowth probably do not growth in only one event and simultaneously.

Appendix **4**

Single sample modeling

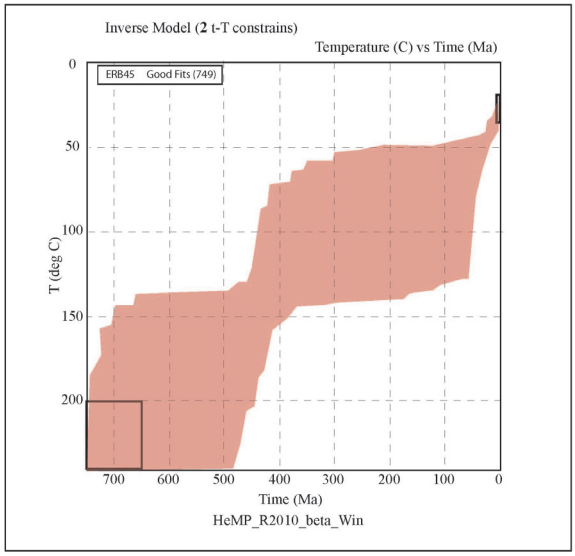

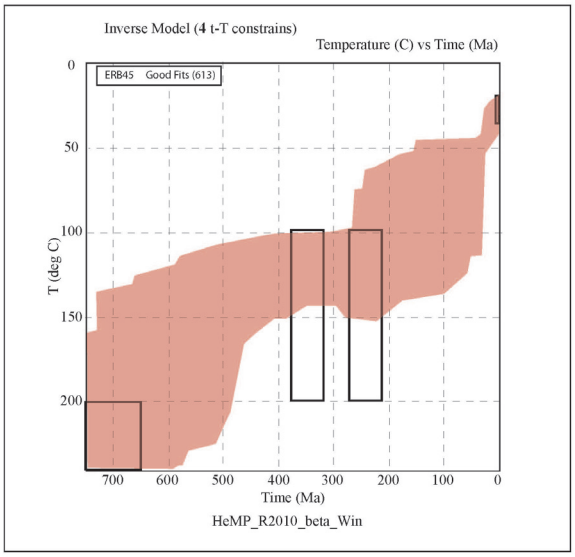

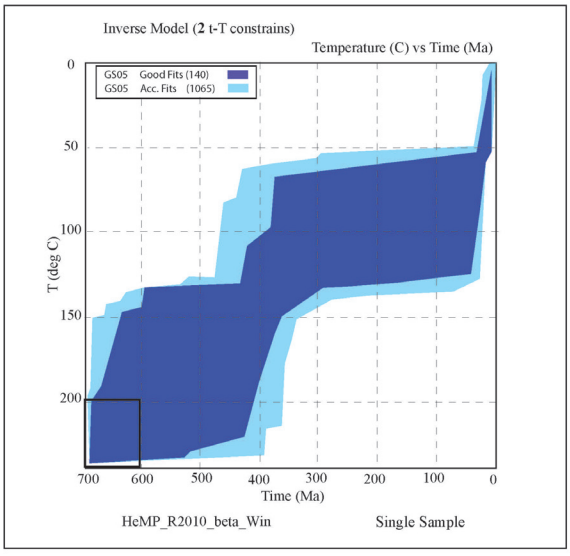

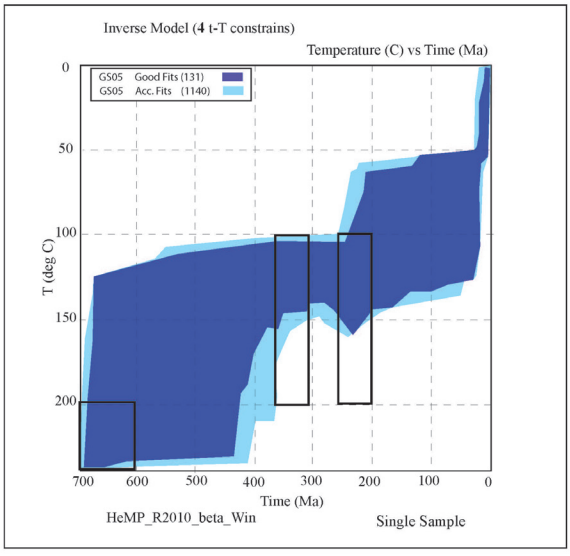

Appendix **4**

Single sample modeling

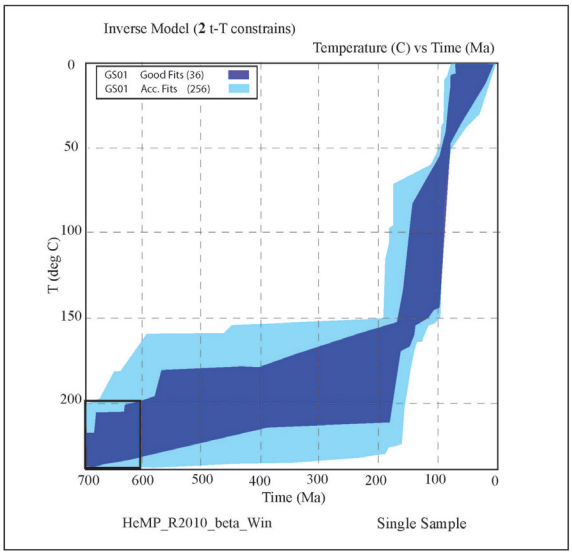

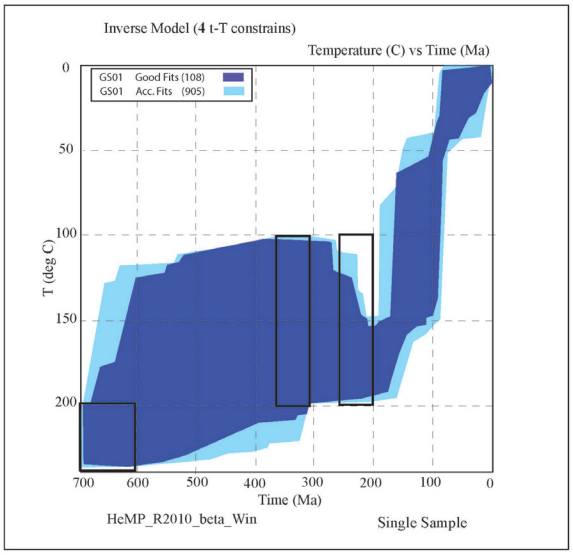

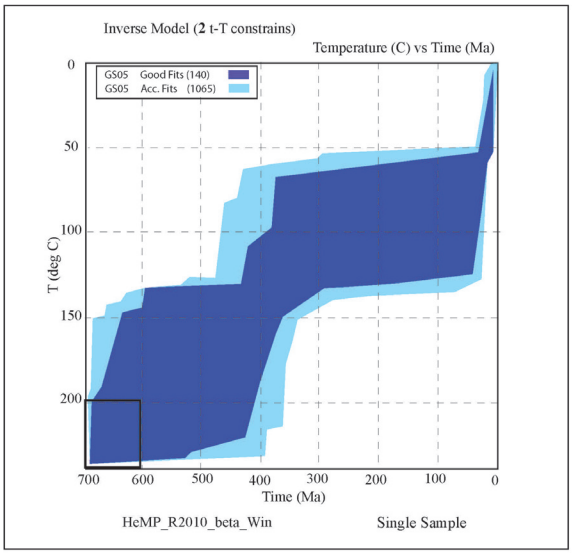

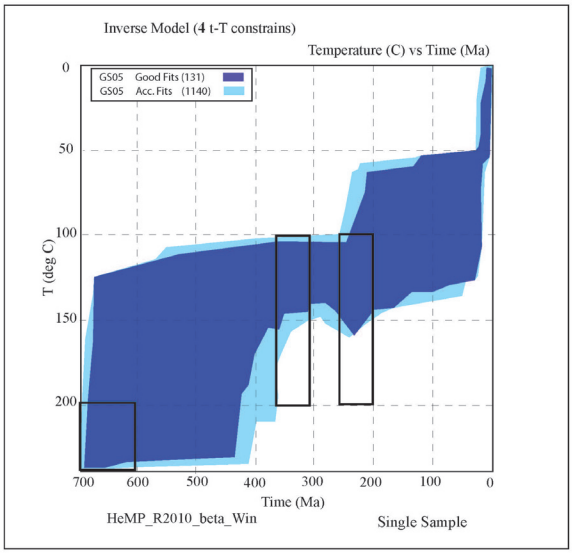

Appendix **4**

Single sample modeling

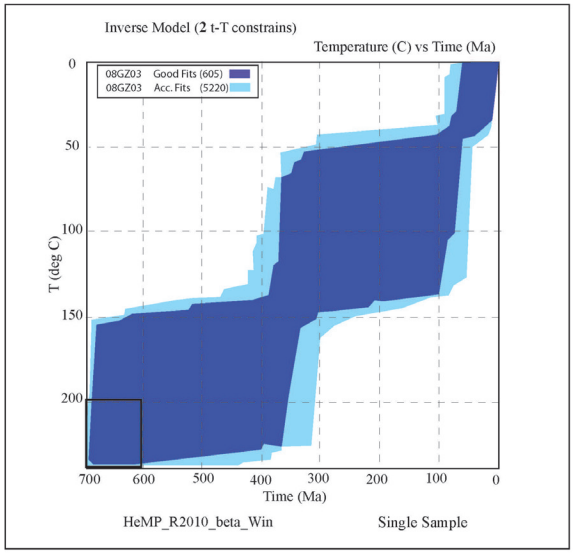

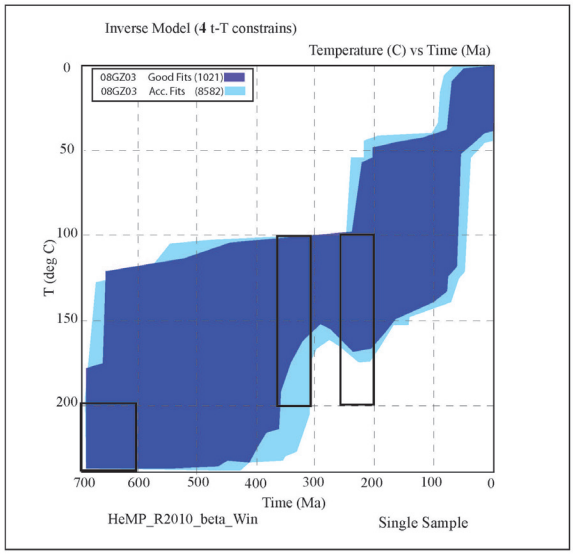

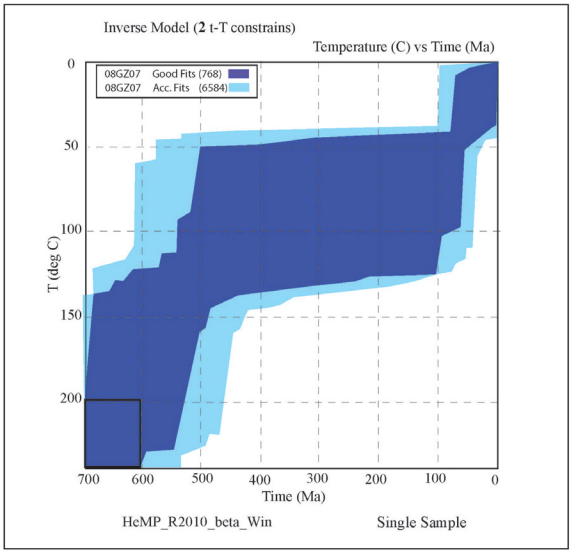

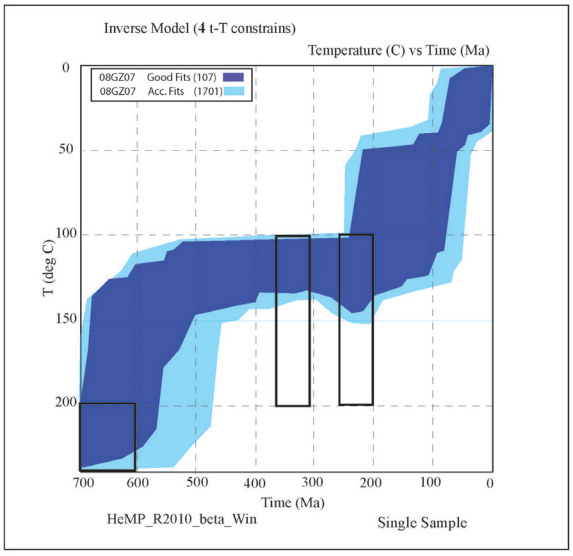

Appendix **4**

Single sample modeling

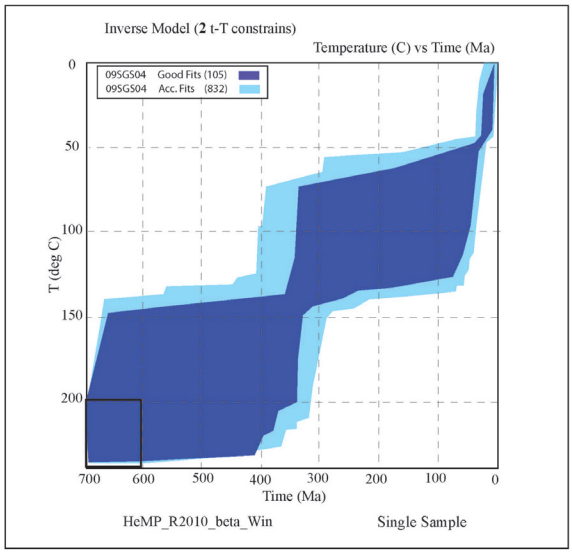

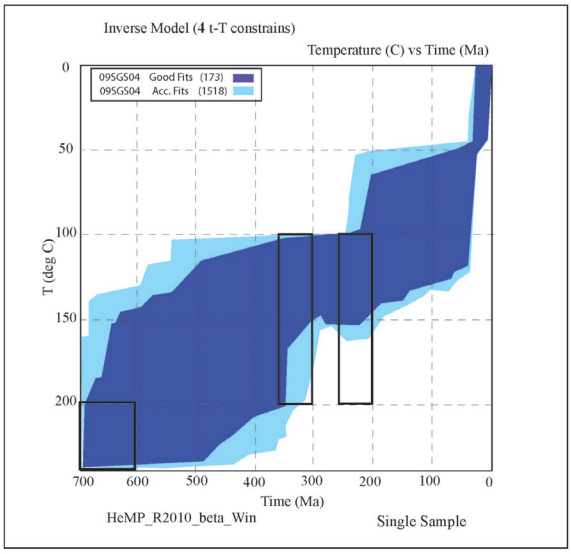

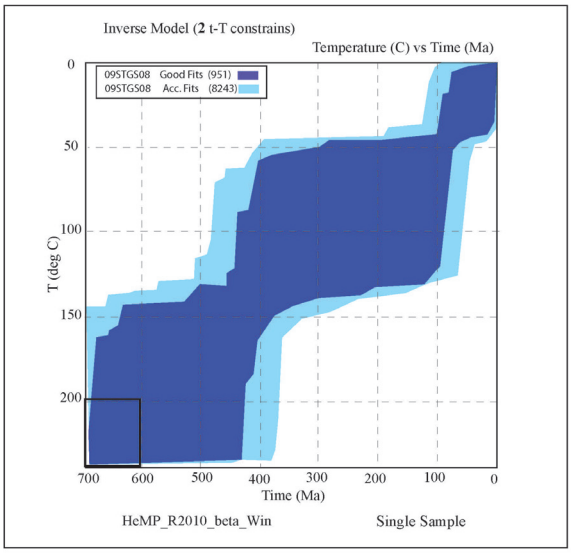

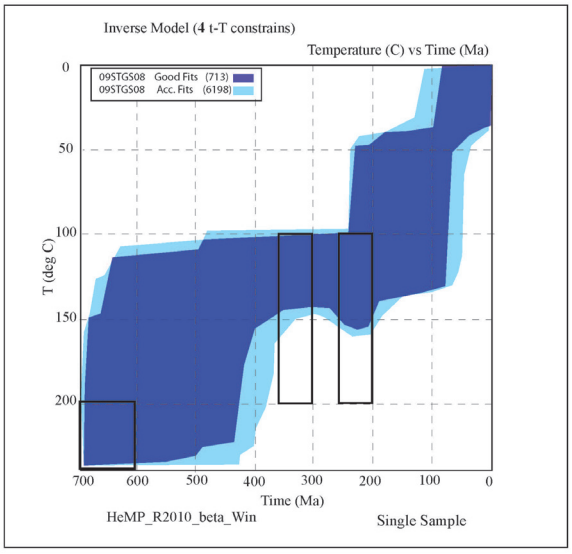

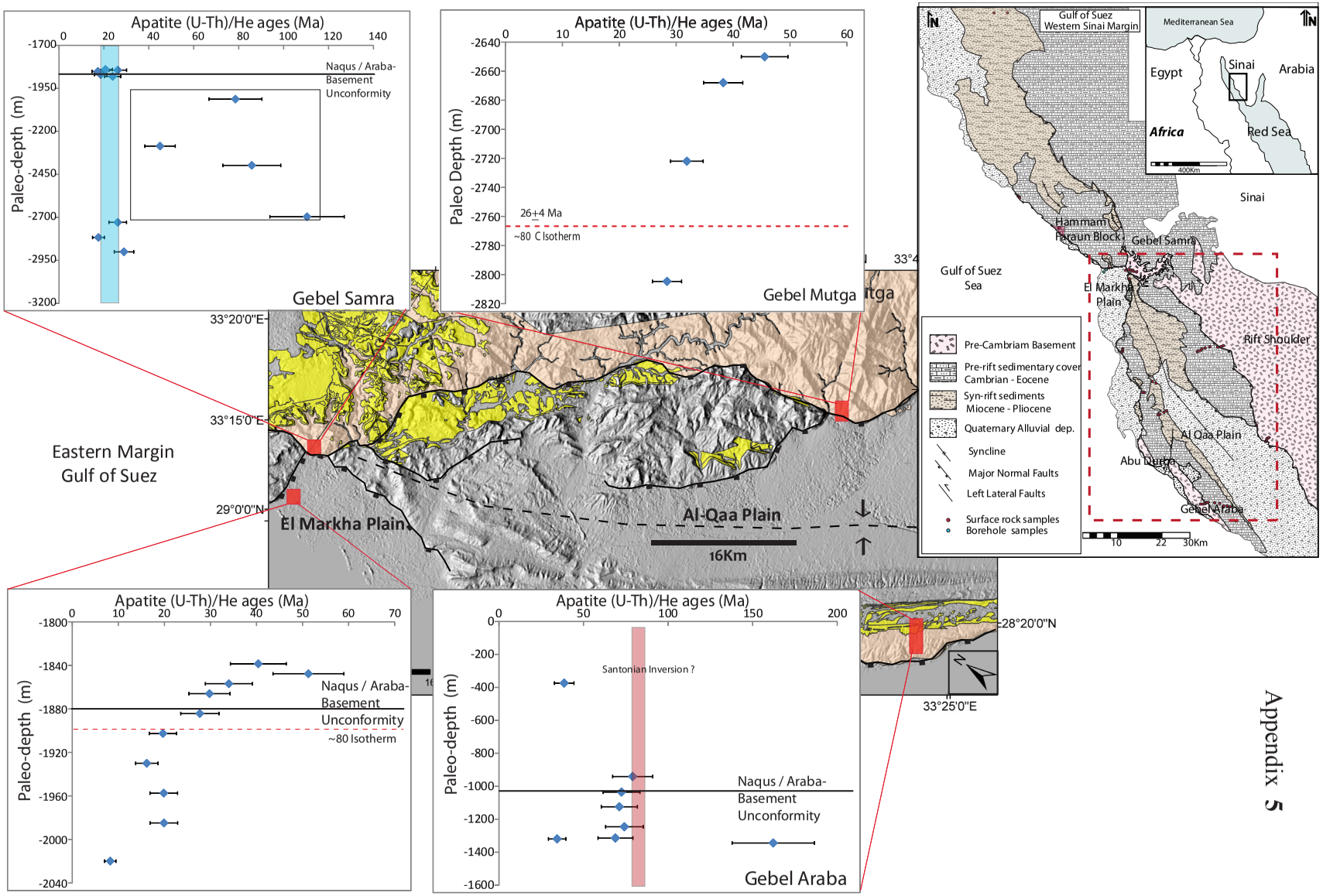
Apatite (U-Th)/He ages (Ma)
Paleo-depth (m)
Naqus / Araba-Basement Unconformity
Gebel Samra
Apatite (U-Th)/He ages (Ma)
Paleo Depth (m)
26±4 Ma
~80 C Isotherm
Gebel Mutga
Gulf of Suez Western Sinai Margin
Mediterranean Sea
Egypt
Sinai
Arabia
Africa
Red Sea
Hammam Faraun Block
Gebel Samra
Gulf of Suez Sea
El Markha Plain
Rift Shoulder
Al Qaa Plain
Abu Durba
Gebel Araba
Pre-Cambriam Basement
Pre-rift sedimentary cover Cambrian - Eocene
Syn-rift sediments Miocene - Pliocene
Quaternary Alluvial dep.
Syncline
Major Normal Faults
Left Lateral Faults
Surface rock samples
Borehole samples
Eastern Margin Gulf of Suez
33°20'0"E
33°15'0"E
29°0'0"N
El Markha Plain
Al-Qaa Plain
16Km
28°20'0"N
33°25'0"E
Apatite (U-Th)/He ages (Ma)
Paleo-depth (m)
Naqus / Araba-Basement Unconformity
~80 Isotherm
Apatite (U-Th)/He ages (Ma)
Paleo-depth (m)
Santonian Inversion ?
Naqus / Araba-Basement Unconformity
Gebel Araba

Appendix 5

Appendix **5**

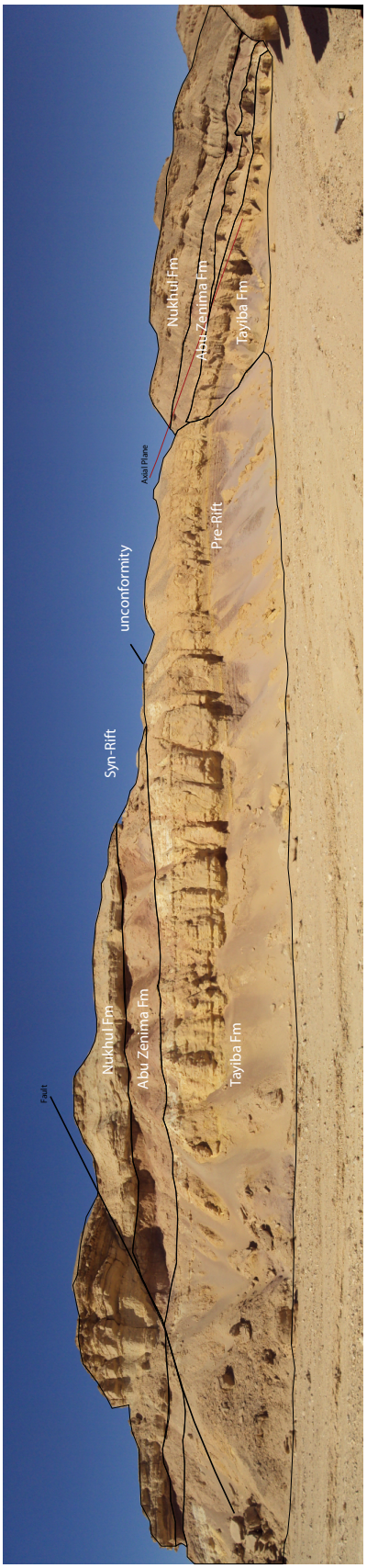
Nukhul Fm
Abu Zenima Fm
Tayiba Fm
Axial Plane
Pre-Rift
unconformity
Syn-Rift
Nukhul Fm
Abu Zenima Fm
Tayiba Fm
Fault

Appendix **5**